Summer 2011

The Investigation of Combustion and Emissions of Jp8 Fuel in an Auxiliary Power Unit

April Covington

THE INVESTIGATION OF COMBUSTION AND EMISSIONS OF JP8 FUEL IN AN AUXILIARY POWER UNIT

by

APRIL COVINGTON

(Under the Direction of Valentin Soloiu, PhD)

ABSTRACT

The US Army Single Fuel Forward policy mandates that deployed vehicles must be able to operate with aviation fuel JP-8. It is for this reason that it is vital that an investigation into the impact of JP-8 on a diesel engine performance be conducted. The author investigated the injection, combustion, and performance of JP-8, 20-50% by weight in diesel no. 2 mixtures in a small indirect injection, 77mm separate three vortex combustion chamber engine, with a high compression ratio, in order to evaluate its' effectiveness for application in Auxiliary Power Units (APUs). The new fuel mixtures were created at room temperature. For proper injection, the diesel engine requires a fuel viscosity between 1-10cSt, therefore, the new fuel can contain up to 100% JP-8 (J-100). This was verified by the piston-plunger type pump injection system. All blends were shown to have a good ignition with the ignition delay remaining constant in correlation with the amount of JP-8. The heat release for all blends displayed a similar development compared with the diesel fuel, the premixed phase being combined diffusion combustion. The maximum combustion pressure remained relatively constant for all fuel blends. The maximum temperature shifts later in the crank angle as JP-8 percentage increases, all the while retaining a higher temperature for a longer duration. The exhaust temperatures remained relatively constant for all blends. The heat flux in the engine cylinder showed similar values for all fuels, while the cylinder heat losses were at a minimum during combustion before TDC with increased convection losses at TDC for all fuels and first part of power stroke. The heat losses associated with the system increased slightly with the addition of JP-8 without any shifts extending for the duration of cycle. The engine investigation demonstrated that up to 50% JP-8 by weight in diesel can be injected and burnt in a diesel engine at a residence time of 5ms from the start of injection, while maintaining the overall efficiency performance. The study validates that the JP-8 is an excellent source for power generation in a diesel APU (auxiliary power unit) based on its combustion characteristics.

INDEX WORDS: Alternative fuels, Internal combustion engine, JP-8, Thermodynamics, performance, Heat transfer, Diesel

THE INVESTIGATION OF COMBUSTION AND EMISSIONS OF JP8 FUEL IN AN AUXILIARY POWER UNIT

by

APRIL COVINGTON

B.S., Georgia Institute of Technology, 2009

A Thesis Submitted to the Graduate Faculty of Georgia Southern University in Partial

Fulfillment

of the Requirements for the Degree

MASTER OF SCIENCE

STATESBORO, GEORGIA

2011

THE INVESTIGATION OF COMBUSTION AND EMISSIONS OF JP8 FUEL IN AN AUXILIARY POWER UNIT

by

APRIL COVINGTON

Major Professor: Valentin Soloiu
Committee: Gus Molina
Anoop Desai
Norman Schmidt

Electronic Version Approved:
June 2011

DEDICATION

I dedicate this paper to my parents. It is their love, support, and money that have gotten me through the past twenty-four years. They have provided the roof over my head, the car I blew up, and the computer whose screen died. Thank you for all the reliable support.

ACKNOWLEDGEMENTS

Thank you to everyone in the Renewable Energy Laboratory and Georgia Southern University.

TABLE OF CONTENTS

LIST OF TABLES

LIST OF FIGURES

CHAPTER 1: OVERVIEW OF THE STUDY

Introduction

In today's modern society, a military forces' success depends as much on their fuel supplies as their food supplies. It is for this reason that governments around the globe have recognized that a large portion in the recipe for success is oil, as numerous battles throughout history have been decided by oil or rather the lack of. Currently the U.S. military operates on three fuels: gasoline, diesel, and jet aviation fuel (JP-8). Three fuels means three separate transportation, storage, and distribution systems. A single fuel would eliminate the planning associated with anticipated fuel usage of a certain type and also eliminate the possibility of mixing up the fuels in the heat of battle. NATO (North Atlantic Treaty Organization) observed this constant problem and recognized the need for the standardization of the fuel through the adoption of a Single Fuel Forward policy, whose purpose is the simplification of the Army logistics through the reduction of the total number of fuels required. The use of a single fuel for both aircraft and ground vehicles would result in the reduction of costs and optimization of logistics, due largely in part to the face that approximately 38.6% of the Army supply is bulk fuel (TARDEC, 2001). Based on this, both NATO and the US Army adopted a policy of a "Single Fuel Forward" for the battlefield, using aviation kerosene fuel MIL-DTL-83133E grade JP-8 with maximum allowable sulphur content of 0.3% (3000 ppm) by weight. This strategic move offers a chance for logistical stream-lining.

The US military's primary mode of vehicle propulsion for both tactical and combat vehicles is that of the diesel engine (TARDEC, 2001). The diesel engine is designed for both military and commercial applications; however, their calibrations and design are based on the

optimization for use of diesel fuel, not military JP-8 fuel. Thus, the operation of the standard engine with JP-8 may result in non-optimal performance. It is possible that these obstacles may be overcome through the use of electronic control units (ECUs); however, a better understanding of the fundamental effects of JP-8 on engine operation and performance is required before such a device may be developed.

Right before the official adoption of this standardized fuel the US Army conducted extensive field test on various pieces of equipment using JP-8 fuel at Fort Bliss, TX, nevertheless without in cylinder combustion analysis. Numerous benefits of using JP-8 in combustion ignition engines were noted as a result of the extensive testing. In terms of the engine itself it was observed that it reduced engine combustion-related component wear, reduced nozzle fouling/deposit problems in both diesel and gas turbine engines, reduced fuel related low temperature operability problems, and improved fuel/lubricant related cold starting (TARDEC, 2001). In terms of the influence on auxiliary systems it reduced potential for fuel system corrosion problems, extended oil change and filter replacement intervals, reduced potential for microbiological growth in fuel tanks, reduced water entrainment and emulsification problems in vehicle fuel tanks, and reduced exhaust emissions and particulate signature (TARDEC, 2001). It can also be noted that an increase in a storage stability of the fuel was observed.

However, a few negative effects were also observed, these being, a reduction in horsepower due to the lower volumetric heat content of JP-8 as compared to diesel, which resulted in a 1 to 5% increase in fuel rate consumption, in order to offset the reduction in horsepower (TARDEC, 2001). It was also observed that consistent reading were unable to be obtained in relation to cetane index, aromatic content, naphthene content, and proportions of other hydrocarbon functional groups. Finally, operational difficulties and problems also

occurred in fuel-lubricated rotary-type injection pumps due to lower viscosity and material incompatibilities with JP-8.

From the above results and the numerous studies conducted on the cumulative impact of replacing Diesel with JP-8, there still exists a need to understand and quantify the fundamental reasons for these phenomenon's, in order to provide a solution for eliminating potential drawbacks. It is for this reason that this study focuses on the investigation into the impact of JP-8 fuel on a diesel engines' combustion characteristics in terms of fuel injection, combustion, and performance.

Purpose of the Study

As members of the Georgia Southern class of 2011, we are part of a new generation of engineers that are more aware of our actions and the consequences that they produce. We realize that our actions may not only affect our lives alone but the well being of the global community as a whole. Our Professors have provided us with all of the tools necessary to change our dreams into reality. It is with this attitude that we have become full supporters of the idea and concept of sustainability, which is in a nut shell, the development that meets the needs of the present without compromising the ability of future generations to meet their own needs.

As members of our global community, our goal is to investigate a current problem facing society at this moment in time. Because we are all members of our global community, we are not just interested in researching and studying the issue, we are also interested in working to bring about some type of change or transformation, by applying the knowledge we have gained thus far on our educational journey.

For this particular study, the problem the researcher intends to conquer is that of the investigation into the combustion and performance characteristics of a compression ignition engine fueled with varying blends of JP-8 in hopes that, future researchers may expand on these results to develop an electronic control unit (ECU) to optimize the engine for use with the JP-8 fuel.

Sustainability

Sustainability can be summed up in one word, that being that sustainability equals equilibrium. Which basically means, that something is considered sustainable if everything evens out, the matter going in "input" equals the matter coming out "output." While on the other hand, sustainable development means that people should be aware of the future and once again that things even out that we leave the world "our community" the same or better than it was before by any means necessary. This does not mean that we cannot use our natural resources, because whether or not we like it, they will eventually be used all up and be gone. So if we choose to use the available natural resources like we are, then we need to provide alternate energy sources as an output. So we evaluate our current situation and the available resources and make sure that when we finish and as we go along that we are able to provide the future generations with the same choices "resources" that we had available. Basically, we need to be able to recognize a crisis before it is too late.

Easter Island provides a historical example of the importance of sustainability that cannot be denied. Easter Island is an island that lies in the southeastern Pacific Ocean, many may know of it because of the large statues of heads that still exist there today. Easter Island was once a tropical paradise, for example, if one were to look up the word paradise in the dictionary, they would see a picture of it. It had everything, beautiful scenery, everlasting water, trees as far as

the eye could see, and an endless supply of food supplied from the ocean. The natives lived luxurious for many moons. However this utopia would not last forever. The natives used countless trees to help build the now famous statues and also to build boats to travel out to get food from the ocean. They begin cutting down the trees at a very rapid rate without ever planting any new ones, and to no surprise the tree supply became obsolete. Without trees for boats the natives had no way to go out into the ocean to retrieve food. So in time the natives became extinct, and to this day the trees on Easter Island are still very thin. So as you can see, this is a classic example of what happens when sustainability is not taken into consideration. This is why the current dwindling supply of natural resources and exponentially increasing energy demand ordeal urgently needs to be taken into consideration and solutions developed.

Energy Demands

It is a known fact that approximately ninety-five percent of the primary energy consumed in the transportation area worldwide is provided by liquid hydrocarbon fuels derived from crude oil. There exists no other sector in the world, which is so completely reliant on a single source of primary energy, and this fuel singularity represents a unique threat to both the environment and global security. The transportation segment as a whole includes automotive, aviation, high performance land utility and marine transportation modes, is responsible for roughly one-quarter of energy-related greenhouse gas emissions worldwide. This is the second largest group contribution with the only greater being that of power generation.

Despite the mounting awareness of the dangers and latent causes of global warming, the potential impact that the climate change could have worldwide as a result of the current transportation industry, until now, has played a relatively minor role in the development of alternative fuels. Many of the fuel technologies which are currently under consideration or in

various stages of commercialization have environmental footprints which are significantly worse than conventional crude oil. They were considered and acted upon for the wrong reasons. So in order to avoid the worst impacts of climate change, the global economy as a whole must quickly embark on the road towards the reduction of the emission associated with current fuels. The transportation industry will continue to increase its carbon footprint as the oil industry and governments are forced to exploit these energy-intensive unconventional oils to satisfy a steadily growing demand for liquid fuels. Basically this energy demand will be meet regardless of its unforeseen consequences. One of the major sources of pollution throughout the world is from the combustion of hydrocarbons in internal combustion engines. Although the ideal case would be a total shift away from the use of any liquid hydrocarbons derived from conventional crude oil, the thought of this idea actually being able to be accomplished in the near future is imprudent. It might as well be thought of nothing more than a mere fantasy. However, the idea that alteration to the industry could be made in order to reduce emissions and increase efficiency is quite obtainable. This is a fantasy that could easily become a reality.

The Environmental Protection Agency

The Environmental Protection Agency (EPA) and other international regulatory agencies are requiring vehicles and powered equipment to substantially reduce emissions. Significant reductions in carbon monoxide (CO), unburned hydrocarbons (UHC), nitrogen oxides (NOx) and particulate matter (PM) will be required in almost all classes of engines. Generally, diesel engines are substantial emitters of PM and NOx, but only small emitters of CO and UHC, whereas, gasoline engines are the greatest emitters of CO and substantial emitters of UHC and NOx, but only modest emitters of PM. It is for this reason that a diesel engine will be used in the experimentation in order to reduce toxic emissions even further. The contraction of the engine

emissions standards for compression ignition engines has resulted in the tightening of fuel specifications. These specifications limit concentrations of sulfur, aromatics, polycyclic aromatic hydrocarbons, and several other fuel impurities. The military even begin taking interest in the development of emission control technologies with the hope that they would be able to reduce cost and perhaps make a profit based on discovered technologies.

Diesel Engine

Diesel engines have been used in light and heavy transport for many decades. Due to increasingly stricter requirements for lower fuel consumption and reduced emissions, further investigations into the diesel engine are required in order to help comply with this demand. One possible solution would be the improvement of the combustion process to optimize consumption and reduce emissions. Thus there is a strong demand to explore new combustion concepts capable of meeting stringent emission standards. In the past engine optimization was done by conducting a series of trial and error physical experiments that were both costly and time consuming. By using engine modeling, the amount of testing required is reduced because most of the testing is done virtually through a simulation.

The creating of an engine model requires a broad range of experimental data. To make an accurate model, the data must span the entire range of operating conditions. However, only a relatively small amount of data is needed. Therefore, the demand is now able to be satisfied through the development of computer models for engine design, the combination of experimental measurements and validated computer model predictions as to provide an added opportunity for improved understanding of in-cylinder combustion and pollutant-formation processes. By the creation of an engine model the analysis and comparison of various alternative fuels can easily

and efficiency be developed. With this new tool in our arsenal the concept of sustainability is finally visible on the horizon.

Government Influence

Ever since WWI, governments everywhere have recognized that oil is a key to national security. Many battles throughout history have been decided by oil or shall I say the lack of. Many nations have experienced many logistics problems created by long supply lines and fuel shortages. Logistics problems are further complicated due to multinational operations. Approximately 38.6 percent of the Army troop supply is bulk fuel (TARDEC, 2001). NATO observed this constant problem and recognized the need for the standardization of the fuel. They believed that the adoption of such would result in lower costs and optimized logistics. Soon after both NATO and the US adopted a standardized fuel, which that fuel being JP-8. JP-8 is important to study because using a single fuel for both aircraft jet engines and military ground vehicles offers a chance for logistical stream-lining. Right before the official adoption of this standardized fuel the US Army conducted extensive field test on various pieces of equipment using JP-8 fuel at Fort Bliss, TX (TARDEC, 2001). These extensive tests resulted in the conclusion that JP-8 could be successful used as a standardized fuel. Numerous benefits of using JP-8 in combustion ignition engines were noted as a result of the extensive testing. It was observed that it reduced engine combustion-related component wear, reduced potential for fuel system corrosion problems, increased fuel filter replacement intervals, reduced nozzle fouling/deposit problems in both diesel and gas turbine engines, reduced exhaust emissions and particulate signature, extended oil change and filter replacement intervals, increased storage stability, extended oil change and filter replacement intervals, reduced fuel related low temperature operability problems, reduced potential for microbiological growth in fuel tanks,

reduced water entrainment and emulsification problems in vehicle fuel tanks, and improved fuel/lubricant related cold starting. However, a few negative effects were also observed, these being, a reduction in horsepower occurred due to the lower volumetric heat content of JP-8 as compared to diesel. This caused a 1 to 5% increase in fuel rate consumption, in order to offset the reduction in horsepower (TARDEC, 2001). It was also observed that consistent reading were unable to be obtained in relation to cetane index, aromatic content, naphthene content, and proportions of other hydrocarbon functional groups. Finally, operational difficulties and problems also occurred in fuel-lubricated rotary-type injection pumps due to lower viscosity and material incompatibilities with JP-8. (TARDEC, 2001)

CHAPTER 2: REVIEW OF RELATED LITERATURE

Introduction

For years, JP-8 has been the leading aviation fuel for the military. It has been examined, tested, and researched, and yet its full effects on CI engines are still unknown. The number of research papers dedicated to JP-8 is indeed limited; however, the studies into JP-8 have undeniably plowed the way for new and in-depth research into the field. It is irrefutably true that without knowledge of what has been, new and innovative research cannot begin to be conducted. It is from past studies that I have built my foundation for which to assemble this research study. It is from these papers that I have developed an in-depth appreciation for the diesel engine, the global community's concern for the environment, the need for sustainability, and the previous research on JP-8.

Compression Ignition Engine

Looking back to the events of days long passed, it can be seen how the repercussions of a single action are capable of forever altering the lives of future generations. One such action occurred during the 19th century with the invention of the reciprocating engine, which has become an indispensable part of today's mechanized society due to its robust versatility, durability, and relative low cost. All reciprocating engines are characterized by a piston that moves back and forth in a cylinder, with the piston geometry being described by the figure below (Heywood, 1988).

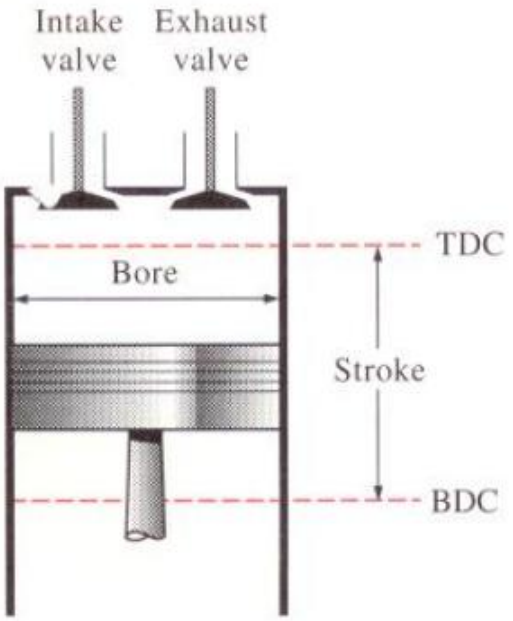

Figure 1 Piston Geometry (Heywood, 1988)

With top dead center (TDC) representing the point at which the piston is at its highest position in the cylinder, and is associated with the minimum cylinder volume and bottom dead center (BDC) representing the point at which the piston is at its lowest position within the cylinder and results in the maximum cylinder volume. This piston movement in turn drives a

crankshaft, which transmits the power to a drive shaft or transmission. The reciprocating engine for all intensive purposes can be described as a mere heat engine defined as a thermodynamic system which operates in a cycle and delivers useful work to the surroundings through the use of a working fluid when heat energy supplied to the system (Shyam, 2006). Heat engines can be classified into two distinct types, external combustion engines and internal combustion engines. A steam engine is an example of an external combustion engine in which, the products of combustion, transfer heat energy released during the combustion process to the working fluid through the walls of a heat exchanger. The working fluid is then used for the production of mechanical or electrical power. However, in an internal combustion engine also referred to as an IC engine, the working fluid used for power production is derived from the products of combustion of the fuel and air mixture. This type of engine is much simpler mechanically due to the absence of the heat exchanger and cooling/recycling facility. Internal combustion (IC) engines can be classified into two distinct types, with the most widely used being that of the spark-ignition (SI) engine that operates using gasoline and the other being a compression ignition (CI) engine that operates using diesel. In 1876, Niklaus Otto is credited with the invention of the SI engine and the statement of its theoretical cycle with Rudolf Diesel developing the CI engine just 7 years later (Weston, 1992). Traditionally, SI engines are employed for light duty applications as they are rated for a lower power range, while CI engines are primary used for heavy-duty applications as they are able to develop more power with the use of a lower amount of fuel consumption.

The Diesel cycle (CI engine) is very similar to the Otto cycle (SI engines) in that both are closed cycles commonly used to model internal combustion engines designed to convert the chemical energy available in the fuel into mechanical energy. This mechanical energy moves

pistons up and down inside cylinders. The pistons are connected to a crankshaft, and the up-and-down motion of the pistons, known as linear motion, creates the rotary motion needed to turn the wheels of a car in a forward direction. It can be observed that both the diesel engines and gasoline engines covert fuel into energy through a series of small explosions or combustions, with the main variation of the two being in the way these small explosions or combustions occur. The difference between them is that the Diesel cycle is a compression-ignition cycle instead of a spark-ignition cycle like the Otto cycle. In a spark-ignition cycle of a gasoline engine, fuel is mixed with air, compressed by pistons and ignited by sparks from spark plugs. In a compression-ignition cycle of a diesel engine, the air is compressed and this compression causes the air to heat up, then the fuel is injected, and ignites when it comes in contact with the associated heat. Basically air heats up when it's compressed, the fuel ignites use fuels that begin combustion when they reach a temperature and pressure that occurs naturally at some point during the cycle and, therefore, do not require a separate energy source to burn. It is important to note that note that most fuels will start combustion on their own at some specific temperature and pressure. But this is often not intended to occur and can result in the fuel combustion occurring too early in the cycle.

The diesel combustion process is an extremely complex process involving fuel sprays, inhomogeneities, vaporization, oxidation, and mixing processes. The diesel engine uses a four-stroke combustion cycle just like a gasoline engine, with the four stokes being, compression stroke, combustion stroke, expansion stroke, and cooling stroke shown in the Figure below (Soloiu V. , 2010).

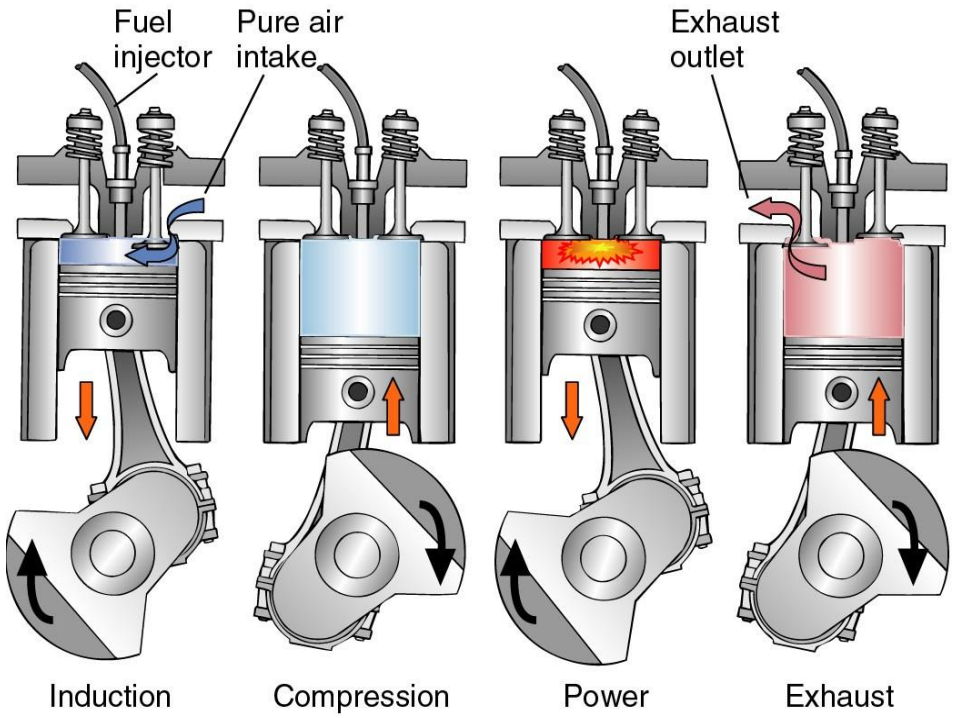

Figure 2 Four Stroke Cycle (Soloiu V. , 2010)

During the Intake Stroke the intake valve is open. The piston starts at TDC and moves to BDC, which creates a vacuum effect causing the air-fuel mixture to be sucked into the cylinder. During the compression stroke, both valves are closed and the air is heated by compressing it; this is accomplished by moving the piston down the cylinder BDC to TDC. It is in this part of the cycle that we contribute work to the air. In the ideal Diesel cycle, this compression is considered to be isentropic (Kondepud & Prigogine, 1998). It is here that the volumetric compression ratio, the ratio of the volume of the working fluid before the compression process to its resulting volume after compression, is determined based on piston/cylinder geometry. During the combustion/power stroke, as the piston reaches the top, fuel is injected at just the right moment and ignited, forcing the piston back down. In moving the piston, the high temperature, high pressure gases also rotate the crankshaft, providing compression to the other cylinders. The gauges exert approximately five times the amount of work on the piston as the piston exerted on

the gas during the compression stroke (Heywood, 1988). The heat during this process is considered to be isochoric. During the expansion/exhaust stroke, fuel is burned to heat compressed air and the hot gas expands forcing the piston to travel up in the cylinder. It is in this phase that the cycle contributes its useful work, rotating the automobile's crankshaft. We make the ideal assumption that this stage in an ideal Diesel cycle and thus can be considered isentropic. During the cooling stroke, the expanded air is cooled down to ambient conditions. This corresponds to exhausting the air from the engine to the environment and replacing it with fresh air. Since this happens when the piston is not moving, it can be assumed that this process is isochoric (no change in volume).

A simplistic view of the process can be described in the following manner. Fuel is directly injected into the combustion chamber near the end of the compression stroke creating a spray of droplets. The compression ratio is intentionally selected high enough so that the air near the end of the compression stroke is sufficiently heated enough to cause the fuel to vaporize and auto ignite very soon after injection. The remaining fuel continues to be injected and can burn at a rate no faster than injected. The fuel injection method creates fuel rich regions, thus producing the observed high concentrations of particulate matter associated with compression ignition cycle.

There are two main types of CI engines; direct injection (DI) and indirect injection (IDI). Direct injection (DI) is characterized by the fuel being injected directly into the combustion chamber, and indirect injection (IDI) is defined by the fuel being injected into a separate

combustion chamber from the main combustion chamber.

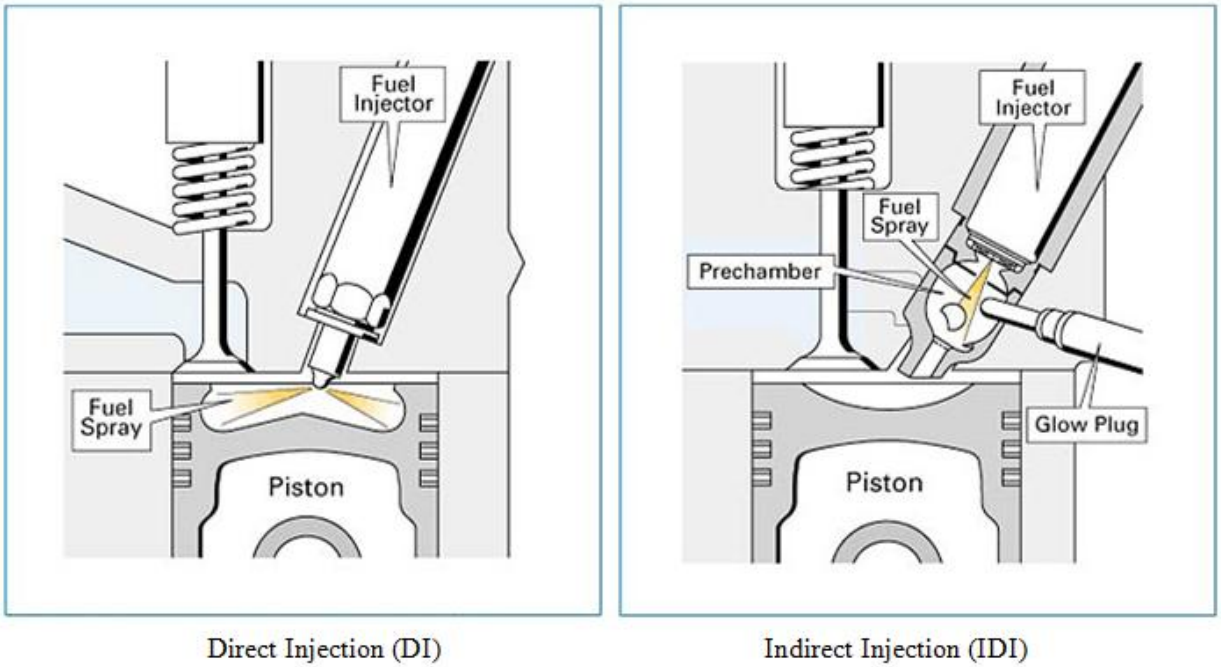

Figure 3 Types of CI Engine Systems (Soloiu V. , 2010)

The DI engine has a combustion bowl in the piston crown and a helical port to generate swirl, while the IDI engine has a prechamber that severs as a swirl chamber of sorts in which the swirl is induced through the location of the fuel injection port. These two types of CI engines have different advantages over the other and are designed for different applications. Although when comparing the DI to the IDI engine it can be noted that the DI engine exhibits reduced thermal stress and a higher possible air charging (Culick, Heitor, & Whitelaw, 1996). IDI engines are known for lower noise characteristics due to the lower maximum combustion pressure and max temperatures (Majewski & Khair, 2006). The brake specific fuel consumption (BSFC) for an IDI engine is typically 15 percent higher than that of a DI engine. This increase in BSFC is due to an increase in friction mean effective pressure, partly offset by the effect of decreasing the importance of heat losses per cycle on efficiency. In terms of emissions NOx

concentrations rise steadily as the air/fuel ratio increases with increases brake mean effective pressure at constant injection timing, with the IDI displaying similar characteristics except that at high loads the NOx concentrations are shown to level off. These characteristics were seen not to change substantially with respect to engine speed. The IDI engine shows significantly lower HC emissions than the DI engine. The high HC is thought to result from fuel mixing to too lean an equivalence ratio. It is for these reasons that it can be concluded that the ideal application for IDI systems are for small high speed diesel engines where the DI applications are best suited for the medium to large size engine subjected for use at all speeds.

(Szybist, Kirby, & Boehman, 2005) explore the diesel injection and combustion processes in an effort to better understand the differences in NOx emissions between biodiesel, Fischer-Tropsch (FT) diesel, and their blends with a conventional diesel fuel. The baseline petroleum diesel fuel, BP325, was 325 ppm low sulfur diesel fuel from BP, the FT fuel was produced from a gas-to-liquid (GTL) process, and the biodiesel used in this study was standard soy-derived methyl ester biodiesel obtained from World Energy Corporation. The study of the various emissions were performed with each fuel at a variety of static fuel injection timing conditions in a single-cylinder DI diesel engine with a mechanically controlled, in-line, pump-line-nozzle fuel injection system. The engine used was a Yanmar L70 EE air-cooled, four-stroke, single cylinder DI diesel engine with a maximum continuous power output of 5.8 hp was operated at high load (75% maximum continuous output) and low load (25% maximum continuous output) at 3600 rpm. These engine performance and emissions studies were performed with a large number of alternative diesel fuels in an effort to reduce particulate matter (PM) and NO*x* emissions from diesel engines. Oxygenates, or fuel with molecularly bound oxygen, are considered to be broad classes of alternative diesel fuels that include renewable fuels

such as biodiesel. A second class of alternative diesel fuels is non-oxygenated synthetic fuels, namely, Fischer-Tropsch (FT) diesel fuel. Both oxygenates and FT diesel fuels have been shown to be effective at reducing PM emissions. In this study it was also noted that biodiesel was able to consistently reduce PM also. They attributed the reduction in PM emissions of the biodiesel fuel to the wt % oxygen in the fuel blend, noting that above 30 wt % oxygen the engine operated with smokeless exhaust. The review of the emissions from FT diesel fuel showed that except at some light load conditions, FT diesel leads to significant reductions in PM emissions, although the % reduction varied with fuel composition and engine technology. The reduction of PM emissions with FT diesel was attributed to a combination of low sulfur content, low aromatic content, and high cetane number (CN). FT diesel fuel reduced NO*x* emissions with nearly the same consistency as it reduced PM emissions, although there were some exceptions in this trend at light load. The reductions in NO*x* emissions were attributed mainly to FT diesel fuel's high cetane number. However, it is important to remember that oxygenated diesel fuels do not produce the same consistent reduction in NO*x* emissions that FT diesel fuels do. An advance in SOI timing was seen for the biodiesel blends, which have a higher bulk modulus than conventional diesel, and a delay was seen for the FT blends, which has a lower bulk modulus. The analysis they conducted showed that changes in the SOI timing, caused by differences in the bulk modulus of the fuel, were largely responsible for the differences in NO*x* emissions. They concluded that there was little or no relationship between NO*x* and DCN or maximum cylinder temperature. There was a strong relationship between NO*x* and the maximum rate of heat release at light load, but this trend was not as strong at high loads. It was also observed that there was a relationship between NO*x* and the timing of the maximum rate of heat release. The relationship

between NO*x* and the timing of the maximum cylinder temperature produced a universally applicable correlation, with strong relationships seen at both the high and low load conditions.

(Aceves, et al., 2001) investigated homogeneous charge compression ignition (HCCI) as an alternative to diesel engines with high efficiency and low NOx and particulate matter emissions. The single zone model they develop proved very successful in predicting the start of combustion and providing reasonable estimates for peak cylinder pressure, indicated efficiency and NOX emissions. It uses a detailed chemical kinetics code (HCT, Hydrodynamics, Chemistry and Transport) to predict HCCI combustion, under the assumption that temperature, pressure and composition are uniform throughout the combustion chamber. This model was being applied to develop detailed engine performance maps and control strategies. It was also used to analyze the problem of engine start ability. The multi-zone model was capable of providing very accurate predictions of the combustion process, including HC and CO emissions. This model takes into full account the effect of temperature (and possibly concentration) gradients inside the combustion chamber. The multi-zone model combines a detailed fluid mechanics code with a detailed chemical kinetics code. Instead of directly linking the two codes, which would require an unacceptably long computational time, the procedure consists of first running the fluid mechanics code to obtain temperature profiles as a function of time. These temperature profiles are then used as input to a multi-zone chemical kinetics code. The success of this procedure is in large part a consequence of the fact that for much of the compression stroke the chemistry is inactive and thus has little influence on fluid mechanics and heat transfer. Then, when chemistry is active, combustion is rather sudden, leaving little time for interaction between chemistry and fluid mixing and heat transfer. The multi-zone model was used in the optimization of combustion chamber geometry and operating conditions to achieve controlled combustion at

high efficiency and low emissions. It was noted that small temperature differences inside the cylinder have a considerable effect on combustion because chemical kinetics is very sensitive to temperature. As a result, heat transfer and mixing are important in forming the condition of the charge prior to ignition. Heat release rate is typically difficult to match analytically because heat release rate is obtained by analyzing pressure traces according to the first law of thermodynamics. Small inaccuracies in pressure can therefore result in great differences in apparent heat release rates. Turbulence, flame propagation and mixing make SI and CI combustion much more difficult to predict with good accuracy than HCCI combustion. They noted Cylinder-to-cylinder variations play an important role in limiting maximum power, and should be controlled to achieve satisfactory performance.

(Nagaraju, Henein, Quader, Wu, & Bryzik, 2008) conducted a study to determine the effect of using B-20 (a blend of 20% soybean methyl ester biodiesel and 80% ultra low sulfur diesel fuel) on the combustion process, performance and exhaust emissions in a High Speed Direct Injection (HSDI) diesel engine equipped with a common rail injection system. The engine used was operated under simulated turbocharged conditions with 3-bar indicated mean effective pressure and 1500 rpm engine speed. The tests were conducted at IMEP (3 bar), engine speed (1500 rpm), and covered a wide range of injection pressures, EGR rates, injection timings, injection duration and a fixed swirl ratio of 3.77(R*s*). The experiments were conducted on a single cylinder, 4-valve, direct injection, 4 stroke, water cooled, diesel engine equipped with a common rail fuel injection system capable of delivering fuel pressure up to 1350 bar. The engine was supercharged with heated shop air. The charge temperature and pressure in the intake surge tank, in addition to the back pressure in the exhaust surge tank were adjusted to simulate actual turbocharged engine conditions. In the intake manifold, tangential and helical ports were

throttled to different degrees by using gate valves to attain a swirl ratio of 3.77. An EGR valve was incorporated which facilitated different EGR levels of 0, 25, 50, 60 and 64% to be attained. Based on their research, biodiesel was found to increase NO_X emissions when compared with regular diesel fuel due to physical properties such as the higher bulk modules of biodiesel, which promotes an advance in fuel injection timing and produce higher cycle temperatures. The increase in NO_X was reported to be more prominent in the pump-line-nozzle and unit injection systems, but was not relevant in high-pressure common rail injection systems. They discovered that B-20 did not contribute in the initial stages of fuel evaporation and the formation of an ignitable mixture under all the operating conditions tested. There was no statistically significant difference in start of injection between B-20 and B-00. The B-20 fuel showed a 29% lower ignition delay than B-00 that was significant at the 95% confidence level. B-20 enhanced the exothermic reactions leading to the premixed combustion. This was thought to be caused by the contribution of the oxygen atom in biodiesel. The peak of the premixed combustion rate of heat release was higher with B-20 than B-00 under different operating conditions. Statistically the maximum rate of heat release (RHR Max) for B-20 was 8% higher than that for B-00. The mixing and diffusion controlled combustion fractions were higher with B-20 than B-00, causing higher exhaust gas temperature for B-20 than B-00. Indicated specific fuel consumption was higher with the B-20 when compared to B-00. Increased fuel consumption with B-20 can be attributed to its lower heating value and late release of energy in the expansion stroke. Statistically it was found that B-20 decreased NOX (4%) relative to B-00 contrary to some previous studies. Though the effect was small it was significant near the 95% confidence level. The incomplete combustion products of HC, CO and Soot are lower for B-20 than for B-00.

(Giannelli, Nam, Helmer, Younglove, Scora, & Barth, 2005) analyze an emissions inventory model developed by the EPA known as MOVES (Motor Vehicle Emissions Simulator). The first version of the model outputs fuel consumption based on available modal data. However, due to the limited heavy-duty vehicle data, MOVES rates needed to be supplemented with rates determined with the Physical Emission Rate Estimator (PERE). PERE combines vehicle tractive power together with vehicle power train parameters specific to the class of vehicle; the vehicle weight, shape, engine type, and transmission. Vehicle fuel consumption is directly related to the vehicle power consumption which has an implicit time dependence realized in the speed-time trace or cycle under which the vehicle has been driven. They determined that vehicle emission models would be more accurate if they would take this into consideration. There are four major components of this model, (i) engine friction and efficiency, (ii.) engine maximum torque map, (iii) vehicle transmission, and (iv) vehicle road load parameters. All of these components, but the vehicle transmission parameters, can be derived from a relationship for fuel consumption. They use Willans line methodology to determine both the engine efficiency and the engine friction of the heavy duty diesel engines studied in this report. To construct the Willans line for these engines, instantaneous values of fuel IMEP and BMEP were determined from measurements of fuel flow, engine speed, and engine load.

(Said, Buttsworth, & Yusaf, 2009) present a review of radiation heat transfer measurement in the diesel engine environment using the principles of the two-colour method. Heat transfer in internal combustion engines has a significant impact on energy efficiency and emissions, and in the case of diesel engines, radiation heat transfer within the cylinder has been identified as a significant component of the total heat transfer process. Based on the relationship

between the radiation heat transfer from the soot and the engine operating and performance parameters they try to determine key processes to optimize engine efficiency and emissions for new fuel blends. There are two types of radiation heat transfer measuring methods: shielded surface junction thermocouple technique; and the two colour method. For the shielded surface junction thermocouple technique, a fast-response surface junction thermocouple or pyrometry detector is located behind a quartz or sapphire window that acts as a filter for convective heat transfer to receive only radiation heat transfer from the combustion zone. So only changes in temperature with respect to time are measured, and these can be converted to values of transient heat flux. The two-colour method, utilizing an assumed soot emissivity, relies on the Hottel-Broughton equations in order to deduce flame temperature and soot concentration with the assumption of uniformity of temperature and soot concentration within a particular volume. The goal of the two-colour technique is to obtain instantaneous in-cylinder flame temperature and a relative soot concentration by an optical technique. There are three principal advantages of the two-colour method. First, the method detects the light emission from soot particles so that there is no need for an external light source. Second, as a non-intrusive method, it makes use of an optical probe which causes minimal interference with the combustion process. Finally, use of fast-response photodetectors enables real-time monitoring of soot concentration. The main problem of radiation heat transfer probe is the soot deposits on the window surface. Soot, solid particles that comes from unburned fuel in fuel-rich region in vapour phase, causes attenuation of the signals.

(US Department of Energy: Energy Efficiency and Renewable Energy, October 2004) state that biodiesel is defined for all partical purposes as a renewable fuel manufactured from vegetable oils, animal fats, and recycled cooking oils. There are a variety of ways that biodiesel

can be ultilzed. For example, 1% to 2% biodiesel can be used as a lubricity additive to increase the lubricating properties of some fuels in particular, ultra low sulfur diesel fuels (ULSD, less than 15 ppm sulfur), which are notoriously known to have poor lubricating properties. The diesel fuel known as B20 is actually a blend 20% biodiesel with 80% diesel fuel. While diesel fuel known as B100 is just simply biodiesel in its pure form. The chemical nature of biodiesel allows it to be blended with any kind of distillate, or diesel fuel. This includes light fuels such as jet fuel, kerosene, No.1 diesel, or military fuels (JP8, JP5), as well as normal diesel fuel like No. 2 diesel for diesel engines or gas turbines, and heating oil for boilers or home heating. Once biodiesel is blended thoroughly with diesel fuel, it stays together as one fuel and does not separate over time. Research shows that vegetable oil or greases used in CI engines at levels as low as 10% to 20%, can cause long-term engine deposits, ring sticking, lube oil gelling, and other maintenance problems and can reduce engine life. These problems are caused mostly by the greater viscosity, or thickness, of the raw oils (around 40 mm^2/s) compared to that of the diesel fuel for which the engines and injectors were designed (between 1.3 and 4.1 mm^2/s). To avoid viscosity-related problems, vegetable oils and other feedstocks are converted into biodiesel. Through the process of converting vegetable oil or greases to biodiesel, we reduce viscosity of the fuel to values similar to conventional diesel fuel (biodiesel values are typically between 4 and 5 mm^2/s). The specification for biodiesel (B100) is ASTM D6751-03. This specification is intended to insure the quality of biodiesel to be used as a blend stock at 20% and lower blend levels. Any biodiesel used in the United States for blending should meet ASTM D6751 standards. B20 is also the minimum blend level allowed for Energy Policy Act of 1992 (EPAct) compliance.

Review of JP-8 Case Studies

(TARDEC, 2001) states that numerous extensive field test using JP-8 fuel were preformed on US Army equipment at Fort Bliss, TX. These extensive test resulted in the conclusion that JP-8 could be successful used as a standardized fuel. Numerous benefits of using JP-8 in combustion ingniton engines were noted as a result of the extensive testing. It was observed that it reduced engine combustion-related component wear, reduced potential for fuel system corrosion problems, increased fuel filter replacement intervals, reduced nozzle fouling/deposit problems in both diesel and gas turbine engines, reduced exhaust emissions and particulate signature, extended oil change and filter replacement intervals, increased storage stability, extended oil change and filter replacement intervals, reduced fuel related low temperature operability problems, reduced potential for microbiological growth in fuel tanks, reduced water entrainment/emulsification problems in vehicle fuel tanks, and improved fuel/lubricant related cold starting. However, a few negative effects were also observed, these being, a reduction in horsepower occurred due to the lower volumetric heat content of JP-8 as compared to diesel. This caused a 1 to 5% increase in fuel rate consumption, in order to offset the reduction in horsepower. It was also observed that consistent reading were unable to be obtained in relation to cetane index, aromatic content, naphthene content, and proportions of other hydrocarbon functional groups. Finally, operational difficulties and problems also occurred in fuel-lubricated rotary-type injection pumps due to lower viscosity and material incompatibilities with JP-8.

(Fernandes, Fuschetto, Filipi, Assanis, & McKee, Impact of military JP-8 fuel on heavy-duty diesel engine performance and emissions, 2007) researched and evaluated the effect of using JP-8 fuel in a heavy-duty diesel engine on fuel injection, combustion, performance, and

emissions, and subsequently utilized the obtained results to propose changes to the engine calibration to mitigate the impact of the trade-offs. JP-8 is important to study because using a single fuel for both aircraft jet engines and military ground vehicles offers a chance for logistical stream-lining. Approximately 38.6 percent of the Army troop supply is bulk fuel. Therefore, the standardization of the fuel would result in lower costs and optimized logistics. It was observed that Jet A-1 fuel has the similar properties to winter diesel fuel (DF-1) and the only difference between Jet A-1 and JP-8 is the addition of three fuel additives. The US Army adopted a policy of a "Single Fuel Forward" for the battlefield using DTL-83133E grade JP-8 with a maximum allowable sulfer content of 0.3 percent (3000 ppm) by weight. The EPA, along with CARB and the US Army, classifies JP-8 as an alternative fuel for on-road buses and trucks. However, in 1994 the EPA set regulations that mandated a maximum allowable sulfer level of 0.05 percent (500ppm) by weight in diesel. They were able to shown that the density of the fuel can have a direct effect on the build-up of fuel pressure in the injection system and a consequent effect on the dynamic start of the fuel injection. The cetane number (CN) of the fuel is the measure of its propensity for autoignition. In other words, it provides a measure of the ignition delay, or the time required from the start of fuel injection to the start of combustion. They conducted experiments using a Detroit Diesel Corporation (DDC) S60 engine. The engine was equipped with exhaust gas recirculation (EGR), variable geometry turbocharging (VGT), electronic unit injection (EUI), and charge air intercooler. Their results indicated that the torque and fuel economy of diesel fuel can be matched, without smoke or NO*x* penalty, by increasing the duration of injection to compensate for the lower fuel density. The lower cetane number of JP-8 caused an increased ignition delay, retarded start of combustion, and increased premixed combustion, and their cumulative effect led to relatively unchanged combustion phasing. They

observed that directly replacing diesel fuel with JP-8 leads to a performance reduction, due to the lower density and consequently less mass of fuel injected for the same injection pulse width. Also that it is possible to match the performance of the engine with diesel fuel by increasing the pulse width of a JP-8 injection to match the mass of fuel per stroke. Due to increased mechanical losses in the fuel system pumping higher rates of volumetric flow, the correction of injection pulse width at higher loads may need to be adjusted beyond direct compensation for lower density of JP-8. The higher compressibility of JP-8 fuel causes a slower pressure build-up in the high-pressure fuel pump element as compared to diesel fuel. However, advancing the injection timing is not recommended, since increased fraction of premixed burning compensates for retarded ignition, thus preserving desired combustion phasing. Under almost all conditions, JP-8 led to lower NO*x* and particulate matter (PM) emissions and shifted the NO*x*–PM trade-off favourably. In particular, the soot formation is drastically reduced due to beneficial effects of higher volatility of fuel and the increased ignition delay on mixing. A simultaneous reduction of NO*x* is attributed to a lower aromatic content of JP-8. The beneficial effect of EGR on emission tradeoffs is relatively unchanged with JP-8. The overall trends captured with the NO*x*–PM tradeoff curves are shifted in the direction of the lower optimum, with a strong bias towards lower amounts of PM.

(Coordinating Research Council, Inc., 1983) states that how a fuel ignites depends on its physical properties. The properties of aviation and turbine fuels that relate to ease of ignition are flash point, flammability limits, vapor pressure, autoignition temperature, distillation range, and electrostatic susceptibility. The Coordinating Research Council determined that the properties associated with JP-8 fuel were as follows: flash point obtained by closed-cup method at sea level was 95°F to 145°F, no flash point was obtained by air saturation method, lower flammability

limt was 0.6%, upper flammability limt was 4.9%, temperature range for flammabile mixtures was 95°F to 165°F, vapor pressure was 0.1lb/sq in, autoignition temperature was 440°F to 475°F, the freezing point was -40°F to -58°F, the boiling point was 325°F to 450°F, and the pool rate of flame spread was 100ft per minute of less.

(Rogers, et al., 2003) analyzed diluted exhaust from a selection of Air Force ground support vehicles operated on diesel and JP-8 fuels was subjected to gravimetric, carbon, and size distribution analyses in September 1999.

(Schihl, Hoogterp, Pangilinan, Schwarz, & Bryzik, Modeling JP-8 Fuel Effects on Diesel Combustion Systems, 2006) explain a methodology for determining the evaporation rate of JP-8 in a direct injection diesel engine to predict energy release rate profiles and subsequent cylinder pressure rise rate in a current military diesel engine through extrapolation of the current knowledge base for heavy hydrocarbon ignition toward a medium worst case cetane number scenario. The evaporation process in a diesel jet under the constraint that ignition occurs during the injection event can be modeled as a steady-state jet whose evaporation rate is mixing controlled under the assumption of a finely atomized spray with an advantageous surface area to volume ratio promoting a saturated state at the bulk break-up length of the jet. They developed a model based on applying the conservation of mass, momentum, and energy to a rectangular control volume that encompasses a propagating conical fuel jet whose tip has reached the saturated state condition. The model was able to produce results that agreed with the experiemental data acquired for a variety of heavy-hydrocarbon fuels under thermodynamic conditions experienced in a diesel engine under ‘warmed up’ conditions through comprehensive constant volume experiments. This means that this assumption is not valid for cold start or light load under extremely cold ambient conditions. It was revealed the possibility of three surrogate

subcomponents: dodecane, tetradecane, and cetane based on the distillation properties of JP-8. Each of these three possible subcomponents cover the necessary boiling point range of JP-8, HMN, and DF-2 and also either have published thermodynamic property relationships or derived property sets. They determined that the boiling point of JP-8 based on a 90% distillation point was 496K. The proposed strategies for properly assessing multicomponent surrogate evaporation rate of JP-8 were based on determining subcomponent mass fractions by a boiling point weighting scheme and then either weighting the individual subcomponent liquid length predictions or weighting the evaporation coefficient and subsequently determining the resulting liquid length. The former approach is referred to as the Mean Liquid Length (MLL) method while the latter is referred to as the Mean Evaporation Coefficient Method (MEC). Based on the MEC method it was determined that one potential JP-8 blend is 18% tetradecane/82% dodecane. Since this blend is predominately dodecane, it is reasonable to also assess the possibility of using a single component surrogate for JP-8 as dependent on the variance between the two possible surrogates. The primary issue with modeling JP-8 ignition is that the cetane number can drastically vary depending on the supply source since JP-8 does not have a cetane number specification (MIL-DTL-83133). Data collected by Defense Energy Support Center in 2004 emphasizes this issue where the indirectly measured cetane index ranged from 29 to 51 with a mean of 43.9 and a variance of 13.69. Though cetane index is a not a precise indicator of ignition quality it still provides a sense of cetane number variability in CONUS. Therefore published data on DF-2 that covers a variance of cetane numbers was used to extrapolate the ignition delay period associated with using JP-8 in a diesel engine. Such data revealed that an average 30% increase in the ignition delay period would occur for a decrease of ten in the cetane number assuming that kinetics dominates the ignition delay processes. Based on their research

they discovered that in CONUS there have been a number of reports concerning excessive piston erosion problems while operating on JP-8 that suggests a potential combustion system issue revolving around spray targeting. To address this issue, an engine was instrumented with typical performance and combustion measurements and run on both DF-2 and CONUS JP-8. The former had a cetane number of approximately 45 while the latter was 49. However, their experiment yielded no evidence of erosion so a comprehensive spray study was undertaken to extrapolate the combustion system behavior for a JP-8 with a CONUS representative cetane number of near 40. JP-8 liquid length is 30% to 40% shorter than DF-2 which is not a surprise considering the 80K difference in the 90% distillation point. The predicted vapor fraction at ignition reveals that JP-8 is 15% to 30% higher in comparison to DF-2 and thus it is anticipated that JP-8 would yield both higher premixed phase heat release and pressure rise rate. For a given fuel, a decrease in the cetane number increases the premixed fuel mass causing an increase in pressure rise rate which is further augmented by fuels with higher volatility that again tend to increase the premixed fuel mass.

(Owens, E. C.; LePera, M. E.; Lestz, S. J., 1989) state that JP-8 is similar in properties to arctic grade diesel fuel. Concerns about the use of JP-8 in higher ambient temperatures included power loss, hot startability and idle, fuel consumption, and durability. The test engines used for the JP-8 fuel evaluations were a two-stroke General Motors (GM) Detriot Diesel (DD) 6V-53T, the natural aspirated General Motors (GM) Detriot Diesel (DD) 6V-53N, the Teledyne Continental Motors LDT-465-1C, General Motors (GM) 6.2L, and the Cummins NHC-250.

Engine Designation	DD 6V-53T	DD 6V-53N	LDT-465-1C	GM 6.2L	Cummins NHC-250
Engine Type	Turbocharged, Direct Injection, Uniflow Scavenged, Two-Stroke Compression Ignition	Naturally Aspirated, Direct Injection, Uniflow Scavenged, Two-Stroke Compression Ignition	Turbocharged, Direct Injection, Four-Stroke, Compression Ignition, M.A.N. Combustion Chamber Design	Naturally Aspirated, Ricardo Swirl Pre-Combustion Chamber, Four-Stroke, Compression Ignition	Direct Injection, Naturally Aspirated, Four-Stroke, Compression Ignition
No. of Cylinders, arrangement	6, V	6, V	6, in-line	8, V	6, in-line
Displacement, liters (in.^{3})	5.2 (318)	5.2 (318)	7.8 (478)	6.2 (380)	14.0 (855)
Bore x Stroke, mm (in.)	98.43 x 114.30 (3.875 x 4.500)	98.43 x 114.30 (3.875 x 4.500)	115.8 x 123.7 (4.56 x 4.87)	101 x 97 (3.98 x 3.82)	139 x 152 (5.50 x 6.00)
Rated Power, kW (Bhp)	224 (300) at 2800 rpm	157 (210) at 2800 rpm	104 (140) at 2600 rpm, 15.5°C (60°F) and 29.82 in. Hg	96.6 (130) CUCV, 107.7 (145) HMMWV at 3600 rpm	186 (250) at 2100 rpm
Rated Torque, Nm (ft-lb)	834 (615) at 2200 rpm	603 (445) at 1500 rpm	597 (429) at 2000 rpm	325 (240) at 2200 rpm	892 (658) at 1300 rpm
Compression Ratio	18.7:1	21:1	22:1	21.3:1	15.8:1
Oil Capacity, liters (gal.)	19 (5)	19 (5)	21 (5.5)	6.62 (1.75)	20.8 (5.5)
Injection System	DDA N70 Unit Injectors	DDA N50 Unit Injectors	Bosch Rotary Distributor With Density Compensator	Stanadyne DB-2 F/I Pump With Bosch Pintle Injectors	Cummins PT System

Figure 4 Description of Test Engines (Owens, E. C.; LePera, M. E.; Lestz, S. J., 1989)

The different engines were each operated over either the Army/Coordinating Research Council (CRC) 240 hour cycle for tracked vechicles, or the Army/CRC 210-hour cycle for wheeled-vehicles, depending on the type of vehicle in which a particular engine is used. The 240 hour cycle was only used for the 6V-53T engine. All the rest of the engines were operated over the 210 hour cycle except for the GM 6.2L engine which used the NATO AEP-5 400 hour diesel engine test procedure for a single evaluation. The base fuel was No.2 diesel fuel (AL-12069-F). The specification requirements for this fuel, commonly referred to as Caterpillar 1H/1G reference as set forth by ASTM STP 509A. The JP-8 test fuel (AL-14216-F) used in these endurance test met the requirements of MIL-T-83133B Aviation Turbine Fuel. The cetane number, although not a regulated specification requirement for jet fuels, was found to be 41. While the minimum cetane number requirement for VV-F-800D diesel fuel is 40. The JP-8 fuel

was blended so that the fuel viscosity was close to the average viscosity of JP-8 being procured by the US military.

Table 4. Properties of JP-8 Test Fuel

Property	Method	MIL-T-83133B JP-8/NATO F-34 Requirements	Test Fuel AL-14216-F	Vehicle Performance Test Fuel AL-17629-F
Color	D 156	(a)	+15 (Saybolt)	>+30
Total Acid Number, mg KOH/g	D 3242	0.015 max	0.005	0.004
Aromatics, vol%	D 1319	25.0 max	19.0	9.3
Olefins, vol%	D 1319	5.0 max	0	1.5
Sulfur, total wt% (XRF)	D 4294	0.3 max	<0.01	0.03
Mercaptan Sulfur, wt%	D 3227	0.001 max	0.0002	>0.0001
Distillation, °C	D 86			
Initial Boiling Point		(a)	171	168
10% Recovered		186 max	184	178
20% Recovered		(a)	188	181
50% Recovered		(a)	200	188
90% Recovered		(a)	222	204
End Point		330 max	238	
Flash Point, °C	D 93	38 min	56	47
Gravity, °API	D 1298	37-51	40.3	49.4
Density, kg/L at 15°C	D 1298	0.775-0.840	0.8232	0.7819
Freezing Point, °C	D 2386	-50 max	-55	-47
Kin. Vis., cSt, at -20°C	D 445	8.0 max	4.14	3.68
at 40°C	D 445	NR*	1.26	1.16
Net Heat of Combustion, MJ/kg (Btu/lb)		42.8 (18,400) min	43.106 (18,532)	43.264 (18,600)
Hydrogen Content, wt%		13.5 min	13.69	14.4
Smoke Point, mm	D 1322	19 min	22.2	29.5
Copper Corrosion, 2 hr at 100°C	D 130	1B max	1A	1A
Thermal Stability (JFTOT), Code	D 3241	<3	1	1
Change in Pressure Drop, mm Hg		25 max	0	0
Existent Gum, mg/100 mL	D 381	7.0 max	0.2	0.2
Particulate Matter, mg/L	D 2276	1.0 max	1.1 (b)	0.5
Water Reaction, interface rating	D 1094	1b	1b	1
Water Separation Index, modified	D 2550	70 max	--	60
Fuel System Icing Inhibitor		0.10-0.15	0.01, 0.04	0.11
Corrosion Inhibitor		NR	(c)	(d)
Fuel Electrical Conductivity, pS/m	D 2624	200-600	170, 90	130
Filtration Time, minutes, Apdx A	MIL-T-5624	15 max	72	--
Cetane Number		(e)	41	49
BOCLE, scar diameter, mm (f)		(e)	0.34	--

Figure 5 Fuel Properties of Test Fuel (Owens, E. C.; LePera, M. E.; Lestz, S. J., 1989)

The 210 hour testing used a qualified MIL-L-2104D (6) OE/HDO-30 army reference oil, utilizing a magnesium detergent-dispersant and with a sulfated ash content of 0.84 wt%. The 6V-53T test used the CRC reference engine oil REO-203, an SAE 30-grade lubricant. The REO-203 oil uses a calcium detergent-dispersant and has a sulfated ash content of 0.93. An external

fuel supply system was used to ease the transition between test fuels and to measure the vehicle fuel flow rate. This system was connected to the engine through existing quick disconnects or at the fuel system fittings near the engine. An onboard data logger recorded the fuel flow and temperature during the runs.

(U.S. Air Force, 2008) state that JP-8 is primarily developed for use in military applications. It is used to power a variety of military aircrafts, tanks, other high performance vehicles, power generators, and space heaters, just to name a few. It is made by refining crude petroleum. The primary ingredient in JP-8 is kerosene (99.8% by weight). It also contains trace amounts of benzene and various additives to inhibit icing, prevent static charge buildup, avoid oxidation, and decrease corrosion.

JP-4 fuel has a low vapor pressure and JP-5 fuel has a high flashpoint. Less volatile jet fuels such as grade JP-7 and JP-8 are thermally stable. During the 1990s, many units of the U.S. Air Force changed their usage of fuel from JP-4, in use since the 1950s, to JP-8. JP-4 is a wide-cut petroleum distillate exhibiting compounds from the lighter naphtha fraction as well as the kerosene fraction of petroleum. JP-8 typically ranges in composition from 6-carbon hydrocarbons to 18-carbon hydrocarbons. The properties of JP-8 are as follows: Specific Gravity is 0.8, color is yellow, distillation boiling point initial is 159.5C, distillation boiling point final is 263.5C, distillation boiling point average is 215.2C, freezing point is -48C, and flash point is 56C (Karthikeyan, Davis, Mankin, Erickson, & Kulakow, 1999).

JP-8 Environmental/Health Concerns

JP-8 is able to enter the environment through evaporation into the air from here it can migrate into the soil and water. Once it has evaporated into the air it is able to form other compounds by reacting with other substances in the air or by being exposed to sunlight. If JP-8

gets in the soil, it can remain there for years until bacteria and other organisms present in the soil cause it to break down into other substances, or it begins to slowly migrate into the groundwater in various forms. Once it gets in the water, some of its components will attach to other particles in the water and settle to the bottom and the cycle will continue repeating. An individual can be exposed to JP-8 in a variety of ways. The effects of JP-8 on human health is currently unknown and under investigation. Some predictions were made on possible health effects based on knowledge of kerosene. Some possible health effects expected include skin irritation and sensitization, breathing in large amounts of jet fuel will make breathing painful and may cause the individual to feel like as if they are suffocating, high exposures can also cause headaches, difficulty concentrating, fatigue and trouble with balance or coordination, breathing in small amounts of jet fuel vapors over a long period of time might result in sleep disturbances or dizziness, accidentally swallowing a small amount of JP-8 has not been shown to cause any significant health problems, and swallowing large amounts of JP-8 is dangerous and can result in coma, convulsions and even death. Currently, no specific guidelines or regulations for jet fuel exposure exist and no definitive scientific study results are available to help set appropriate limits. In the absence of such regulatory standards, the Air Force Medical Operations Agency (AFMOA) in the USAF Surgeon General's Office establishes standards. The current standard for JP-8 is an occupational exposure limit (OEL) of 350 mg/m^3 for an 8-hour time weighted average exposure and a 15-minute short-term exposure limit (STEL) of 1800 mg/m^3 (U.S. Air Force, 2008).

(Karthikeyan, Davis, Mankin, Erickson, & Kulakow, 1999) state that the environmental impact of spills of JP-8, a kerosene-based jet fuel, has been studied very little. For the more volatile JP-4, earlier studies showed that biodegradation was less important than evaporation but

for JP-8, evaporative loss from soil is very slow. The Air Force is now in the process of changing operations at its installations within the continental U.S. to use JP-8 in place of JP-4. This changeover has required the alteration of many environmental impact estimates. There are few studies conducted on fate and environmental effects of JP-4 and JP-8. Results of experiments conducted in aquatic systems indicate that evaporation was the major loss for low molecular weight hydrocarbons in JP-4 and JP-8. An experimental study on fate of JP-8 in soil showed that higher molecular weight hydrocarbons were removed significantly faster in soils with indigenous microbial populations than in sterile soil.

CHAPTER 3: METHODOLOGY

Introduction

The scientific aspects of this project will develop over time, as experience is gained. This section discusses the present understanding of the methods and constraints that are believed to yield clear, interpretable results with regard to the basic prediction of a correlation to previous studies with identifiable states of collective consciousness. The ability to gather and interpret scientific evidence depends fundamentally on a clear statement of the hypothesis or the question that is being asked. The author uses operational definitions to ensure that the reader is able to extract quantitative conclusions from data, with specific relevance to scientific questions. The author has used more than one defined analysis over the course of the experiment, for which the detailed descriptions are provided.

Experimental Setup

The purpose of this study is to investigate if the JP-8 fuel mixture is a viable substitute for military application for power generation in a diesel auxiliary power unit (APU), meaning it is able to burn efficiently in a diesel engine without special features, requirements, or modifications to the existing design and being able to obtain the same performance and power as that of diesel no.2 fuel. This was determined by observing the injection and combustion properties in a single cylinder indirect injection diesel engine. The experimental setup schematic is described below in Figure 6.

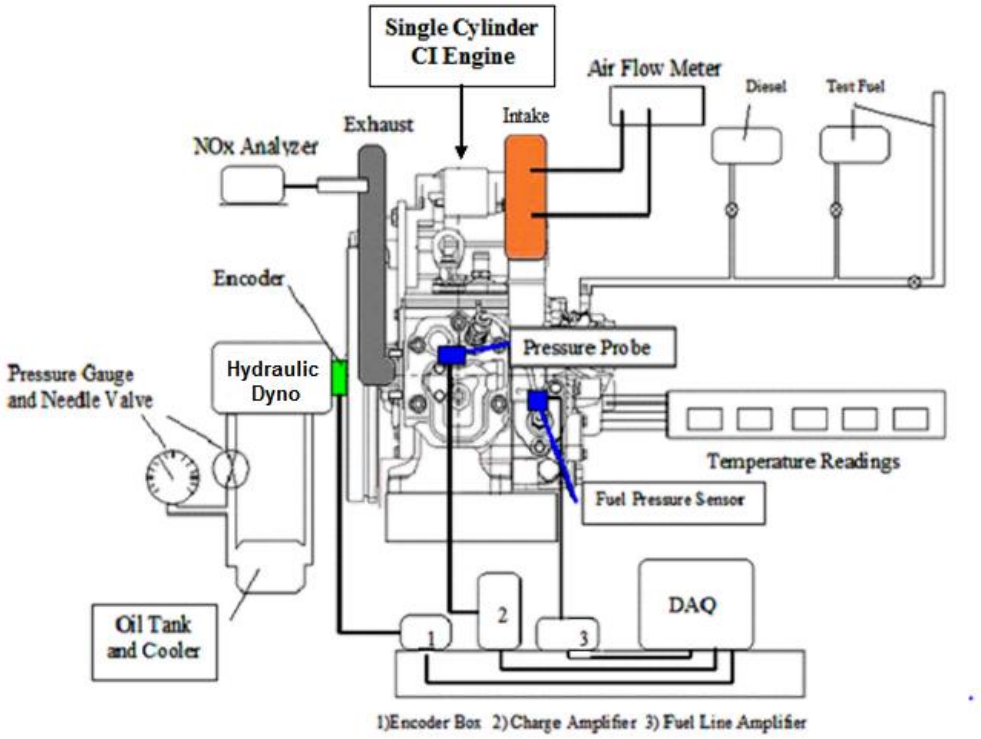

Figure 6 Experimental Engine Test Setup (Nelson, 2010)

The engine has been mounted to a hydraulic dynamometer and investigated at continuous power of 2.9kW (5 bar BMEP) at 2000 rpm. The engine was fueled with four varying

percentage fuel blends of JP-8, which were diesel no. 2, 20% JP-8 (J20), 35% JP-8 (J35), and 50% JP-8 (J50). The fuel was aged for eight months prior to testing in order to verify its storage stability. Before testing, the visual inspection of the fuel revealed no separation and displayed no signs of instability, and based on this inspection, the fuel was deemed stable for use after eight months storage.

Instruments and Equipment

The engine was not modified, except for the attached diagnostic instrumentation; a time base taken with a rotary encoder 2000 pulses per crank shaft revolution, non-cooled piezoelectric high pressure sensor introduced through the glow plug connected to a charge amplifier, clamp injection line pressure sensor with amplifier, high speed data acquisition system, laminar air flow meter with attached integral flow computer monitoring system, NOx analyzer, and Smoke Meter.

The injection system employed was of a piston-plunger type pump and the injector had 1x0.200mm nozzle with a pintle needle and the injection pressure was 147 bars. The engine worked with the original factory settings and was able to maintain the specifications given by the manufacture even after 50 hours of operation on JP-8.

Engine

The engine used in this research was a by Kubota EA-330 single cylinder, indirect injection with a separate three vortex combustion chamber, 4 stroke, liquid cooled, compression ignition, naturally aspirated engine, with no EGR.

Figure 7 Kubota EA330 Model Engine

The specifications of the engine given by Kubota are shown below in Figure 8.

Model		EA330-E3-NB1
Emission Regulation		Tier 4
Type		Horizontal 4-cycle liquid cooled Diesel
Number of Cylinders		1
Bore	mm (in)	77 (3.03)
Stroke	mm (in)	70 (2.76)
Displacement	L (cu.in)	0.325 (19.83)
Combustion System		IDI (TVCS)
Aspiration		Naturally Aspirated
Maximum Speed	rpm	3000
Output: Net Intermittent	kW	5.15
	HP	6.9
	PS	7.0
Oil Pan Capacity	L (gal)	1.3 (0.34)
Starter Capacity	V-kW	12-0.8
Alternator Capacity	V-A	12-3.5
Length	mm (in)	566 (22.28)
Width	mm (in)	411 (16.18)
Height (1)	mm (in)	457 (17.99)
Dry Weight	kg (lb)	54 (119)

Figure 8 Specification Sheet for EA-330 Kubota Engine

The performance curves given by Kubota for the EA-330 model engine are shown below in Figure 9.

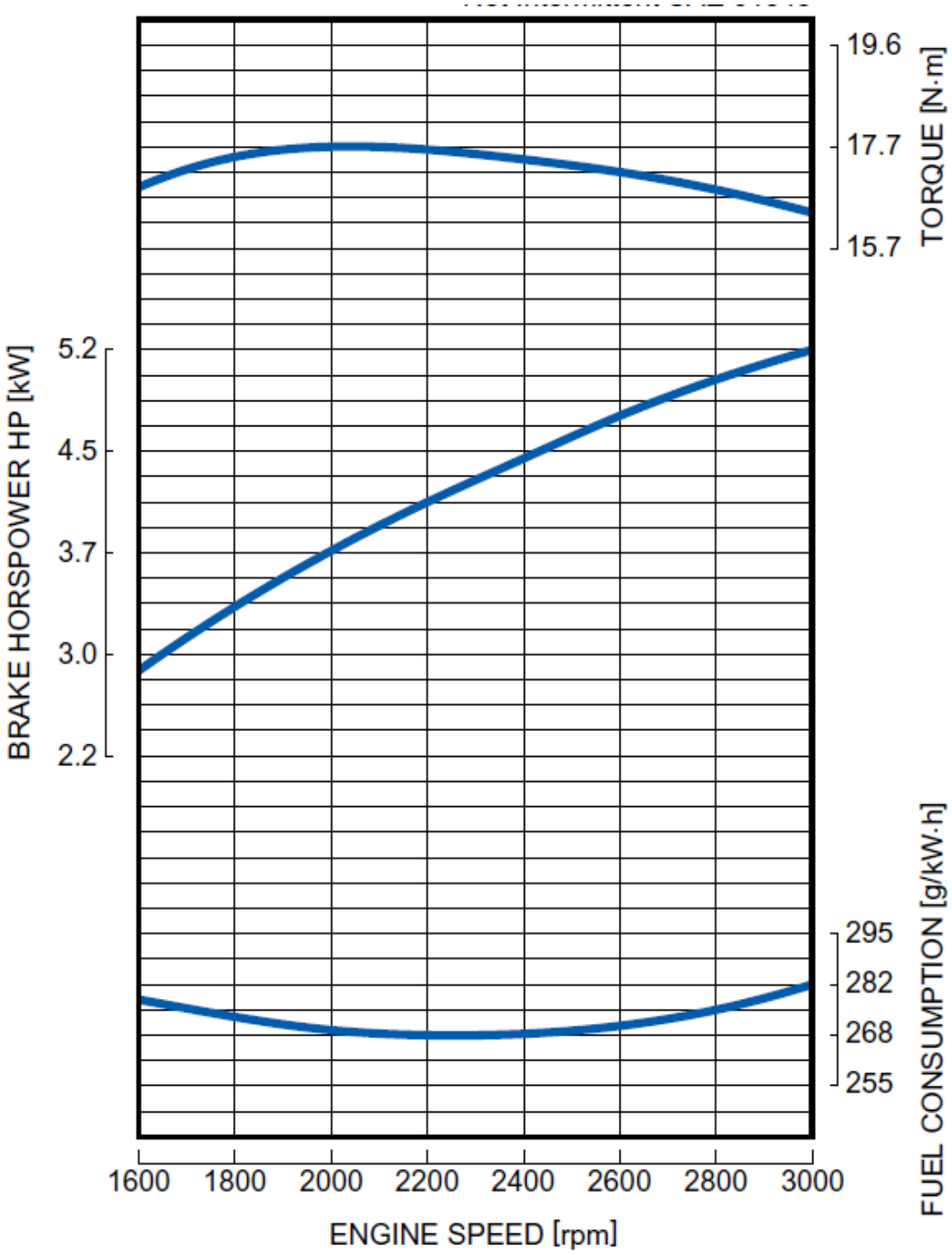

Figure 9 Kubota Performance Curve

Based on the performance curve, it was be seen that the engine has a maximum RPM of 3000, and is advertised to produce 17.7 Nm of torque and 5.15kW of power, Although it is important to note that during the course of this research it was uncovered that the performance curve given by

Kubota (Figure 9) represents the engine operating at its smoke limit or 120%. Typically a 100% load represents the engine's optimal load, with any amount beyond that being outside its optimal range up until it reaches its smoke limit at around 120%.

Hydraulic dynamometer

In order to properly assess the performance of the engine the use of a dynamometer was employed. The importance of a dyno is that it allows researchers to simulate diverse operating conditions on an engine by placing various loads on the engine during a trial run. A dynamometer or more commonly known as dyno is a device used for acquiring the measurements of force, torque, and ultimately power of a machine. With torque representing moment of force that acts through the longitudinal axis of an object and power simply being the moment of force multiplied with the angular velocity. The use of this type of measuring apparatus was first proposed by William Froude, who is credited with the invention of the hydraulic dynamometer in 1877. However, it was Dr. Osborne Reynolds who was the first who was able to make the dynamometer a practical success in 1894 with his design of the dyno shown in Figure 10 below.

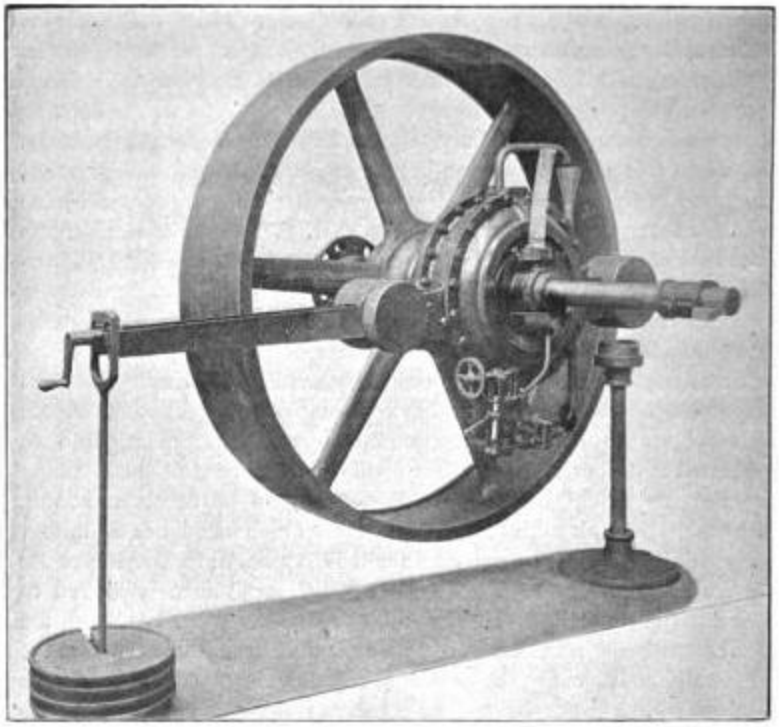

Figure 10 Reynolds Dynamometer Design (Blaine, 1897)

This Dynamometer was designed to work up to a maximum turning effort of 26,400 lbs-feet at 200 revolutions per minute (Blaine, 1897). However, as it can be seen from Dr. Reynolds design, the earliest dyno's were quite bulky in design, as time has progressed so has the design of the dynamometer.

There are several different types of dynamometers that currently exist in today's society with the basic setup being the same for all types, in which, the engine is typically clamped on a test bed and its' shaft is connected to the dynamometer rotor. The schematic of the operation principle of the dynamometer is shown below in Figure 11.

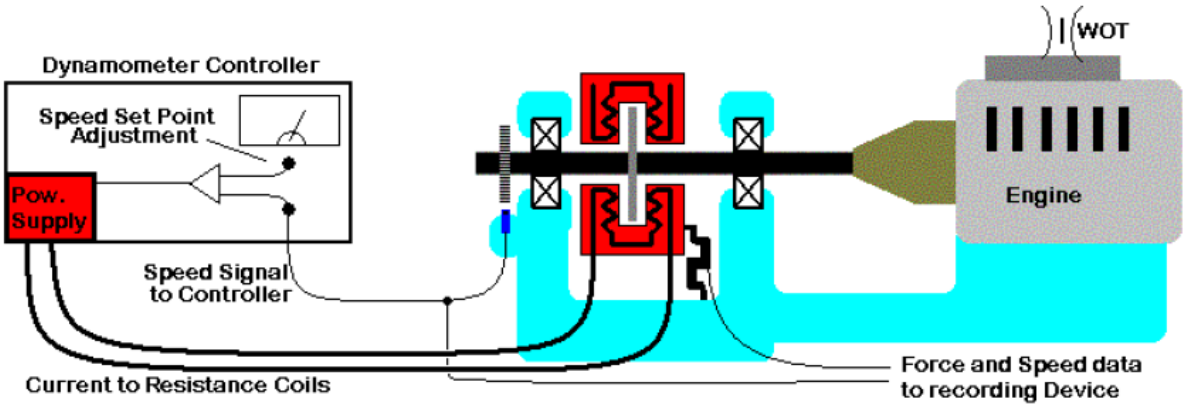

Figure 11 Schematic of Principle of Operation of a Dynamometer

The rotor is coupled electromagnetically, hydraulically, or by mechanical friction to a stator, which is supported by low friction bearings. The stator is then able to be balanced with the rotor being stationary. The torque exerted on the stator is able to be measured with the rotor tuning by placing the stator in equilibrium through the utilization of weights, springs, or pneumatic means (Heywood, 1988).

The dyno system employed for this research was a hydraulic dynamometer, it was a relatively small and simple system that was both constructed and designed by students at Georgia Southern University. The hydraulic dynamometer works on the principle of dissipating the power in fluid friction rather in dry friction. In principle its construction is remarkably similar to that of a fluid flywheel. The hydraulic dyno system used in this research is shown below in Figure 12.

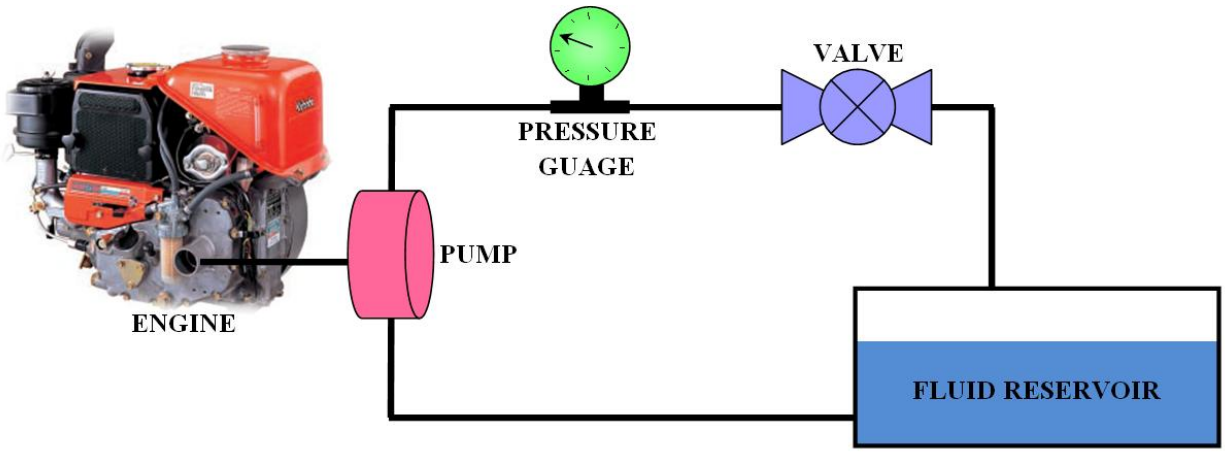

Figure 12 Hydraulic Dyno Schematic

The hydraulic dyno system employed for this particular study involves: the engine, a hydraulic pump, hydraulic hose, pressure gauge, needle valve, fluid reservoir, sprockets, and coupling. A #16 chain sized sprocket (Figure 13) was placed on both the PTO shaft of the Kubota engine and pump, with only the number of teeth differing to ensure the correct pumping ratio of 0.4 was achieved; the sprocket placed on the engine shaft contained 22 teeth, while the sprocket placed on the pump contained 55 teeth.

Figure 13 Sprocket

The sprockets were connected through the use of a coupling, which allowed the engine to translate its rotational motion to be used to drive the pump. The pump then pumps hydraulic fluid throughout the system where a needle valve is used to control the pressure in the lines and a

pressure gauge is used to measure the pressure in the lines. In short the system enables the dyno to place a resistive load on the engine through the reduction of hose size imposed by the needle valve. For system calibration purposes it was assumed that the power required to turn the pump is equivalent to that which the engine produces; therefore losses associated between the connection of the pump and engine may be considered as negligible. The pump used in this system had a 1.403 in^3/rev displacement and a safety factor of 1.5, while being able to maintain a steady accurate pressure in the system in relation to time elapsed.

In order to ensure the integrity of the thermodynamic calculations performed for this study, researchers were able to eliminate several unknown variables associated with the dynamometer through the utilization of a cooling system to maintain a relatively constant temperature of the hydraulic fluid employed by the system. Based on the thermodynamic calculations it was determined that the optimal temperature range for the hydraulic fluid was 38-42 ^oC. Through research of cooling systems it was deemed that the most practical cooling system design for this experimental facility would be of a simple heat exchanger type shown in Figure 14 .

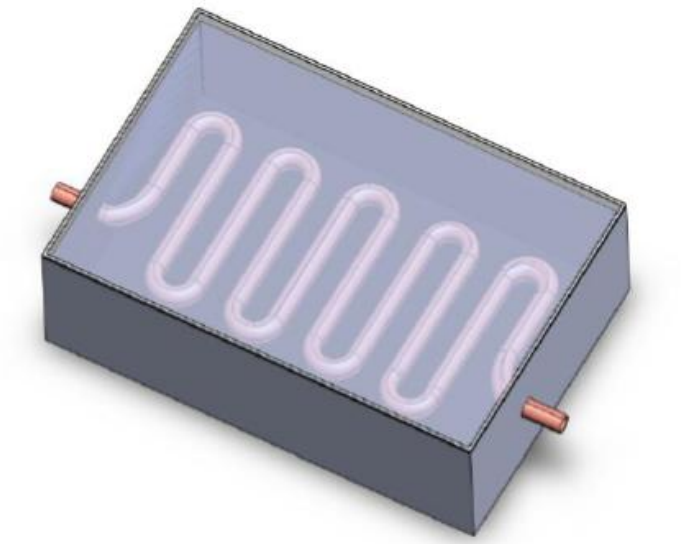

Figure 14 Simple Heat Exchanger

As members of the global community and under oath to the order of the engineer for the dedication to the concept of sustainability lead researchers to modify the original design to include materials that were saved from further infesting the beauty of mother earth. The final design of the dynamometer cooling system is presented below in Figure 15.

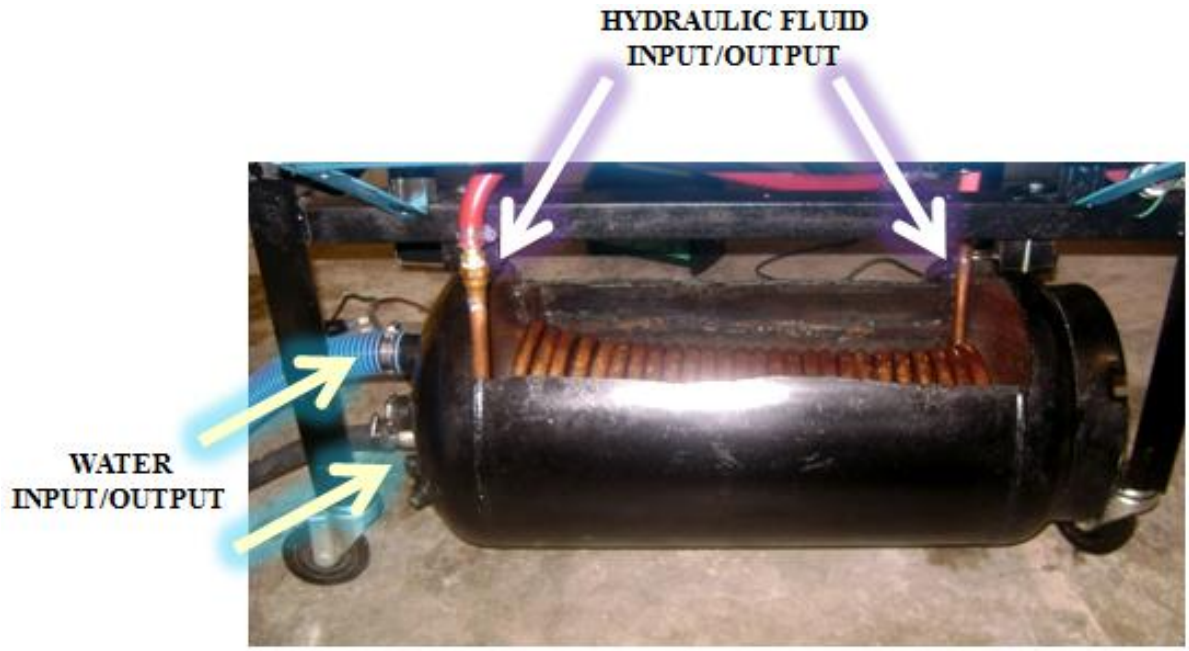

Figure 15 Dyno Cooling System

This system is still of a simple heat exchanger design type in which the hot hydraulic fluid is pumped through a coil constructed of copper tubing placed in a container filled with a moving fluid, in this case water, the hot fluid transfers heat into the moving fluid through convection. The copper tubing was chosen for two reasons, with the first being due to safety concerns as its maximum allowable pressure exceeds far beyond any pressure the dyno is capable of producing, and the second being the coppers excellent convection coefficient for the application.

In order to perform an accurate analysis of the data obtained from engine testing it is vital that the load on the engine be known at any given point in time with respect to the known parameters of speed and applied pressure in the system. This is able to be calculated by using the following equation.

$$P_{pump} = \frac{pv}{1400}$$

Where P_{pump} represents the power in terms of horsepower, p represents the pressure contained within the dyno system [lbs/in^2], and v represents the flow rate of the hydraulic fluid [gallons/minute] and the number 1400 representing a constant used to transform the unit of power to the US standard horsepower [HP]. The torque is then able to be calculated by using the equation shown below.

$$T = \frac{5252 P_{pump}}{N_{pump}}$$

Where T represents Torque [lb-ft], N_{pump} represents the speed of the pump in terms of [RPM] and 5252 represents a constant used to transform the unit of torque to the US standard, lb-ft. In order for the results of this analysis to be compared to other studies, the mean effective pressure (MEP) needs to be determined as it serves as the bench mark for engine testing comparison. The MEP of an engine is derived from the following equation.

$$MEP = \frac{T n_c}{V_d} 2\pi$$

Where *T* represents the torque, η_c represents the number of revolutions per cycle (this being 2 for a four stroke engine), and V_d represents the volumetric displacement of the engine. Through the manipulation of the equations above, the MEP and load can be determined for a given speed.

Rotary encoder

For an accurate analysis of the results collected from this research it is vital that the position of the piston be known, in order to obtain an isolation of an individual cycle. This is accomplished through the use of a rotary encoder attached to the engine shaft. A rotary encoder can be defined as an electro-mechanical device used to convert the angular position of a shaft to

an analog or digital code by emitting light from a light emitting diode (LED) through a slotted disk and recognizing the escaping light through the use of a photo sensor, and transforming it into a pulsating signal in the form of a square wave (Figure 17), with its basic components being described in Figure 16.

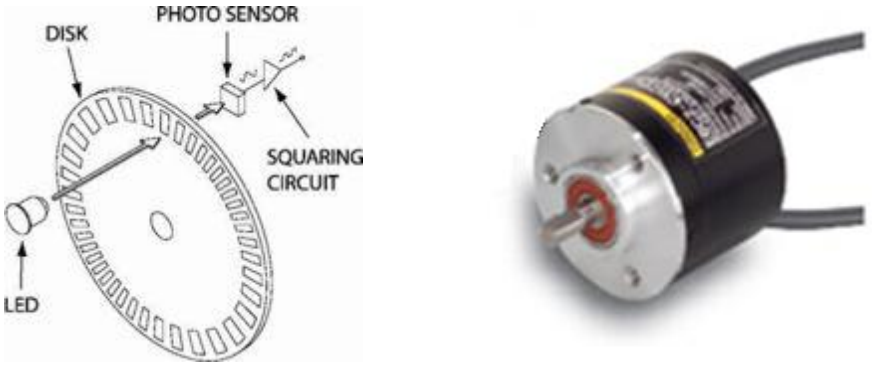

Figure 16: Basic Internal Parts of an Optical Encoder (Omron, 2010)

The encoder used for this particular research was an Omron optical rotary encoder with 2000 pulses/revolution for channels A and B, and 1 pulse/revolution for channel Z (Figure 17,Figure 16).

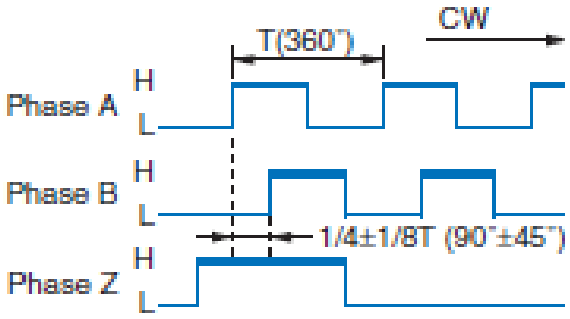

Figure 17 Rotary Encoder Output Signal

The rotary encoder was mounted to the flywheel cover of the engine with the use of a flange, in order to be concentric, parallel, and maintain a shaft to shaft revolution ratio of 1:1. The flange fabricated is shown in Figure 18 through Figure 20.

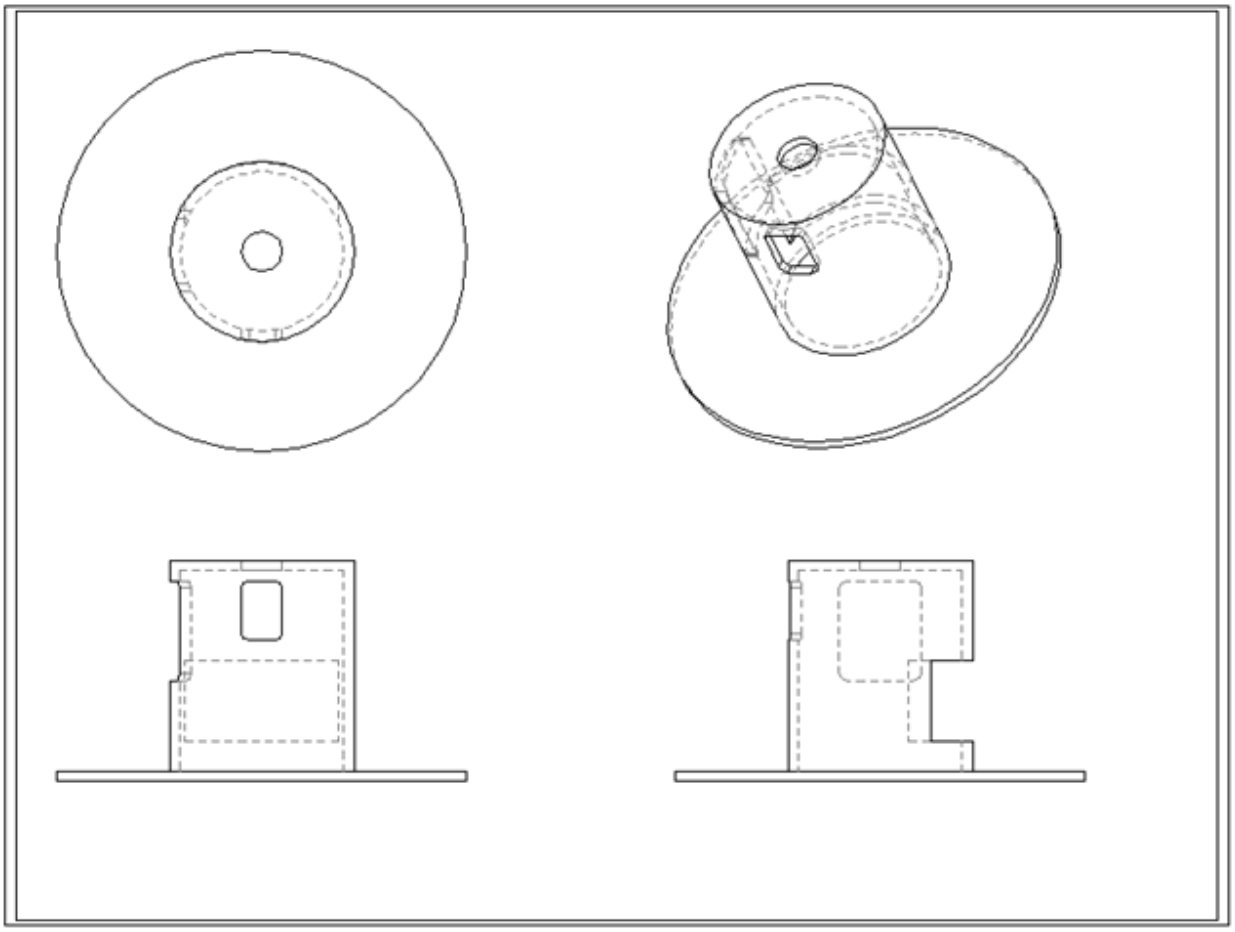

Figure 18 Final Drawing of the Encoder Flange (Nelson, 2010)

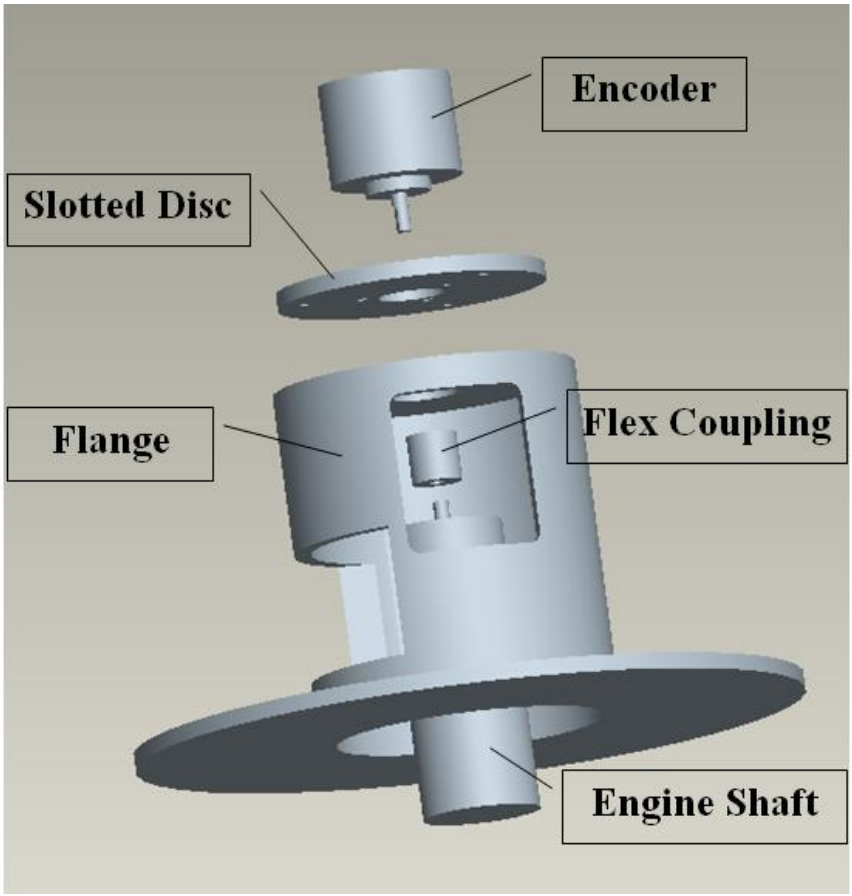

Figure 19 The Mounting Setup of the Encoder (Nelson, 2010)

Figure 20 Illustration of Actual Encoder Mounting (Nelson, 2010)

Once mounted, channel Z of the encoder (one pulse/rev) was synchronized with the TDC position of the engine.

Cylinder pressure sensor

One of the most important measurements that can be made in order to investigate the combustion characteristics of a particular fuel in an engine is that of the pressure inside the cylinder throughout the duration of the cycle. This was accomplished through the use of a Kistler piezoelectric 6056A pressure sensor.

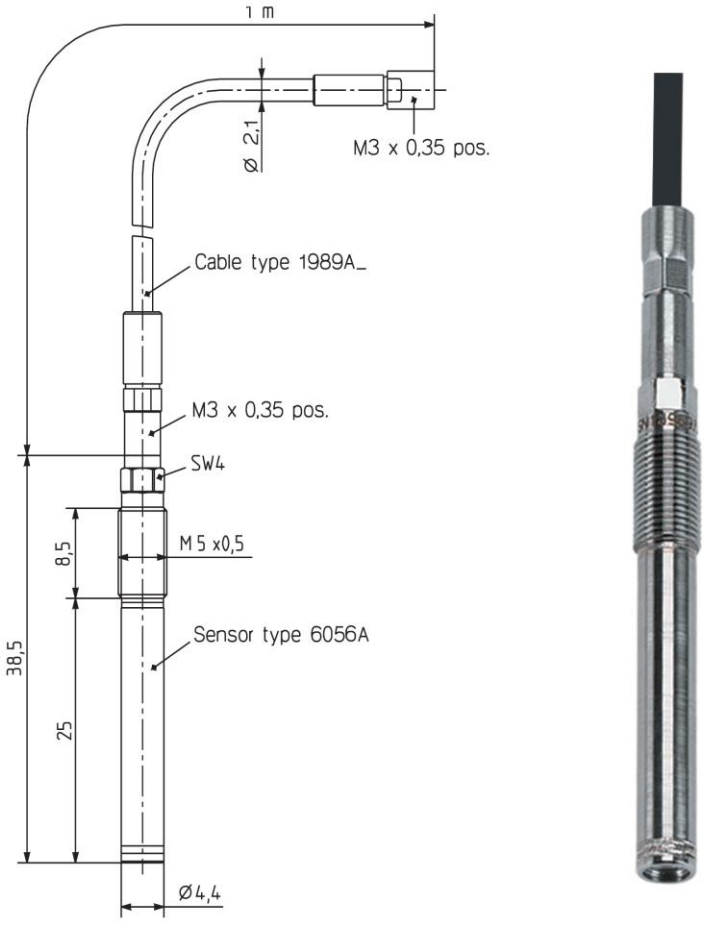

Figure 21 Kistler Pressure Sensor Type 6056

This type of pressure sensor was selected due to its high rigidity and small size allowing it to possess excellent high frequency response with accompanying rapid rise time capability. Acceleration compensation makes it virtually unresponsive to mechanical motion, i.e. shock and vibration. Another benefit being it is capable of withstanding exposure to high pressure and temperature ranges during the course of a test, due in part to the front seal on this sensor, which allows for excellent heat dissipation permitting a maximum operating temperature of up to 400 ºC. The technical specifications for this sensor are display below in Table 1.

Table 1 Kistler Pressure Sensor Specifications

Measuring Range	0-300	bar
Calibrated Partial Ranges	0-100,0-200, 0-300	bar
Overload	350	bar
Sensitivity	-19	pC/bar
Acceleration Sensitivity		
axial	< 0.0005	bar/g
radial	< 0.0005	bar/g
Thermal Shock Error (at 1500 1/min, p_{mi}=9bar)		
Δp (short time drift)	≤± 0.7	bar
Δp_{mi}	≤± 3	%
Δp_{max}	≤± 1.5	%
Natural frequency, nominal	≈ 160	kHz
Linearity in all ranges (at 23◦C)	≤± 0.4	%/FSO
Operating temperature range	-450	◦C
Insulation resistant (at 23 ^{o}C)	≥ 10^{13}	Ω
Shock resistance	2 000	g
Tightening torque	1,5	N·m
Capacitance, without cable	5	pF
Weight with cable	30	G

The sensitivity changes by not more than ± 0.5 % over a temperature range of 200±50 °C. This allows for a high thermal stability to be achieved with is an excellent property for

application with this research. A piezoresistive high pressure sensor involves a crystal that is able to produce an analogous voltage signal when stressed in compression by pressure acting on the diaphragm of the sensor. This pressure, by virtue of diaphragm area, is converted to compressive force which strains the crystals linearly with applied pressure producing an analog voltage signal. the voltage generated by the crystals is fed to the gate terminal of the FET input stage of an impedance converting IC amplifier which drops the impedance level 10 orders of magnitude. Also, the electrical output of the crystal is in the form of a charge (coulombs), therefore a charge amplifier is required in order to convert the small charge output from the mechanical loads applied to voltage.

Figure 22 Kistler Charge Amplifier

The charge amplifier linearizes the conversion from charge to volt for the ease of converting electrical signals to a mechanical force. This is all done by use of the charge amplifier with complimentary settings for the transducer being used Table 2.

Table 2 Kistler Amplifier Specifications

Frequency response: Standard filter	Hz	180, 000
Accuracy	%	≤ ±0.50
Time Constant (range dependent):		
Long	s	0...100000
Medium	s	1…10000
Short	s	0.01…100
Time Constant Resistor:		
Long	Ω	>114
Medium	Ω	111
Short	Ω	19
Noise:		
referred to with input shield	pCrms	0.0036
1 pC/V max	μVrms	500
100 pC/V max		300
100000 pC/V max		200
Drift MOSFET leakage current	pC/s	≤± 0.03
Zero Offset in Reset typical	mV	0.5
Output:		
Impedance	Ω	100
Voltage Range	V	±10
Current Limit	mA	5
Display	type	LCD 16 chars.
Serial Interface (RS-232C)		
Connector		9 pin D-Sub.
Baud Rates		150…9600
Maximum Cable Length	m/ft	20/65 (2500pF)
Temperature Range Operating	oF	32…122
Temperature range storage	oF	-1…158
Humidity Non-condensing	%	10…90
Power Line:		
Voltage	VAC	89…135
Frequency	Hz	48…62
Power Consumption max.	VA	14
Weight without case	lb	2.8

Table 3 Settings used for Charge Amplifier and the Corresponding Reasons

Setting	Value	Units	Justification
Transducer Sensitivity	22.3	pC/MU mV/MU	Sensitivity setting matching desired parameters from calibration sheet (0…250bar, 350^{o}C).
Scale	10	MU/Volt	Ease of conversion and also fits within the range of amplifier voltage output (±10V)
Time Constant	Medium	-	Recommended for engine applications
Mode	Charge	-	Required mode for 6056A pressure sensor

For this particular study the time constant on the amplifier was set to medium as it was recommended for use with engine applications.

CHAPTER 4: COMBUSTION INVESTIGATION

Fuel Composition

The composition of the fuel used in the application has a strong effect on quality and quantity of emissions. Variation in fuel properties such as density, cetane number, distillation characteristics, sulfur, and aromatic content have all been shown to affect combustion and emissions. Diesel fuels are mixed so as to combust reliably at the proper thermal state so that Diesel cycle engines run more efficiently. Some of these properties are dependent on each other and it is difficult to completely isolate the effect of each. It can be seen that there is an indirect relationship that exist between the density and other fuel parameters such as cetane number, viscosity, volatility, and distillation characteristics (boiling point range). Reducing the high end distillation temperatures reduced the fuel density by excluding the heaviest compounds. A fuel with a lower density will result in lower engine power, and will therefore affect specific fuel consumption.

Diesel fuel is a distillate blend, whereas, aviation fuels are typically of a kerosene-type. The fundamental difference between kerosene-type and distillate type fuels is the temperature at which they are separated in a distillation column.

JP-8 has many characteristics that make it very appealing to the military, one being its' low volatility in comparison to previously used JP-4 (Korres, Karonis, Lois, Linck, & Gupta, 2008), which is extremely important in terms of safety as the vehicles and aircrafts have the potential to be exposed to enemy fire. JP-8 is almost identical to the standard commercial airline aviation fuel (Jet A-1). The main difference between the two is the fact that JP-8 contains three additives required for military operation these include (U.S. Air Force, 2008):

- Fuel System Icing Inhibitor (MIL-DTL-85470),

- Corrosion Inhibitor /Lubricity Improver (MIL-PRF-25017),

-Static Dissipater Additive

There is no standard formula for jet fuels. Their exact composition depends on the crude oil from which they were refined. JP-8 is a mixture of many different hydrocarbons, with modern analytical techniques being unable to separate all the individual molecular species present in the jet fuel. The range of their sizes in terms of molecular weight and carbon number is restricted by the distillation, freezing point, and smoke point requirements. As a result of this variability, little information exists on the exact chemical and physical properties of jet fuels. JP-8 typically has a carbon number distribution between about 8 and 16 carbon numbers. Most of the hydrocarbons in jet fuel are members of the paraffin, naphthene, or aromatic classes. JP8 differs so widely in bulk properties due to the fact that they contain different proportions of the three classes of

hydrocarbons. A comparison of diesel no.2 to that of JP-8 has been made and is shown below (Coordinating Research Council, Inc., 1983) (U.S. Air Force, 2008):

Table 4 Comparison of Fuel Properties

Property	**Diesel**	**JP-8**
Density @ 15°C (kg/L)	0.835	0.806
Distillation (°C)		
10% Rec. Temperature	218	151
50% Rec. Temperature	283	200
90% Rec. Temperature	348	238
Aromatic Content, % vol	28.4	13.6
Sulfur Content, %wt	0.033	0.25
Flash Point	65	44.5
Cloud Point (F)	9	-40

Diesel consists of a mixture of numerous hydrocarbon compounds of various densities and molecular weights. Thus, the overall density and molecular weight is a function of the composition of the fuel and provides an indirect relationship to other fuel parameters such as cetane number, viscosity, volatility, and distillation characteristics. For a diesel engine, fuel is injected into the combustion chamber using a volume-based metering system, therefore, lower density will result in lower engine power and will therefore affect brake specific fuel consumption (BSFC). It has also been shown that the density of the fuel may have a direct effect on the build-up of fuel pressure in the injection system and a consequent effect on the dynamic start of fuel injection (Soloiu, Covington, Nelson, & Lewis, 2011). The cloud point of diesel is 9 F compared to -40 F for JP-8, with the cloud point being defined as the temperature at which

wax crystals separate and cloud the fuel. This is provides an advantage for JP-8 as it means that this fuel will not experience any starting issues when exposed to a cold climate. JP-8 is more refined than diesel and therefore, it is less likely to plug filters or leave deposits in the injection nozzles.

Viscosity

The viscosity is one of the most important properties of a fuel because of its prominent effect on the operation of the fuel injection equipment. Viscosity can be defined as a measure of a liquid's resistance to flow under pressure, generated by either a gravity or mechanical source. For diesel engines, the fuels' viscosity is essential as it provides a significant influence on the droplet size, penetration, and mixing rate with the air, vaporization, emissions, smoke, and wall deposits (Heywood, 1988). This is especially true at low temperatures where the increase in viscosity can lead to poor spray due to injector clogging and inadequate fuel atomization (Balat & Balat, 2008). The poor atomization leads to increased carbon deposits causing increased wear to develop which in turn effects performance, with respect to mechanical efficiency and power output. The aliphatic and aromatic hydrocarbons in petroleum diesel exhibit a smaller viscosity range with lower viscosities due to their lack of oxygen that in turn effects the fuel spray atomization and ultimately, the formation of carbon deposits in the engine (Knothe & Steidley, 2007) (Tsuji & Neto, 2008). The viscosity of JP-8 varies from batch to batch due to variation in the amount and type of hydrocarbons it contains. Although, viscosity is generally more reliant on carbon number than on the type of hydrocarbon class, for a given carbon number, naphthenes generally have slightly higher viscosities than paraffins or aromatics. For all the JP-8-diesel fuel mixtures developed in the previous studies, the viscosity has been investigated at various speeds (shear stress) with a Brookfield Viscometer DV II Pro type, fitted with the small sample adapter

attachment. This instrument choice came from the conditions that the viscometer had to work from 0 to 100 °C, handle high viscosity substances, robust, with easy cleaning and resistant to contamination. Precise viscosity experiments were performed at temperatures between 25 °C and 45 °C using a small increment step, as seen below in Figure 5. The results showed that viscosity decreases in proportion with the amount of JP-8 content introduced into the mixture, which corresponds to results obtained from previous studies

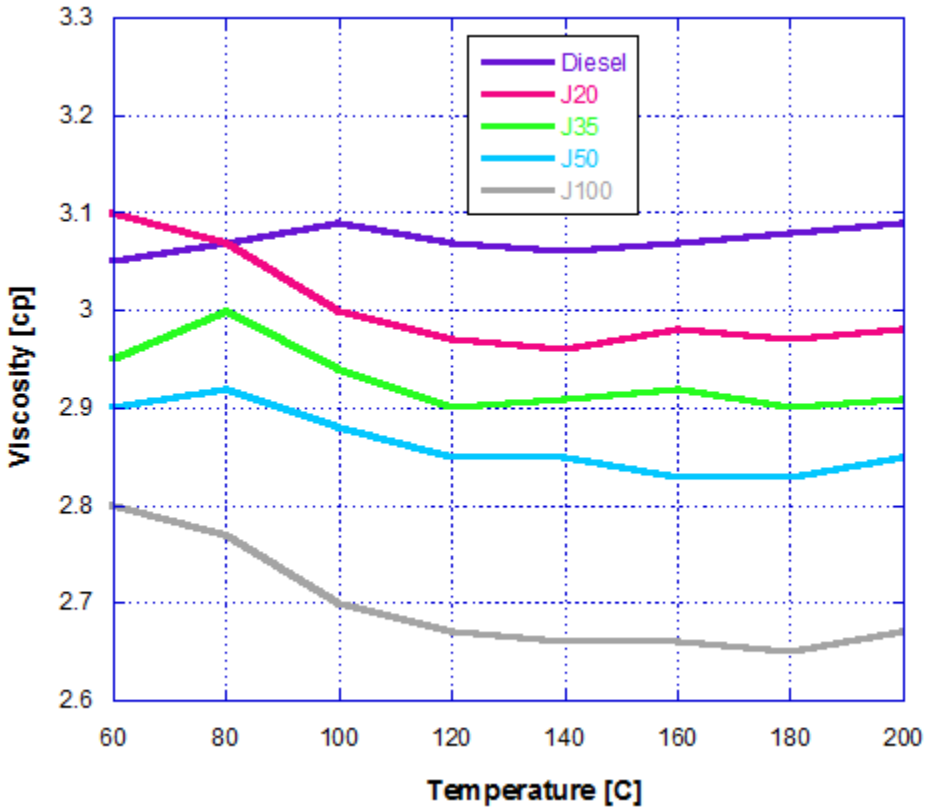

Figure 23 Viscosity Comparison (60-200 °C)

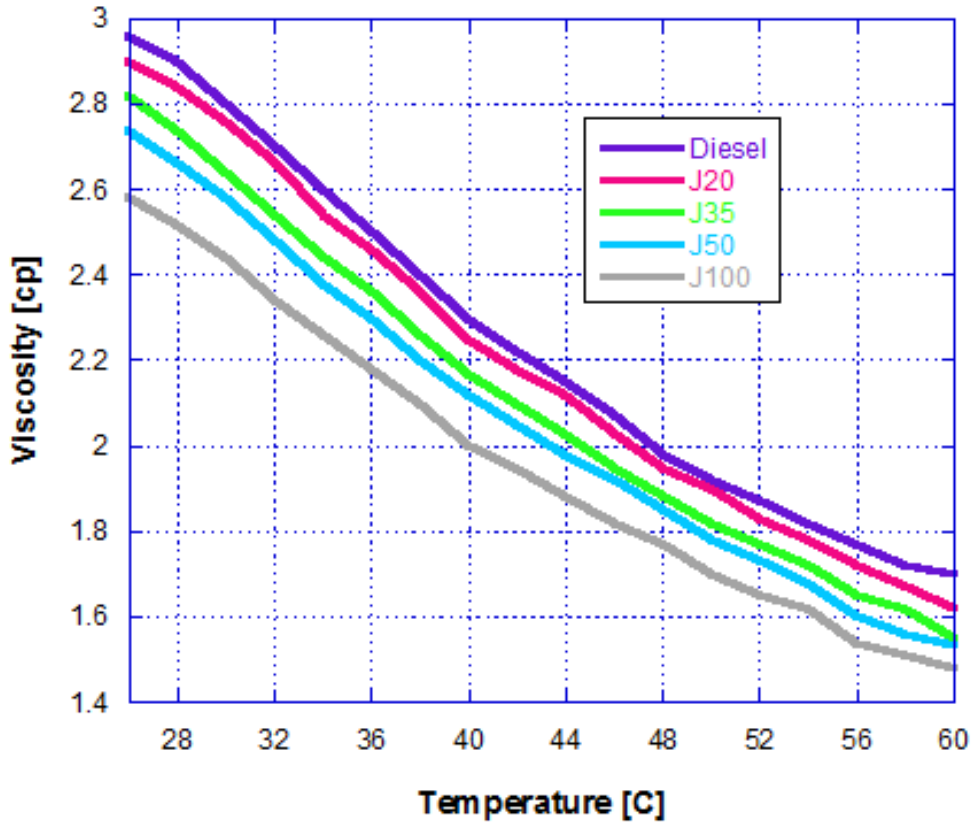

Figure 24 Viscosity Comparison (26-60 °C)

The lower viscosity characteristic of the JP-8 is one reason it is used for aviation application. At high pressures the jet fuel is injected into the combustion chamber section of the turbine engine though the nozzles. This lower viscosity in conjunction with the fact that viscosity decreases in relation to temperature allows the fuel to be injected in the form of a fine spray of fuel droplets that are able to be evaporated as soon as they mix with air. If the fuel viscosity was any higher the engine would be extremely difficult to relight in flight. It is for this reason that there has been an upper limit placed on the viscosity of the fuel. Due to the lower viscosity of the JP-8, diesel blends containing up to 50% JP-8 by weight will considered for this study.

Density

Density is an essential parameter to measure due to the fact that fuel is delivered by volume but energy is measured by mass. Due to the fact that JP-8 has such a large variation in its chemical composition, the density of the fuel will vary in correlation to the amount of compounds it contains. The correlation between the hydrocarbon compounds and their corresponding densities are shown in the table below (U.S. Air Force, 2008).

Table 5 Hydrocarbon Density Correlation

Compound Name	Hydrocarbon Class	Carbon Number	Density [g/m3] @20C
n-Octane	n-Paraffin	8	0.7027
2- Methylheptane	lsoparaffln	8	0.6979
1-Methyl -1-ethylcyclopentane	Naphthene	8	0.7809
Ethylcyclohexane	Naphthene	8	0.7879
o -Xylene	Aromatic	8	0.8801
p-Xylene	Aromatic	8	0.861
Cis - Decalin	Naphthene	10	0.8967
Tetralin	Aromatic	10	0.9695
Naphthalene	Aromatic	10	1.175
n - Dodecane	n - Paraffin	12	0.7488
2-Methylundecane	Isoparaffin	12	0.7458
n - Hexylbenzene	Aromatic	12	0.8602
n - Hexadecane	n-Paraffin	16	0.7735
n - Decylbenzene	Aromatic	16	0.8554

As is apparent by observing the table above, there is a relation in which the density increases in correlation to the carbon number for compounds in the same class. For compounds with the same carbon number, the order of increasing density by class is as follows, paraffin, naphthene, and aromatic. The density of the JP-8 fuel blends used in this particular study were obtained in the laboratory by determining the weight associated with a given volume of fuel.

These measured values corresponded with results obtained by other studies (TARDEC, 2001) and fall within the acceptable standard range dictated by the military. These experimental results are displayed in the figure below.

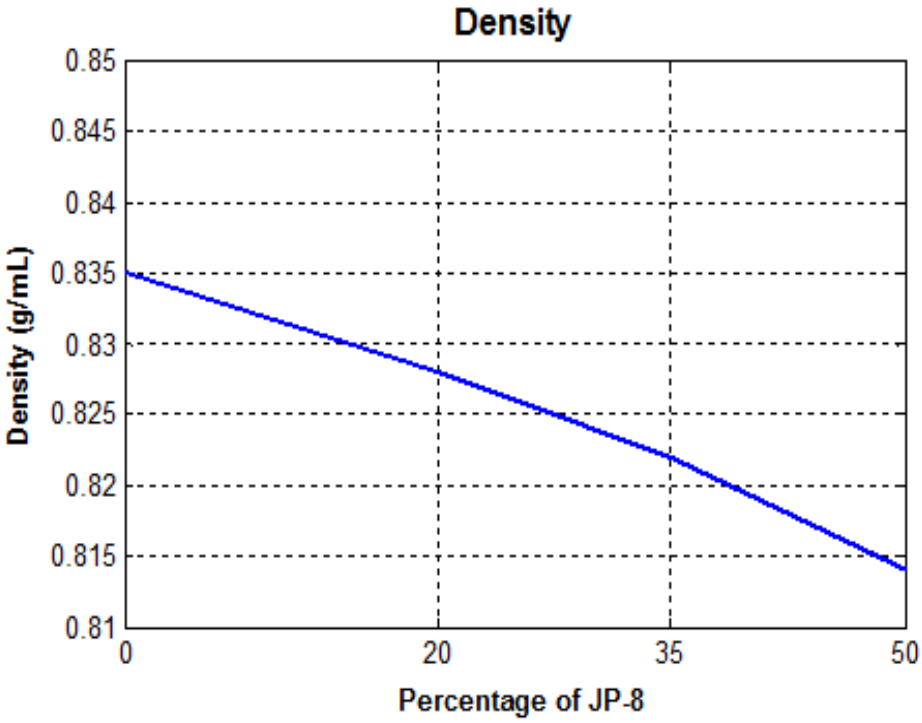

Figure 25 Fuel Density of Various Blended Fuels

After analyzing the figure above, a trend becomes apparent. The Density of the fuel decreases in correlation to the percentage of JP-8 content present in the mixture.

Lower heating value

The heat of combustion also known as the heating value is numerically equal to the enthalpy of reaction, but opposite in sign. However, for fuels in which the exact fuel composition is not known, the enthalpy of the reactants cannot be determined from the enthalpies of formation of the reactant species. The heating value of the fuel is simply measured directly,

such as in the case of this research study. The heating value or calorific value of the fuel is the magnitude of the heat of reaction at constant pressure or at constant volume at a standard temperature (25°C) for the complete combustion of unit mass of fuel (Heywood, 1988), with complete combustion meaning all carbon is converted into carbon dioxide, all hydrogen is converted into water, and all sulfur is converted in sulfur dioxide.

The lower heating value (LHV) of the fuel is defined as the amount of heat released from the fuel by burning specified quantity of the fuel with the assumption that the latent heat of vaporization of water in the fuel is not recovered. The lower heating value of the fuel was determined experimental by using a Calorimeter.

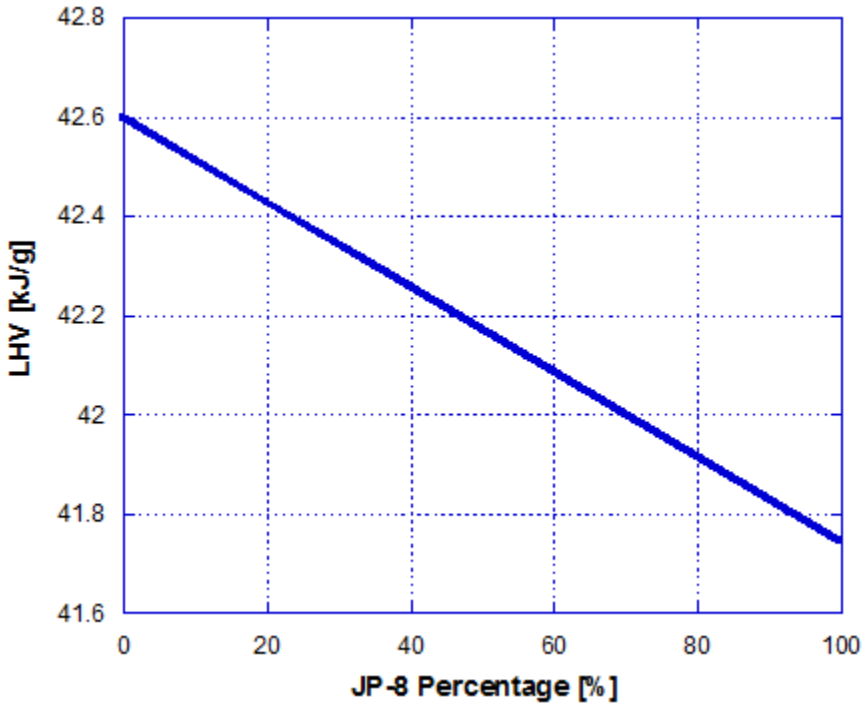

Figure 26 LHV Comparison

Based on the figure above one can easily see the trend, as the percentage of JP-8 by weight in diesel increases the LHV decreases. Because the energy content of the individual hydrocarbons

can differ in relation to the jet fuel composition, the particular batch of jet fuel has an effect on the energy content. This effect is usually able to be predicted by the fuel density. Typically, the higher the density of the fuel the higher volumetric energy content it will have while the lower density jet fuels have higher gravimetric energy content. The correlation between hydrocarbon and energy content is shown in the table below (U.S. Air Force, 2008).

Table 6 Hydrocarbon Energy Content Correlation

Compound Name	Hydrocarbon Class	Carbon Number	Net Energy Content @ 25C			
			Gravimetric		Volumetric	
			[MJ/kg]	[Btu/lb]	[MJ/L]	[Btu/gal]
n-Octane	n-Paraffin	8	44.42	(19,090)	31.21	(112,000)
2- Methylheptane	lsoparaffln	8	44.38	(19,080)	30.97	(111,100)
1-Methyl -1-ethylcyclopentane	Naphthene	8	43.57	(18,730)	34.02	(122,100)
Ethylcyclohexane	Naphthene	8	43.4	(18,660)	34.2	(122,700)
o -Xylene	Aromatic	8	40.81	(17,550)	35.92	(128,900)
p-Xylene	Aromatic	8	40.81	(17,550)	35.14	(126,100)
Cis - Decalin	Naphthene	10	42.62	(18,320)	38.22	(137,100)
Tetralin	Aromatic	10	40.52	(17,420)	39.06	(140,200)
Naphthalene	Aromatic	10	40.12	(17,250)	47 .14	(169,100)
n - Dodecane	n - Paraffin	12	44.11	(18,960)	33.03	(118,500)
2-Methylundecane	Isoparaffin	12	44.08	(18,950)	32.87	(117,900)
n - Hexylbenzene	Aromatic	12	41.8	(17,970)	35.96	(129,000)
n - Hexadecane	n-Paraffin	16	43.95	(18,890)	33.99	(122,000)
n - Decylbenzene	Aromatic	16	42.23	(18,160)	36.12	(129,600)

As can be noted from the table shown above, for hydrocarbon compounds containing the same carbon number, the order of increasing energy content per unit weight by class is aromatic, naphthene, and paraffin. The order is simply reversed on a volume basis, with paraffin's having the lowest energy content per unit volume and the highest being that of the aromatics.

Air/fuel ratio

The Stoichiometric Air-Fuel Ratio (AFR) can be defined as the mass ratio of air provided to completely burn one kg or one kmole of the fuel during combustion. It is of interest because it lends influence to the maximum bulk gas combustion temperature, apparent heat release, and net power. If the mixture is lean it will produce higher maximum bulk gas combustion temperatures and lower power, while rich mixtures result in lower bulk gas combustion temperatures due to the excessive amount of carbon which oxidizes to form carbon monoxide rather than carbon dioxide (Najt & Foster, 1993). The Stoichiometric Air-Fuel Ratio (AFR) of JP-8 fuel blends were determined based on their chemical compositions and are displayed in the figure below.

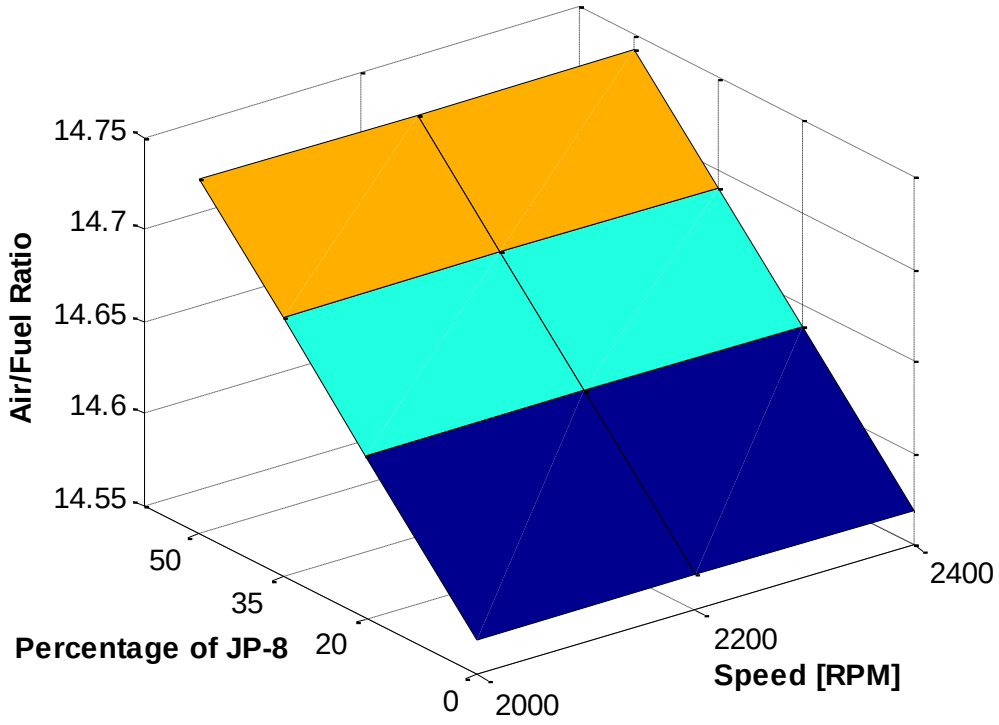

Figure 27 Air/Fuel Ratio Surface Plot

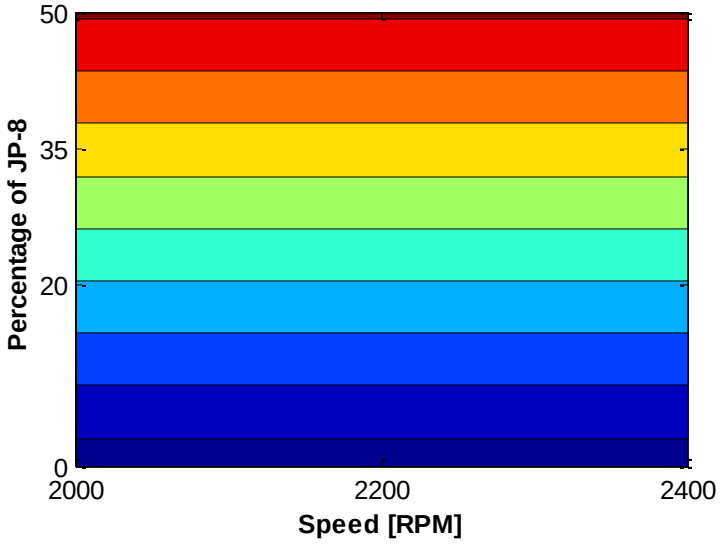

Figure 28 Air/Fuel Ratio Control Plot

Thermal analysis

In differential thermal analysis (DTA), the temperature difference between a reactive sample and a non-reactive reference is determined as a function of time, providing useful information concerning the temperatures, thermodynamics and kinetics of reactions. Thermogravimetric analysis (TGA) determines the weight gain or loss of a condensed phase due to gas release or absorption as a function of temperature weight as the sample is heated in an atmosphere of choice, for this particular study it was air. This is useful for locating the temperature where reactions occur such as for melting, phase changes, and oxidation.

Stability

A stable fuel can be defined as simply a fuel whose properties remain unchanged in relation time (storage stability) and prolonged exposure to high temperatures in the engine or environment (thermal stability). JP-8 becomes unstable through the same process for both causes of instabilities, that being through multi-step chemical reactions, that attack the

elastomers of the fuel and result in the formation of soluble gums and insoluble particles (Coordinating Research Council, Inc., 1983).

In terms of application for use in aircrafts, the thermal stability is one of the most important fuel characteristics due to the fact that the fuel serves as the cooling system (heat exchange medium) for the engine and aircraft components. This exposure to high temperatures accelerates the chemical reactions that lead to particle and gum formation, resulting in deposits accumulating on fuel filters (increasing the pressure drop across the filter and reducing fuel flow), in fuel injector nozzles (disrupting spray patterns causing hot spots in the combustion chamber), and in the main engine control (disrupting fuel flow and engine system control) (Coordinating Research Council, Inc., 1983).

The storage stability of the fuel is typically compromised due to the more reactive fuel components in the fuel composition. However, it may also be influenced by the storage conditions, instability reactions occur quicker and to a greater extent at higher ambient temperatures. This may be combated through the use of additional additives if the fuel shall be stored in a less than ideal location. In terms of fuel stability during storage, it is not usually an issue due to the fact that the fuel is typically used within weeks of manufacturing. However, since this study is for military application, it shall be assumed that the fuel may be stored for an extended period before use; therefore, the fuel used in this study was stored for eight months after production, before being tested in order to verify its storage stability.

Parameters

Table 7 shown below, describes the design parameters associated with the engine that were used in the thermodynamic calculations described throughout this paper.

Table 7 Engine Parameters

Parameter	Symbol	Unit	Value
Displacement Volume of the Piston	Vs	[L]	0.325
Compression Ratio of Engine	ε	N/A	23.5
Bore	D	[mm]	77
Stroke	S	[mm]	70
Number of Cylinders	I	N/A	1
Number of Strokes	τ	N/A	4
Engines Effective Power	P_e	[kW]	2.9

In-Cylinder and Fuel Line Pressure

The in-cylinder pressure with respect to crack angle was acquired through the use of a piezoresistive high pressure sensor (Kistler 6056A) introduced through the glow plug in order to investigate the combustion characteristics of the JP-8 fuel blends. Absolute pressure referencing was accomplished by pegging the cylinder pressure to the intake plenum pressure. The crank angle at which peak pressure developed inside the cylinder was determined for each fuel blend and compared to the reference sample of diesel no 2 in terms of peak pressure magnitude and crank angle location. Factors that influence peak pressure include but are not limited to, compression ratio, load, piston geometry design, volumetric efficiency, combustion chamber design, and fuel properties. The maximum cylinder pressure can also be influenced by abnormal phenomena such as knock and incomplete combustion.

It is desirable that the engine is capable of producing a relatively high pressure as one of the main purposes of an engine is simply to generate internal pressure which is used to produce work. However, the limits of the engine must be known as a proper assessment of the fuel prior to testing is vital to avoid potential engine damage as a result of the new fuel blend. The indicated diagram presented in Figure 29 displays the baseline reference cycles for diesel no.2

fuel taken for varying speeds (2000 RPM. 2200 RPM, 2400 RPM) at a continuous load (4.78 BMEP). This relationship is able to give a gross indication of the engine performance.

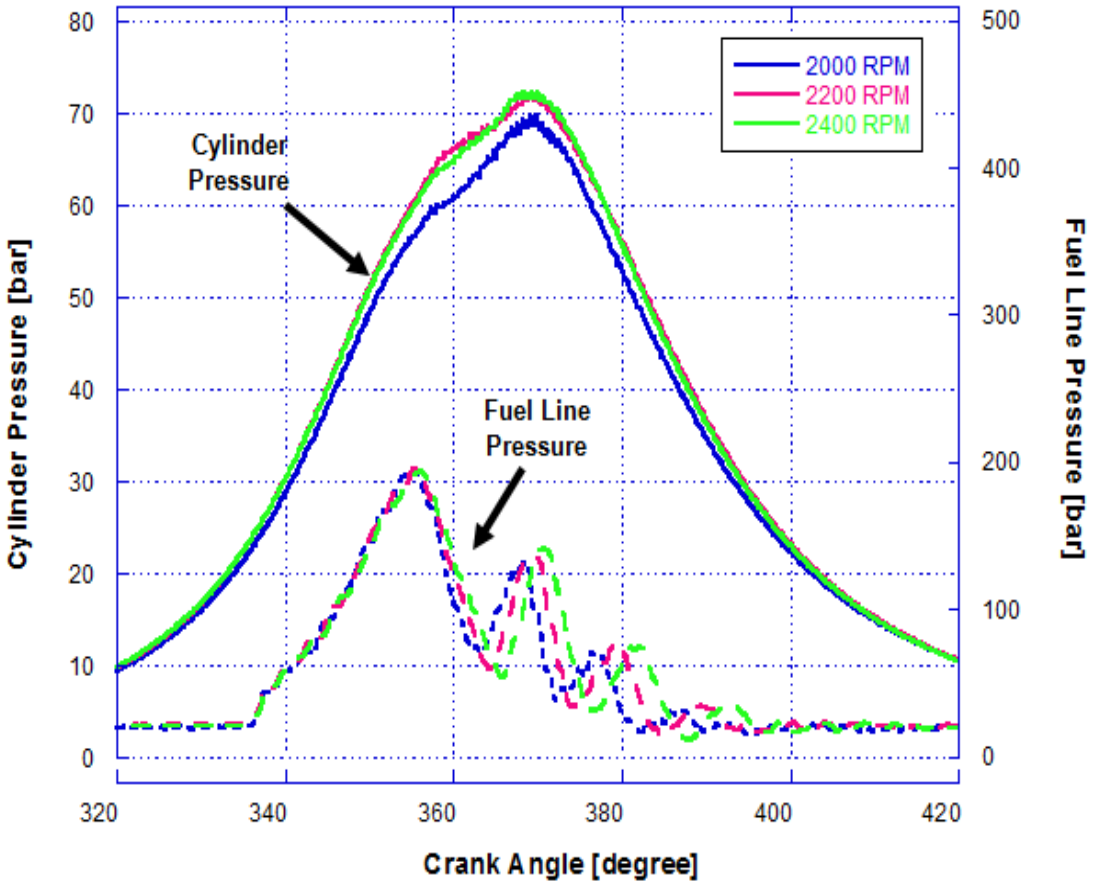

Figure 29 Diesel Cylinder and Fuel Line Pressure Comparison

Based on the reference cycles (Figure 29) collected for diesel, it can be seen that a change in speed has a direct correlation with the cylinder pressure. As the speed of the engine is increased, the pressure inside the cylinder is also increased, while, the fuel line pressure experiences no change in the region relevant to this study. Although it may be noted that an increase in the speed of the engine does result in more visible noise in the fuel line pressure data especially in the wave propagation after the start of injection.

After the reference diagrams were obtained in each experiment, the load was kept at 100% and the maneuver from diesel to JP-8 was made without stopping the engine.

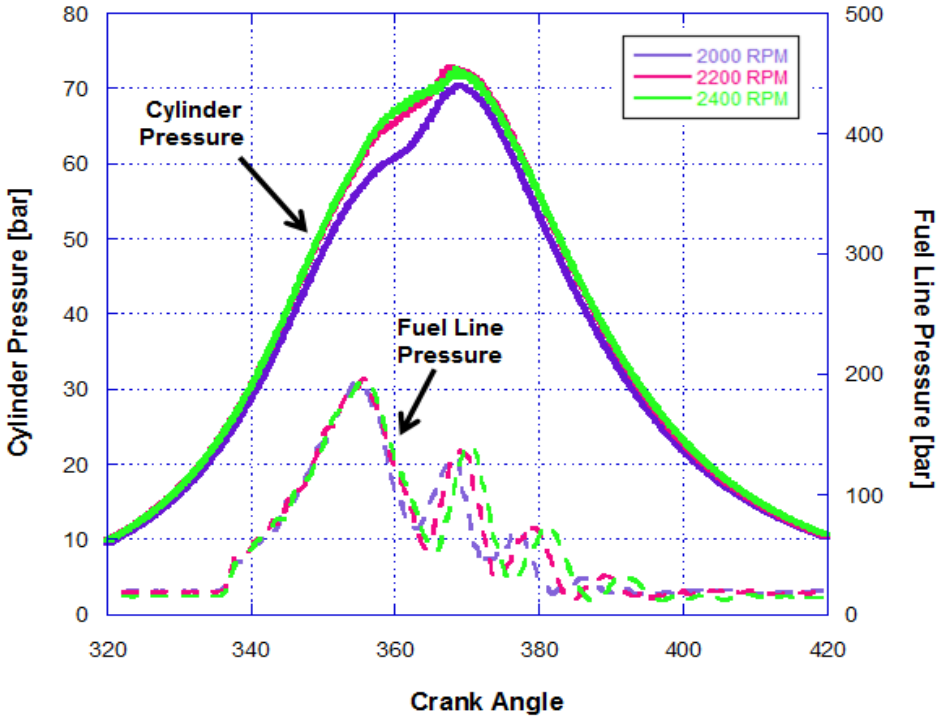

Figure 30 J20 Cylinder and Fuel Line Pressure Comparison

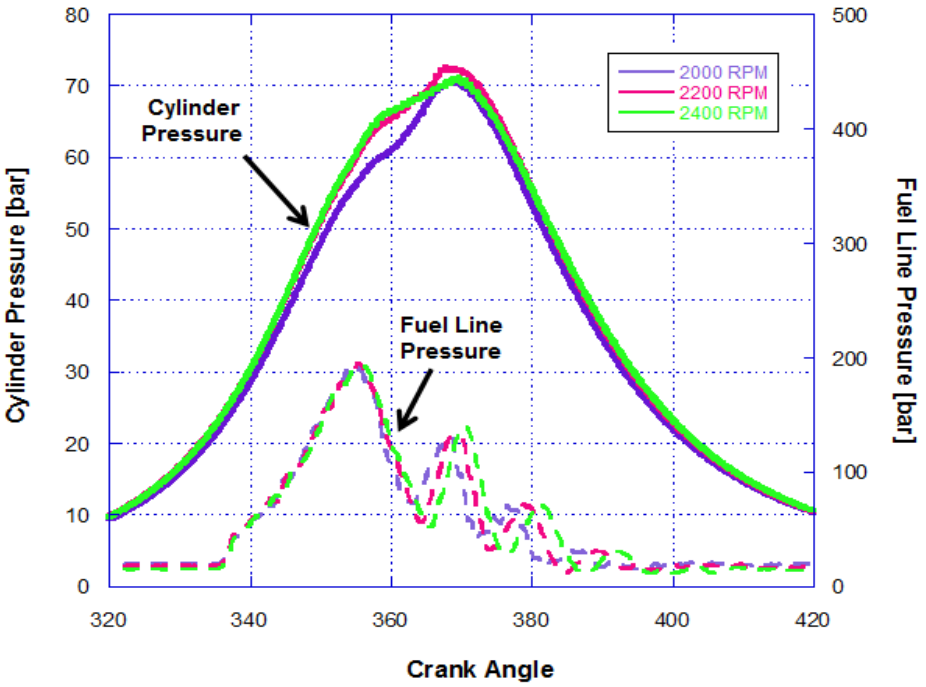

Figure 31 J35 Cylinder and Fuel Line Pressure Comparison

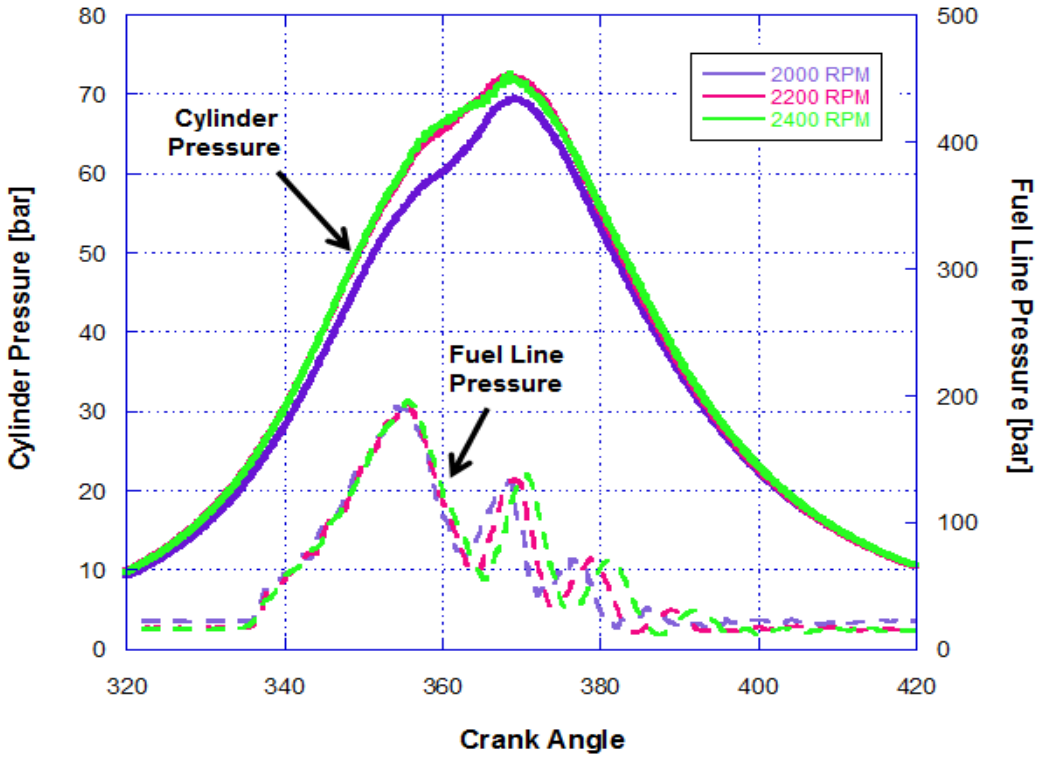

Figure 32 J50 Cylinder and Fuel Line Pressure Comparison

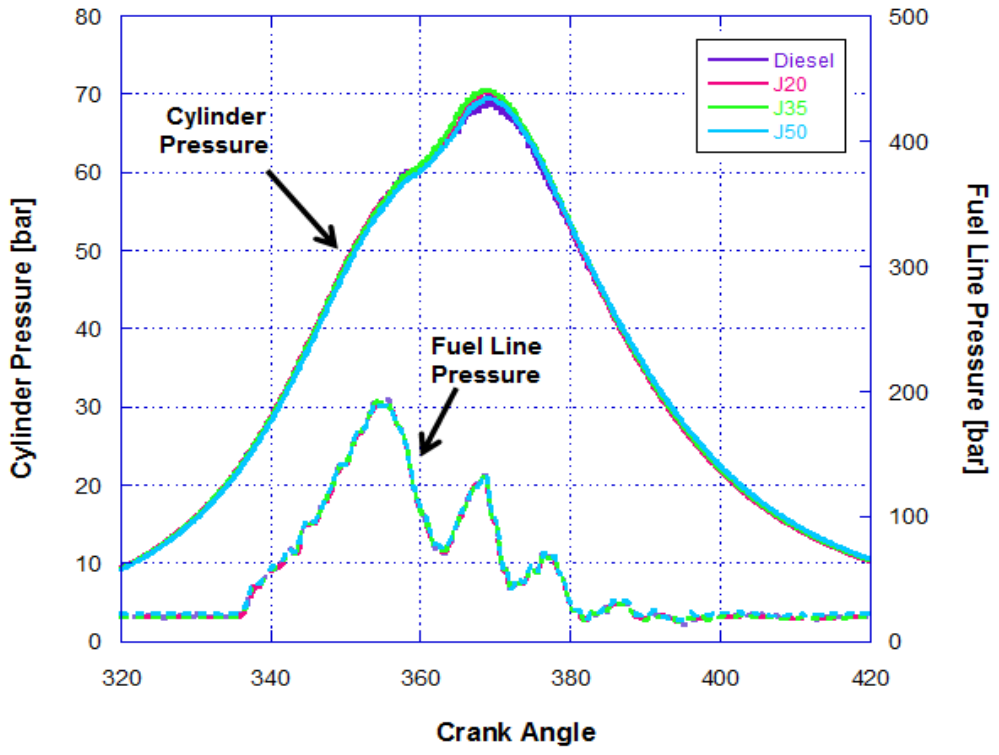

Figure 33 Cylinder and Fuel Line Pressure Comparison @ 2000 RPM (4.78 BMEP)

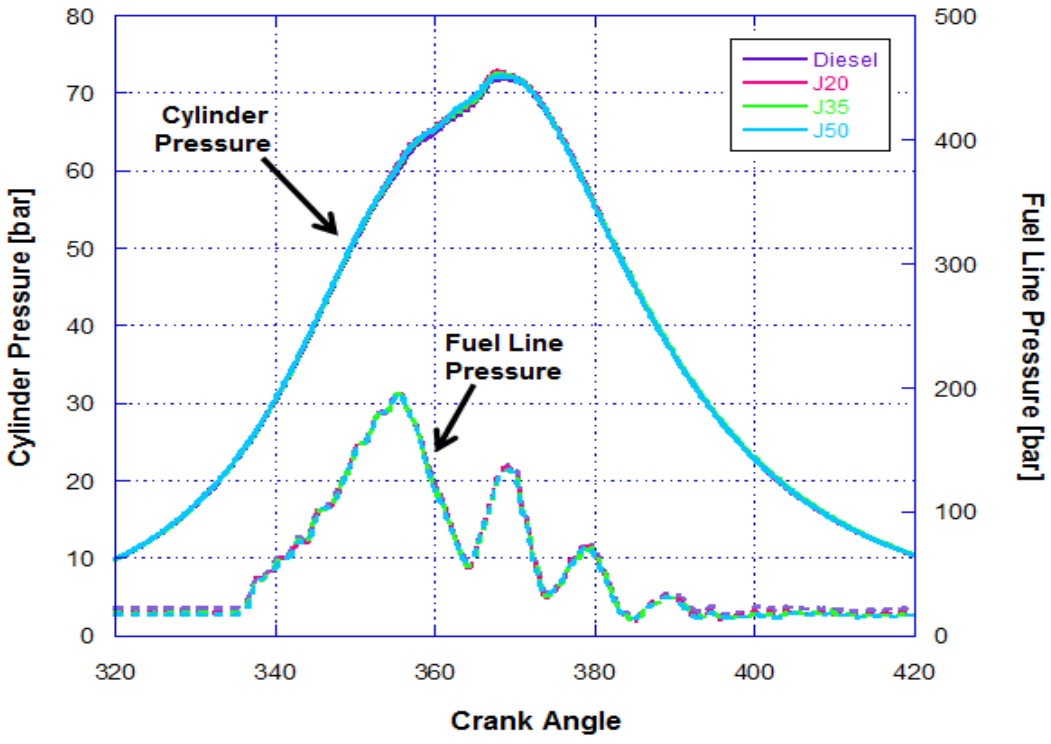

Figure 34 Cylinder and Fuel Line Pressure Comparison @ 2200 RPM (4.78 BMEP)

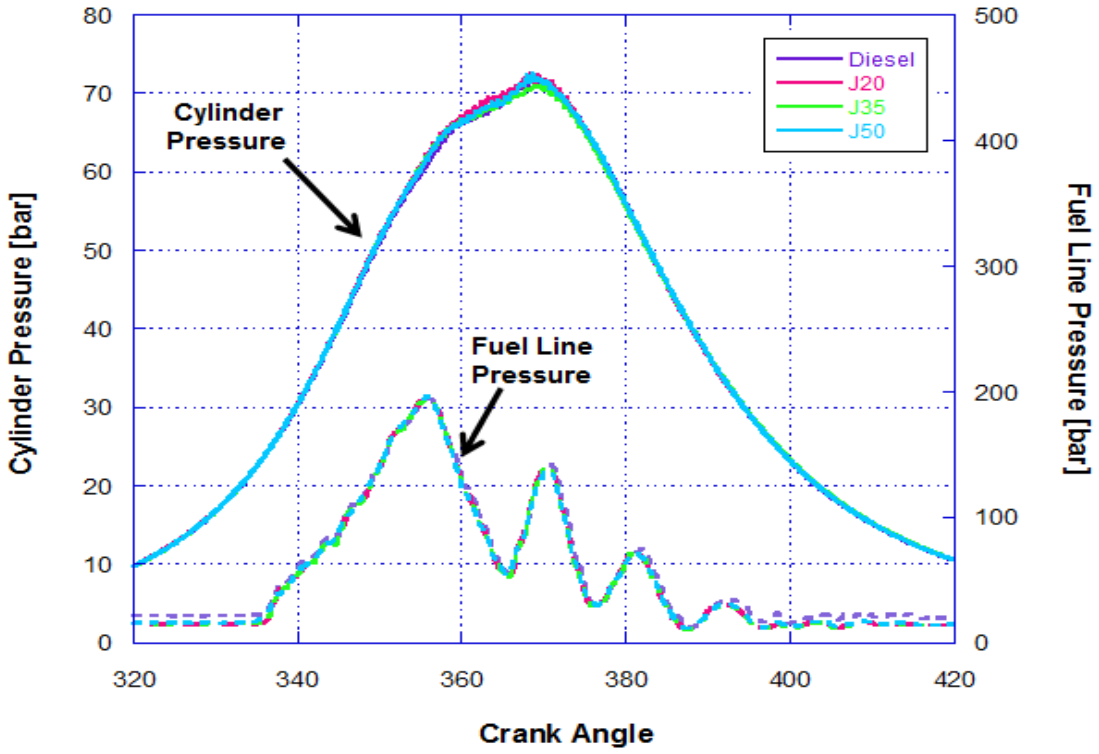

Figure 35 Cylinder and Fuel Line Pressure Comparison @ 2400 RPM (4.78 BMEP)

Based on the pressure records it can be concluded that the change in the amount of JP-8 introduced into the system has a minimal effect on the average maximum combustion pressure, with the maximum combustion pressure remaining relatively constant for all fuel blends, 72.7 bar for diesel and decreasing slightly by 0.4 bar for the J-50 blend, with the peak pressure position into the cycle being delayed by about 0.5 degrees for the JP-8 fuel J50 blend. The same can be said for the fuel line pressure as both the JP-8 and diesel match despite the differences in both viscosities and densities. The reductions that occurred in the peak pressure for increasing JP-8 content blends are expected due to the reductions in the energy content of the blends. Based on the magnitude of the peak cylinder pressure for all JP-8 blends, it may be concluded that since the peak pressures obtained were less than that of diesel no.2, there should be no effects on engine durability observed. It is also important to note that based on the indicated diagram, no

knock in the system was visible. The “diesel knock” phenomenon is developed due to an abrupt pressure gradient characterized by a sudden pressure rise due to the initial ignition of the fuel and air mixture inside the cylinder. This abrupt pressure change represents an extremely powerful excitation force that excites the oscillation of the burned gases in the combustion chamber in the piston.

It is important to note the ram effect that occurs for all test fuels (Figure 36) beyond speeds of 2000 RPM, due to the design of this particular engine. The ram effect can be described as an increase in the static air pressure inside of the intake manifold, which results in a greater mass flow through the engine and a reduction in the intake air velocity. This reduction in the gas velocity correlates with a reduction in the dynamic pressure and increase in static pressure. The increased static pressure in the intake manifold has a positive effect on engine power, due in part to its influence on the cylinder and fuel line pressure.

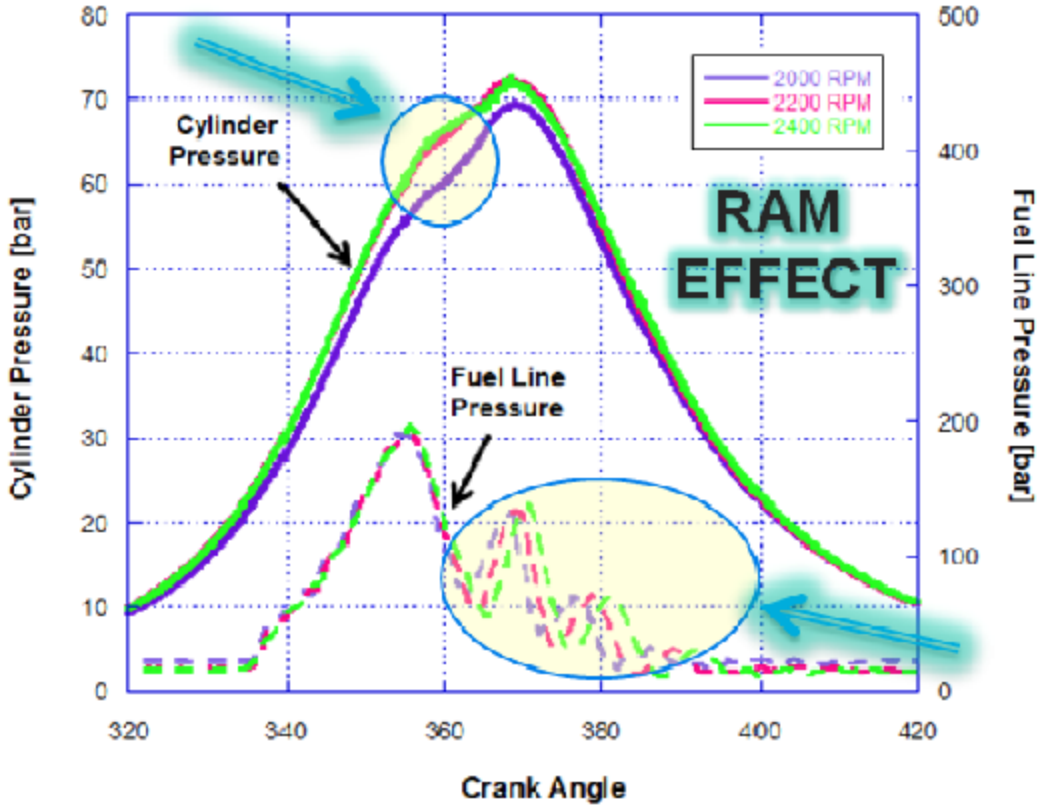

Figure 36 Ram effect

The fuel's bulk modulus, density, and viscosity can modify the needle lift and injection law in a hydraulic plunger-barrel injection system. Higher bulk modulus may cause a steeper rise in fuel pressure at the start of injection and the injector needle to open sooner. The experimental results for the fuel line pressures presented in the figures above do not display any symptoms of the fuel line injector opening prematurely for the JP-8 blends. The mechanical injection system associated with this experiment using JP-8 with 147 bar injection pressure displayed no visible modifications in the injection timing. The engine was able to run relatively smooth and stable using the JP-8/diesel mixtures with no ignition difficulties observed.

Indicated Diagram

One vital parameter when performing the combustion analysis is the piston displacement throughout the cycle. The piston displacement or sometimes referred to as engine displacement can be defined as the measure of the volume moved by the piston in a cylinder of an internal combustion engine as it moves though a single complete revolution (Heywood, 1988). Therefore, the piston displacement, X_D, is found by using the equation shown below:

$$X_D = r\left[(1 - cos\alpha) + \frac{r}{4l}(1 - cos2\alpha)\right]$$

Where r is the radius, α is the crank angle, and l is the length of the crank shaft. As a general rule, the higher the displacement, the more power the engine produces, and thus the more fuel it consumes. Displacement is typically a way of expressing engine size. It's a measure of the total volume of all the cylinders and usually is given in cubic centimeters or liters. The linear movement of the piston is able to be converted to a rotating movement via a connecting rod and crankshaft. The piston movement, X_p, is found by using the equation shown below:

$$X_p = \left[(1 - cos\alpha) + \frac{r}{4l}(1 - cos2\alpha)\right]$$

It can be observed that the piston displacement is simply the piston movement multiplied by the radius of the piston. The graph displayed below in Figure 37 represents the pistons linear movement in relation to the crank angle throughout the cycle.

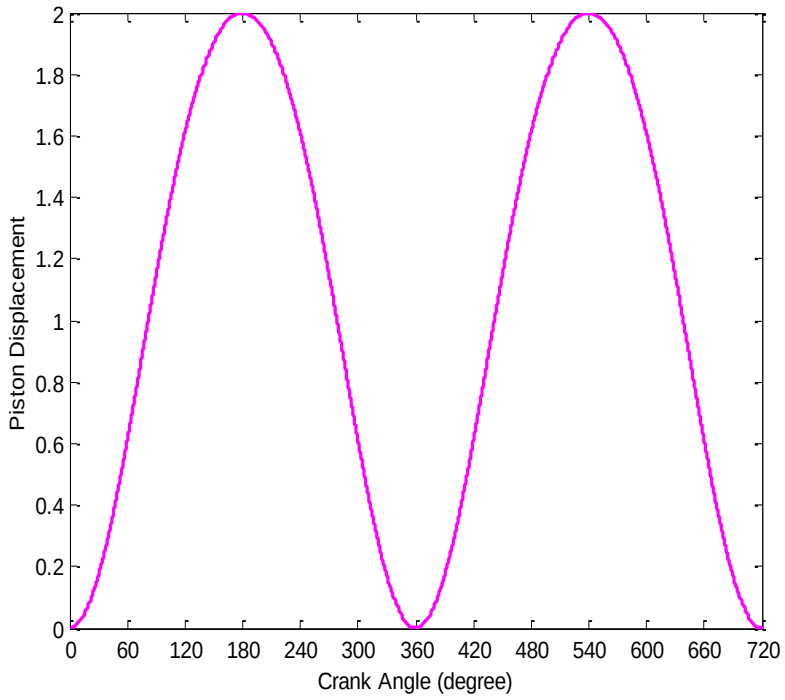

Figure 37 Piston Movement vs Crank Angle

It can be clearly observed from the figure above the distinct movement of the piston is divided up into four main zones occurring every 180 degrees. Zero degrees occur when the piston is at the top of the cylinder. Since there are 360 degrees in one revolution, the piston is at the bottom when the crank angle is 180 degrees. The distance traveled by the piston from zero degrees to 180 degrees is called the stroke of the piston. As stated previously, the piston makes four strokes and the crankshaft makes two revolutions between combustion firings thus the cycle is able to be defined by 720 degrees.

Based on the calculated piston displacement an Indicated diagram is then able to be constructed. The Indicated diagram contains a plot of the pressure and volume variations for an engine. The significance of this chart lies in the fact that the work done during the cycle can be

gauged from the area enclosed within the loop of the graph. The experimental p-v diagram is shown in Figure 38 below.

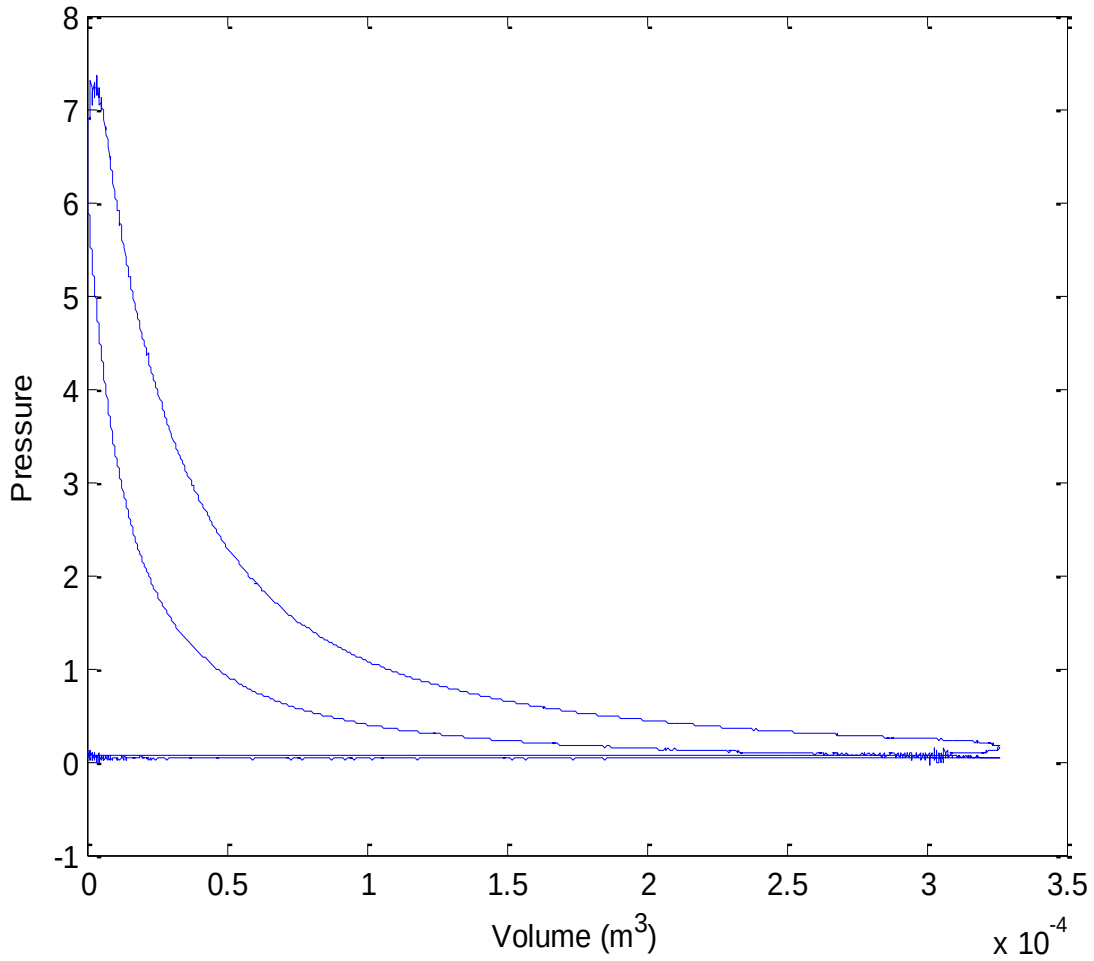

Figure 38 Experimental PV diagram

Based on equation for work, which states that the area underneath the curve of this graph can be defined as the indicated work, a great deal of combustion related information can be ascertained from the in cylinder pressure data using these calculations, such as the indicated mean effective pressure (IMEP). The angular integration span used in this project includes all four strokes. The work produced is due to the gas pressure on the piston. Assuming that the pressure in the crank case is atmospheric, and then the gas pressure will be relative to the crank

case pressure. This means that for a small displacement, defined as dx, the work can be defined as dW. Therefore, the following relationship for work (dW) can be developed:

$$dW = F\,dx = PA\,dx = P\,dV$$

For a finite volume change, work is given by the following equation shown below:

$$W = \int PdV$$

The pressure in the cylinder changes during the expansion stroke. First increasing due to the heat addition, and then decreasing due to the increase in cylinder volume. We can define a mean effective pressure to determine the work.

$$W = \int PdV = P_{mean}V_d$$

The mean effective pressure is defined as a constant hypothetical pressure which if applied to the head of a piston during one stoke would yield the same amount of new that is available at the shaft. The brake mean effective pressure or more commonly referred to as BMEP cannot be measured because the BMEP of an engine does not exist. Instead it is a derived mathematical value. The pressure force in which the piston is forced downward by gas pressure is known as the indicated mean effect pressure or more commonly IMEP. IMEP is that pressure if applied to the head of a piston during one stoke would yield the same amount of work the cylinder produces during the complete cycle. This power producing stroke would yield the same amount of work the cylinder produces during the complete cycle. During a real cycle the pressure is only significant during the compression and power strokes. During the compression stoke work is done on the gas mixture residing in the cylinder. Hence, the net pressure would be the difference

between these two. Therefore, it is expected that the IMEP value be approximately equal to the difference between the average pressures on the power and compression strokes. In summary the Indicated work is work done by the gas while the Brake work is work done by the crankshaft. The difference between the two lies in the fact that in one the work is done against friction and in the other the work is done by pumps and gears. Some of the work that IMEP does is not delivered to the shaft. Reducing engine friction increases BMEP without increasing IMEP thus resulting in a change in the mechanical efficiency of the engine. BMEP is an extremely important parameter since it is proportional to torque.

The indicated mean effective pressure (IMEP) is a normalized performance measure of an engine's work output and is obtained by dividing the work per cycle by the cylinder volume. It is an indication of the torque produced by a cylinder and has the units of force per unit area, or pressure. It is found by using the equation shown below:

$$IMEP = \frac{\int dW}{V} = \frac{\int PdV}{V}$$

Where P and dV represent cylinder pressure and rate of change in cylinder volume, respectively, and dW is defined as the work.

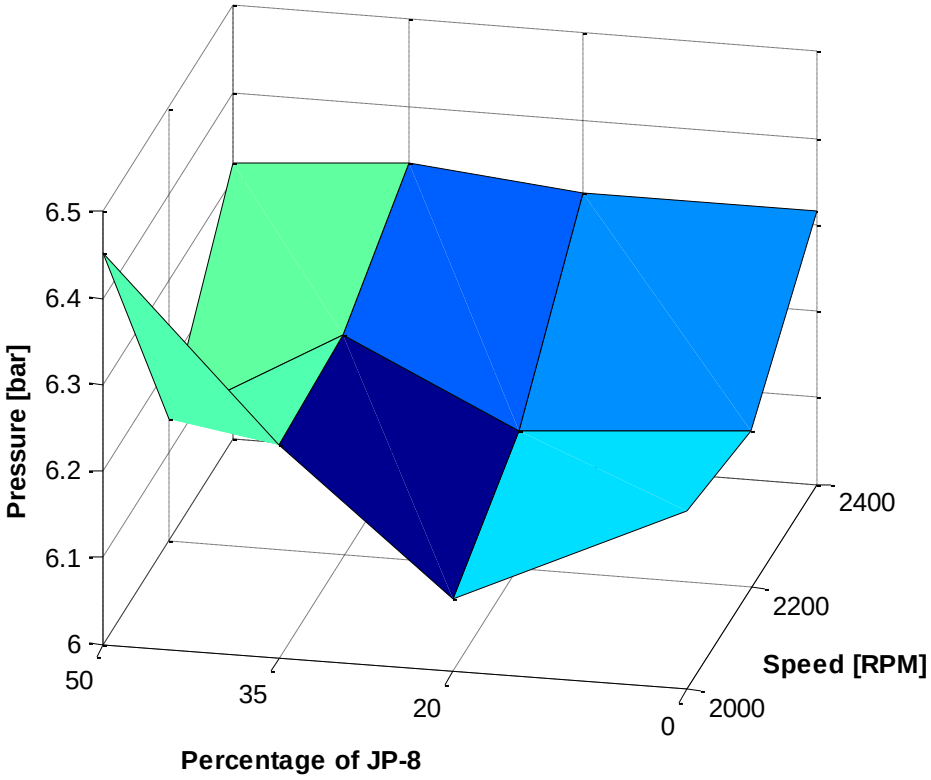

Figure 39 IMEP Surface Plot

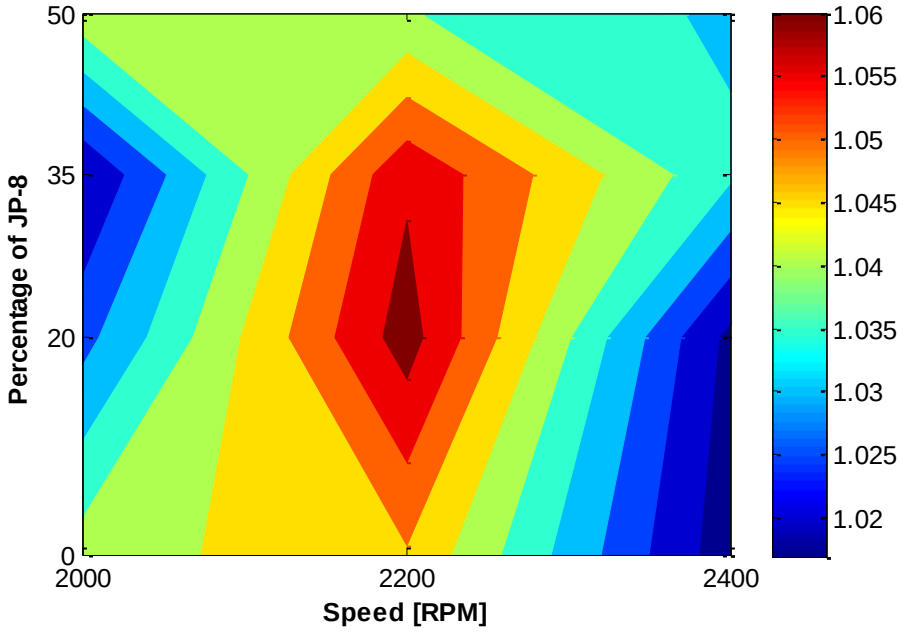

Figure 40 IMEP Contour Plot

Indicated Power (IP) is the power obtained at the cylinder. It can be obtained from the indicator diagram, and can be calculated by using the equation shown below:

$$\mathrm{IP} = \frac{\mathrm{PiLANn}}{60\mathrm{x}}$$

Where Pi is the indicated mean effective pressure, in N/m2, L is the stroke length (m), A is the area of cross section of the piston, m2, N is the engine speed in rev/min, n is the number of cylinders, and x is 1 for 2 strokes and 2 for 4 strokes. In order to find the energy produced per cycle the following formula is used:

$$\dot{W} = \frac{WN}{n60}$$

Where n is the crank revolutions per cycle which is 2 for a four stroke engine, N is the crankshaft speed in rpm and W is the indicated work associated with the PV diagram.

In naturally aspirated engines, such as the one employed for this study, BMEP is not stress limited; instead it reflects the product of volumetric efficiency (the ability to induct air), air/fuel ratio (effectiveness of air utilization in combustion), and finally fuel conversion efficiency (Heywood, 1988). Maximum BMEP values for an IDI engine is typically higher than those for a DI engine of equivalent size because without the need to generate swirl during the intake process, the intake port and valve are less restrictive and volumetric efficiency is higher, and because the IDI engine can be run at lower air to fuel ratios with smoking

Maximum Gas Temperature

The maximum instantaneous volume averaged gas temperature is a very important parameter when investigating the combustion within an engine. When rapidly compressing a gas

to a specific pressure, with minimal heat transfer, significant energy is converted into increasing the gas temperature. The heat transfer within a compression cylinder is quite complex due to the varying flows within the cylinder and the varying coefficients. The analysis is further complicated by the fact that during compression and expansion, the heat transfer can be out of phase with the temperature difference between the bulk gas and the wall. A prime reason that the bulk gas temperature does not closely follow the wall temperature is that the surface area to volume ratio in the piston is typically quite small (Soloiu V. Y., 2010). Assuming that all chemical species are considered to behave as ideal gas and the mixture is considered to be homogenous and there is no spatial-gradient throughout the combustion chamber the following analysis can be conducted.

An ideal gas is defined as one in which all collisions between atoms or molecules are perfectly elastic and in which there are no intermolecular attractive forces. One can visualize this as simply a collection of perfectly hard spheres which collide but which otherwise do not interact with each other. In such a gas, all the internal energy is in the form of kinetic energy and any change in internal energy is accompanied by a change in temperature. It is for this very reason that the ideal gas law is used to calculate the spatially averaged temperature in the combustion chamber. This is because it can be viewed as occurring from the kinetic pressure of gas molecules colliding with the walls of a combustion chamber in accordance with Newton's laws. But there is also a statistical element in the determination of the average kinetic energy of those molecules. The temperature is taken to be proportional to this average kinetic energy. Thus it is assumed that the forces of gravity and friction forces of low value be treated as negligible. The ideal gas law is shown below:

$$Pv = nRT$$

Where P is the pressure, V is the displacement volume, R is the molar gas constant, and T is the temperature. The molar gas constant can be defined as 3.314472(15)J/(Kmole). One mole of a pure substance has a mass in grams equal to its molecular mass. Based on this equation is conjunction with the conversion factor dealing with converting one mole of an ideal gas to a volume quantity is shown below:

$$22.4\text{L} = 1\text{mole}$$

This conversion only holds true when operating under standard temperature and pressure. From this the number of moles can be calculated with minimal effort. Next the volume of the combustion chamber, Vc, is found by using the equation show below (Heywood, 1988):

$$\text{V}_\text{c} = \frac{\text{V}_\text{s}}{\varepsilon - 1}$$

Where Vs is the displace volume and ε is the compression ratio of the engine. The Ideal Gas law is then able to be rearranged to get in terms of Temperature. The temperature associated with the heat transfer of the wall can be calculated by using the equation shown below:

$$T = T_s + \left[X_p \frac{\pi D^2}{4} + V_c\right]\frac{P}{nR}$$

Where Ts is the surface temperature of the cylinder wall, D is the bore, Vc is the volume of the combustion chamber, P is the pressure in the cylinder, n is the number of moles, and R is the molar gas constant. The number 8.314472 m^2 kg s^{-2} K^{-1} mol^{-1} is the value of the molar gas constant. It is vital to remember when performing the calculated stated above that the units are in the International standard. This means that the lengths are measured in meters, Temperatures

in Kelvin, and Pressure in Pascal. This experimental maximum instantaneous volume averaged gas temperature is shown below:

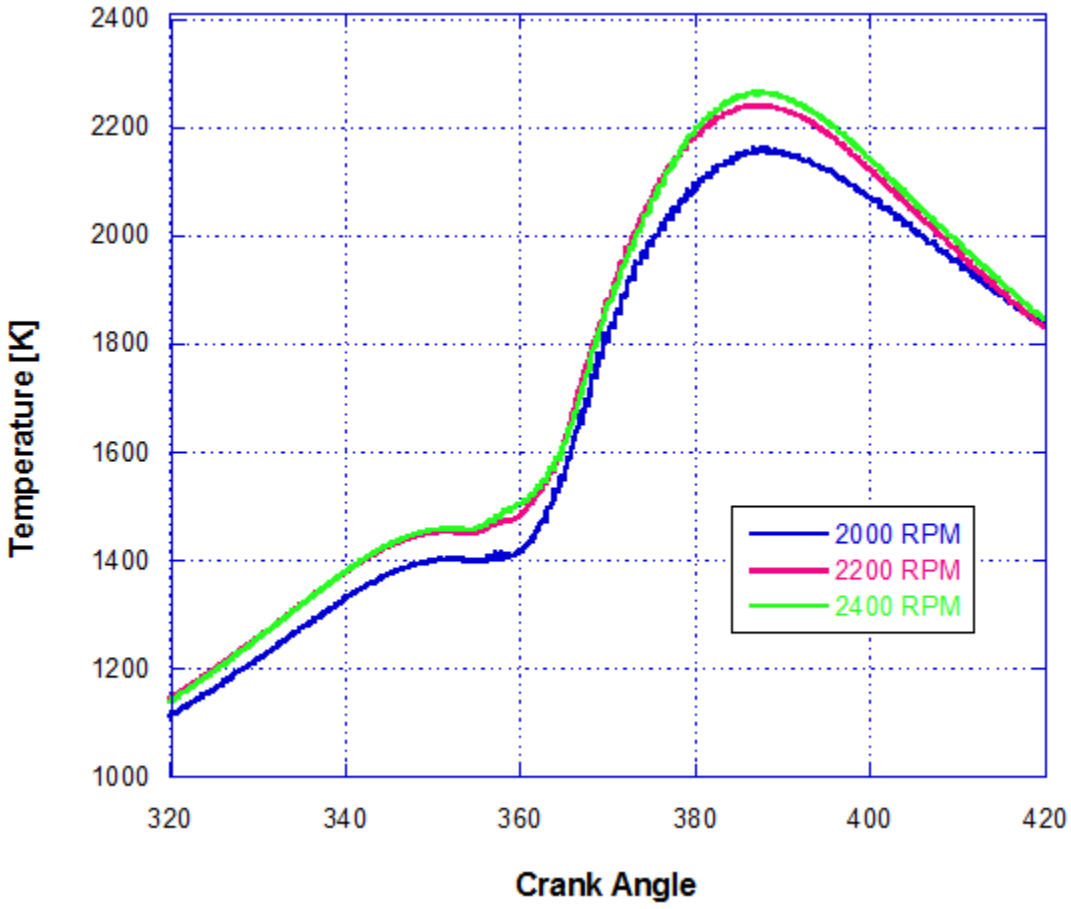

Figure 41 Diesel Instantaneous Volume Averaged Gas Temperature

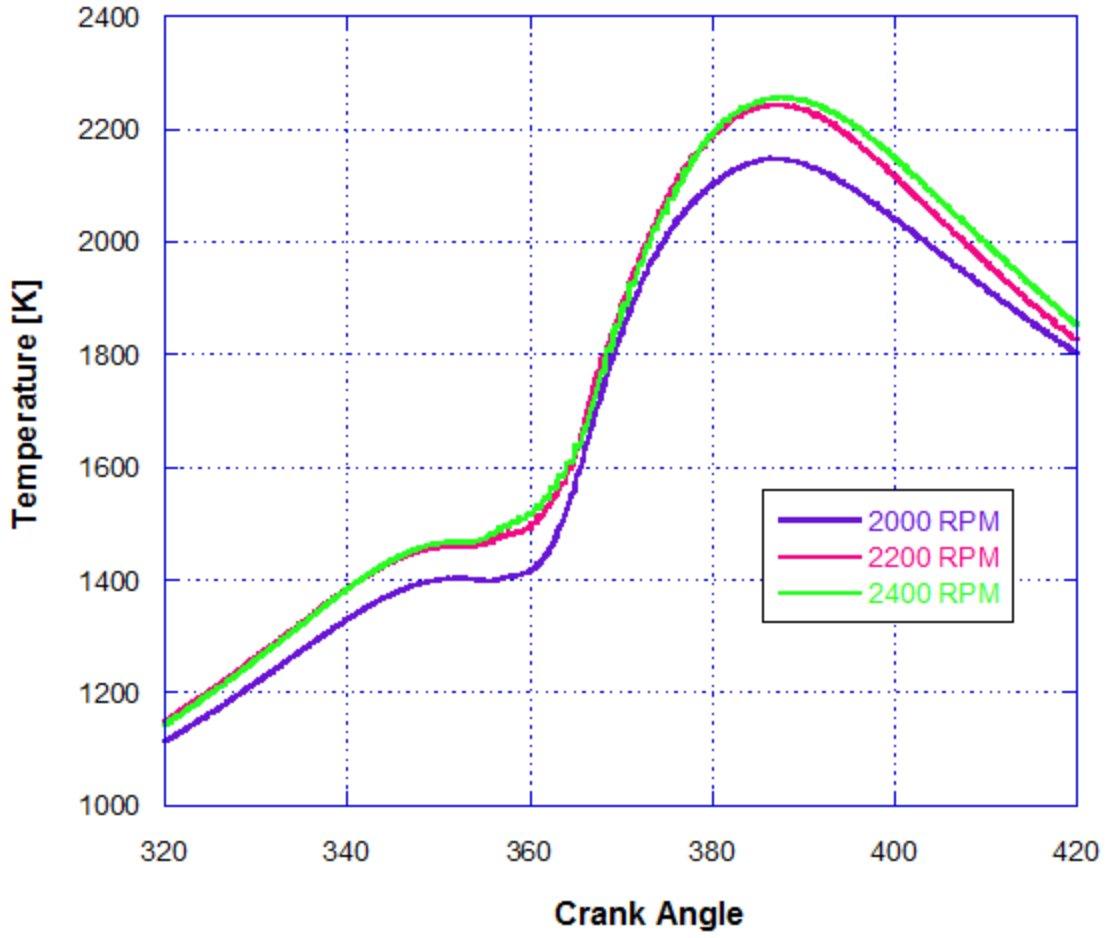

Figure 42 J20 Instantaneous Volume Averaged Gas Temperature

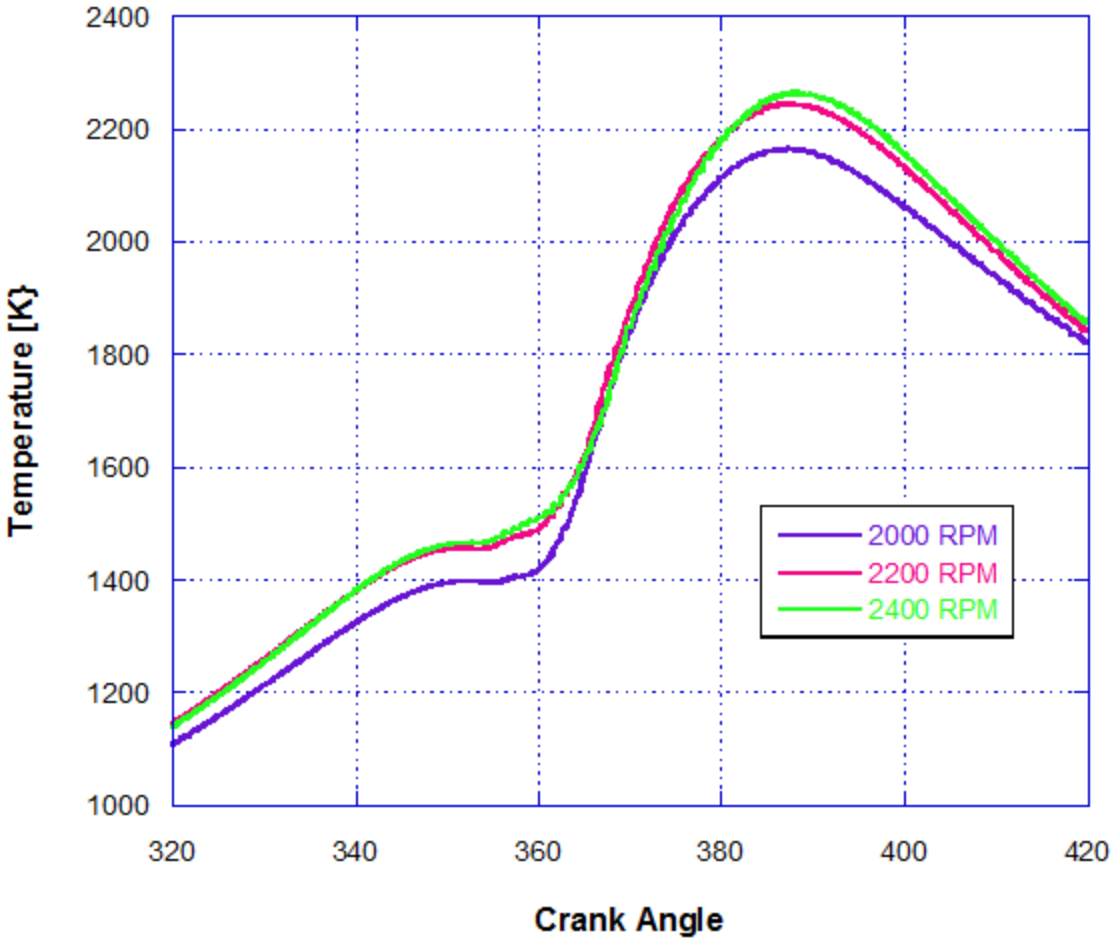

Figure 43 J35 Instantaneous Volume Averaged Gas Temperature

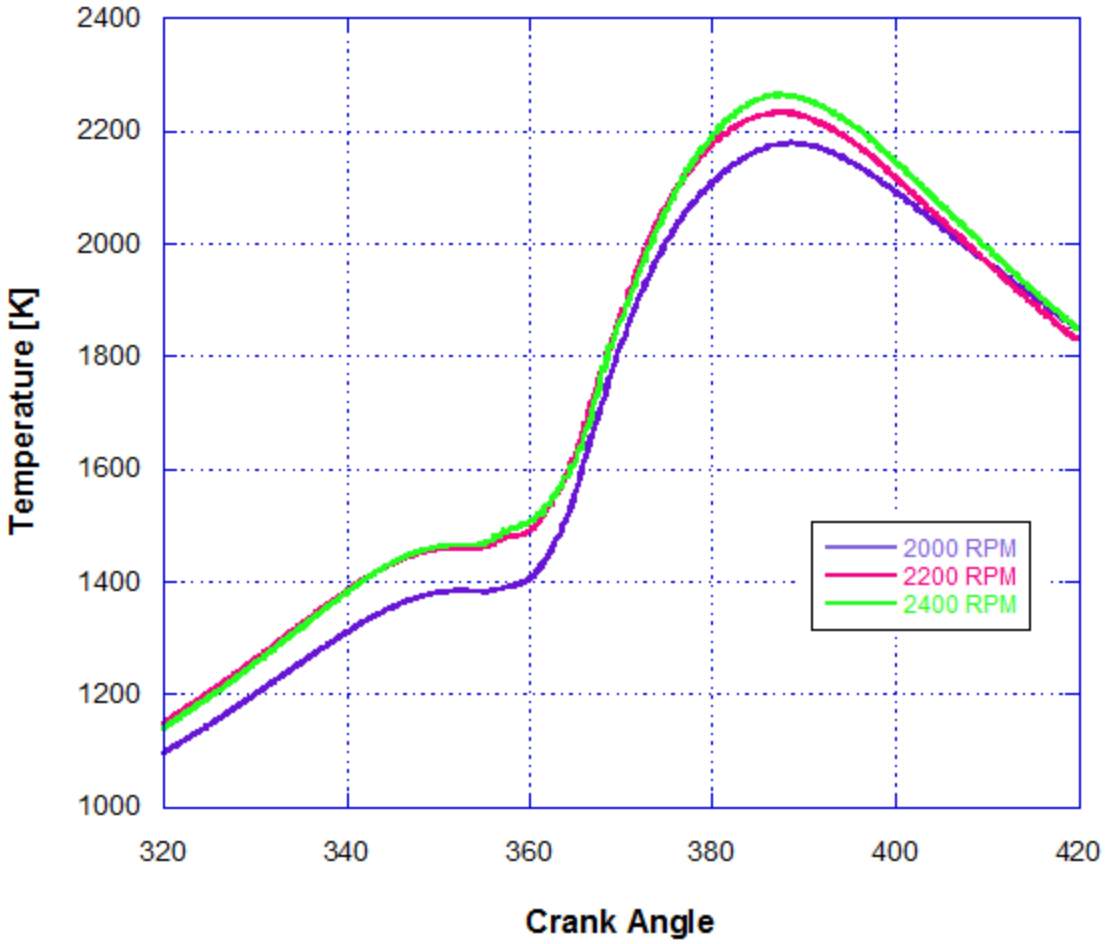

Figure 44 J50 Instantaneous Volume Averaged Gas Temperature

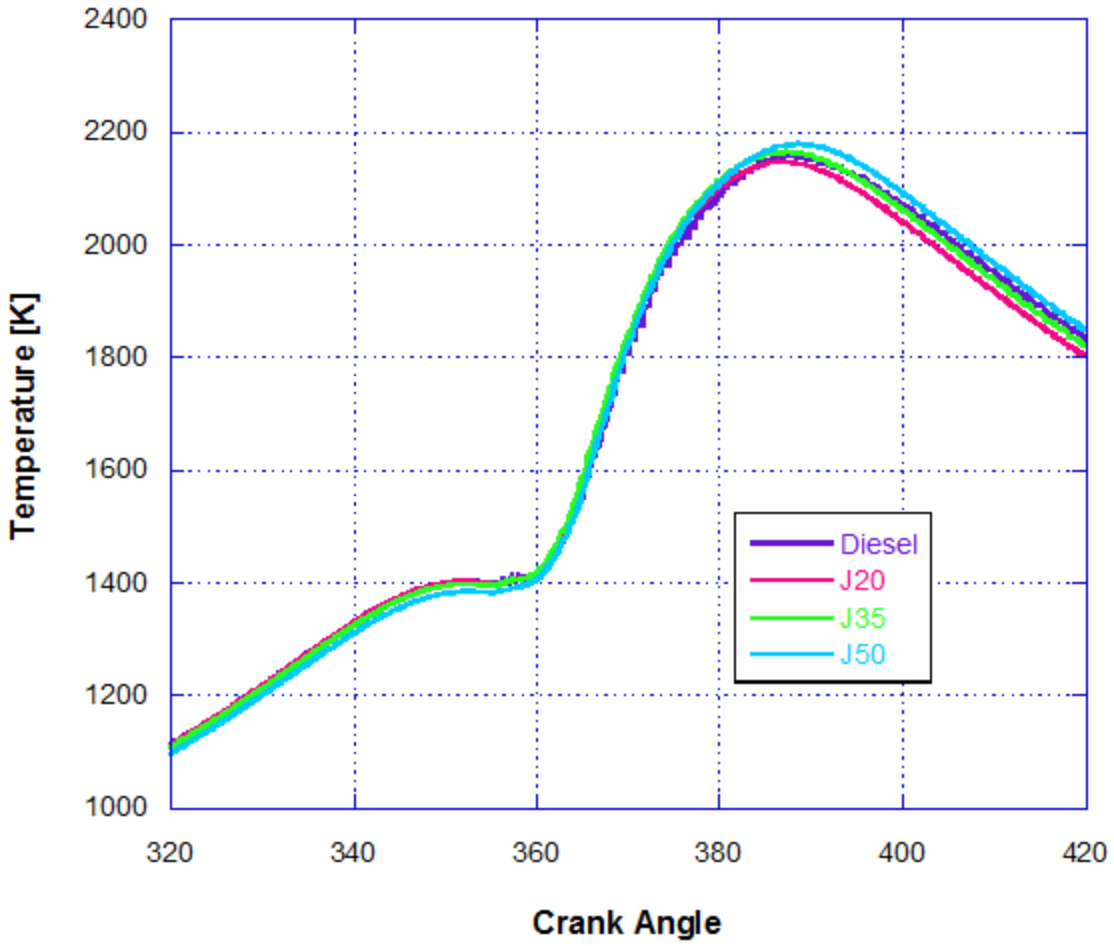

Figure 45 Instantaneous Volume Averaged Gas Temperature @ 2000 RPM

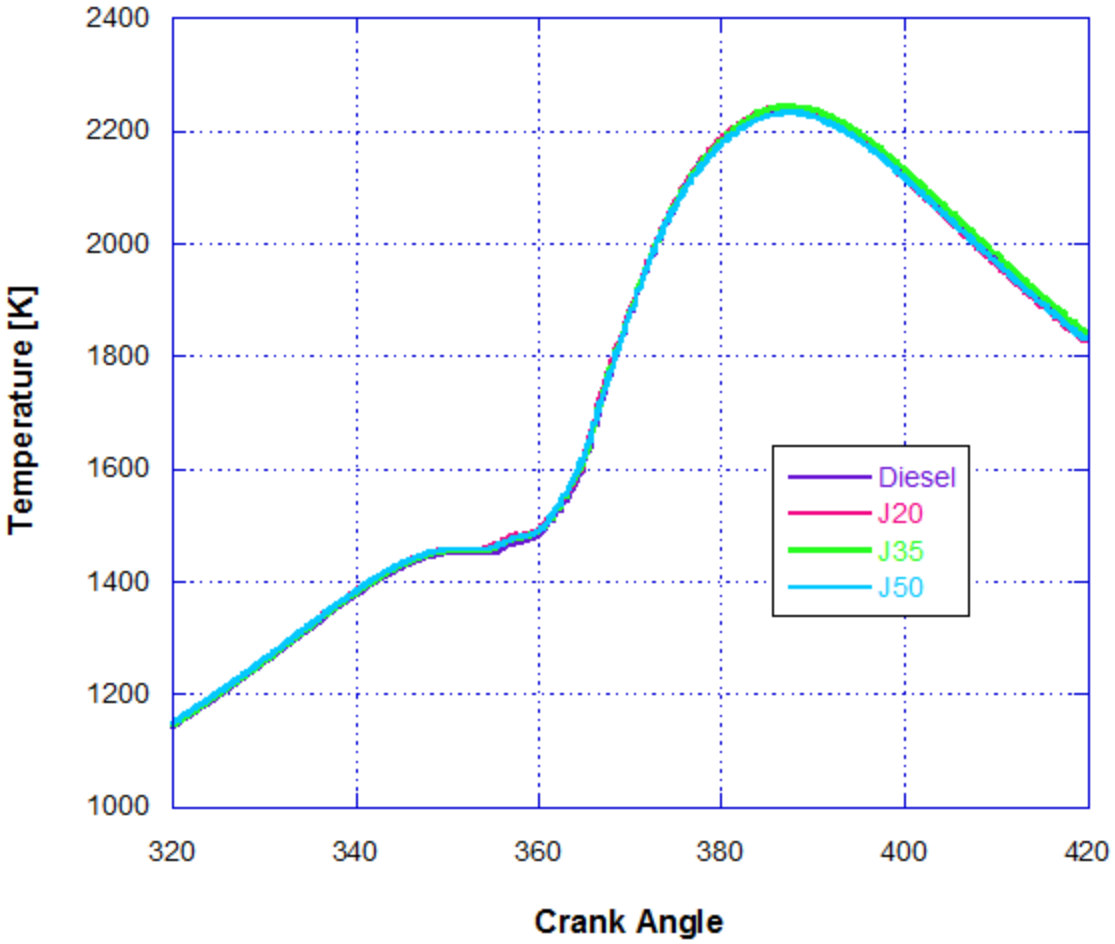

Figure 46 Instantaneous Volume Averaged Gas Temperature @ 2200 RPM

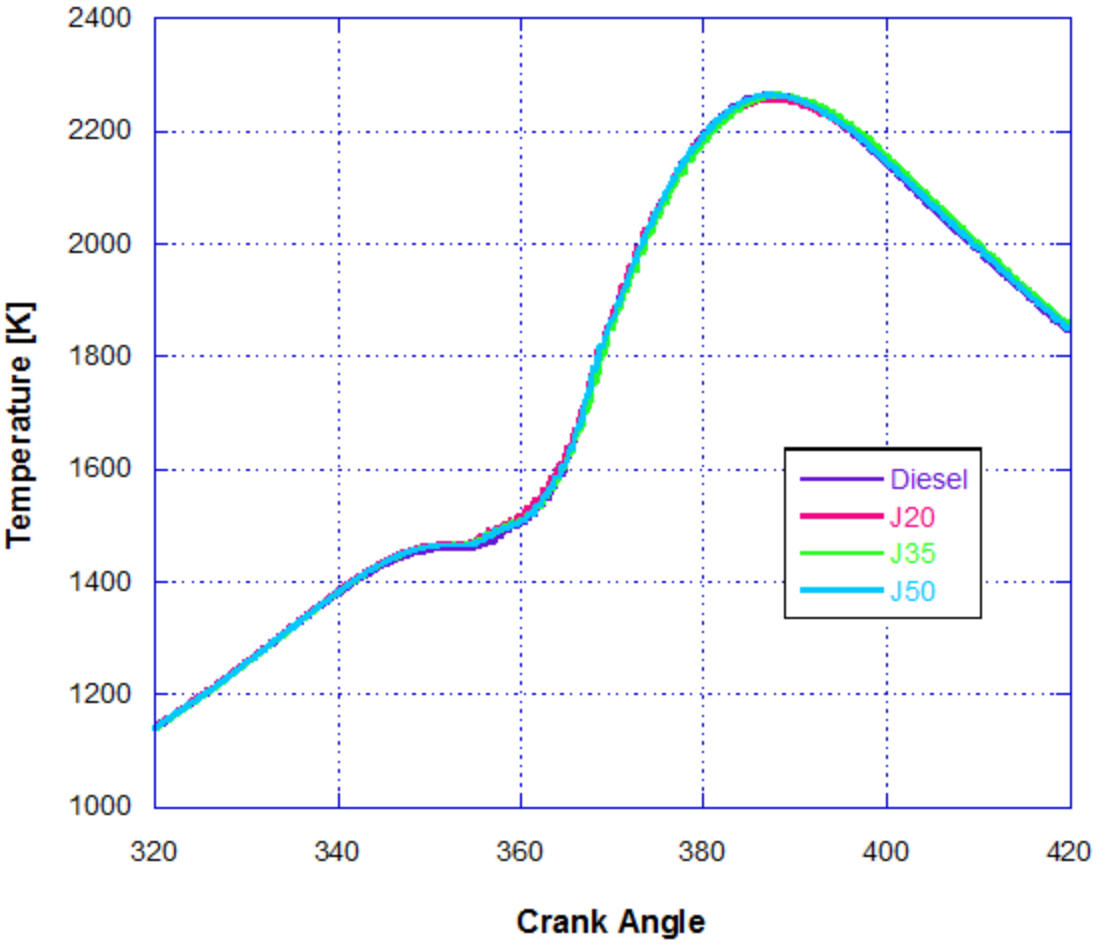

Figure 47 Instantaneous Volume Averaged Gas Temperature @ 2400 RPM

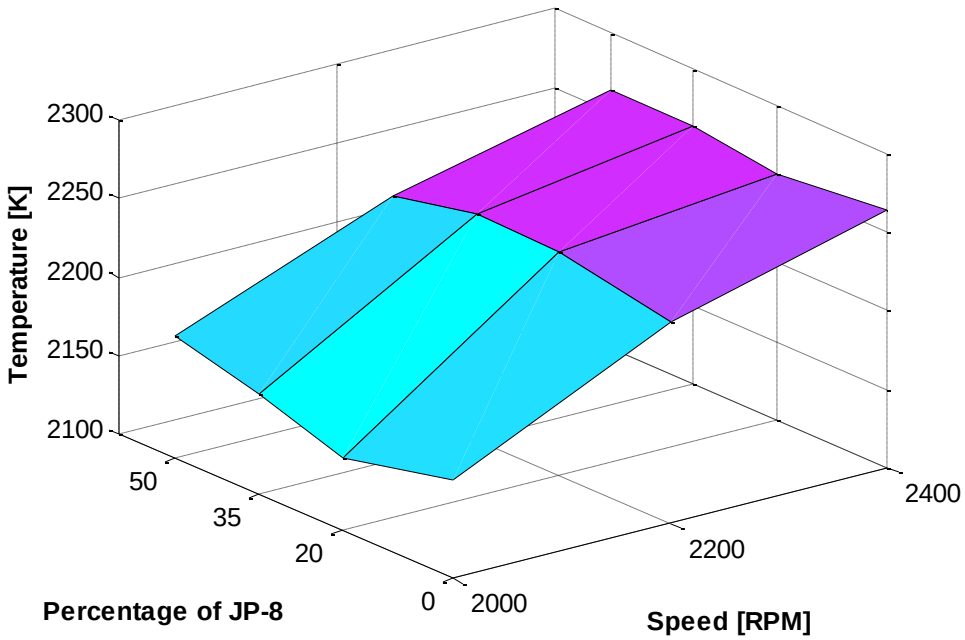

Figure 48 Maximum Instantaneous Volume Averaged Gas Temperature Surface Plot

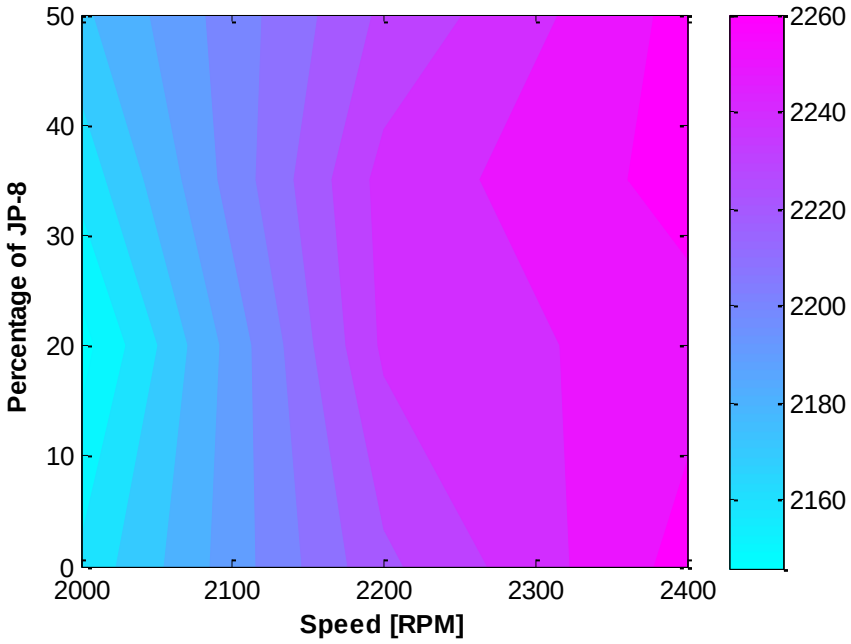

Figure 49 Maximum Instantaneous Volume Averaged Gas Temperature Contour Plot

The instantaneous volume averaged gas temperature shifts later in the crank angle as the JP-8 percentage increases, while retaining a higher temperature for a longer duration (0.21ms for

diesel vs J50 at 2000 rpm), with the position of the occurrence of the maximum temperature of combustion being slightly delayed when compared to diesel. When analyzing a particular fuel blend over the range of speeds tested it becomes noticeable the influence of the ram effect (discussed previously) at speeds beyond 2000 rpm. It is for this reason that the greatest temperature occurs at the highest speed (2400 rpm) and largest percentage of JP-8 (J50) tested.

Gas Density

The density of the gas in a SI engine explosion is four to seven times greater than that of the atmosphere with that amount being substantially higher for a diesel engine. The density of gases depends upon the temperature. The higher the temperature, the more the molecules are spread out and the lower the density. This density is of great importance in terms of its influence on spray characteristics, as the interactions that occur between fuel and air is the most important element in spray formation. For instance, if the air density is near zero, the jet of fuel mixture is unable to break up. By using the instantaneous volume averaged combustion temperature and pressure records from the varying fuel blends, the gas density throughout the cycle can be determine by using the equation shown below.

$$\rho = \frac{pressure(273)(1.3)}{Temperature}$$

With ρ representing the gas density; the gas density throughout the cycle is shown below in Figure 50.

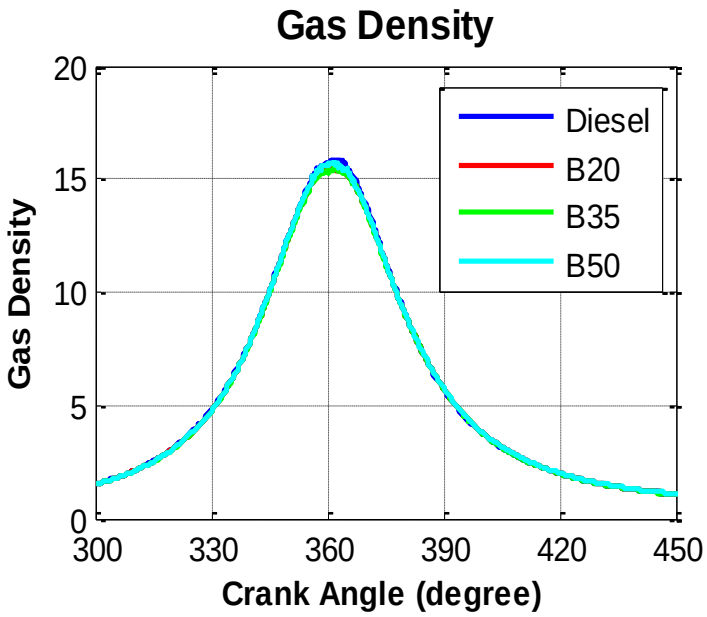

Figure 50 Gas Density

As can be seen from the figure above the gas density throughout the cycle for the varying fuel blends remains relatively constant. This trend remained true regardless of the speed tested.

The exhaust temperature was confirmed by direct measurement in the exhaust valve port shown below in Figure 51.

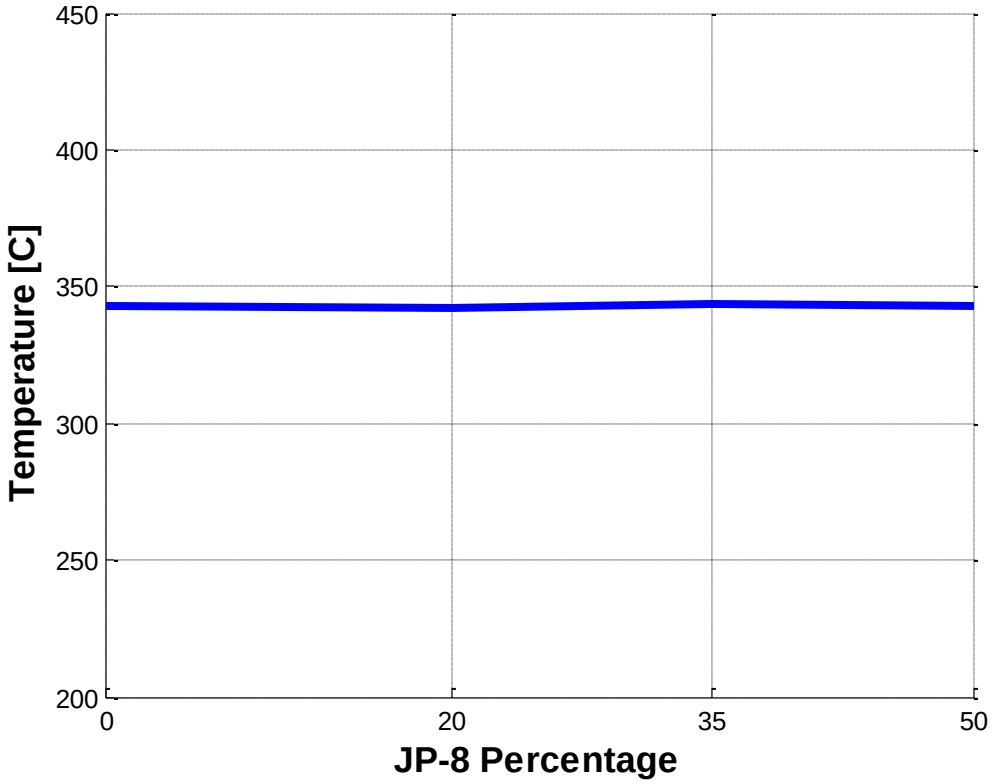

Figure 51 Average Exhaust Temperature

The exhaust temperatures have been relatively the same for all fuels at all loads. The exhaust temperature experienced no large gradient with increasing JP-8 content. When the engine was tested at 100 percent load and a speed of 2000 rpm, the exhaust temperature stayed in the range of 335-338 °C. The NO_x emissions depend on the maximum temperature of the gas in the cylinder and the exhaust gas temperature.

Apparent Heat Release

By rapid measurements of combustion chamber pressures at every 0.18 degrees (.01ms), it is possible to infer with high accuracy the work done on the piston, the increase in internal energy of the trapped mixture, the heat transfer occurring through the combustion chamber walls,

and to total these quantities to calculate the heat released during each increment of crankshaft rotation.

The gases inside the cylinders have different temperatures than the cylinder's walls resulting in heat transfer between the gases and the walls. Before combustion, heat flows from the walls to the gases; after combustion heat flows from the gases to the walls. The measured heat release rate is therefore the heat released by the fuel minus the heat transfer losses.

The dominant heat transfer mechanism in the typical engine is forced convection from the bulk gas to combustion chamber walls. In order to conduct this analysis several assumptions have been made. Despite the fact that combustion in an IC engine is heterogeneous, the contents of the combustion chamber are assumed to be homogeneous, and the system shall be considered a closed system with no mass transfer occurring across the boundaries.

In order to conduct the heat transfer calculations, the following assumptions have been made: the contents of the combustion chamber are assumed to be homogeneous, the system shall be considered a closed system with constant mass throughout the cycle (neglected mass changes due to fuel injection, crevice flow, and blow by), and the mixture inside the combustion chamber behaves as an ideal gas. The first law of thermodynamics, an expression of the principle of conservation of energy, states that energy cannot be created or destroyed it can only change forms (a, a, & Yang, 2005). Although in many processes the energy transformation occurs in the form of heat to the environment. When dealing with problems involving heat flow, work, and efficiency in a heat engine it is vital to remember that all real engines lose some heat to their surroundings. It is convenient for this purpose to focus on changes in the internal energy (U) and

assume there occurrence due to a combination of heat (Q) added to the system and work done by the system (W). Based on this principle, the energy associated with a closed system is defined as:

$$\partial \mathrm{Q} - \partial \mathrm{W} = \mathrm{dU}$$

However, based on the indicated diagram it can easily be observed that,

$$\partial \mathrm{W} = \mathrm{PdV}$$

It can also be noted that the following relation for the internal energy of the system is,

$$\mathrm{dU} = \mathrm{mC_v dT}$$

These can be transformed through the use of the Ideal gas law, so that the following equations can be able to be obtained:

$$mdT = \frac{1}{R}(PdV + VdP)$$

$$dU = \frac{c_v}{R}(PdV + VdP)$$

The volume in the cylinders was never measured, but the dimensions of the engine are known. Using the connecting rod length, the radius of the cylinder and the compression ratio, the volume inside the combustion chamber can be related to the crank angle using the equation shown below:

$$V = V_c\left(1 + 0.5(r-1)\left(R + cos(\theta - \pi) - \left(R^2 - \left(sin(\theta - \pi)\right)^2\right)^{.5}\right)\right)$$

By substituting these equivalent equations into the conservation of energy and simplifying the following equation is obtained:

$$\frac{\partial Q}{d\theta} = \frac{1}{\gamma - 1} V \frac{dP}{d\theta} + \frac{\gamma}{\gamma - 1} P \frac{dV}{d\theta}$$

With γ being the ratio of specific heats, pressure, *p*, is the in-cylinder pressure and *V* is the volume. Because all of the data triggered every crank angle degree, the differential volume and pressure values can be found using the finite difference approximation. The resulting apparent heat release rate is shown below:

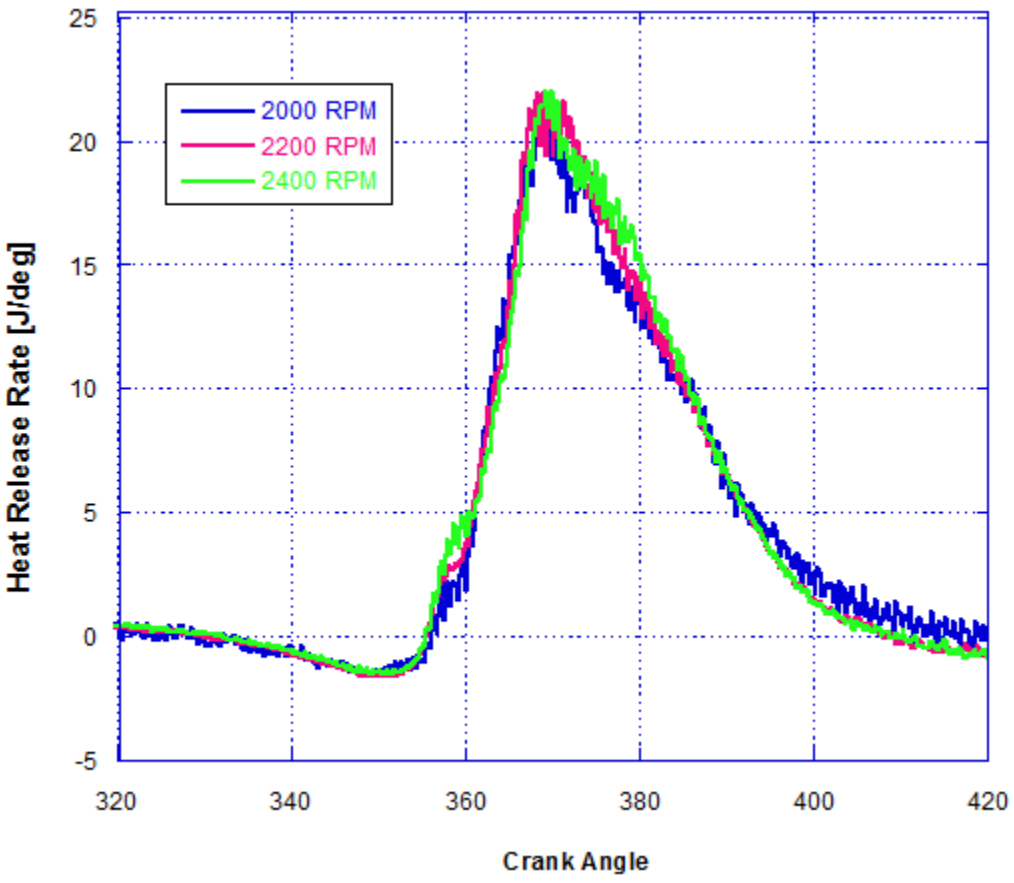

Figure 52 Diesel Apparent Heat Release

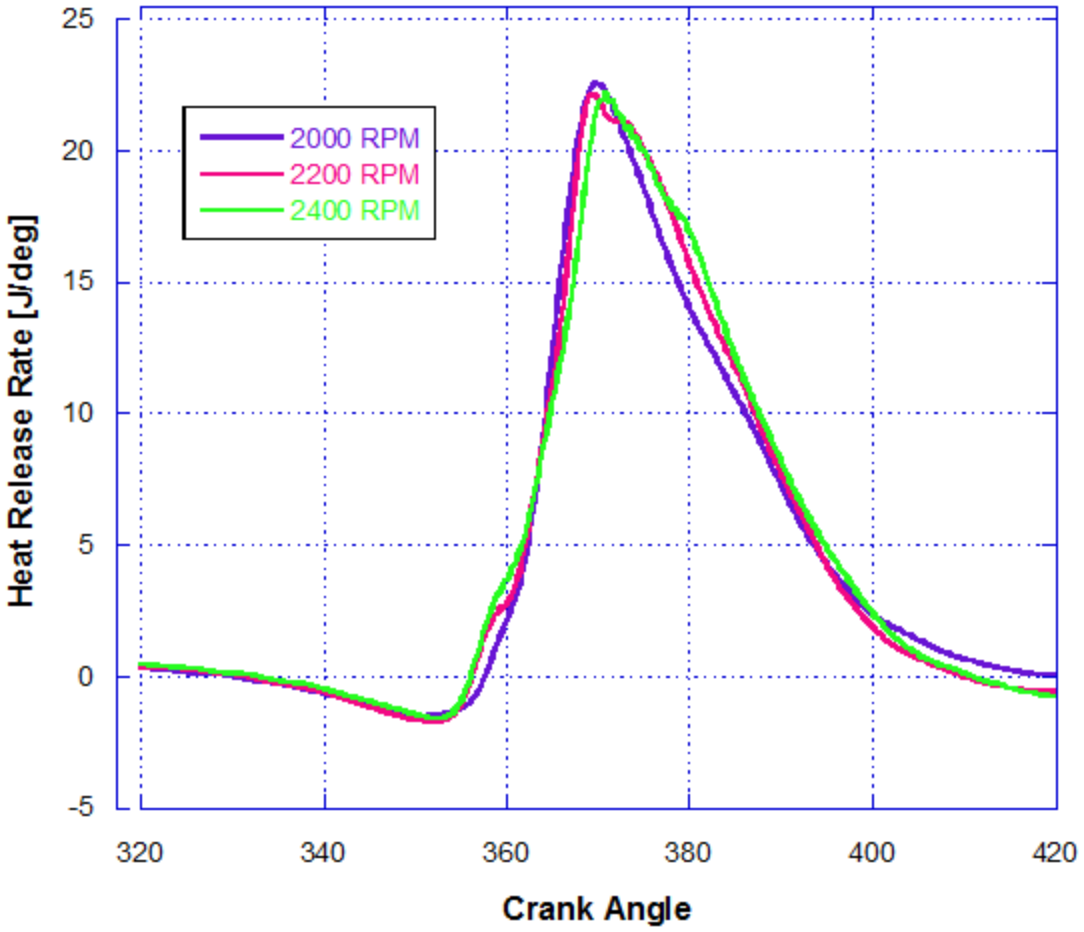

Figure 53 J20 Apparent Heat Release

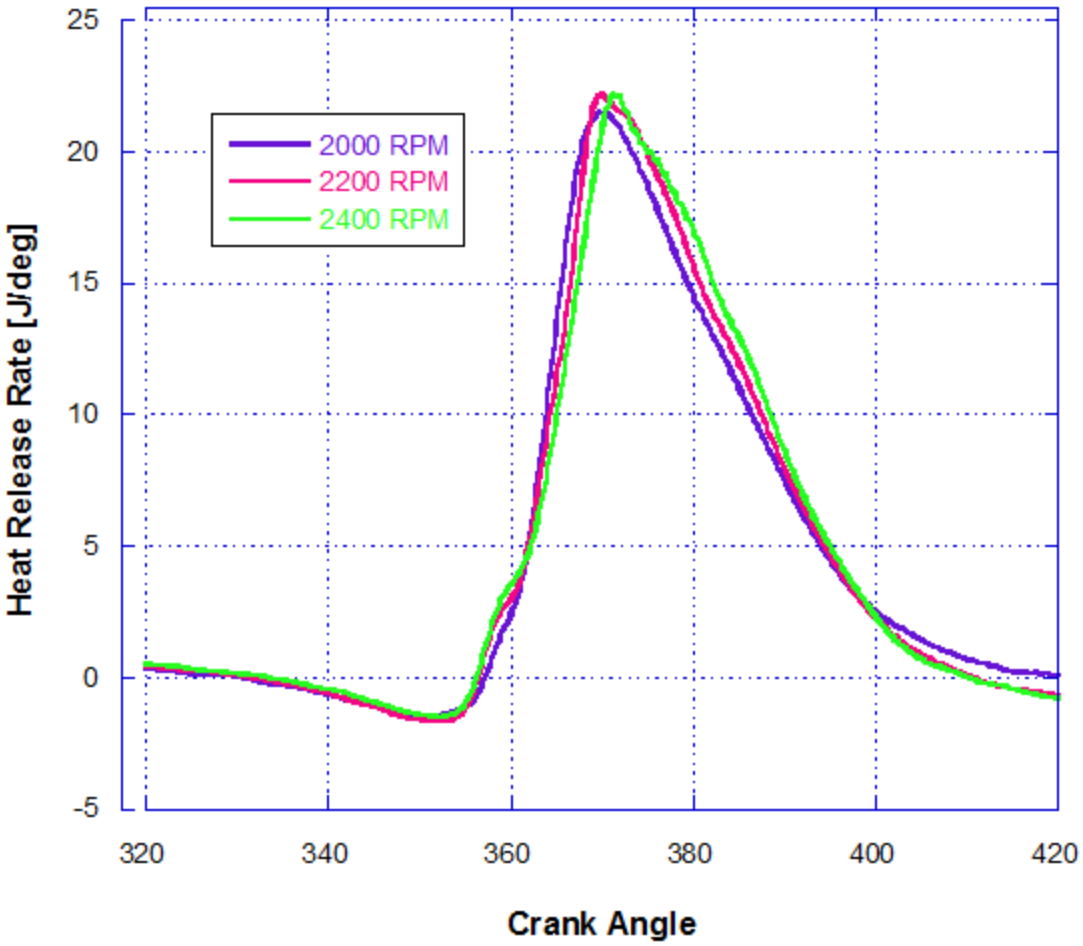

Figure 54 J35 Apparent Heat Release

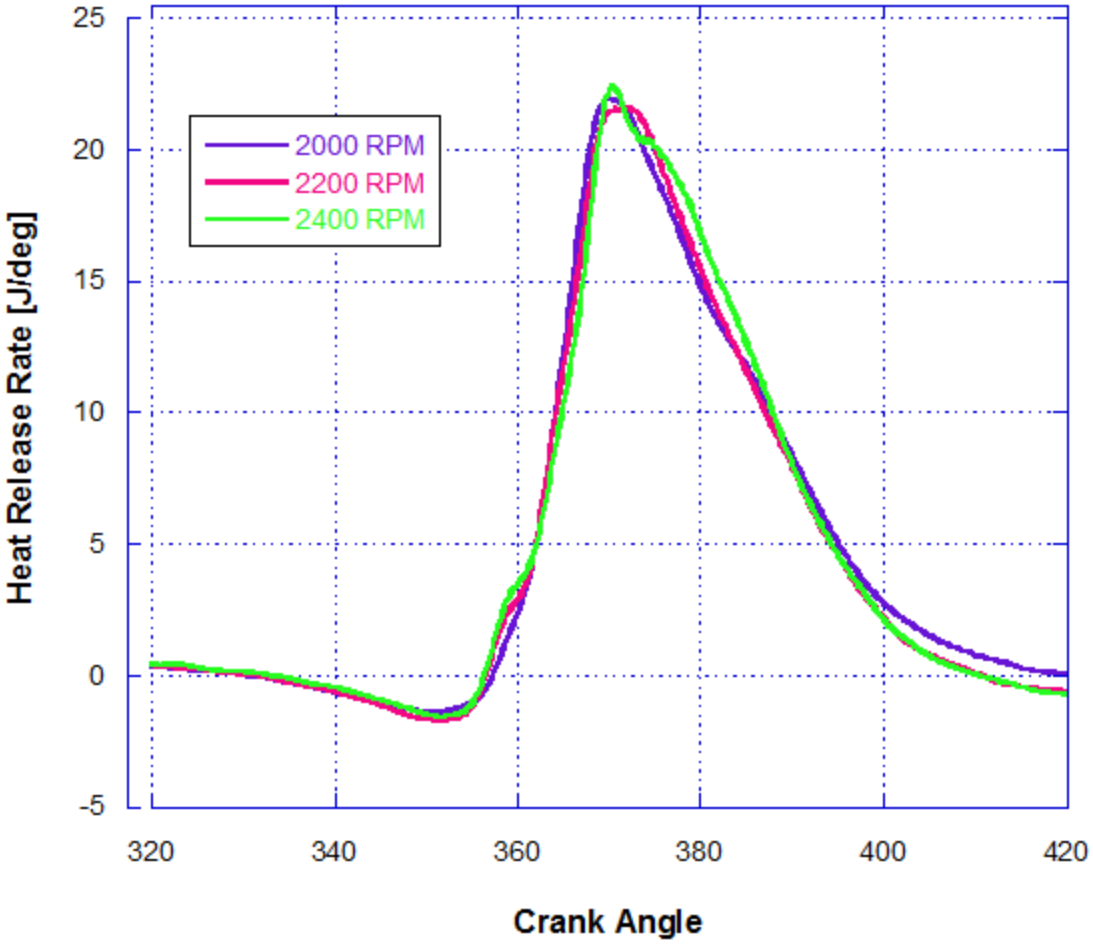

Figure 55 J50 Apparent Heat Release

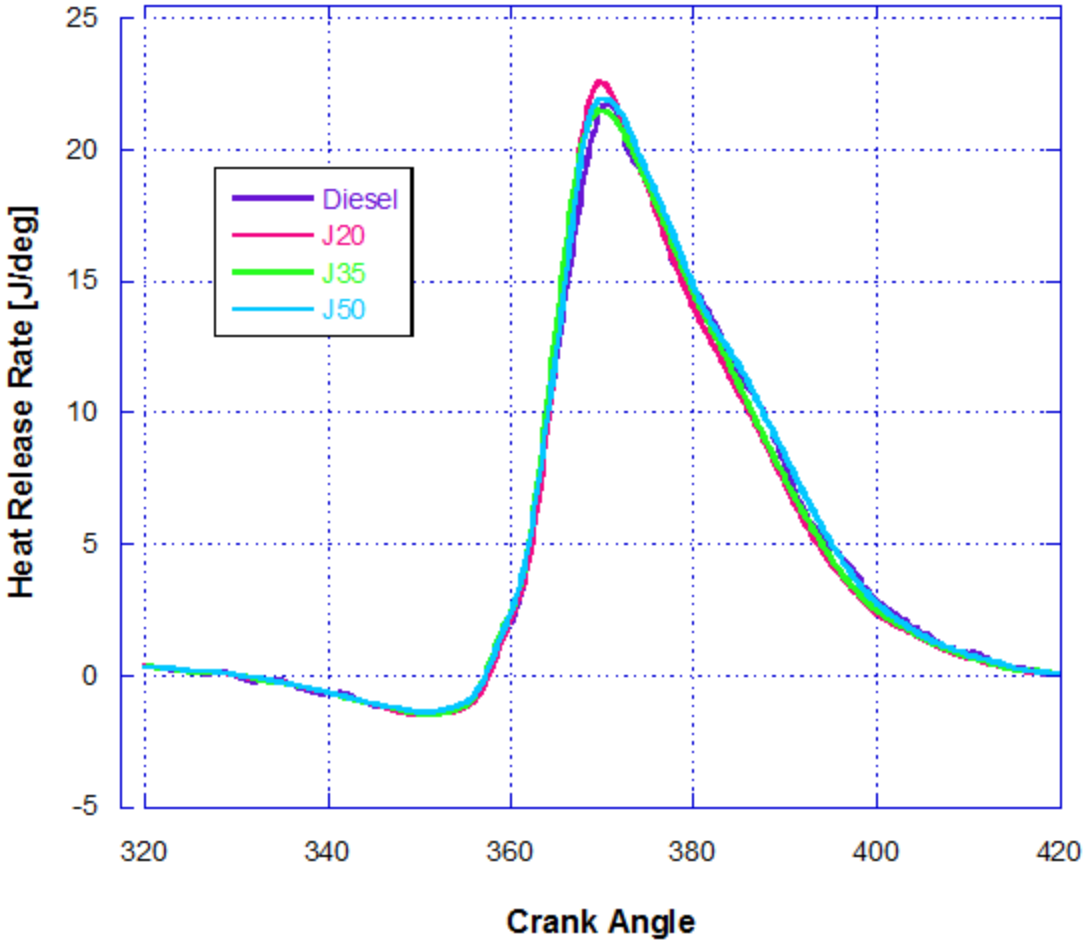

Figure 56 Apparent Heat Release @ 2000 RPM (4.78 BMEP)

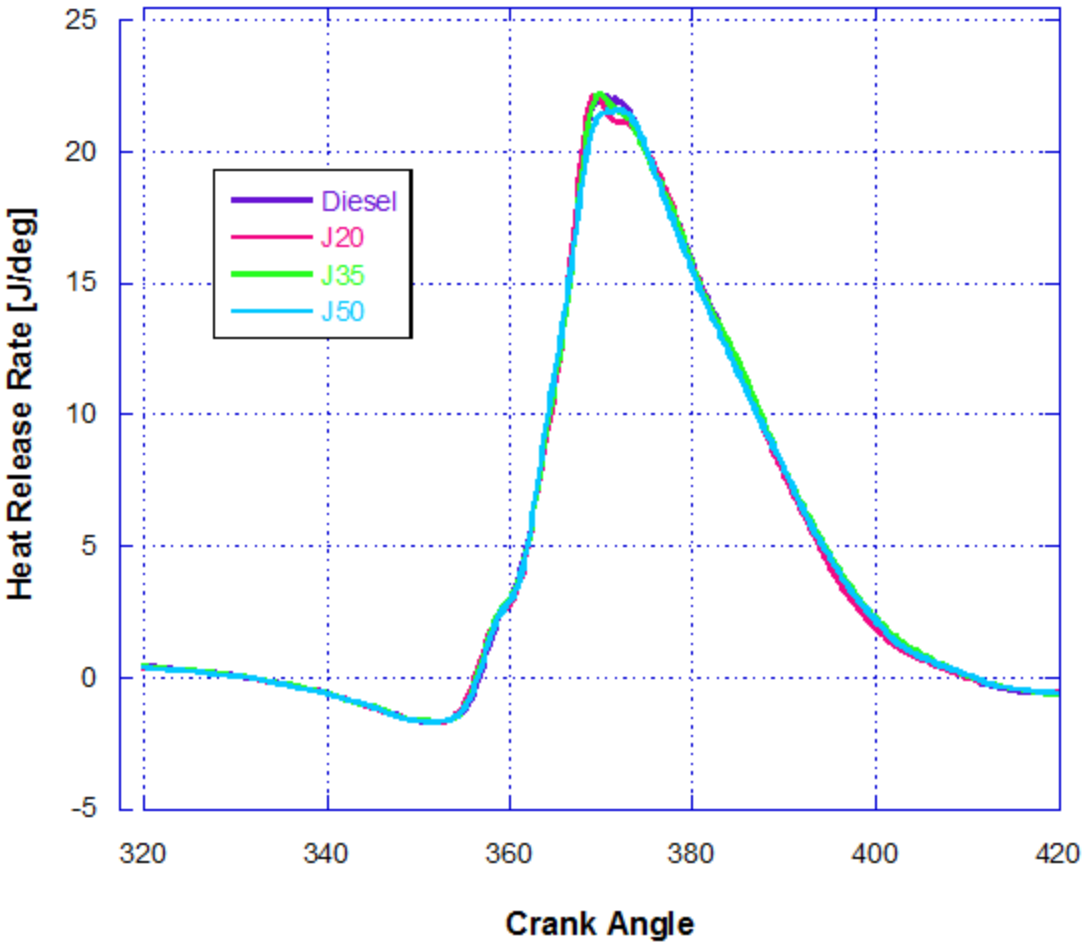

Figure 57 Apparent Heat Release @ 2200 RPM (4.78 BMEP)

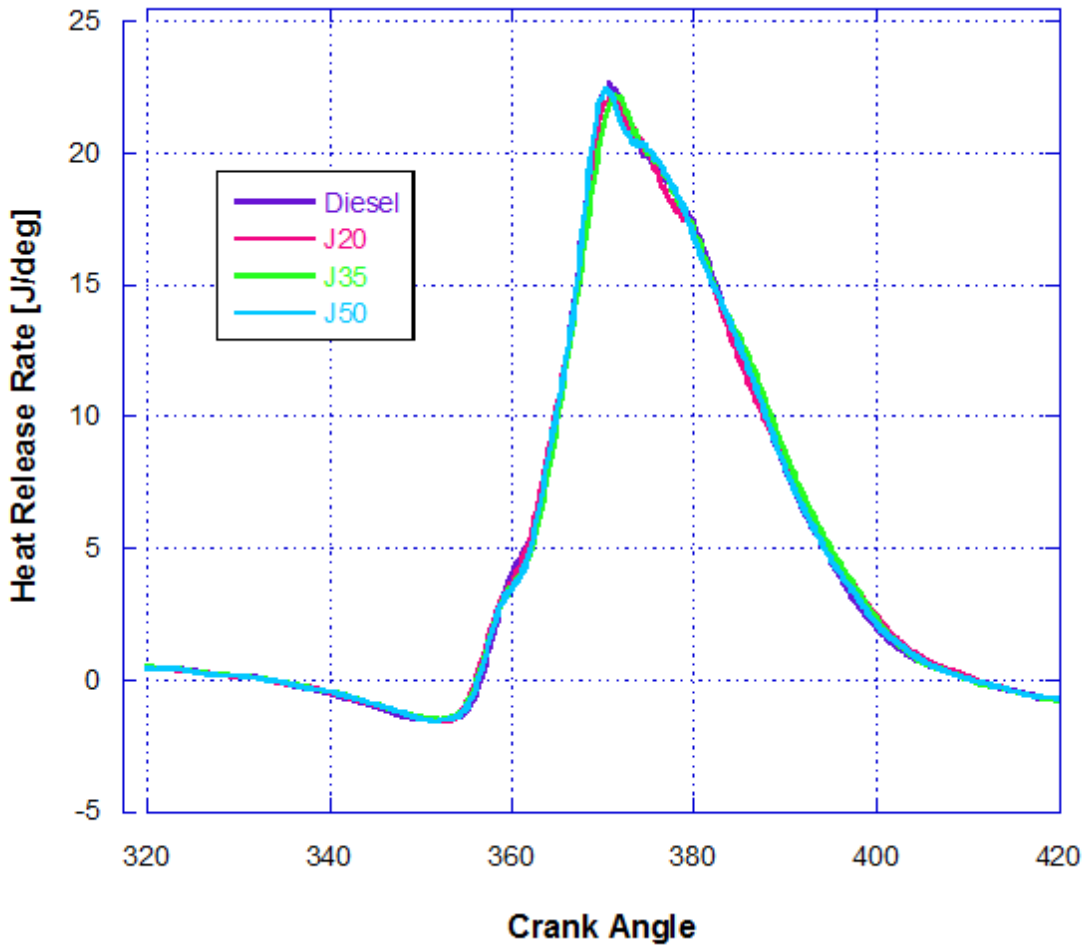

Figure 58 Apparent Heat Release @ 2400 RPM (4.78 BMEP)

The heat release rate generated from these equations is not a direct measure of the heat released by the fuel. Instead, this equation generates the apparent or net heat release. Because the gases inside the cylinders have different temperatures than the cylinder's walls, there is heat transfer between the gases and the walls. Before combustion, heat flows from the walls to the gases; after combustion heat flows from the gases to the walls. The measured heat release rate is therefore the heat released by the fuel minus the heat transfer losses. The peak that occurs in the heat release rate shortly after the start of injection is due by part to the occurrence of the early maximum in turbulent kinetic energy. Approximately at the end of injection a second distinct

bend can be observed after which the heat release rate decreases rapidly, with this bend being caused by the reduction of available fuel mass once the injection process has ceased.

When the curve is followed from left to right, the curves denotes a negative heat release demonstrating that the fuel injected is absorbing heat and is undergoing vaporization after which, the sudden occurring rise represents the heat release related to the combustion of the fuel. Based on the predicted vapor fraction at ignition of JP-8 being 15% to 30% higher in comparison to that of diesel fuel no.2 it was anticipated that JP-8 would yield both higher premixed phase heat release and pressure rise rate (Schihl, Hoogterp, Pangilinan, Schwarz, & Bryzik, 2006). However, based on the results obtained it can be noted that this is not the case, in fact the heat release for all blends of JP-8 and diesel, are relatively the same. The onset of significant heat release being relatively the same for all blends suggests that the blends would posses' similar ignition delays. Due to the differences in viscosity and density of the varying fuel blends it would be expected that the higher content JP-8 blends would experience higher rapid gas expansion associated with an increased premixed burn leading to regions of high shear stress and ultimately an increase in turbulence and turbulent mixing rates. However, in the absence of combustion induced phenomena, the amount of fuel prepared for combustion through mixing induced by injection and air flow was found to be about equal for all blends despite the differences in density and the employment of a mechanical injection system. This assumption in conjunction with the results of the apparent heat release leads researches to conclude that increased mixing induced by the premixed combustion does not occur during this instant.

Ignition Delay

In diesel engines, estimation of ignition delay is of great importance because of its effect on start ability, noise and formation of NOx. The ignition delay time can be defined as the period

between the formation of a combustible mixture, as by the start of injection of fuel into an oxidizing environment, and onset of the rapid reaction phase leading to the rise of pressure and temperature to autoignition (Cosgrove, Church, & Pryor, 1987), with autoignition being defined as the moment when the combustion generated heat has compensated for the energy required to vaporize the fuel. This ignition delay period consists of two basic components being a physical delay, wherein atomization, vaporization and mixing of air fuel occurs and the second being due to a chemical delay attributed to pre-combustion reactions., with both the physical and the chemical delays occur simultaneously. Reduction in ignition delay is said to hold the key for solving emission and noise problems. Higher temperature at the beginning of injection by increased compression-ratio reduces the delay period substantially. The ignition delay has a heavy dependence on the cetane number of a fuel assuming that kinetics dominates the ignition delay processes displaying a 30% average increase in the ignition delay period for a decrease in the cetane number of ten (Fernandes, Fuschetto, Filipi, Assanis, & McKee, 2007). This is of particular concern when dealing with JP-8 as the cetane number can radically differ depending on the supply source, due to the fact that the military specification for JP-8 fuel (MIL-DTL-83133) does not contain a specification for the cetane number. According to the Defense Energy Support Center the cetane index of JP-8 ranges from 29 to 51 with a mean of 43.9 and a variance of 13.69. Although it is important to recall that the cetane index is a not a precise indicator of ignition quality, it only severs to provide a sense of cetane number. Figure 59 displays the information necessary to calculate the ignition delay for the tested fuel.

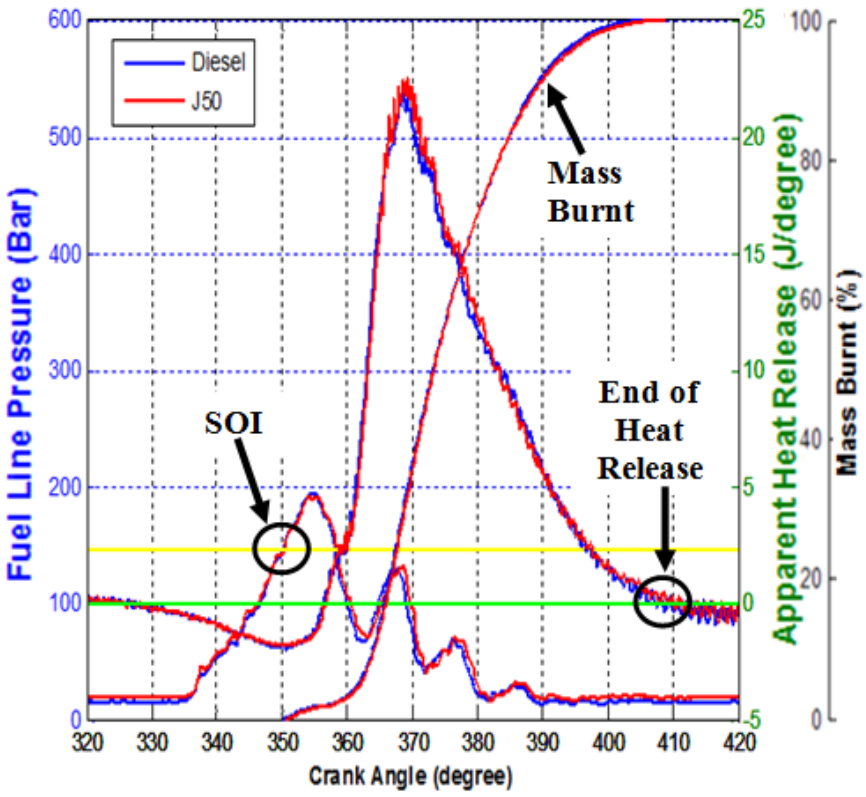

Figure 59 Ignition Delay Comparison

In order to determine the ignition delay, the apparent heat release is integrated over the interval from the start of injection to the moment of autoignition. With the start of injection (SOI) being defined as the moment the fuel line reaches a pressure of 147 bar at which time the fuel is injected. The moment of autoignition being the point after combustion in which the apparent heat release approaches zero (ceases to release heat). The zero crossing is determined by interpolating the cumulative heat release to the nearest 0.18 CAD. The ignition delay is defined as the duration from the crank angle at which the SOI occurred to the crank angle at which 10% of the total mass was burnt (Soloiu, Covington, Nelson, & Lewis, 2011). The quantification of these parameters is extremely useful in characterizing combustion chamber and ignition system

performance. The figure below gives a visual reference to the start of injection in relation to the position of the piston in terms of volume and the percent of mass burnt in the cylinder.

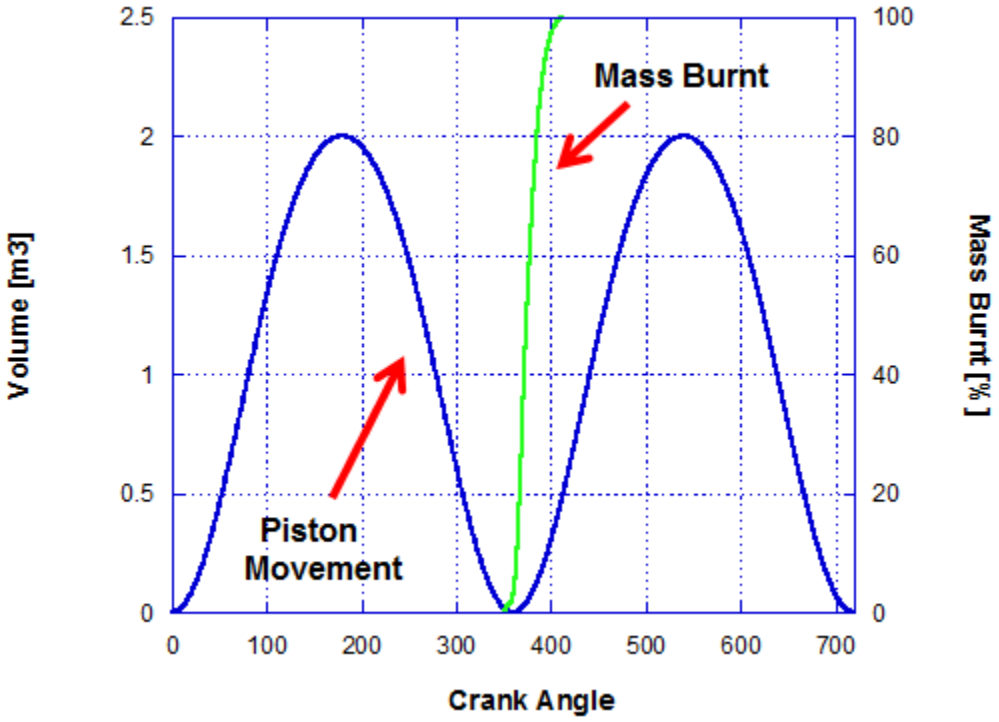

Figure 60 Mass Burnt in Relation to Piston Position

Based on this information the ignition delay was determined and found that the ignition delay remains relatively constant at approximately 1.02-1.06 ms in spite of the amount of JP-8 introduced into the system.

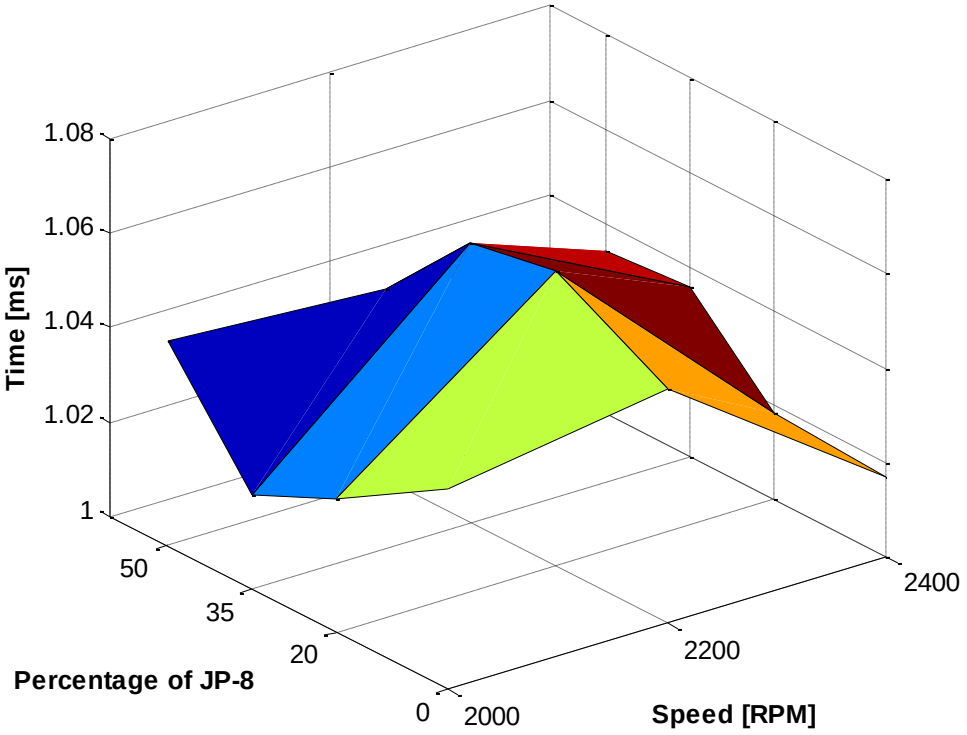

Figure 61 Ignition Delay Surface Plot

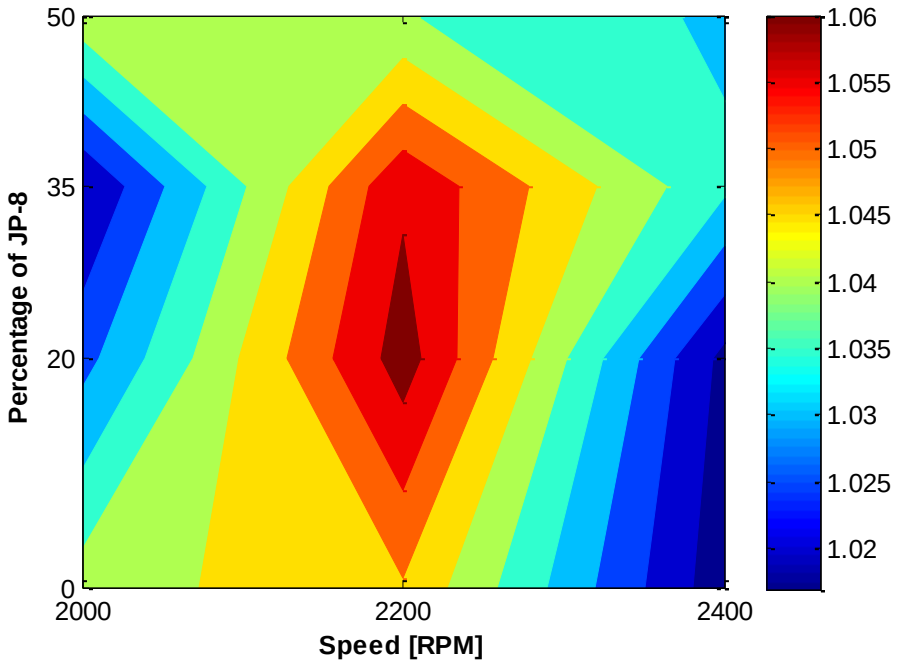

Figure 62 Ignition Delay Contour Plot

The ignition delay definition employed for this study was found to give results closely comparable to ignition delays based on pressure recovery.

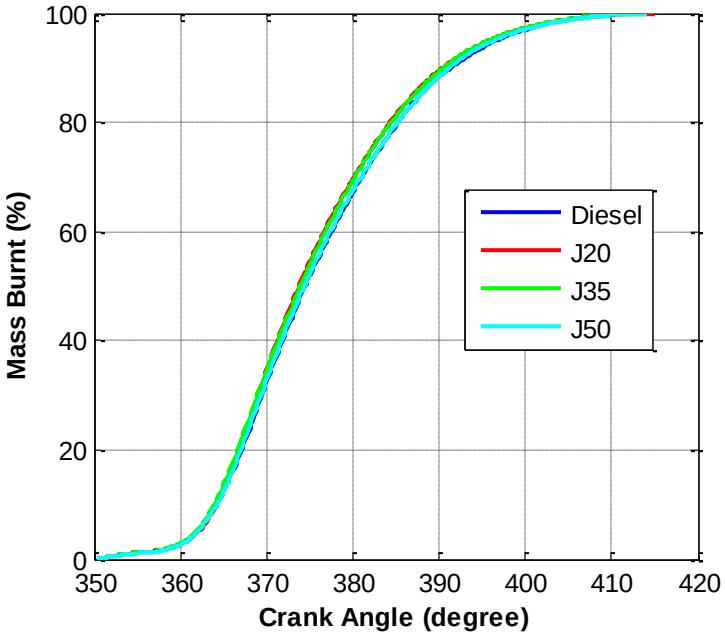

Figure 63 Mass Burnt at 2000 RPM

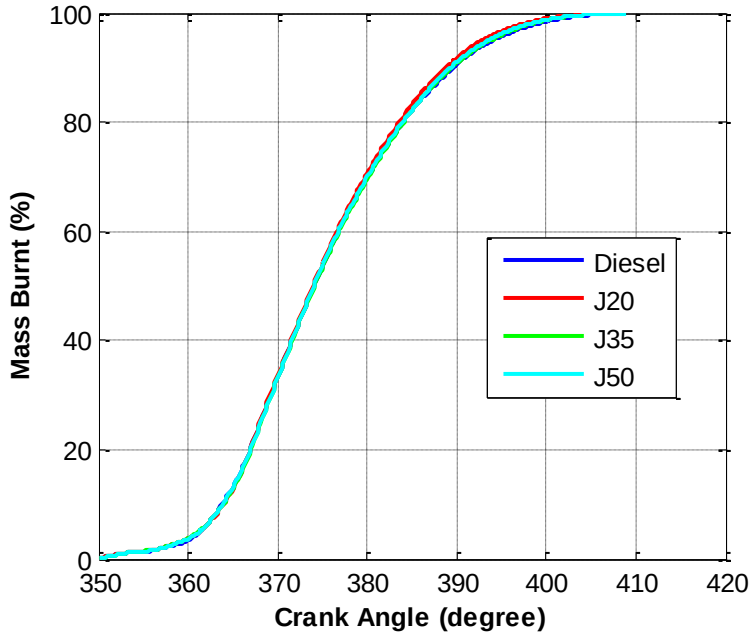

Figure 64 Mass Burnt at 2200 RPM

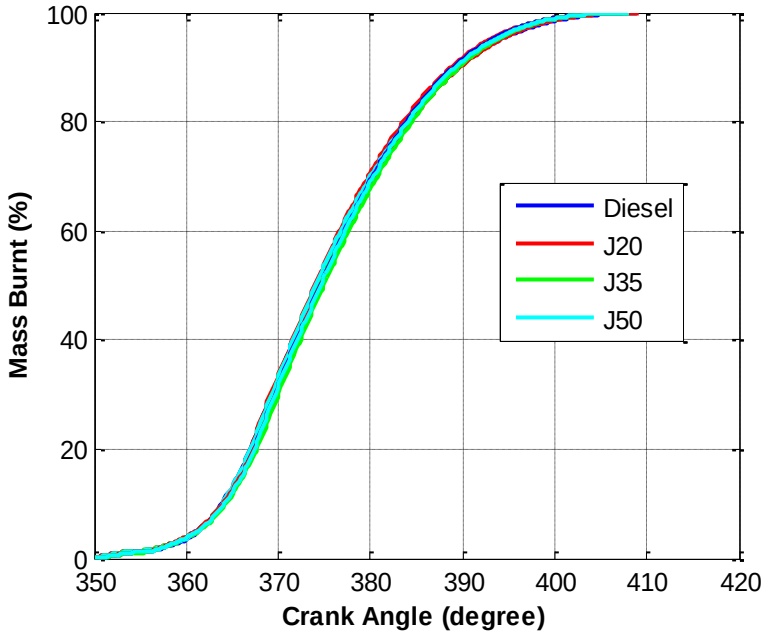

Figure 65 Mass Burnt at 2400 RPM

When comparing the in-cylinder mass burnt percentages for the various fuel blends with the speed and load being kept constant, it can be seen that the rate at which the mass burnt curves

proceed are relatively similar for all blends at each speed tested. However, a difference in the rate at which the curves proceed can be observed in relation to a change in speed with the percentage of JP-8 in the fuel being kept constant (Figure 66-Figure 69).

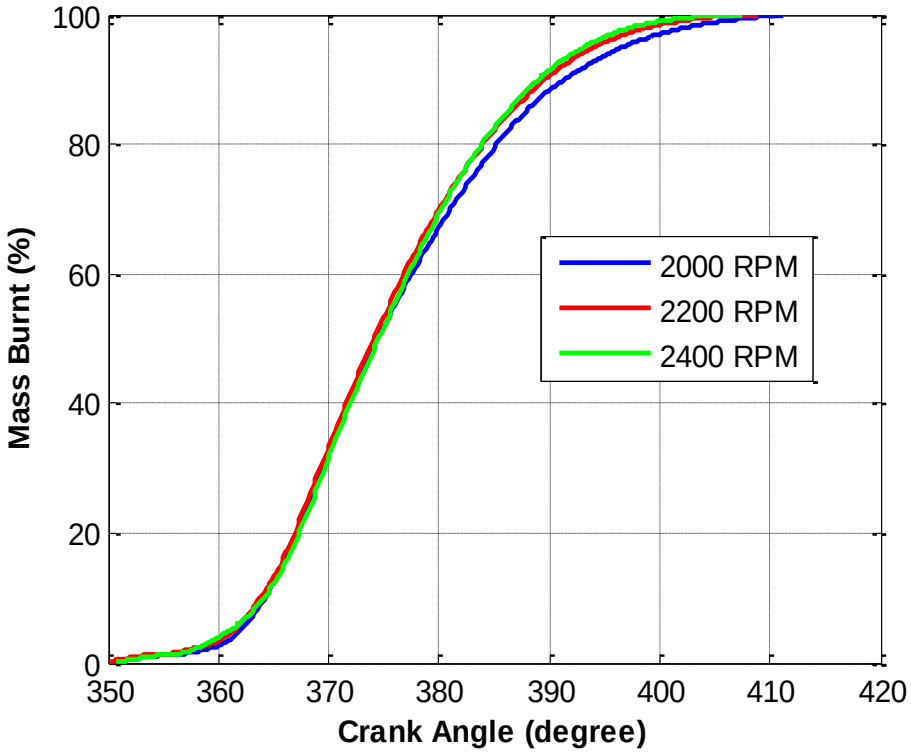

Figure 66 Diesel Mass Burnt

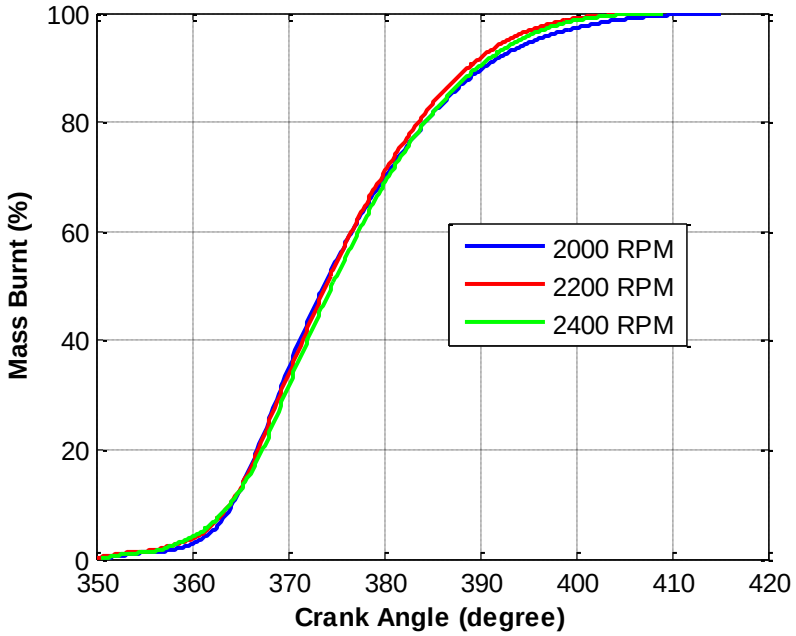

Figure 67 J20 Mass Burnt

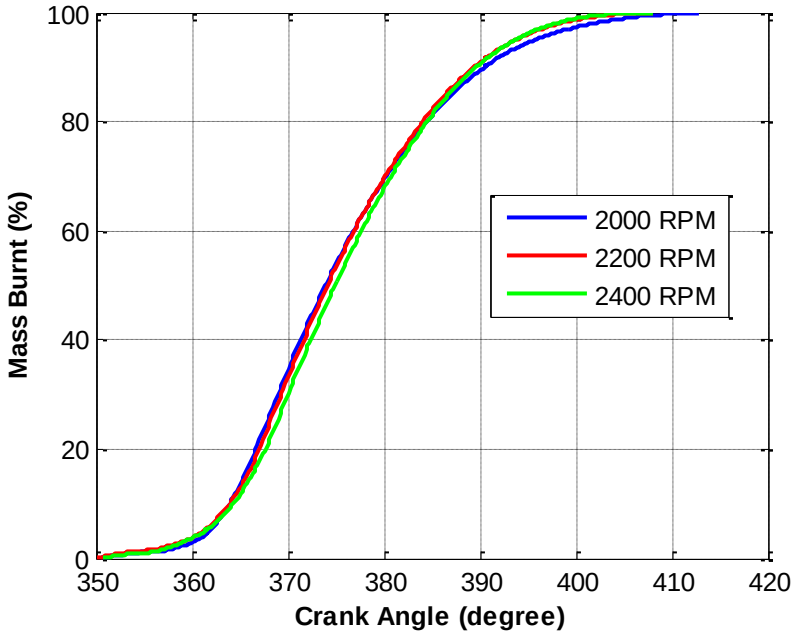

Figure 68 J35 Mass Burnt

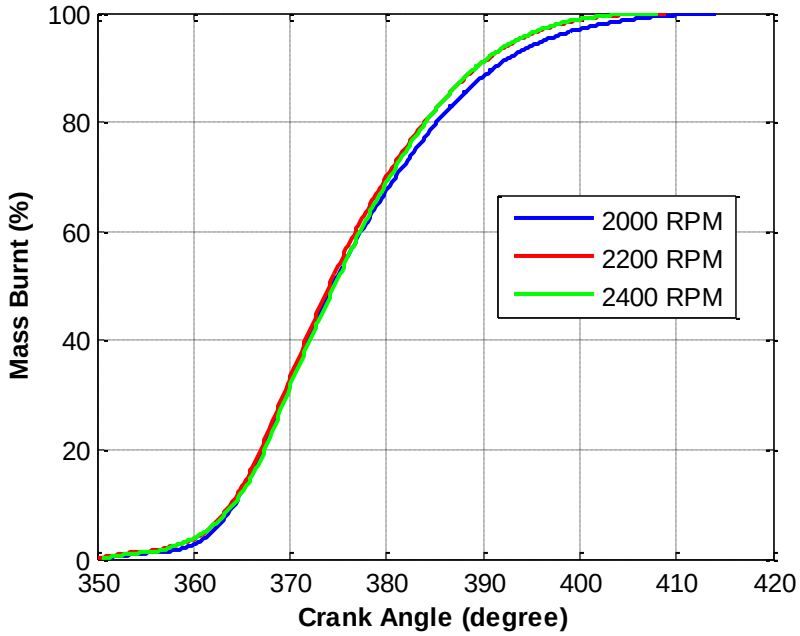

Figure 69 J50 Mass Burnt

Based on the figures shown above, the rate at which the mass burnt curves proceed increased in relation to speed, with the J50 blend displaying the most prominent variation between speeds.

Reynolds Number

The Reynolds number is a dimensionless number that is used to characterize different flow regimes. It can be described as the ratio between two forces, the inertial force which causes movement, and the viscous force which resists the movement of the fluid. In the type of engine usually operated by using JP-8 as its primary fuel source, a jet engine, the source of oxidant is compressed air and the thrust is generated through the formation of combustion products with an increase in the volume and temperature of the air/fuel mixture. Recall that in a diesel engine, liquid fuel droplets are injected into the combustion chamber during the compression stroke, which raises the temperature of the intake air to the ignition temperature of the fuel, and reaction takes place between the vapor phase and the oxygen content of the entrained air with the use of

spark due to the characteristics of the fuel. By increasing the Reynolds number the tendency of the fuel jet to break up into small elements is also increased. Therefore, by using the gas density and viscosity of the varying fuel blends the following figure is able to characterize the flow the fuel throughout the duration of the cycle.

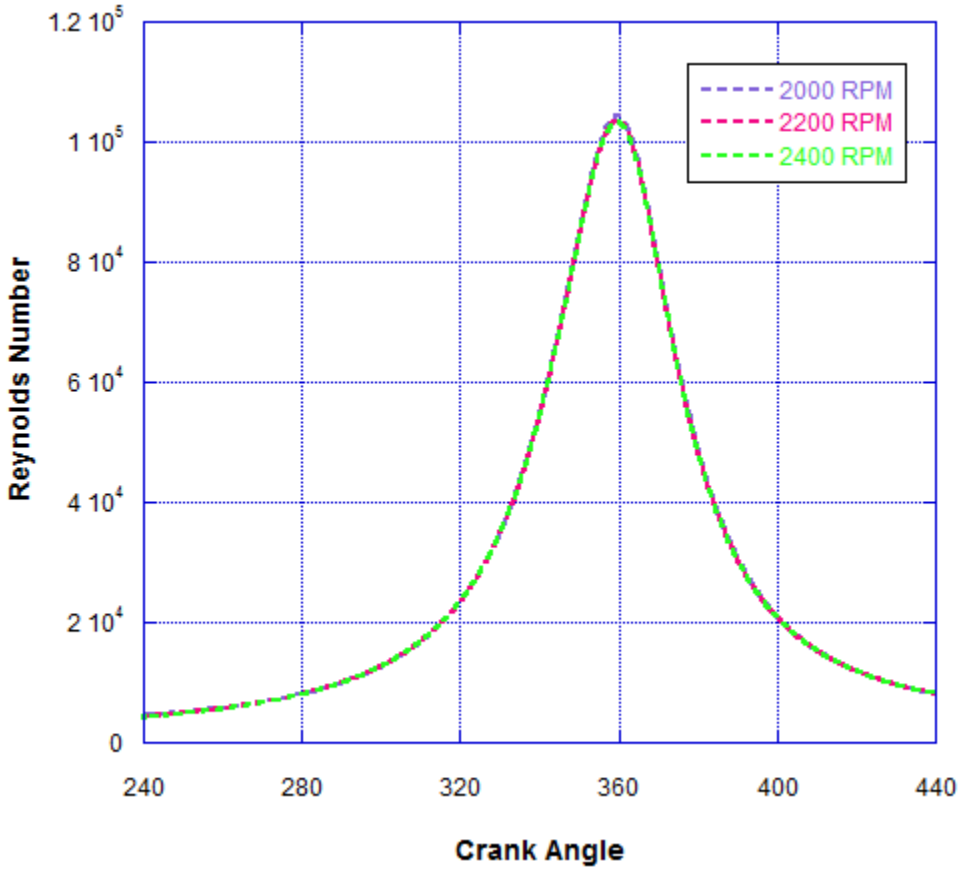

Figure 70 Diesel Reynolds Number Comparison

The Reynolds Numbers of throughout the cycle remains relatively the same for the increasing percentage of JP-8 introduced into the fuel mixture. The flow is considered turbulent for a Reynolds Number greater than 2000. In the laminar flow regimes, the reactants are pre-mixed before entering the combustion volume. In the turbulent flow regimes the velocity is considerably higher and the reactants are separately introduced into the combustion volume with

the extent of the reaction depending on the mixing through the inter-diffusion of the fuel and air streams, while the droplet/air mixture undergoes combustion in which the droplets are consumed by oxidation within the burning mixture. This depends on the vaporization of the droplets and the diffusion of the vapor into the surrounding atmosphere where combustion occurs. Based on the figure above all of the varying blends of fuel tested become turbulent during combustion as is expected. This result confirms the initial statement and provided verification that the engine is capable of handling the lower viscosities of the JP-8/diesel fuel mixtures. In order to modify the Reynolds number the variable of fuel line pressure directly upstream from the nozzle can be changed which results in a change in the injection velocity.

Heat Flux

There exists a direct relationship between heat, loss, and gas density in an explosion type vessel, which is heavily dependent upon two factors, radiation and direct surface loss due to convection and conduction. Typically, when JP-8 is used in a jet engine, small carbonaceous particles are formed early in the combustion and continuously burn until they are completely consumed under suitable conditions. However, these particles can become incandescent under high pressure and temperature conditions leading to an increase in heat available to be transferred to the cylinder wall through radiation. This becomes an issue in terms of wall temperature, where a high temperature could lead to premature engine wear. Therefore, special attention was placed upon evaluation of the heat flux of JP-8 in a diesel engine, due to convection and radiation.

Recall that heat transfer occurs in the form of thin layers that occur in the location between gases in the cylinder and the solid walls. These layers represent thermal boundaries, over which the temperature of the gases exhibits a substantial change with the largest gradient

occurring at the wall. Formally the heat transfer is given by this gradient and the thermal conductivity of the gases. However, since the gradient is dependent upon the transfer properties for energy in the outer part of the boundary layer it becomes influenced by the velocities through the turbulent transport (random convection). The presence of the walls also has a profound influence on the momentum distribution in the gases since the mean velocities and the turbulence must vanish at the walls. The heat transfer at any given location is thus a function of both the thermal boundary layer and the momentum boundary layer (a, a, & Yang, 2005).

The heat fluxes were obtained using a model (Soloiu, Lewis, & Covington, 2011) that was derived from the Annand model, by calculating the instantaneous volume-averaged in cylinder Reynolds number, air viscosity, with the instantaneous volume averaged gas properties, and the convection heat coefficient. For this particular study, the temperature gradients in the axial and circumferential directions are significantly smaller than those that occur in the radial direction. It is for this reason that only the conduction heat transfer occurring in the radial direction shall be considered. During combustion, the heat loss is caused partly by convection from burned gases at high temperature and partly by radiation from soot particles formed during the diffusion flame. The dominant heat transfer mechanism in the typical engine is forced convection from the bulk gas to combustion chamber walls accounting for approximately 80 percent of the total engine heat transfer, which becomes apparent by observing the figures below.

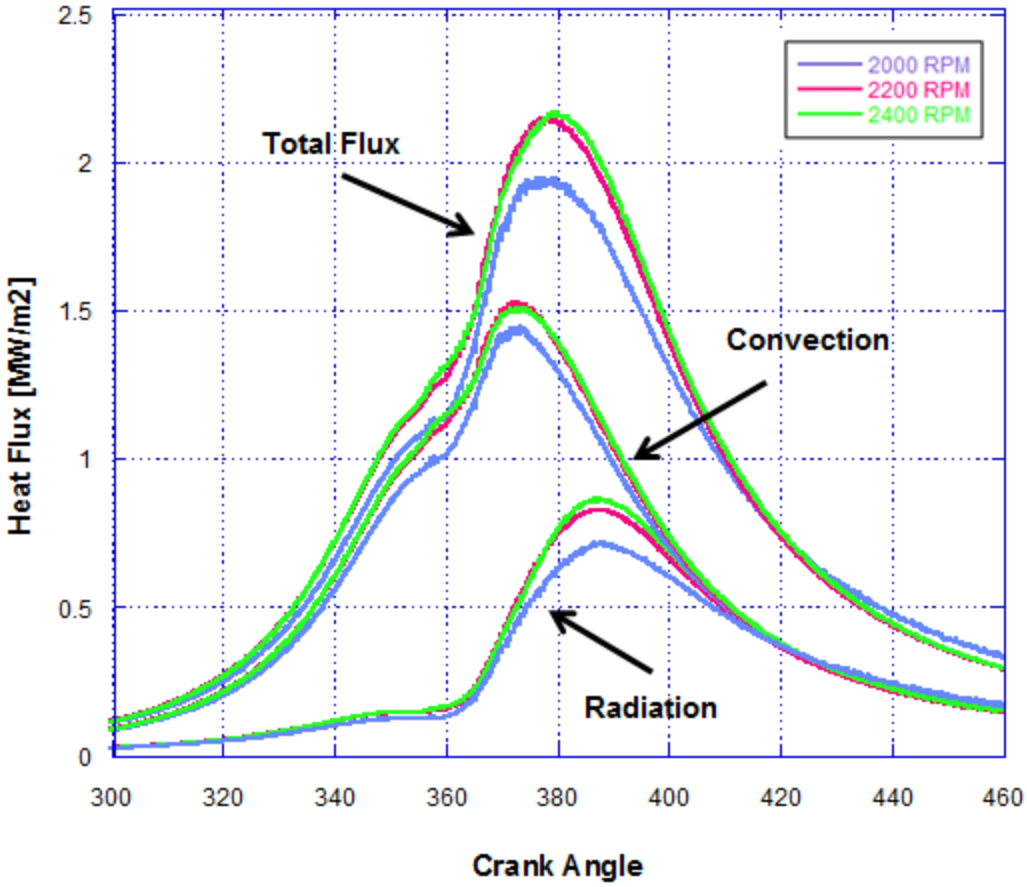

Figure 71 Diesel Heat Flux Comparison (4.78 bar BMEP)

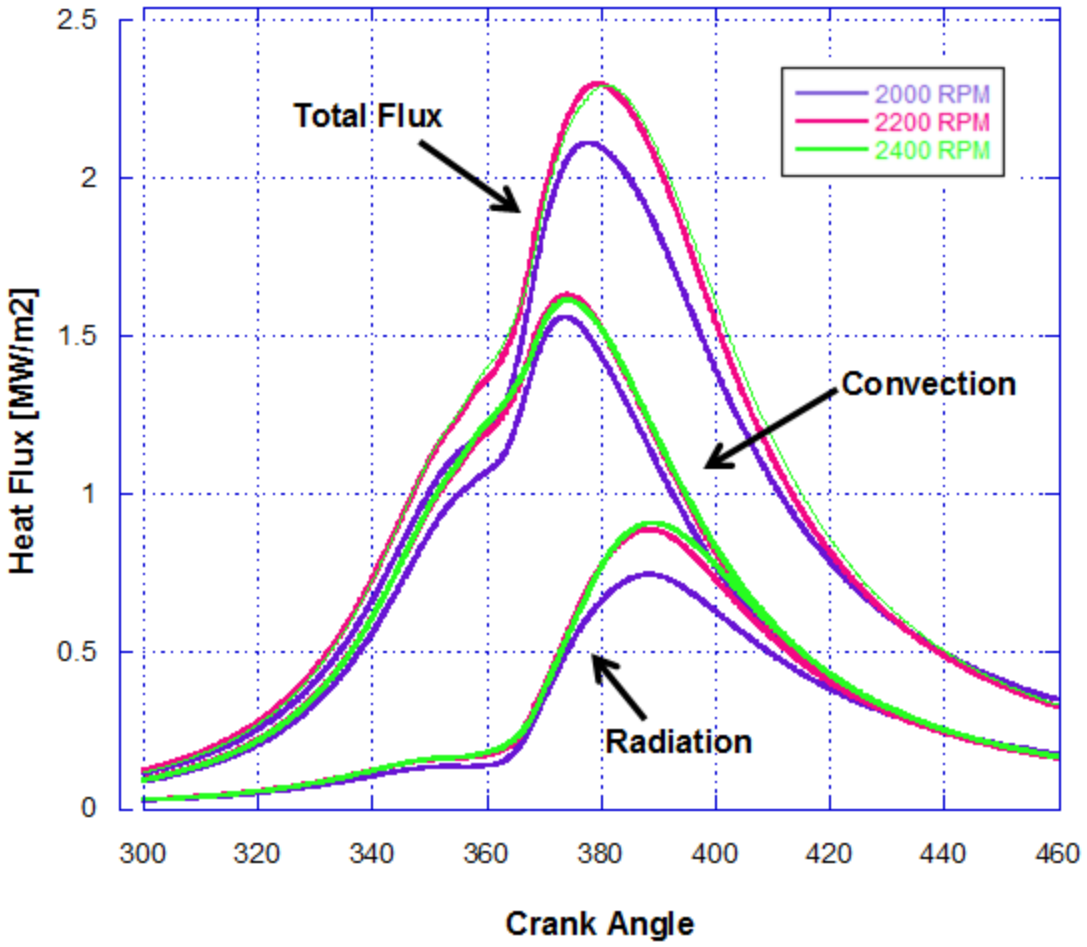

Figure 72 J20 Heat Flux Comparison (4.78 bar BMEP)

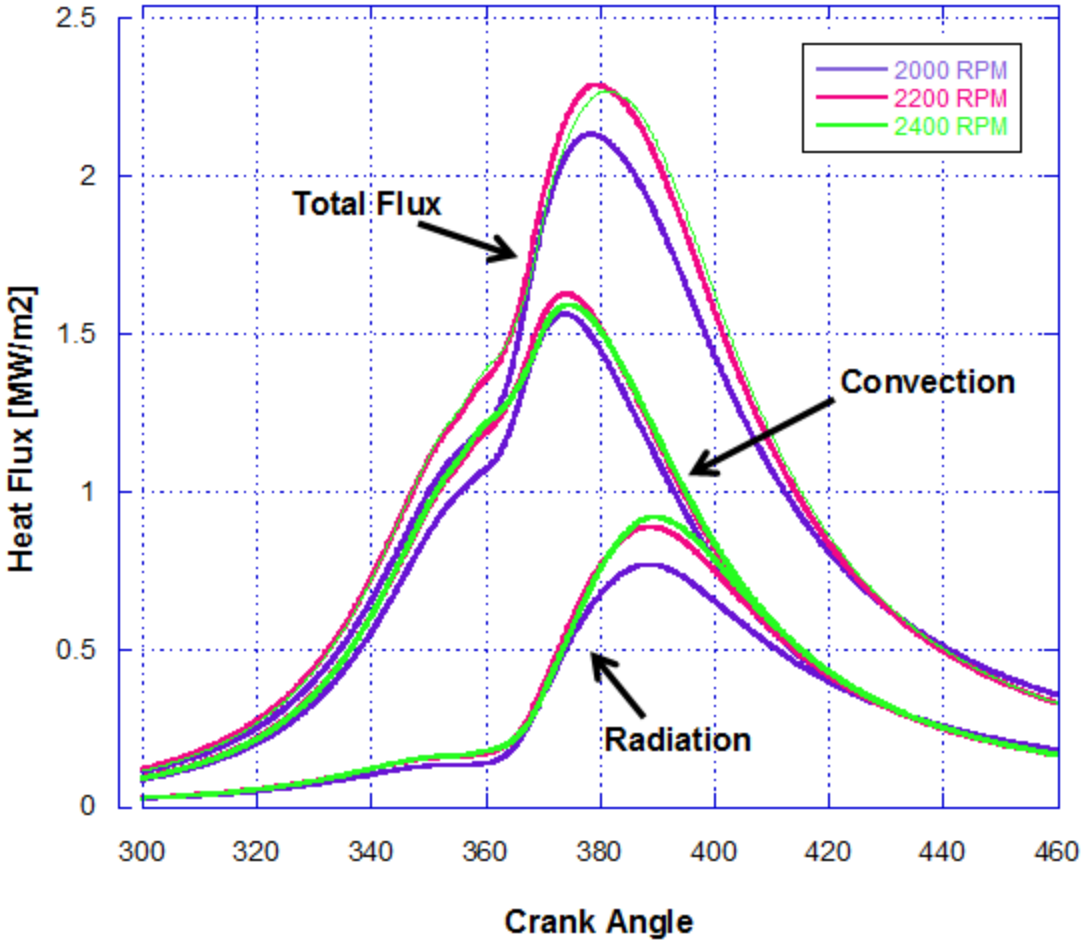

Figure 73 J35 Heat Flux Comparison (4.78 bar BMEP)

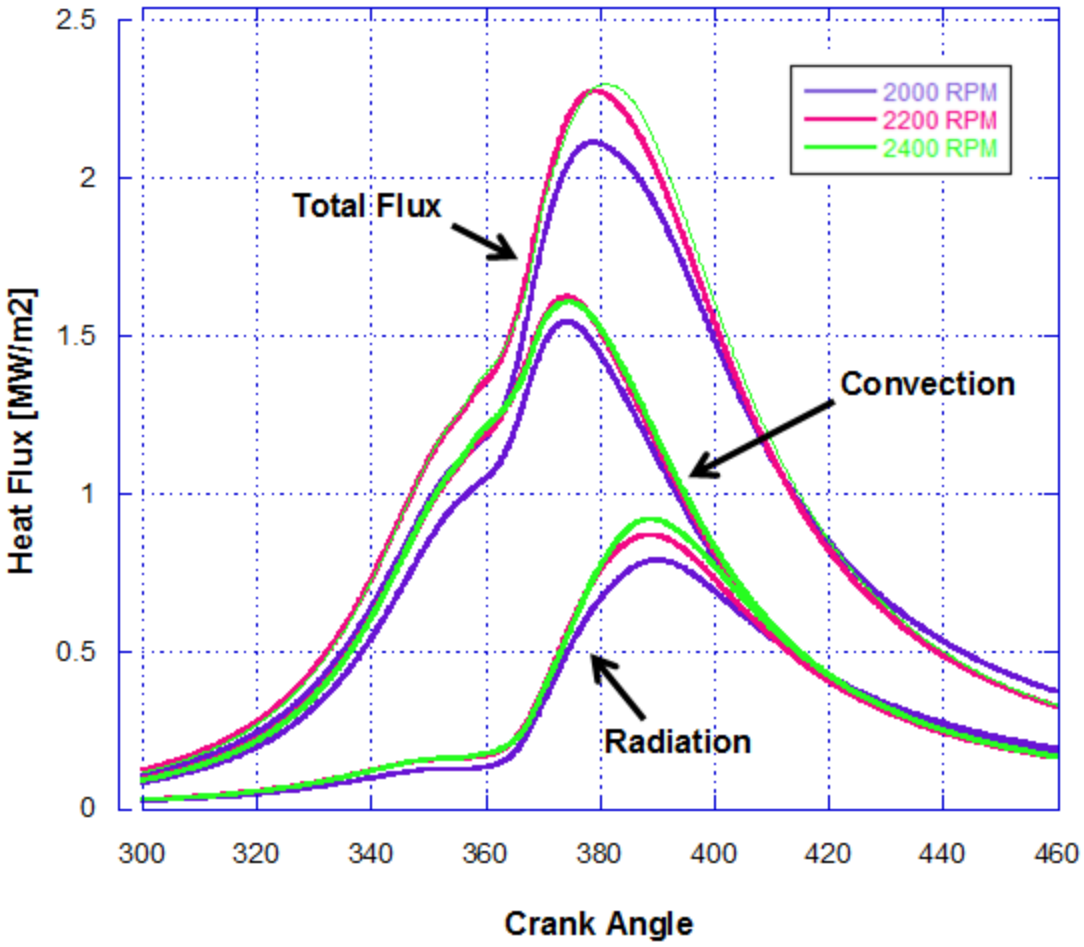

Figure 74 J50 Heat Flux Comparison (4.78 bar BMEP)

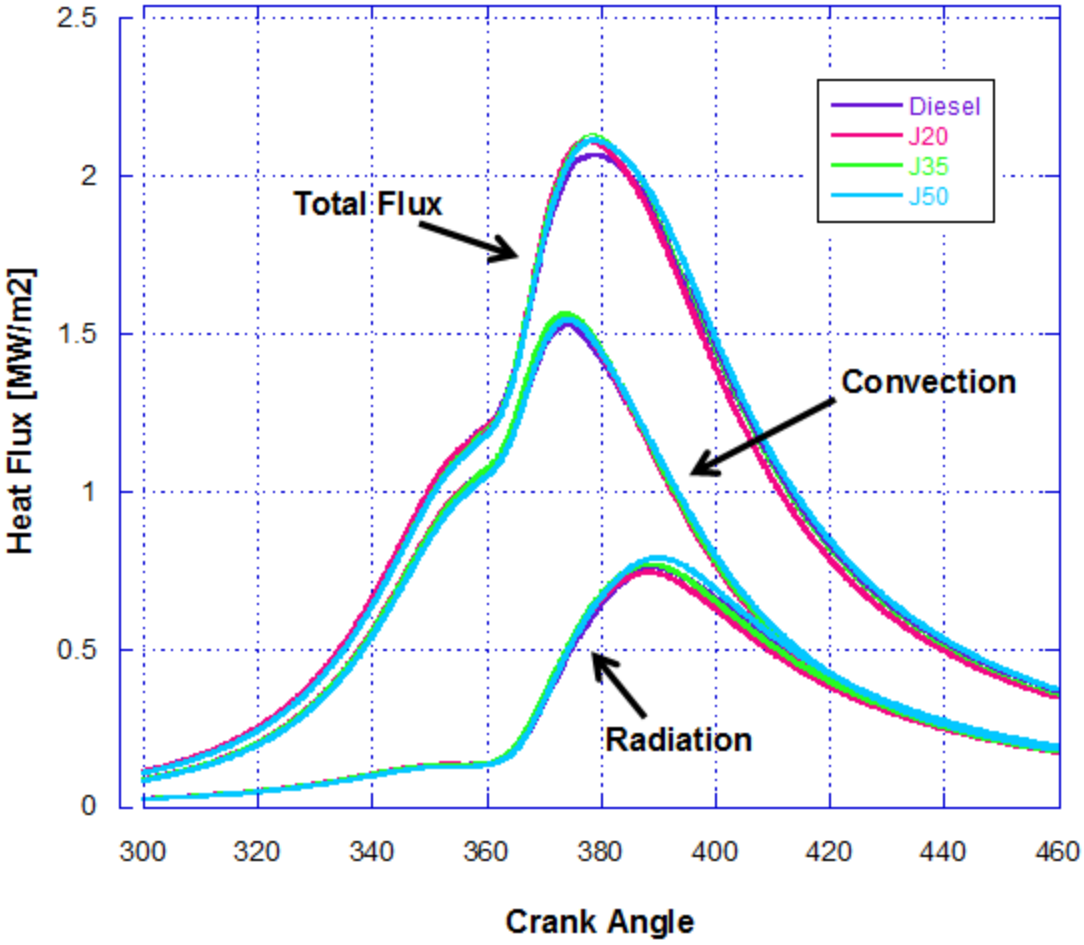

Figure 75 Heat Flux Comparison @ 2000 RPM (4.78 bar BMEP)

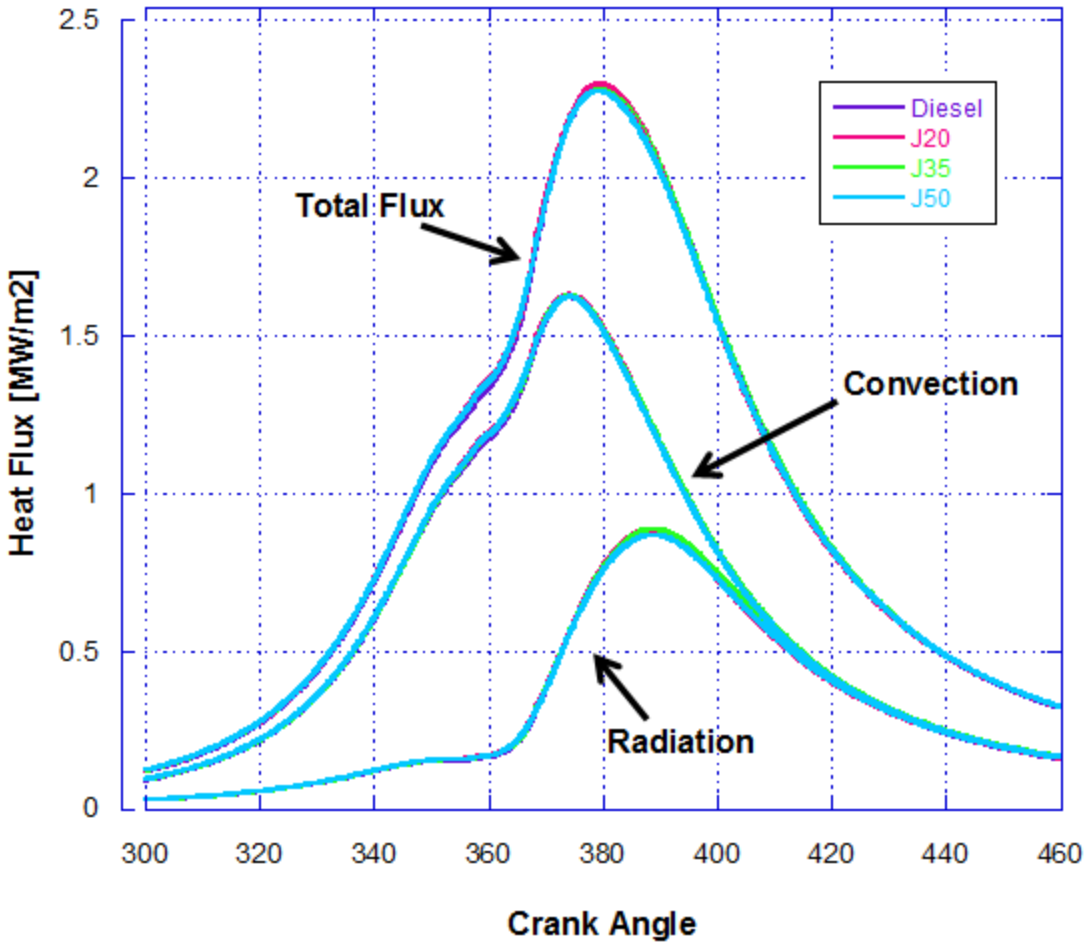

Figure 76 Heat Flux Comparison @ 2200 RPM (4.78 bar BMEP)

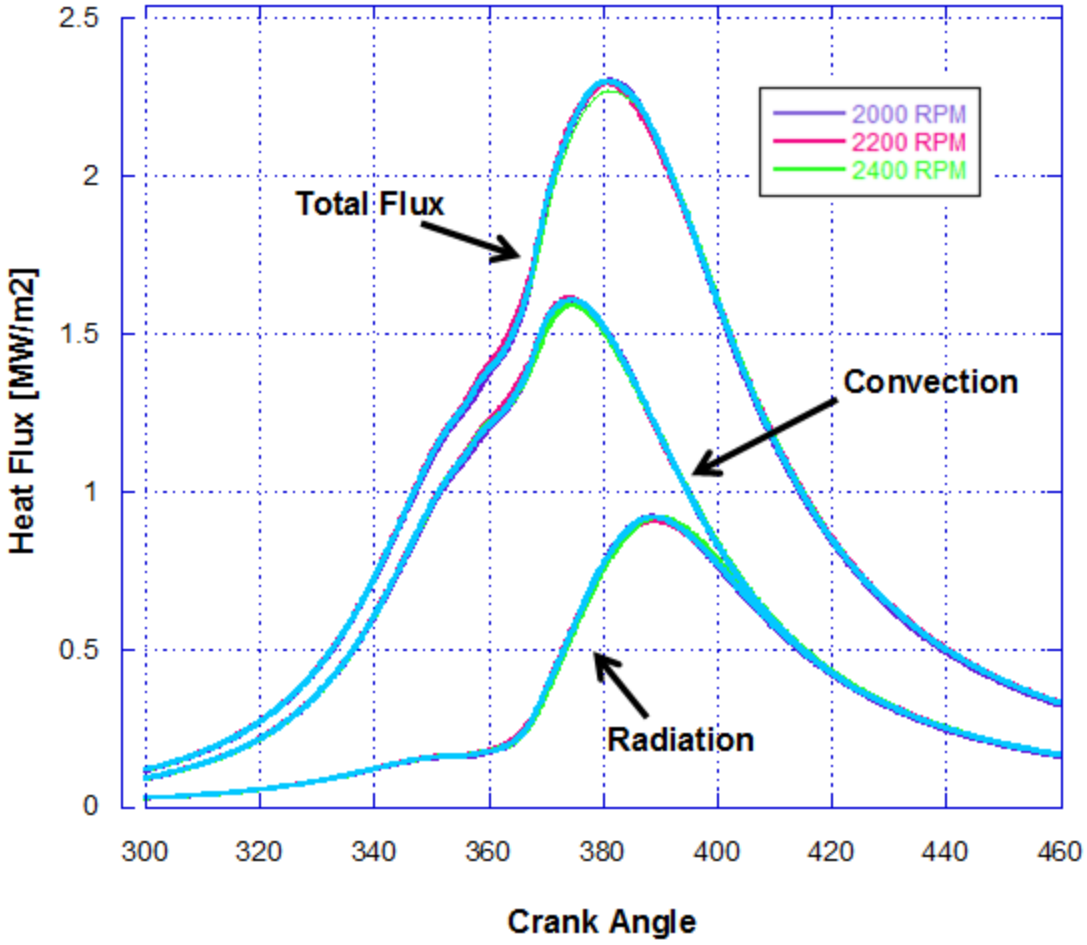

Figure 77 Heat Flux Comparison @ 2400 RPM (4.78 bar BMEP)

The heat flux in the engine cylinder showed similar values for all fuels, with the heat flux maximums for the varying fuel blends being displayed in the Figures below.

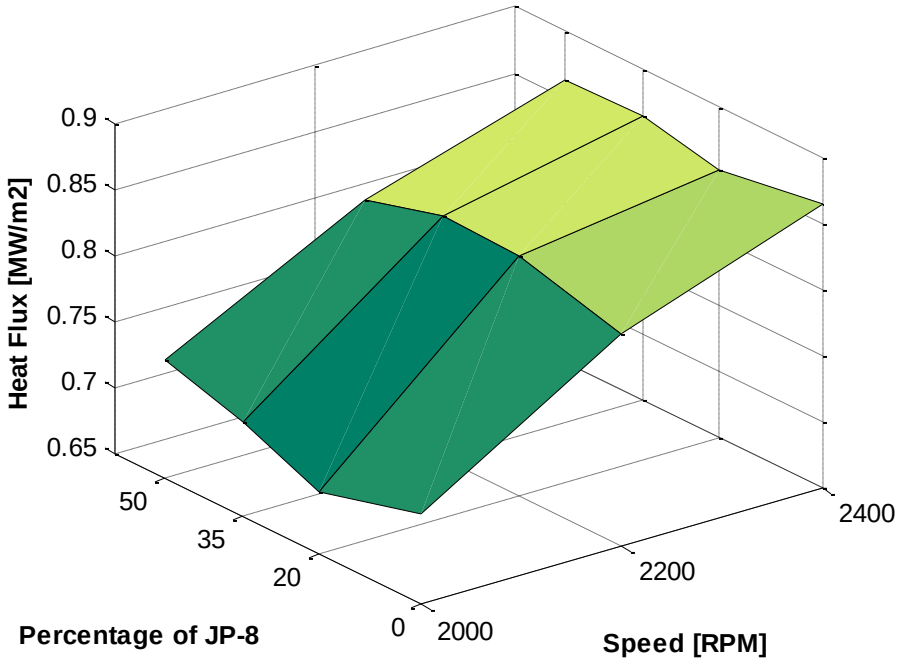

Figure 78 Maximum Radiation Heat Flux Surface Plot

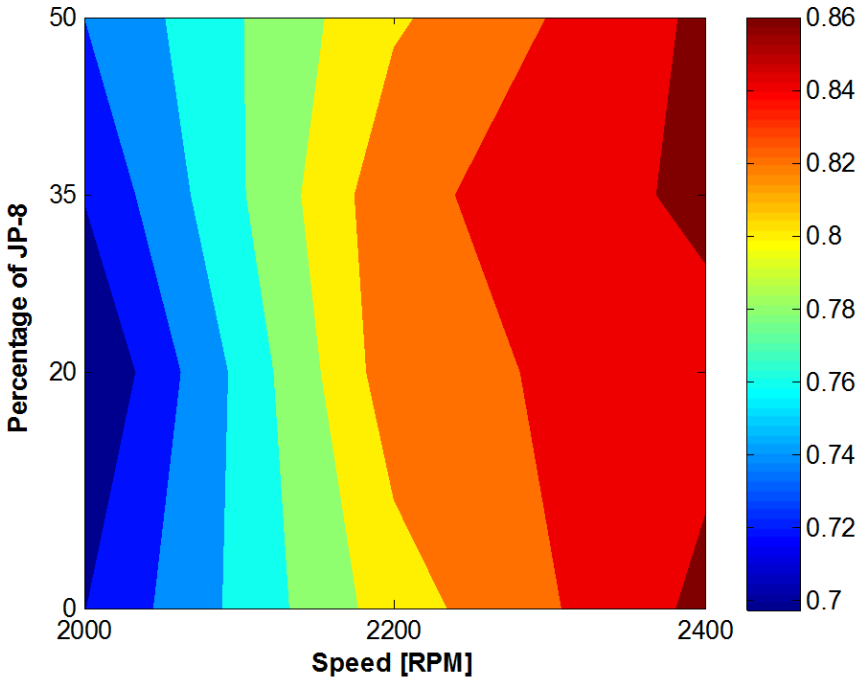

Figure 79 Maximum Radiation Heat Flux Contour Plot

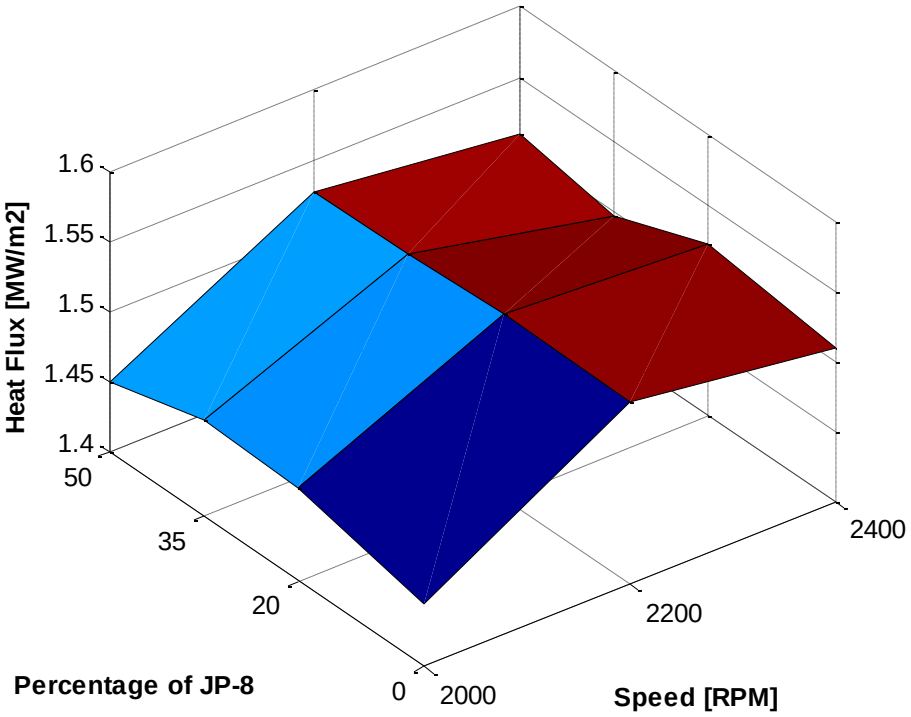

Figure 80 Maximum Convection Heat Flux Surface Plot

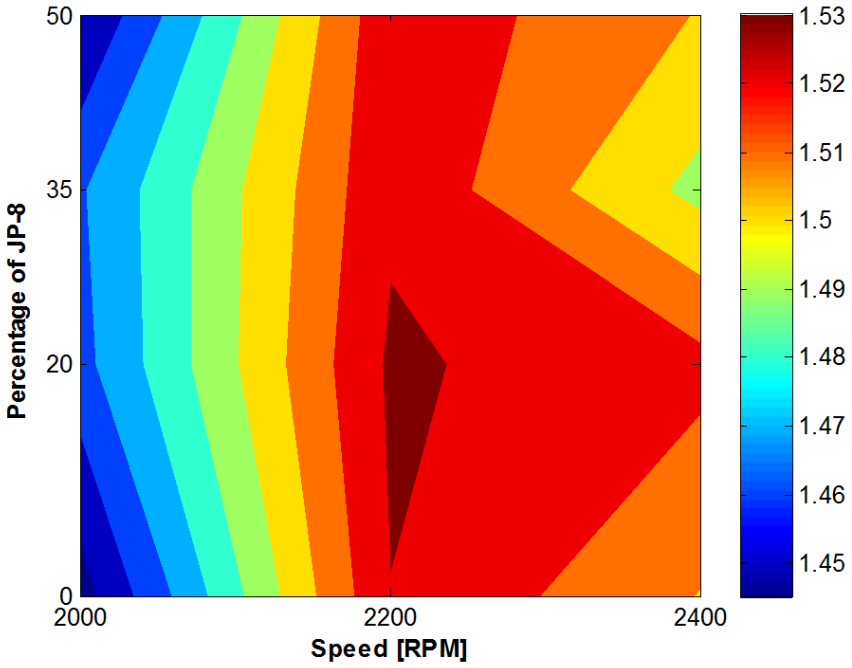

Figure 81 Maximum Convection Heat Flux Contour Plot

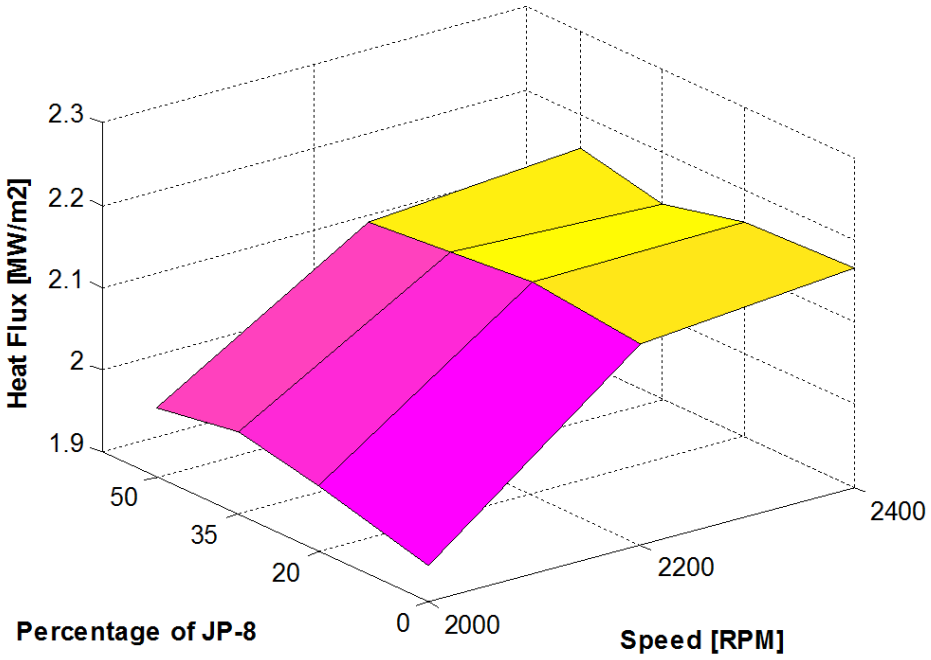

Figure 82 Maximum Total Heat Flux Surface Plot

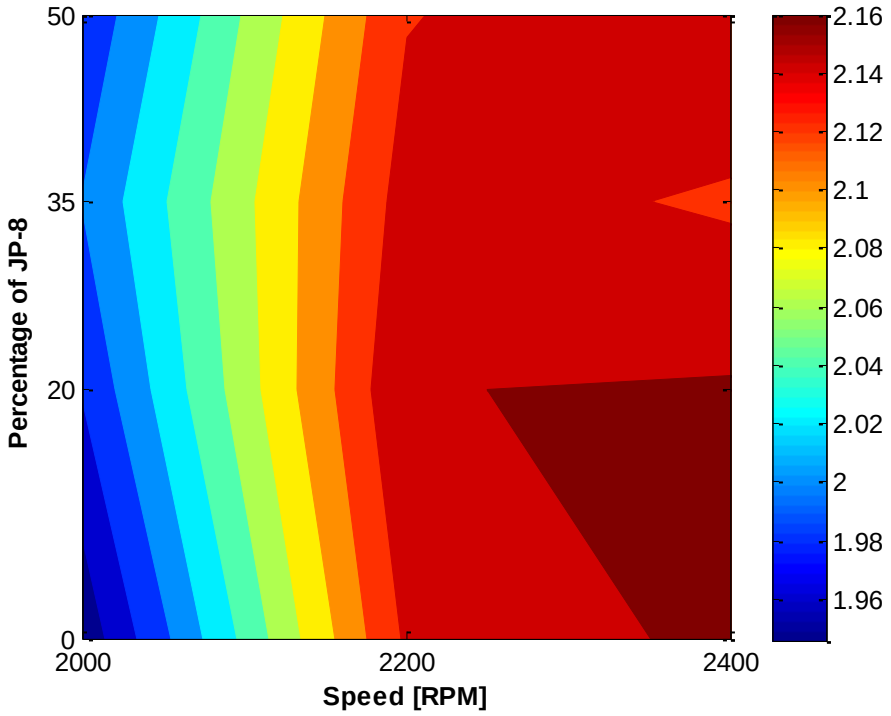

Figure 83 Maximum Total Heat Flux Contour Plot

The convection flux has a maximum earlier in the cycle compared to the radiation flux and following the zone of maximum turbulence location, while the crank angle to which the maximum radiation flux has been obtained is maximum temperature dependent and the results fit well with the study of (Borman & Nishiwaki, 1987) and (Soloiu V. Y., 2010). Due to the short distance between the nozzle and the combustion chamber wall under typical operating conditions, the fuel mixture impinges on the wall in the form of liquid followed by fuel vapor and flame after the onset of auto ignition (Lakshminarayanan & Aghav, 2010). This in conjunction with the fact that the peak radiant heat flux is less than 20% of the total heat flux confirms the dominant role of the flame and spray interaction with the piston bowl (Arcoumenis, Cuter, & Whitelaw, 1998). Radiation heat transfer within the cylinder of a diesel engine has a significant impact on energy efficiency and emission as a significant component of the total heat transfer process in the form of soot, which is formed during the burning of fuel mixture droplets, emitting radiation that is transmitted to the walls of the combustion chamber. The relationship between the radiation heat transfer from the soot of the engine operation and performance therefore, has to be investigated to further understand the influence of the fuel blends on engine efficiency and emissions. The radiation heat flux does not exhibit any major changes on the slope of soot formation (the curve before the peak) or on the oxidation (the curve after the peak) as the content of JP-8 in the mixture is increased (Said, Buttsworth, & Yusaf, 2009), These results verify that the use of JP-8 in a diesel engine will not result in any notable increase in heat flux and thus problems related to engine operation or wear.

Gross Heat Release

Based on the heat fluxes, the heat loses throughout the cycle have been calculated and are presented in the figures below.

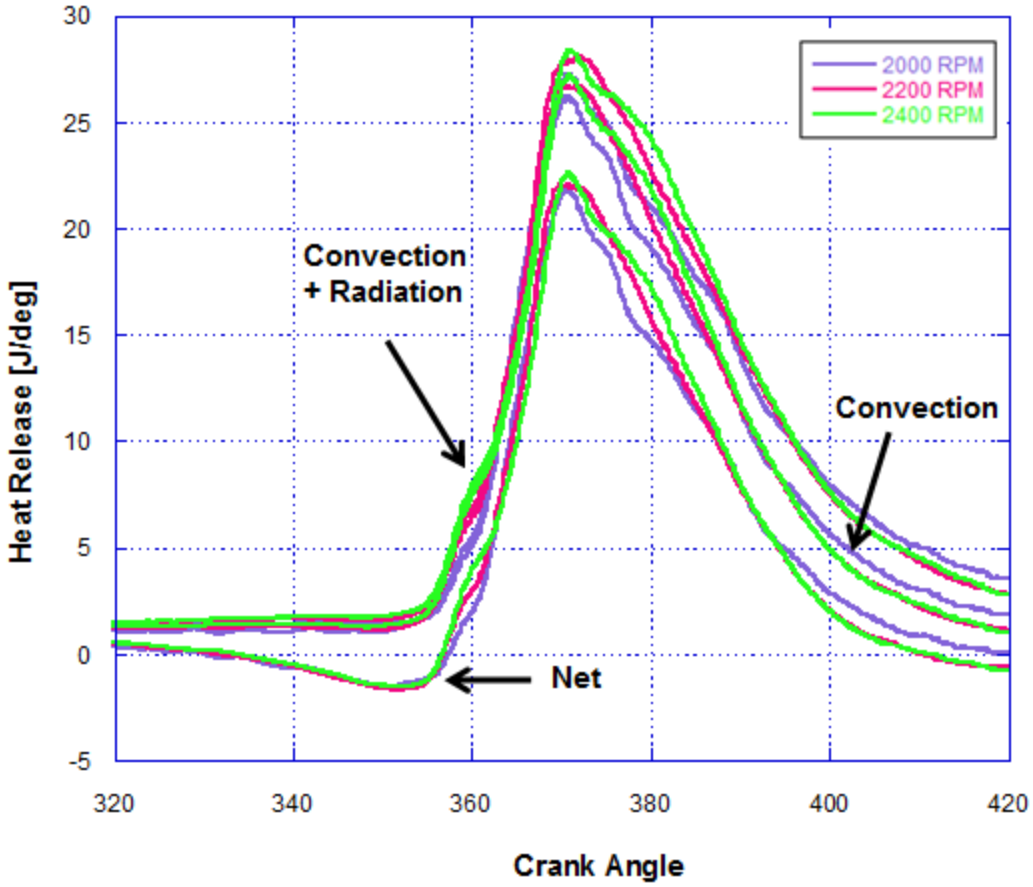

Figure 84 Diesel Gross Heat Release Comparison (4.78 BMEP)

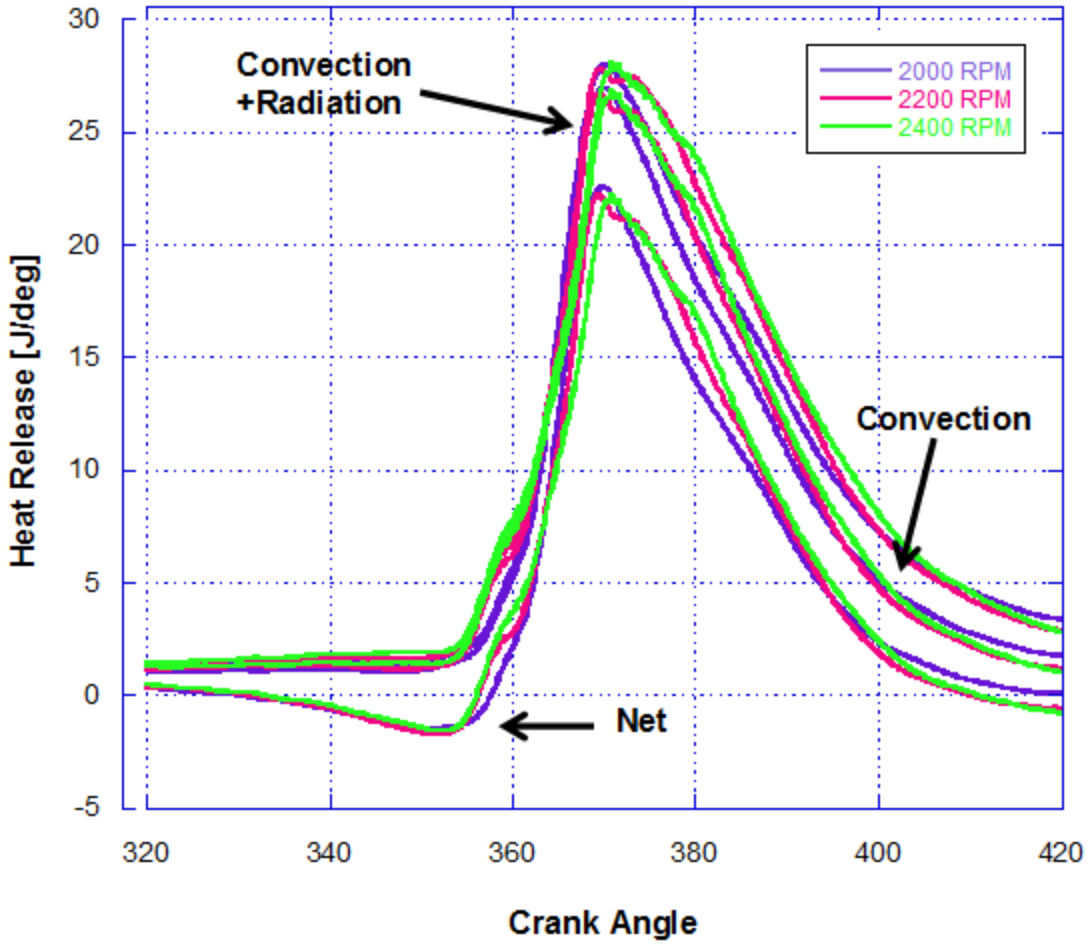

Figure 85 J20 Gross Heat Release Comparison (4.78 BMEP)

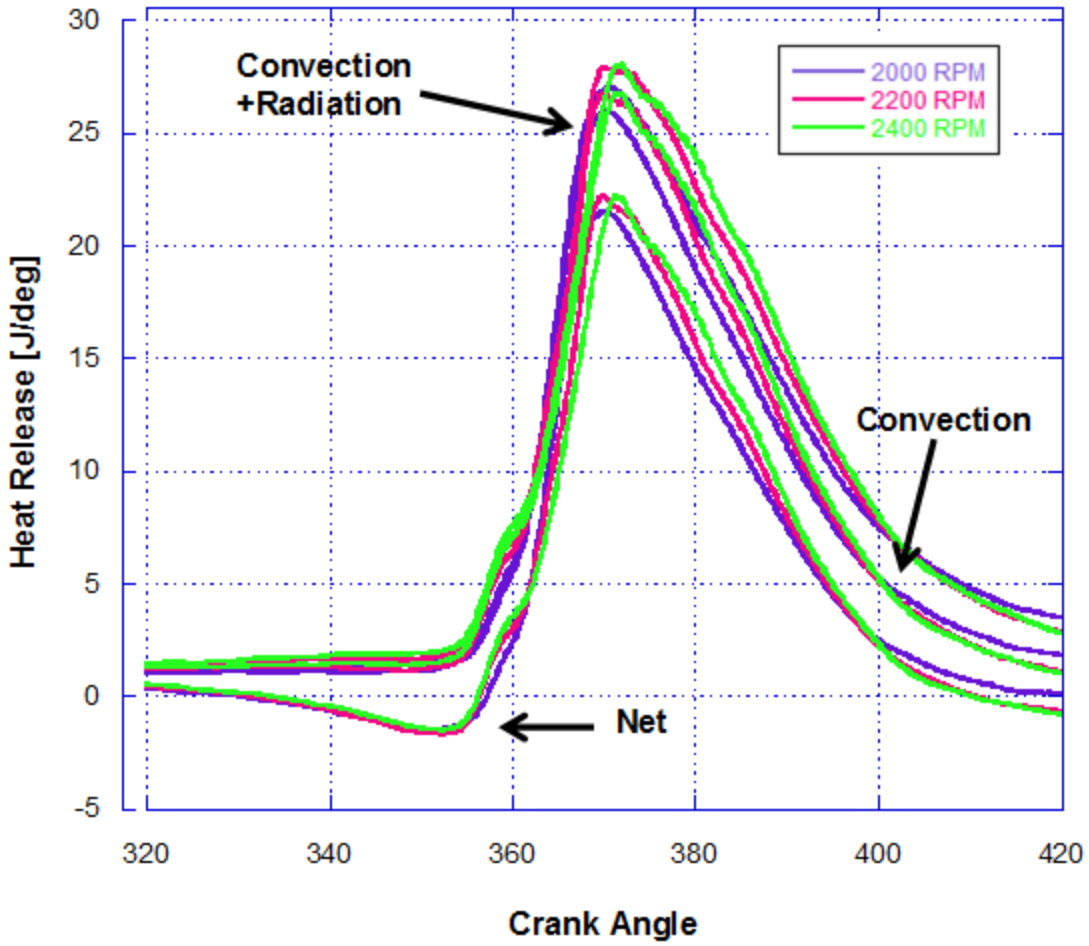

Figure 86 J35 Gross Heat Release Comparison (4.78 BMEP)

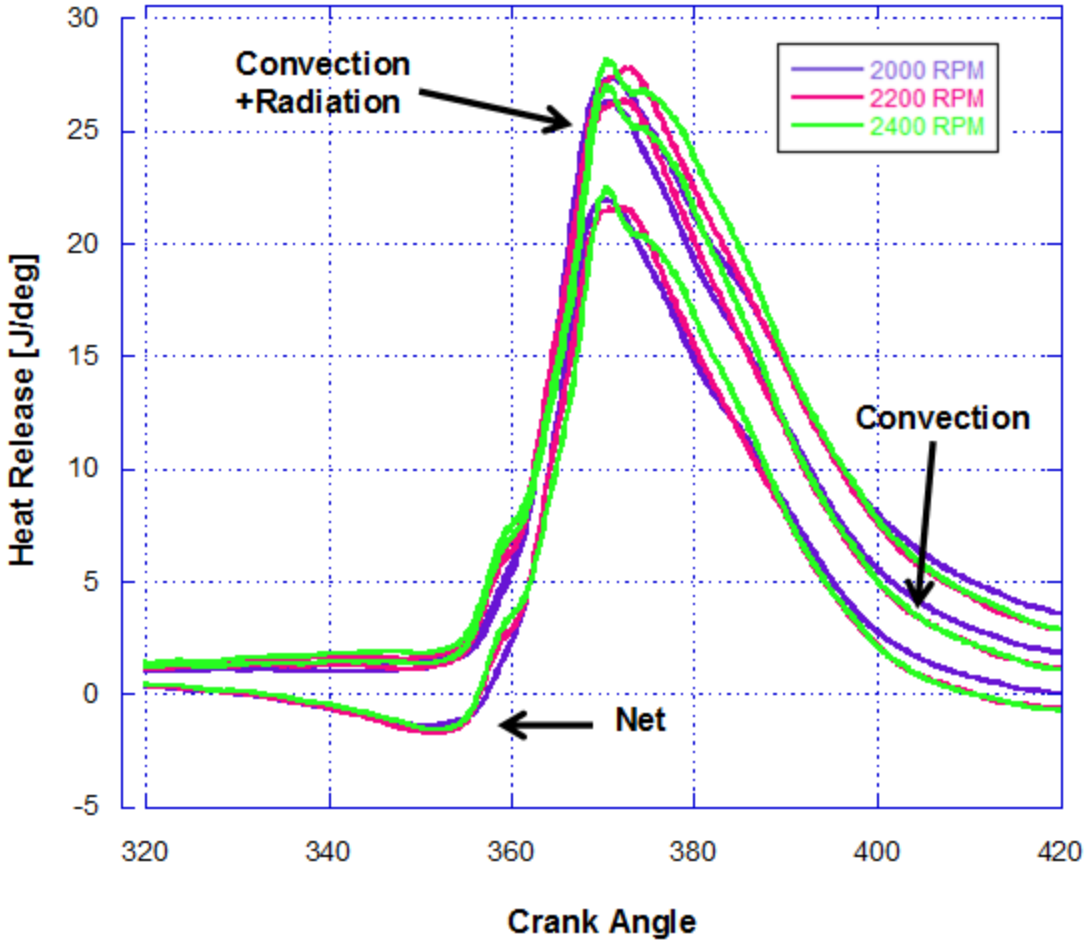

Figure 87 J50 Gross Heat Release Comparison (4.78 BMEP)

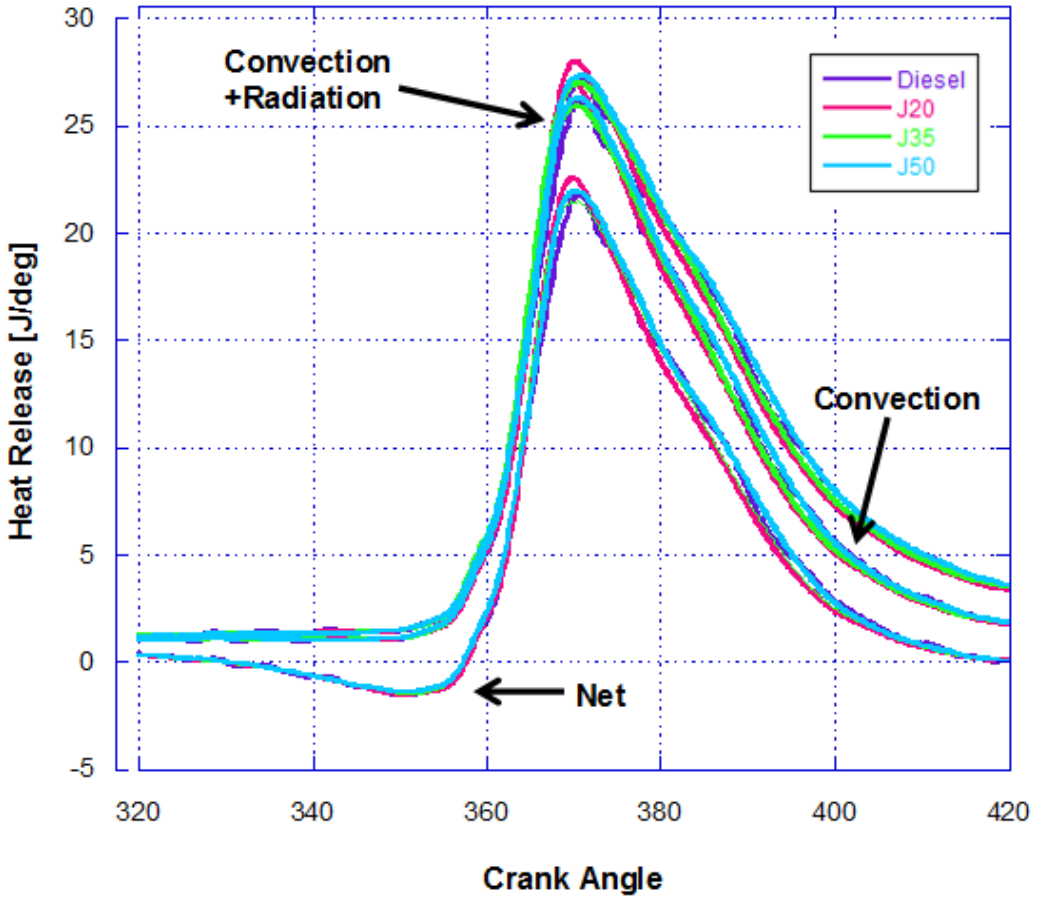

Figure 88 Gross Heat Release Comparison @ 2000 RPM (4.78 BMEP)

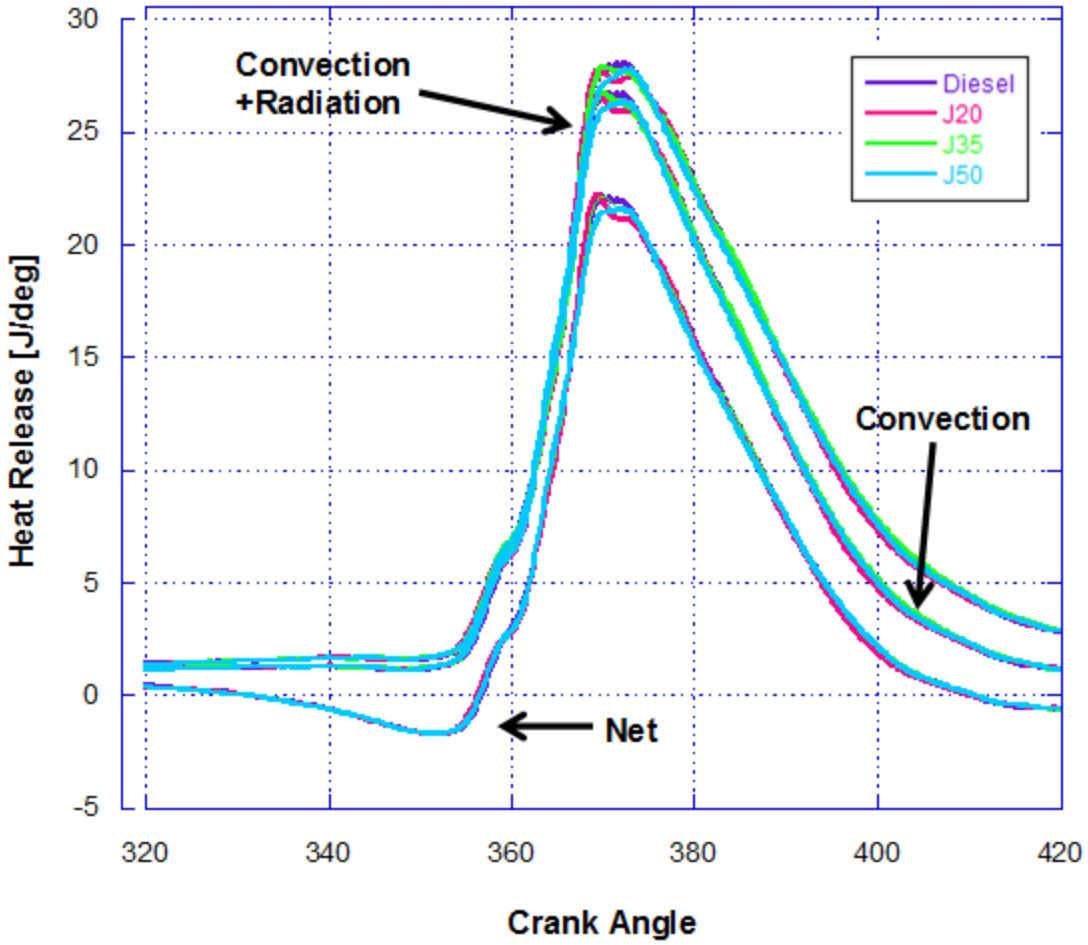

Figure 89 Gross Heat Release Comparison @ 2200 RPM (4.78 BMEP)

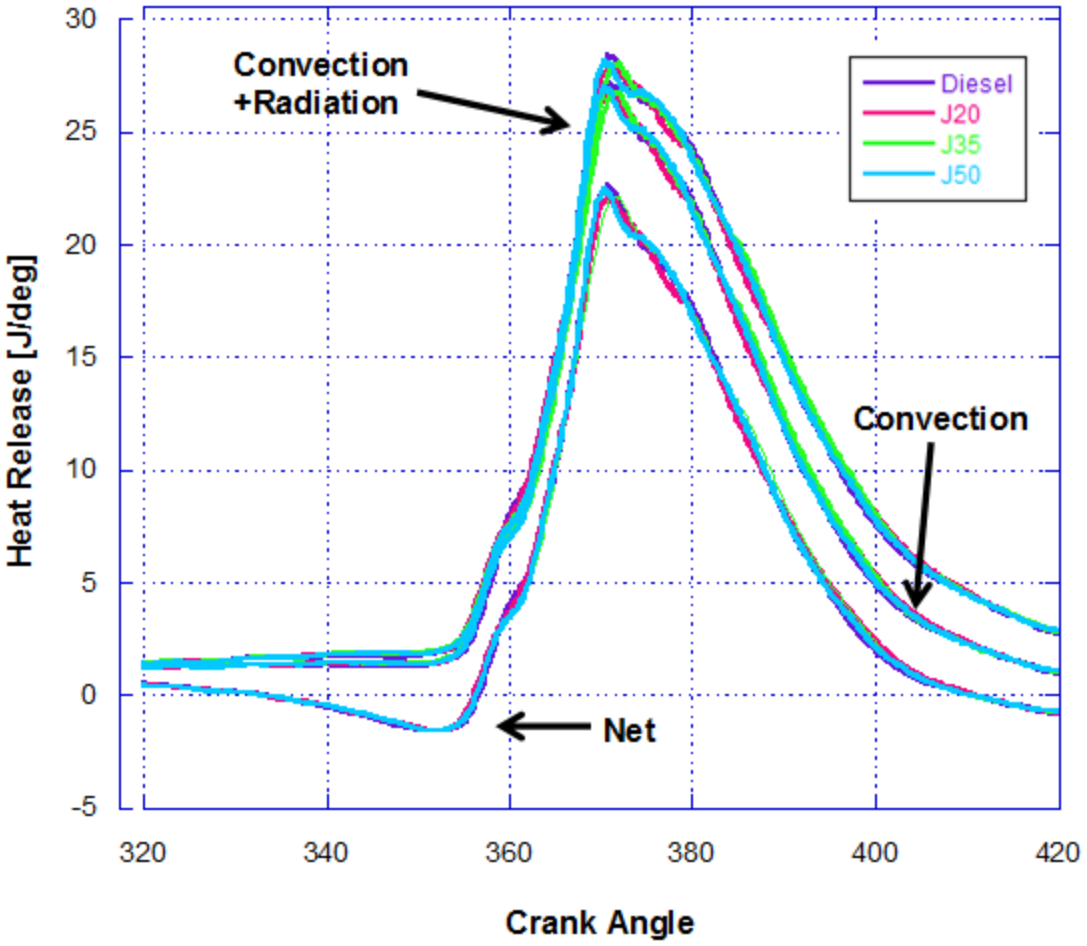

Figure 90 Gross Heat Release Comparison @ 2400 RPM (4.78 BMEP)

The area under inner line represents the apparent (net) heat release, the area between inner and middle line represents the heat lost through convection, and the area between the exterior line and middle line, represents the total heat lost which includes the convection and radiation. From these results seems that the heat loss trend throughout the cycle is very similar for all JP-8/diesel blends. It is very visible that is a minimal heat loss during combustion before TDC with increased convection losses at TDC for all blends and first part of power stroke.

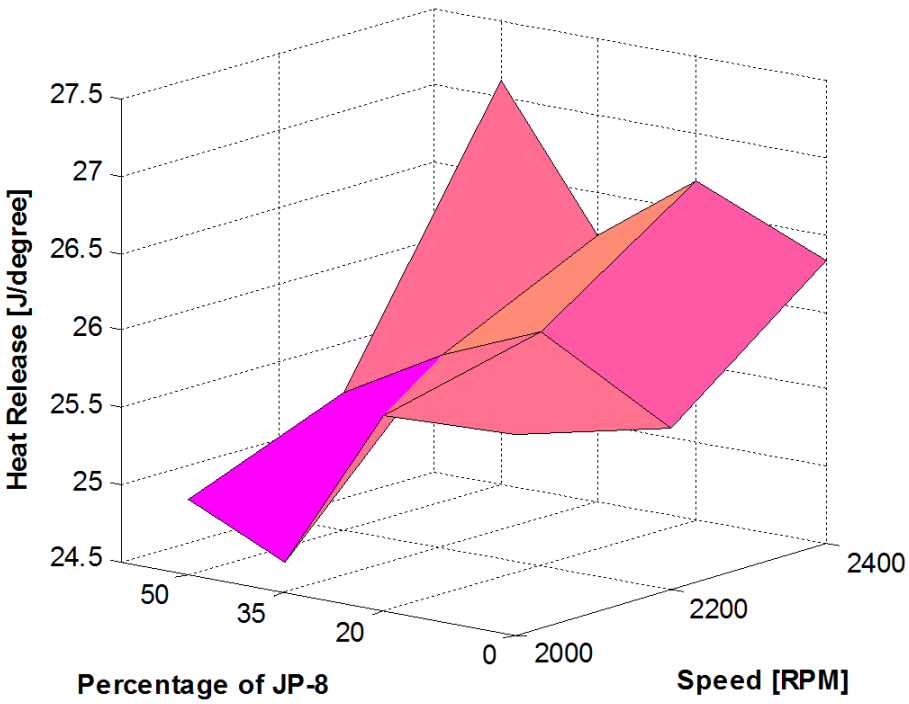

Figure 91 Maximum Gross Heat Release Due to Convection Surface Plot

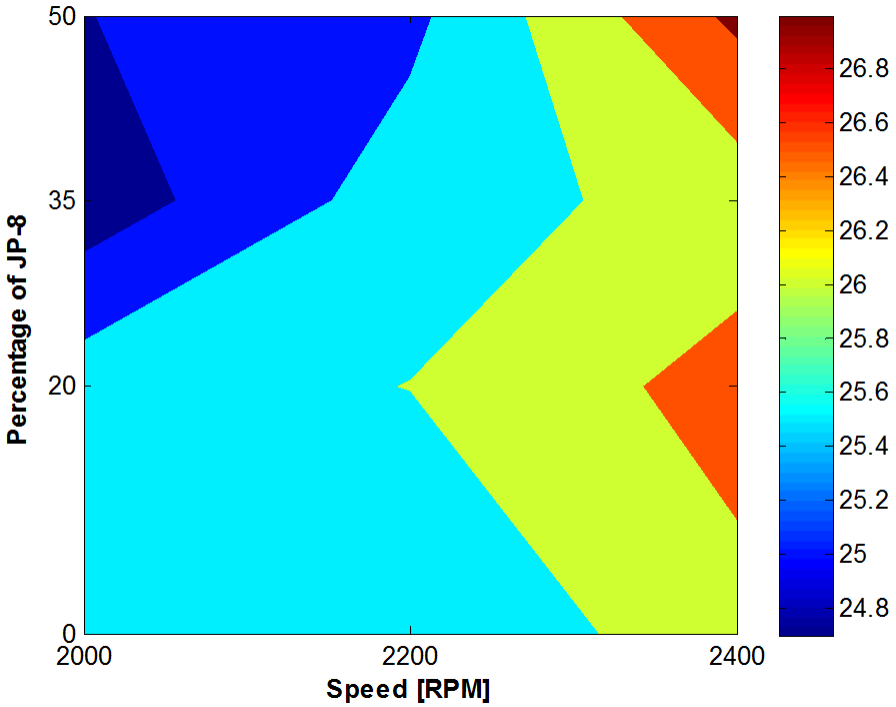

Figure 92 Maximum Gross Heat Release Due to Convection Contour Plot

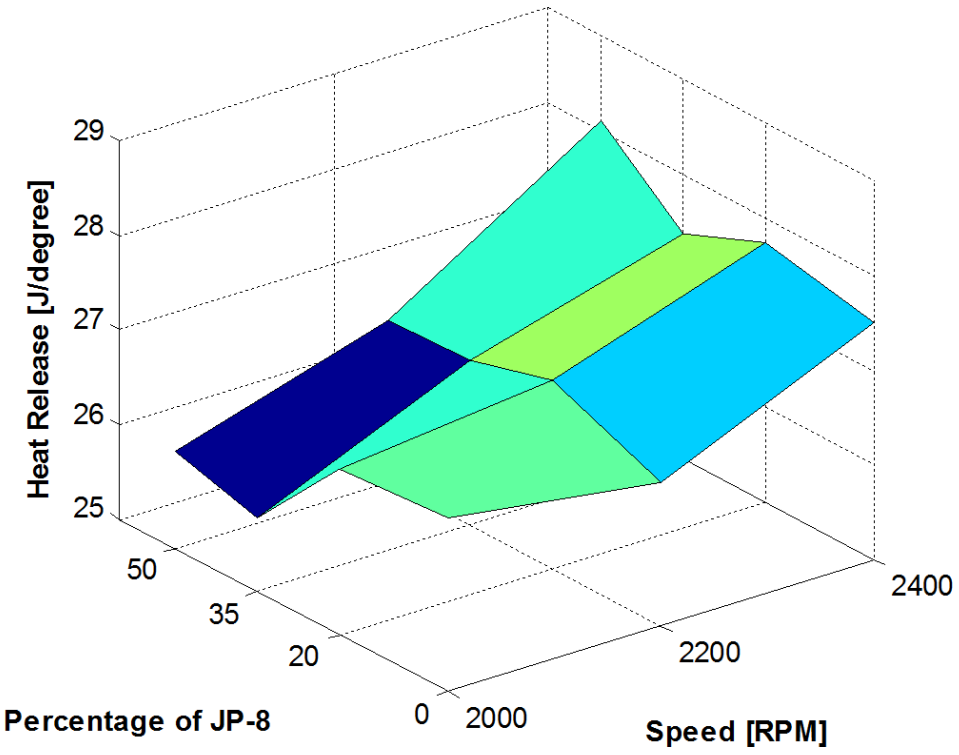

Figure 93 Maximum Gross Heat Release Due to Convection + Radiation Surface Plot

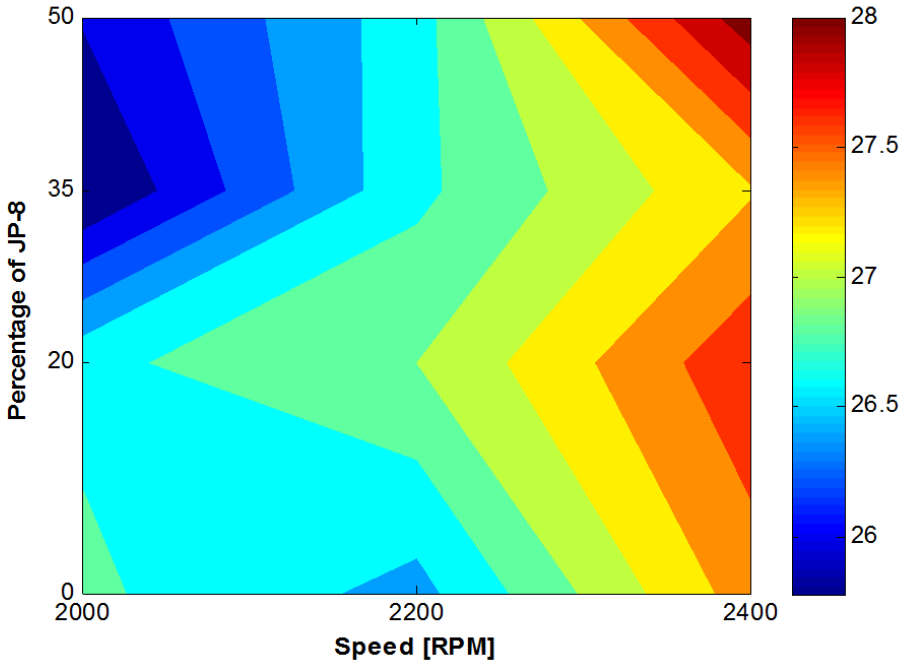

Figure 94 Maximum Gross Heat Release Due to Convection + Radiation Contour Plot

The largest gradient in terms of gross heat release belongs to that of the J50 blend, as it contains both the smallest and largest gross heat release rate value over the tested speeds. This data provides valuable information as it allows researchers to determine which speed and blend will be best for a particular application.

Engine Efficiency

A gross portion of the work that results from the expansion stroke of an engine is used to expel exhaust gases and induct fresh charge in to the engine, with an additional portion being used to overcome the friction of the bearings, pistons, and other mechanical components of the engine. All of these losses described above are grouped in the term friction power. A dynamometer is typically used to measure this value. The engine's mechanical efficiency is defined as the ratio of useful power delivered by the engine to the indicated power. Although it can be transformed in terms of pressure through the manipulation of the torque formula and can be described by the following equation,

$$\eta_e = \frac{BMEP}{IMEP}$$

With η_e representing the mechanical efficiency, BMEP representing the brake mean effective pressure, and IMEP representing the indicated mean effective pressure. Due to the influence of friction, the BMEP of an engine is always less than the IMEP; hence the engine's mechanical efficiency must always be less than 1. It is more desirable that the mechanical efficiency be as close to 1 as possible. The mechanical efficiency provides a good indication of the engine performance, in terms of being able to convert the indicated power into useful power. The value of mechanical efficiency will vary considerably with the design, operating conditions, and use fueled in the engine. It is evident that the mechanical efficiency under idling conditions

would be zero, as all the indicated power developed by the engine is spent in overcoming friction. In order to increase the mechanical efficiency of an engine to a maximum the frictional losses associated with the engine must be reduced to a minimum.

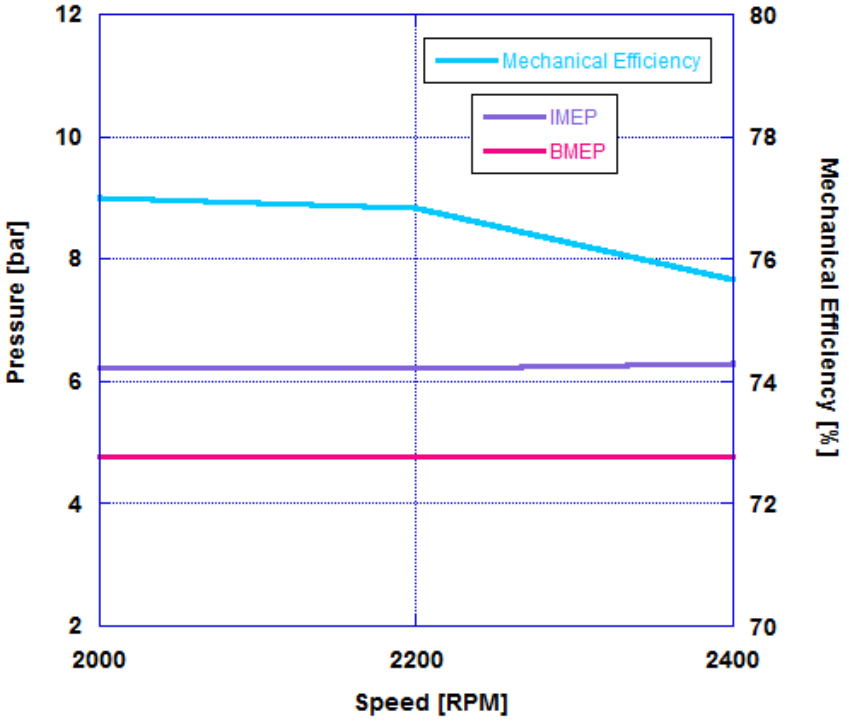

Figure 95 Diesel Mechanical Efficiency Comparison

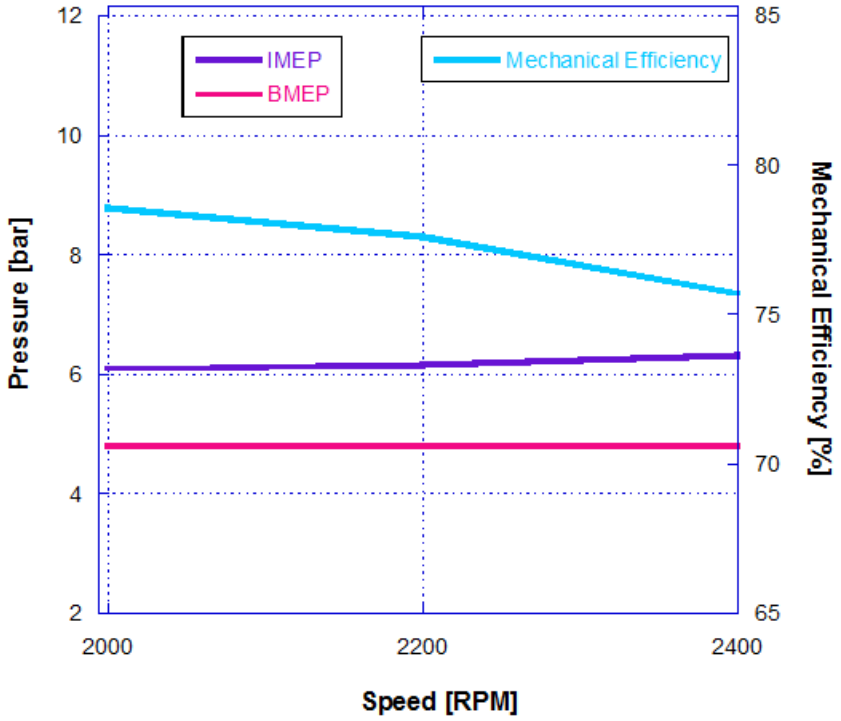

Figure 96 J20 Mechanical Efficiency Comparison

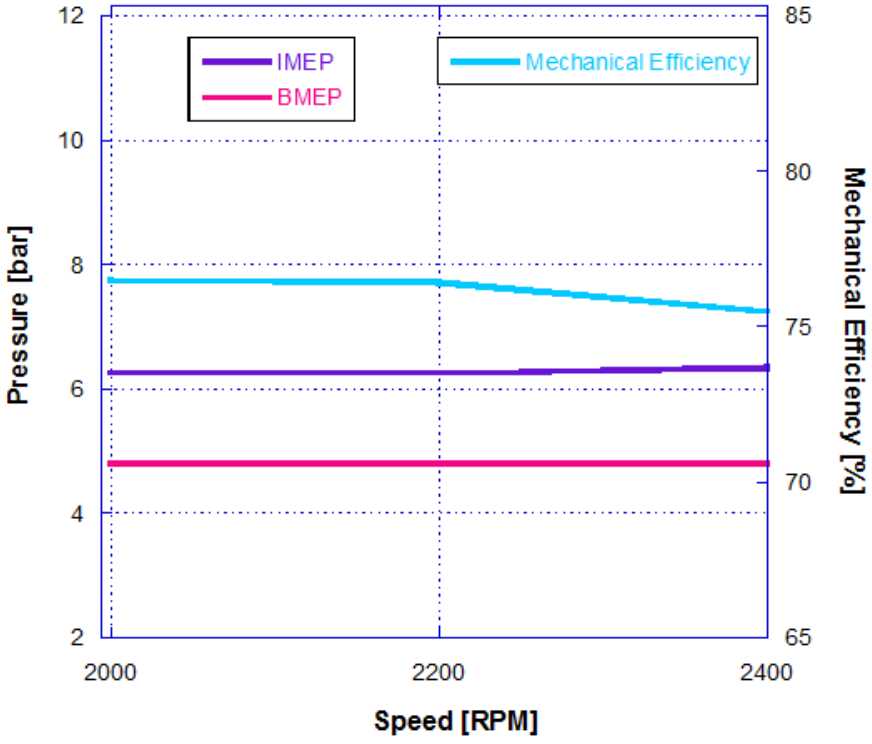

Figure 97 J35 Mechanical Efficiency Comparison

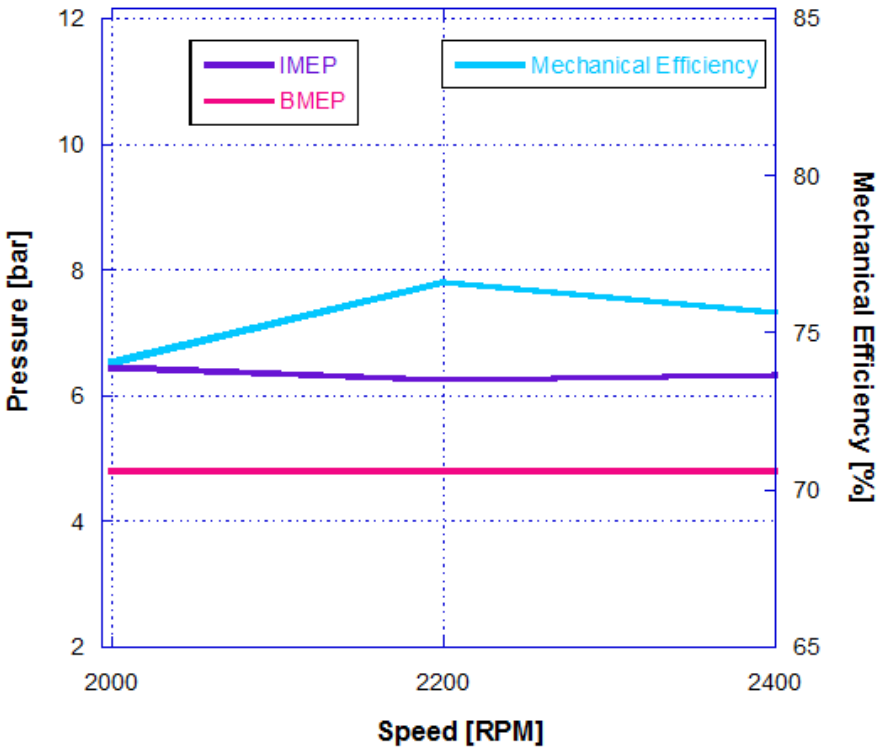

Figure 98 J50 Mechanical Efficiency Comparison

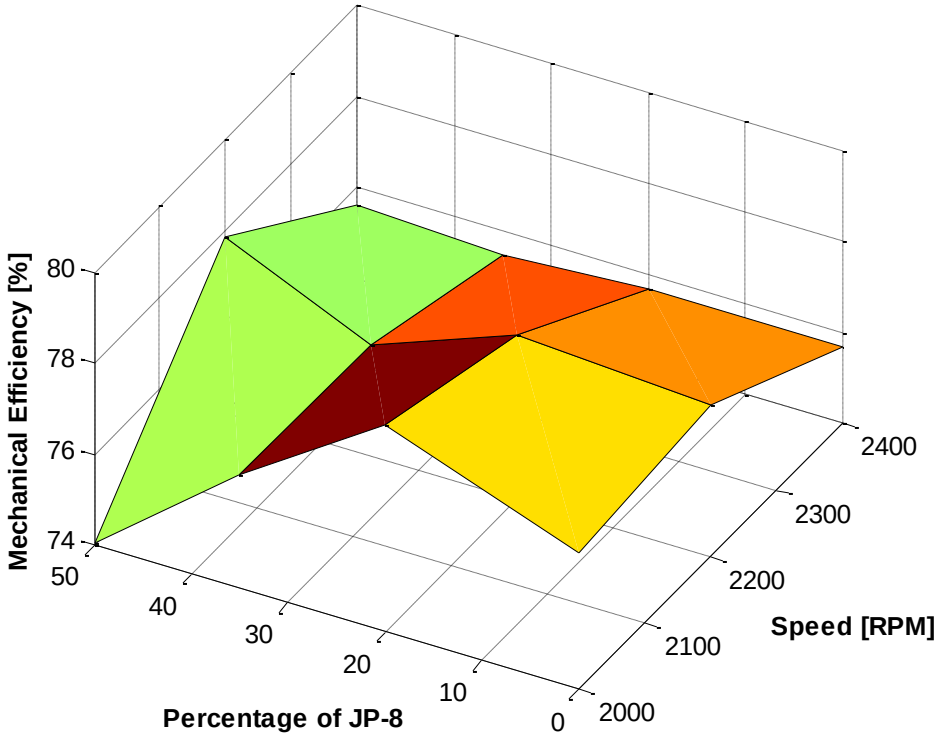

Figure 99 Mechanical Efficiency Surface Plot

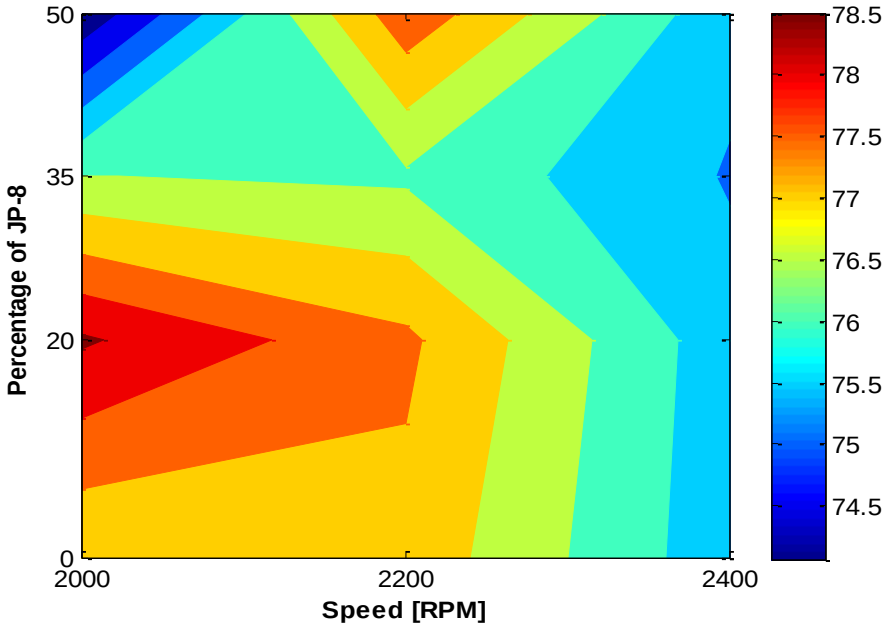

Figure 100 Mechanical Efficiency Contour Plot

For all blends, it can be seen that the engine's mechanical efficiency was at a maximum when the engine was set at a speed on 2200 RPM. The engine's mechanical efficiency with the JP-8 displayed similar values with that of diesel combustion showing a decrease of less than 1 percent for 4.78 bar BMEP at 2000 rpm, despite the increased lubricity of the JP-8 due to the required Corrosion Inhibitor /Lubricity Improver (MIL-PRF-25017) additive.

This result could be explained by an increased mean indicated pressure with the increased percent of JP-8 in the mixture. Another possible explanations for that, would be the increased mechanical work absorbed by the injection pump for the larger amount of fuel pumped in order to compensate for a lower heating value and also the overall combustion characteristics of the JP-8.

Another important factor in this research is the fuel consumption which is defined by the rate of fuel that is consumed within a specific time period, at a given speed, and power that is produced at that speed over a period of time; this is referred to as brake specific fuel consumption (BSFC).

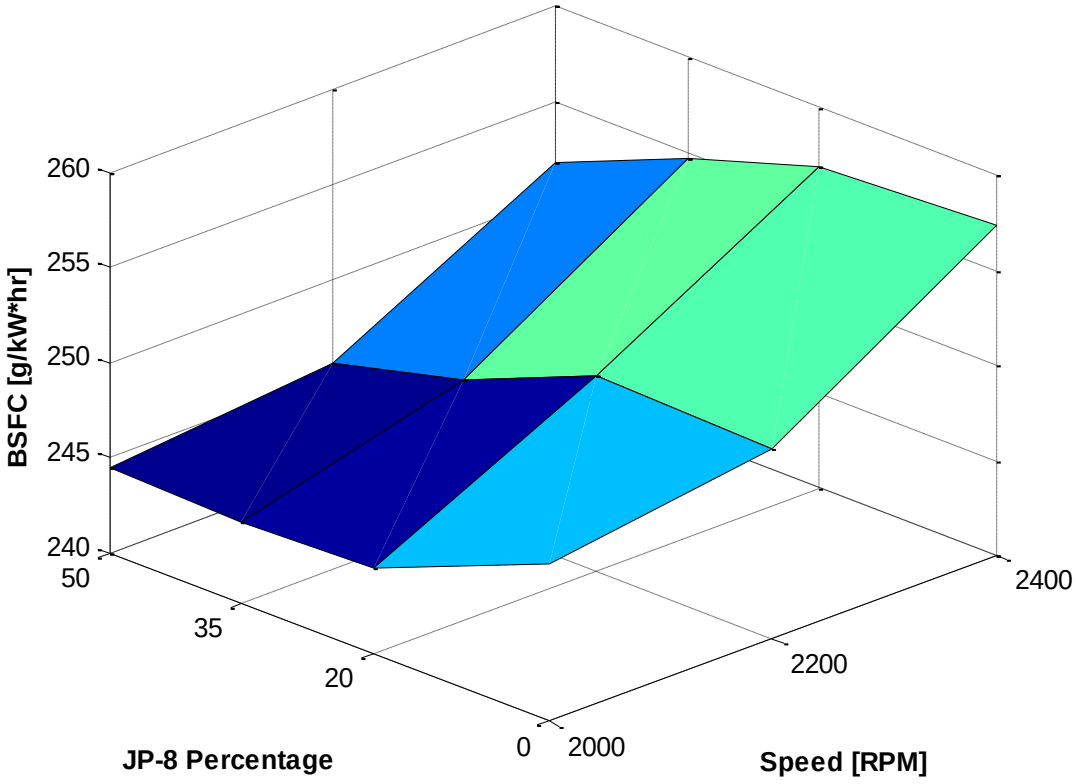

Figure 101 BSFC Surface Plot

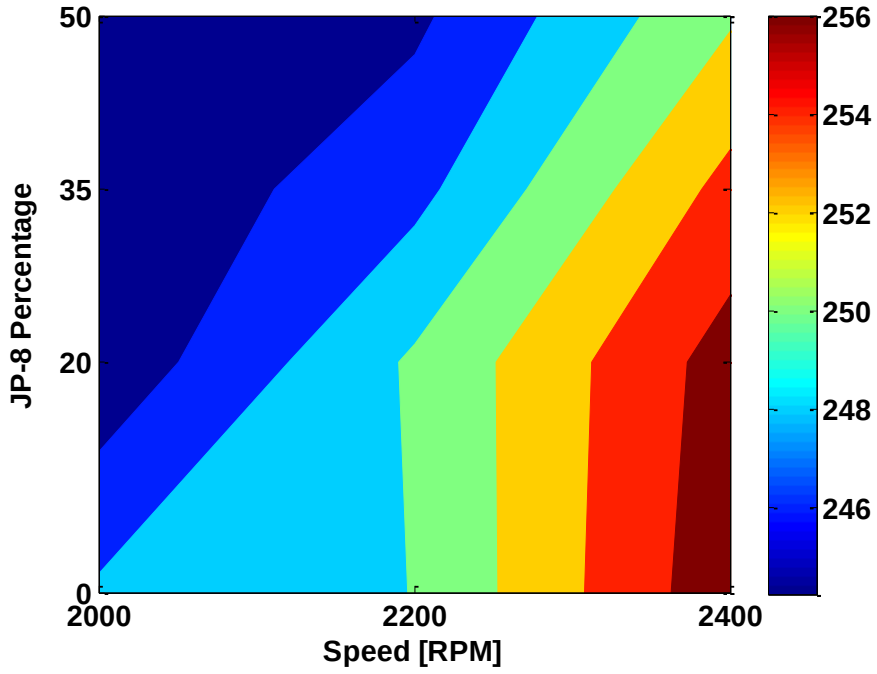

Figure 102 BSFC Contour Plot

The BSFC above in Figure 101-Figure 102 represents values that were averaged over approximately 16,000 cycles. Based on the results, the BSFC increased in relation to speed and decreased in relation to the percentage of JP-8 introduced into the mixture. This correlation became especially strong at higher speeds, where the change could be more dramatically witnessed. However, overall one could conclude that the BSFC remained relatively constant regardless of the amount of JP-8 introduced into the mixture.

During the research, the overall efficiency remained relatively constant at 29% decreasing by only 0.3% as the percentage of JP-8 content in the fuel mixture was increased to 50%. This is an excellent result taking in account the JP-8 lower density and viscosity.

NOx Emissions

Considering the heterogeneous nature of fuel-air mixture in diesel engines, NOx emissions are of a particular concern. Continuous efforts are being made to minimize the quantities of NOx pollutants from the diesel engine exhaust. NOx emission are comprised of NO and NO_2, with NO_2 being formed via the NO molecule. It is widely accepted that NO is formed via a thermal path in diesel engines. Formation of NOx emissions begins rapidly after the start of heat release in a compression ignition engine, with it ending as rapidly as it begin shortly after the end of heat release. This period of rapid NOx formation ends due in part to the temperature of the burned gas decreasing rapidly due to mixing with cooled bulk gas and expansion of the charge. Another important factor influencing the formation of NOx is that of the equivalence ratio. The equivalence ratio can be defined as the stoichiometric air-fuel ratio divided by the actual air-fuel ratio. As the equivalence ratio becomes leaner, it is expected that a significant decrease in the amount of NOx occur. It may also be noted that a higher combustion temperature is expected to result in higher formations of NOx. The combustion temperature may be

increased through advancing the injection timing or increasing the injection pressure which also has the effect of improving combustion efficiency. An increased rate of injection or increased air swirl is able to reduce the amount of exhaust smoke and thus increase the formation of NOx (Ahmad & Plee, 1983). Therefore, it can be seen that a tradeoff exists between the two variables. It was shown in some studies that the addition of diluents to the intake air of a compression ignition engine, such as N_2, CO_2, and exhaust gases were proven to be an effective means of reducing the rate of NO formation and hence the exhaust NOx levels. This is accomplished through the influence of the diluents on lowering the temperature of the peak flame, which serves as the driving force for the formation of NOx (Yu & Shahed, 1981). Thus a correlation was able to be formed on showing the effect of changes in the intake air composition and temperature on NOx emissions. The following NOx emissions were measured for the varying fuel blends subjected to speeds ranging from 2000 RPM to 2400 RPM at 4.78 BMEP, shown in Figure 103 -Figure 104 below.

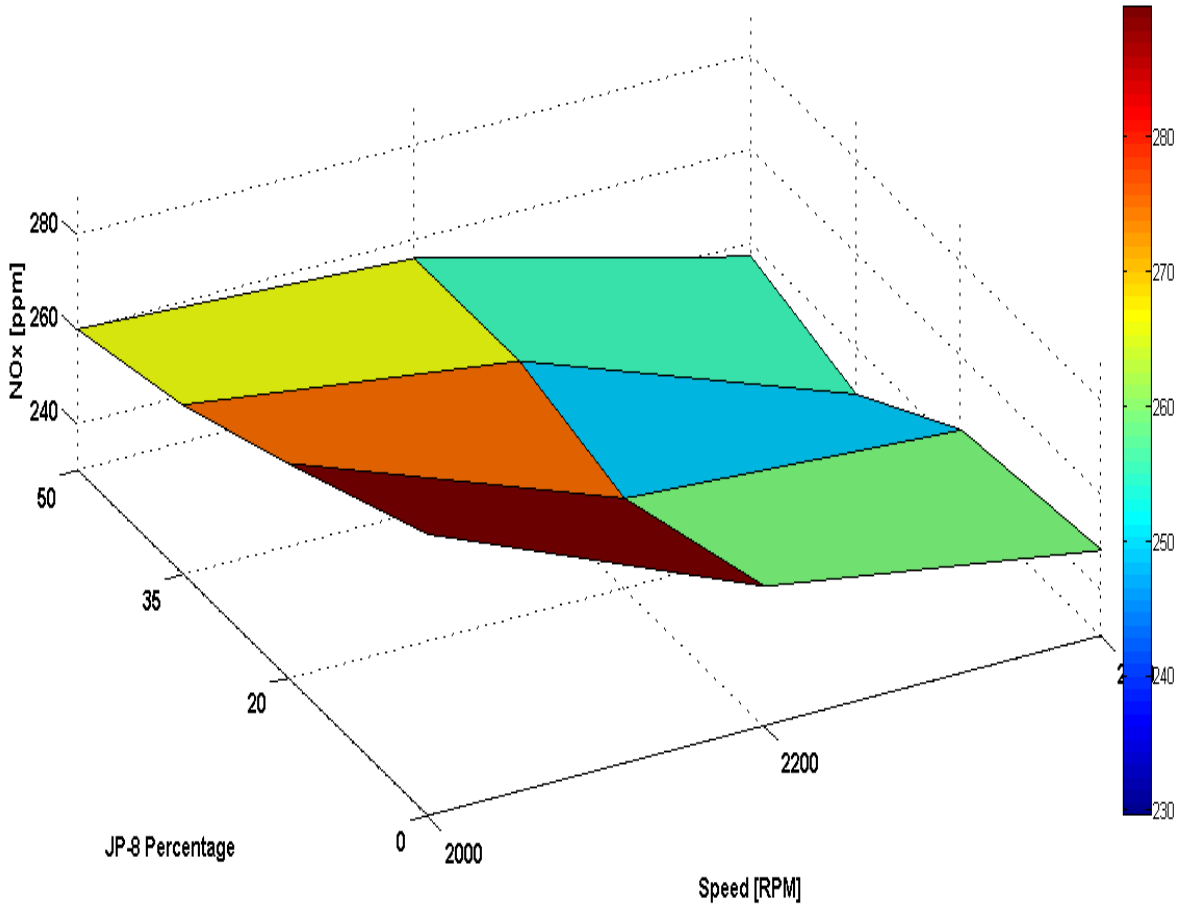

Figure 103 NOx Emissions (4.78 BMEP)

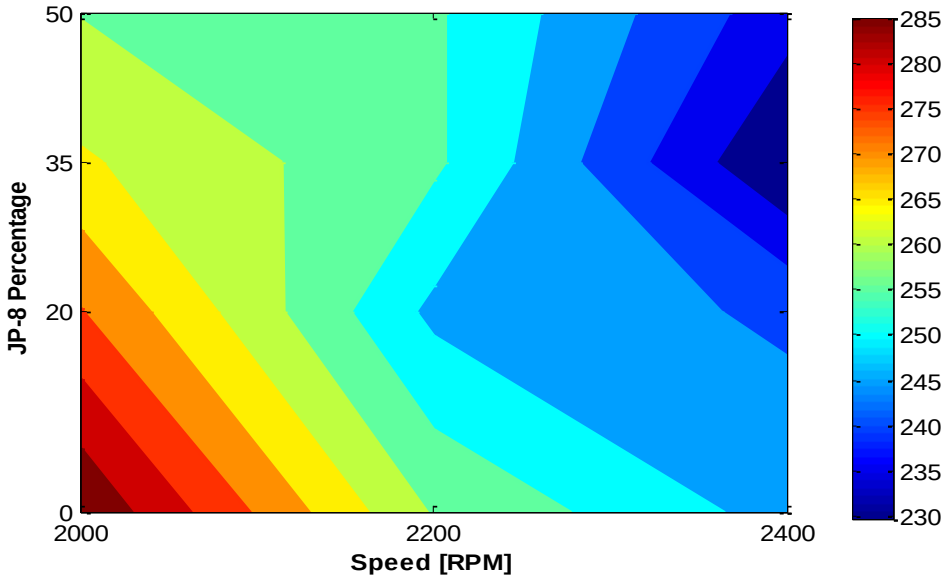

Figure 104 NOx Contour Plot

Based on the NOx figures, it can be seen that the highest concentration of NOx occurs for diesel at 2000 RPM. The NOx decreased in relation to speed and percentage of JP-8 introduced into the mixture. Although the smallest concentration of NOx occurred for the J35 blend at 2400 RPM. In terms of emissions based on these findings it can be suggested that simply adding 20% JP-8 by weight into diesel no.2 fuel shall result in a substantial reduction of NOx, especially at higher speeds.

Soot

The characterization of diesel smoke has remained a challenge in engine development. Diesel particulates consist principally of carbonaceous material or more commonly referred to as soot from smoke generated by combustion on which some organic compounds have become absorbed. Most of the particulate material results from incomplete combustion of fuel hydrocarbons with some being attributed to the contribution of the lubricating oil (Heywood, 1988). The mechanism of soot formation in carbonaceous fuel combustion is very complex and is dependent upon such variables as fuel properties, combustion design, and oxidant-fuel ratio mixing. The air/fuel combustion ratio determines several other properties of the soot particles due to the fact that they are linked to the soot formation process. That is, not only does the oxygen affect the flame temperature, determinant of such factors as mixing, nucleation, and growth rate, but also the particle oxidation rate. Accordingly, particle size distribution and surface area, at least, will be determined by the air/fuel ratio (CHUGHTAI, KIM, & SMITH, 21-43). The structure of n-hexane soot is very similar to that of diesel no.2 and JP-8, with the principle differences being due to the presence of trace elements from the sulfur and other additives in the fuel. This fact revealed among other characteristics, high aromaticity, a high density of unpaired electron spins, and surface carbon-oxygen functionalities. The primary soot

particles range in size from 0.05–0.10 μm geometric diameter spheroids which aggregate to an aciniform morphology (CHUGHTAI, KIM, & SMITH, 21-43). Reactivity of these particles depend primary on the type of fuel used and the combustion conditions of the engine. The following smoke values were measured for the varying fuel blends subjected to speeds ranging from 2000 rpm to 2400 rpm at 4.78 bar BMEP, shown in Figure 105-Figure 106 below.

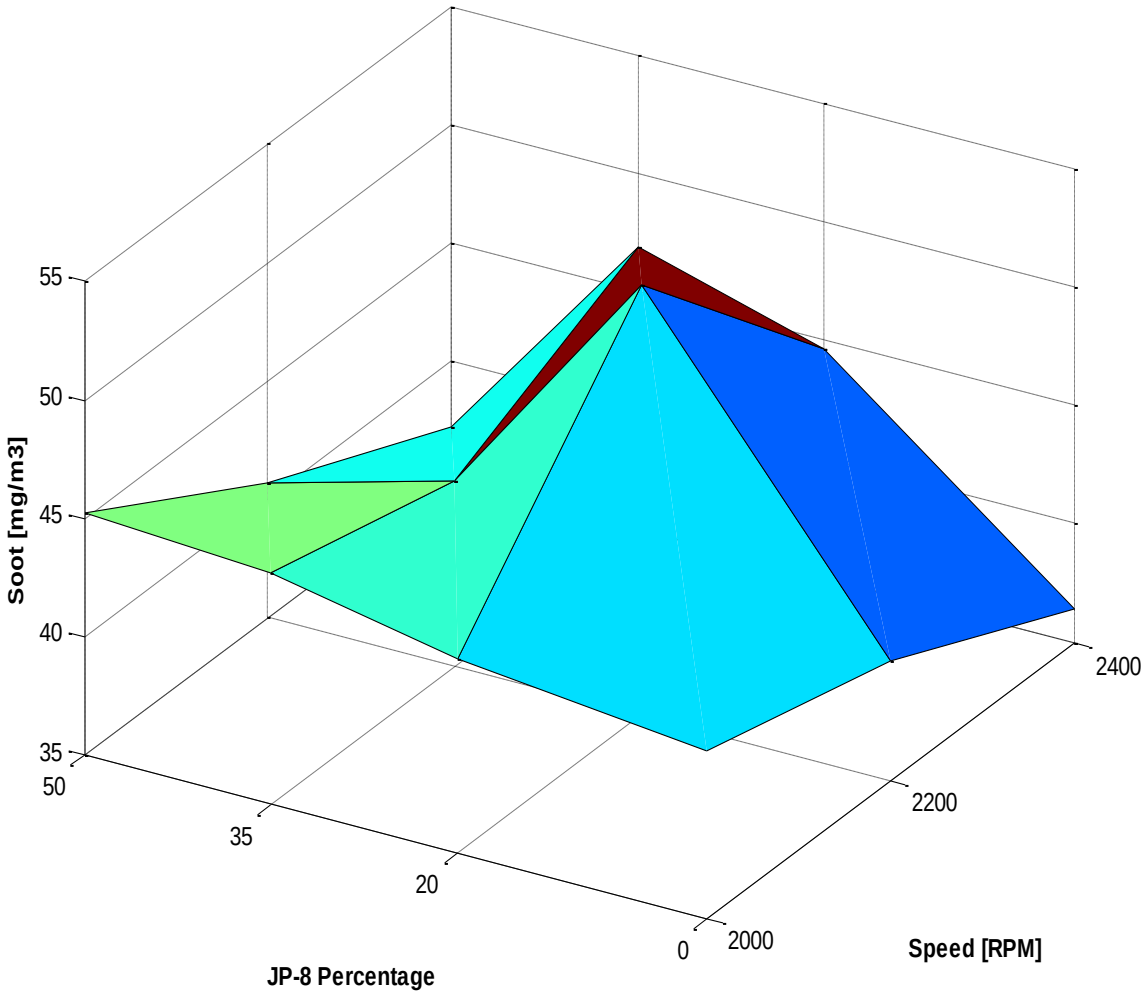

Figure 105 Soot Surface Plot (4.78 bar BMEP)

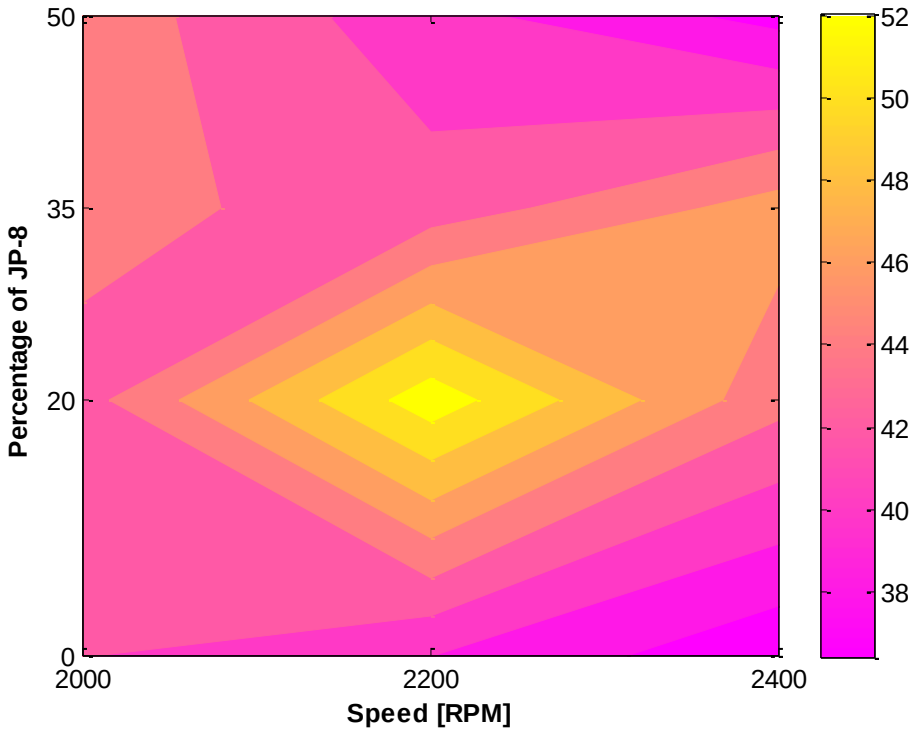

Figure 106 Soot Contour Plot (4.78 bar BMEP)

Based on the measured results it can be seen that the highest concentration of soot occurs for J20 at 2200 RPM. A very popular Method to characterize the particle emission is the light reflection of the soot collected from undiluted exhaust gas on a special paper filter. The filter-type smoke meter used in this study, reports its results as a filter smoke number (FSN) that is similar to the Bosch smoke number (BSN) scale. It operates by drawing a known and variable volume of exhaust gas through a paper filter. The reflectance of the paper is measured to determine the paper blacking and calculation of the smoke level in Filter Smoke Number (FSN). This measurement yields values for the Filter Smoke Number FSN (known as Bosch number) that assumes numbers from 0…10. The principal of operation is similar to the earlier fixed volume Bosch hand pumps, so for all intensive purposes it can be assumed to be comparable to the Bosch number.

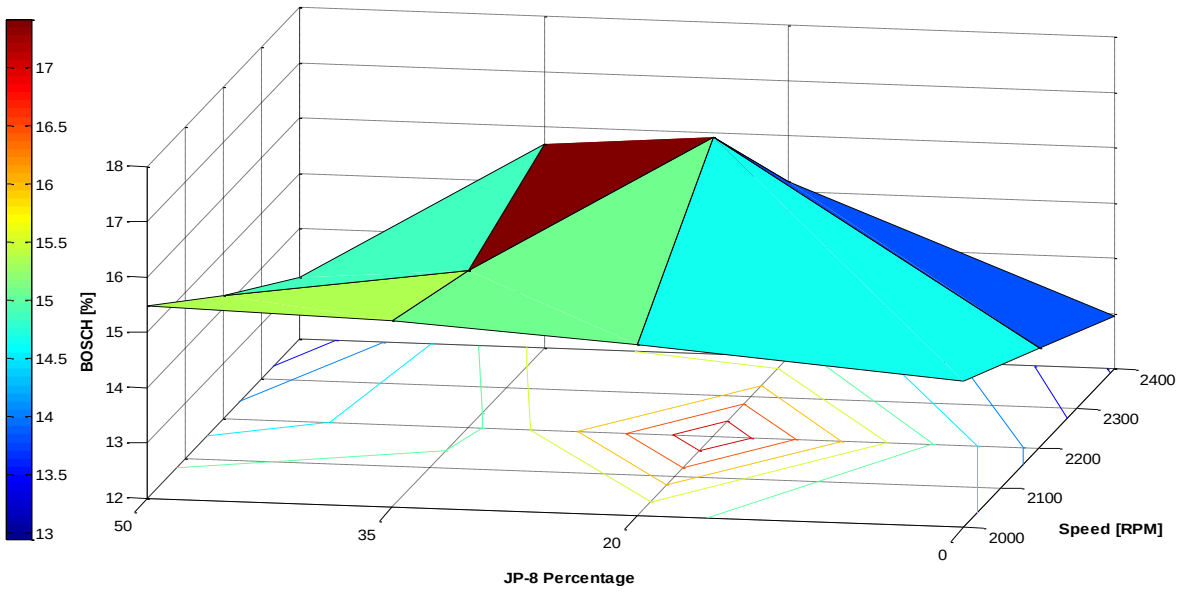

Figure 107 BOSCH (4.78 BMEP) Surface Plot

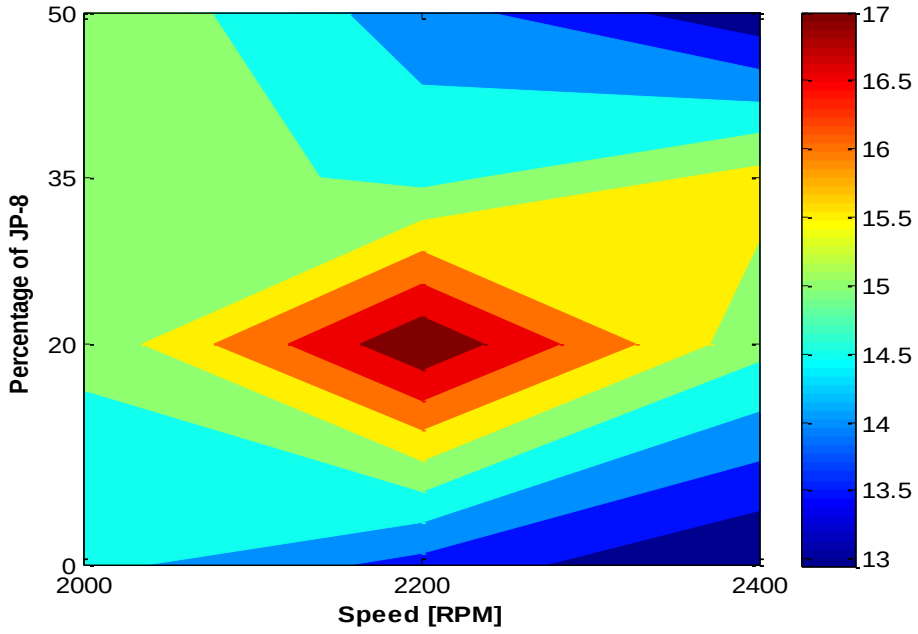

Figure 108 Bosch Contour Plot

The amount of the soot is then able to be calculated as a function of FSN based on an empiric equation with the results being shown in the figures below.

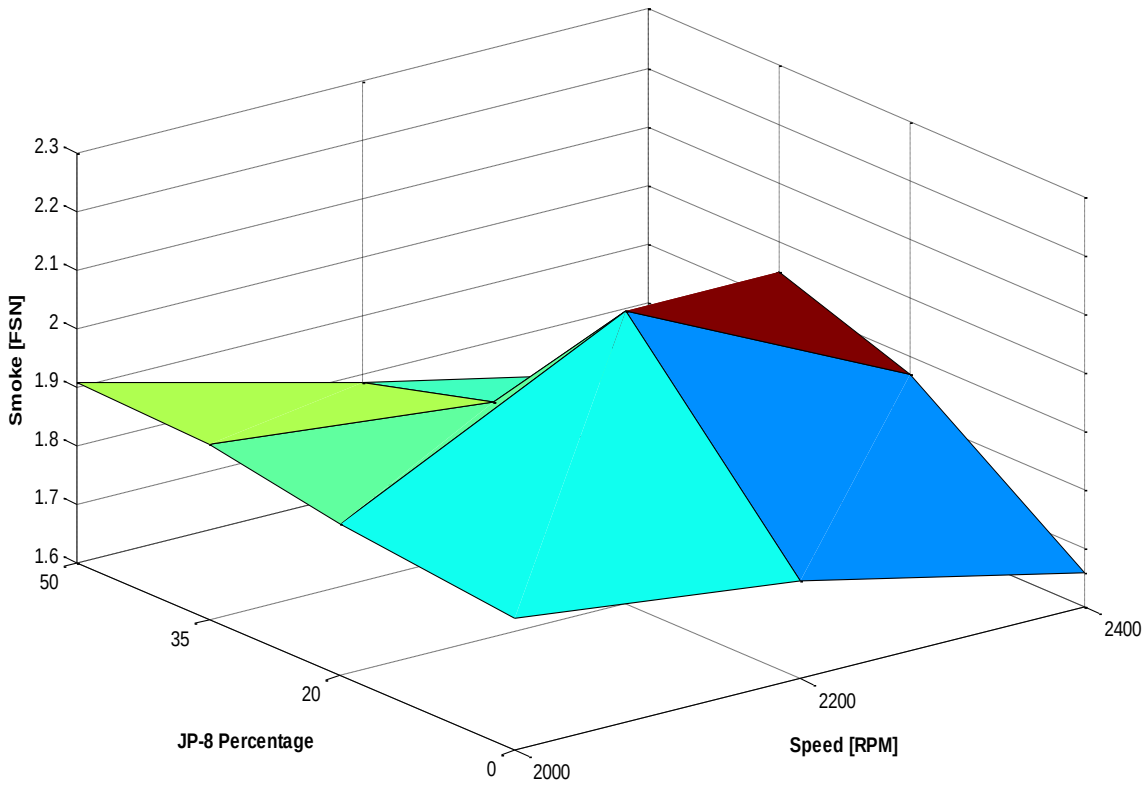

Figure 109 Smoke surface plot (4.78 BMEP)

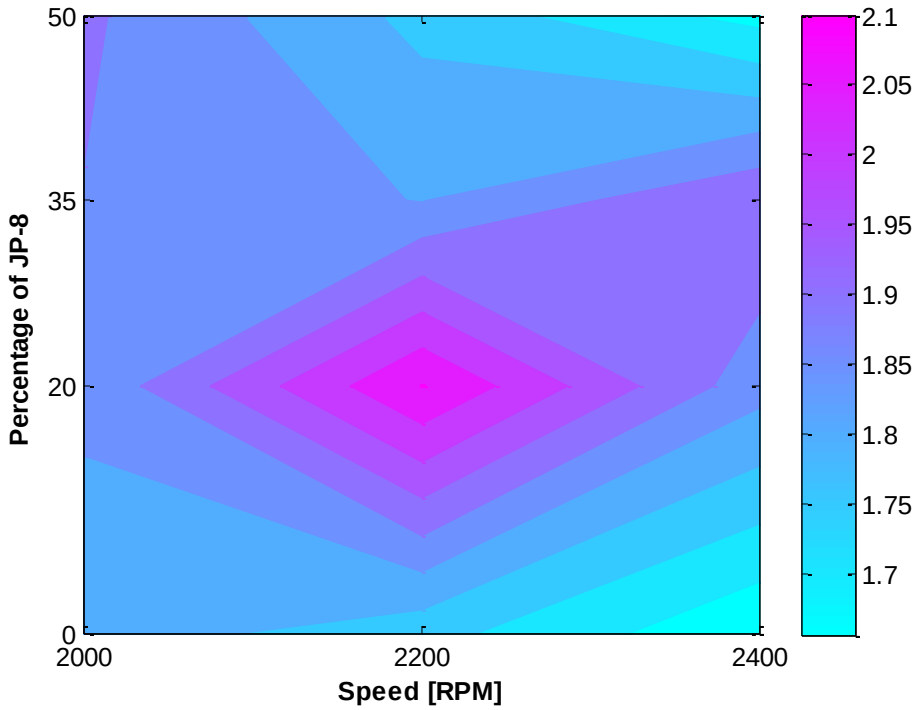

Figure 110 Smoke Contour Plot

The smoke emissions measured displayed an interesting characteristic of displaying a U-shaped behavior in terms of soot concentration, with the heaviest concentration residing for the J20 blend at 2200 RPM. This behavior can be explained due to the predominance of hydrocarbons in the fuels composition at light loads and of carbon at high loads (Heywood, 1988).

CHAPTER 5: THEORETICAL MODELING

Thermodynamic Cycle Simulation

The engines pressure will be modeled based on a model dealing with short term behavior, such as the thermodynamic combustion. This means that the pressure over the cycle will be

broken into several zones and tackled individually. When all of the various zones are described together they will model the experimental pressure cycle. The only input parameters relative to this model shall be simply the parameters related to the design of the engine. The model is based on straight forward representation of the geometry of a single cylinder in an internal combustion engine (Soloiu V. , 2010). This method also requires the use of additional parameters that can fall within a range values. The specific number within that range will vary from case to case and must be determined through a trial and error process. With the chosen values corresponding to the optimal desired result. These additional parameters are shown in the Table below.

Table 8 Additional Case Specific Parameters

Parameter	Symbol	Unit	Range	Value
Mechanical Efficiency	ηm	N/A	0.7-0.87	0.8
Initial Expansion Coefficient	ρ	N/A	1.2-3	1.5
Compression Polytropic Coefficient	m_c	N/A	1.31-1.37	1.27
Expansion Polytropic Coefficient	m_d	N/A	1.20-1.32	1.20
Intake Temperature	T_a	[K]	310-480	399.2
Engine Operating Speed	N	[RPM]	0-5000	2200
Average Temperature of Burnt Gas	T_r	[K]	600-900	850
Pressure into Cylinder during Intake	pa	[MPa]	0.03-0.1	0.08
Pressure into Cylinder during Exhaust	pev	[MPa]	0.1-0.2	0.11
Relative Air-Fuel Ratio	λ	N/A	1.3-1.7	1.33

The engines indicated power, P_i [kW/L], can be determined by using the following equation:

$$P_i = \frac{Pe}{i(Vs)}$$

The parameters are as follows: P_i is the indicated power in [kW/L], P_e is the engines effective power in [kW], i is the number of cylinders, and VS is the displacement volume of the piston in [L]. The mean effective pressure, p_{eff} [MPa] is also able to be calculated by using the equation shown below:

$$p_{eff} = \frac{\tau P_e}{2i(Vs)\eta}$$

The parameters are as follows: P_e is the engines effective power in [kW], i is the number of cylinders, VS is the displacement volume of the piston in [L], τ is the number of strokes for one complete cycle, η is the mechanical efficiency associated with the engine, and p_{eff} is the mean effective pressure in [MPa]. It is important that the mean effective pressure derived is verified to be contained in the following range, 0.8-3.2 MPa, before continuing forward with the analysis. If the derived value for the mean effective pressure is not contained in that range all calculations computed prior should be reviewed for errors, because if it does not lie in that range, it is incorrect. The mean indicated pressure, p_{ind} [MPa] as a function of the number of strokes and speed with the influence of mechanical efficiency can then be found by using the equation shown below:

$$p_{ind} = \frac{p_{eff}}{\eta m}$$

The parameters are as follows: p_{ind} is the mean indicated pressure in [MPa], η is the mechanical efficiency associated with the engine, and p_{eff} is the mean effective pressure in [MPa]. Next, the mean piston speed, w_{pm} [m/s] is found by using the equation shown below:

$$w_{pm} = \frac{s(n)10^{-3}}{30}$$

The parameters are as follows: w_{pm} is the mean piston speed in [m/s], s in the stroke in [mm], and η is the mechanical efficiency associated with the engine. The zone to be considered shall now be that which occurs at the end of compression. During the compression stroke both the intake and exhaust valves are closed thus this system can be treated as a closed system. It is vital to recall from thermodynamics that during compression no heat is transferred to the fuel/air mixture. As the volume is decreased because of the piston's motion, the pressure in the gas in increased. The polytropic transformation of the compression and expansion that occur during the cycle can be characterized by mean polytropic coefficients, mc and md. The initial expansion coefficient, ρ, for a compression ignition engine typically falls within the range of 1.2-3. At the end of compression, the pressure within the cylinder can be described by:

$$p_c = p_a \varepsilon^{mc}$$

Where pc is the pressure within the cylinder at the end of compression, pa in the average pressure into the cylinder during intake, ε is the compression ratio for the given engine, and mc is the compression polytropic coefficient. The temperature associated with the end of compression can be described by the equation given below:

$$T_c = T_a \varepsilon^{mc-1}$$

Where Tc is the temperature within the cylinder at the end of compression, Ta in the average temperature into the cylinder during intake, ε is the compression ratio for the given engine, and mc is the compression polytropic coefficient. Realizing that this is not going to be an ideal diesel cycle like the ones presented in classical thermodynamics, because the gas exchange is not

instantaneous, it can be recognized that the some roundness function must be introduced in order to account for these dramatic changes. Based on this the mean indicated pressure for the system needs to corrected, in the following manner:

$$\grave{p_i} = \frac{1}{\eta_d}\left[p_i + \eta_p(p_{ev} - p_a)\right]$$

With ηd and ηp being coefficients to help round the system, pev being the average pressure in the exhaust, and pi being the mean indicated pressure. The maximum pressure per cycle is limited by design and given by the fuel that is provided per cycle. Based on this the ratio of pressure increase during the combustion phase can be calculated as follows:

$$\lambda p = \frac{\frac{\epsilon - 1}{\epsilon^{mc}}\frac{pi'}{pa} + \left(1 - \frac{1}{\epsilon^{mc-1}}\right)\frac{1}{mc - 1}}{\rho - 1 + \frac{\rho}{md - 1}\left(1 - \frac{\rho}{\epsilon}\right)^{md-1}}$$

With the variables being defined according to values listed in Table 2. From this the maximum pressure of the cycle can be easily obtained by using the equation listed below:

$$p_{max} = \lambda p(pc)$$

With pc being the pressure at the end of compression and λp being the ratio of increase of pressure during combustion. By realizing the influence of the various zones on the volume of the cylinder, the associated volume for each zone can easily be determined. Then by combining the equations associated with each zone the following theoretical p-v diagram is able to be constructed.

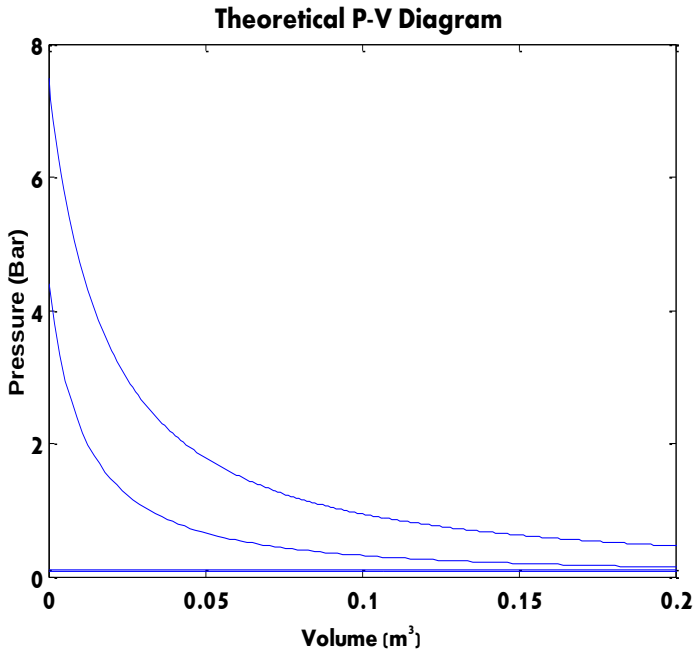

Figure 111 Theoretical PV diagram

This figure appears at first sight to be overall correct due to the fact that its shape follows the expected pattern associated with the four cycles of an internal combustion engine. However, when the theoretical P-V diagram is compared to the experimental PV-diagram some slight differences begin to emerge.

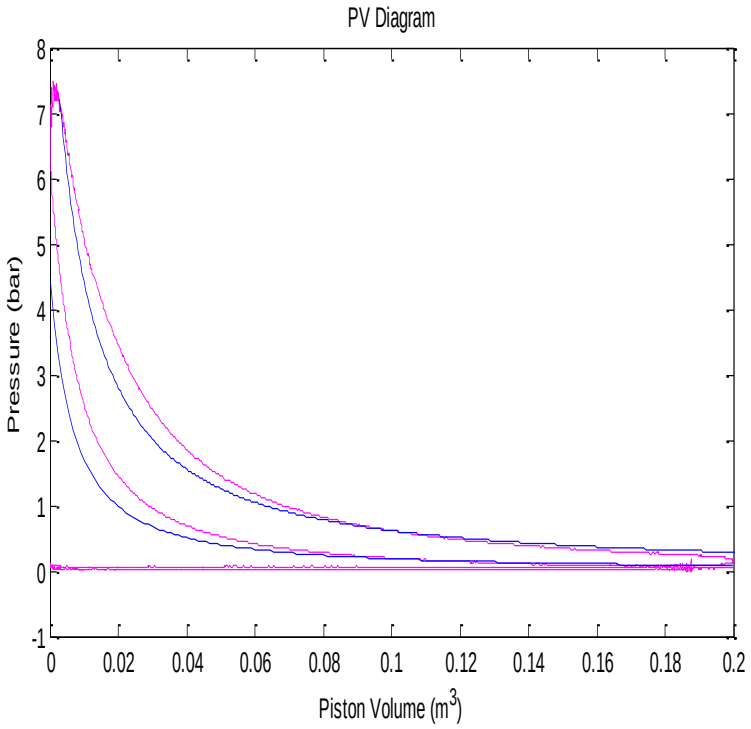

Figure 112 Comparison of experimental and theoretical P-V diagram

Based on the comparison presented above it can be observed that the initial model could be optimized in such a way to help account for the slight variation from the experimental results. One way to optimize the model is the addition of a coefficient exponent and a constant scalar function. After these modifications have been made the theoretical pressure data is plotted against the corresponding crank angle associated with the determined volume and compared to the experimentally obtained pressure vs crank angle data shown below:

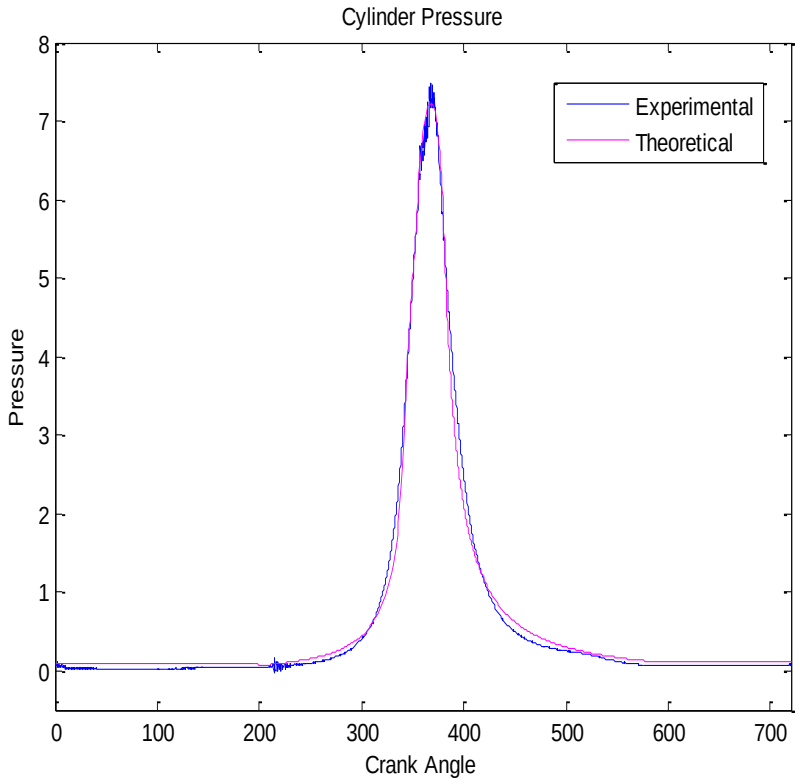

Figure 113 Comparison of experimental and theoretical Pressure vs Crank Angle diagrams

By studying the figure above it can be observed that the modeled theoretical pressure is very similar to the pressure values obtained experimentally and thus the model is valid. This valid pressure model can then be used to approximate the associated bulk gas temperature and heat release associated with the data set.

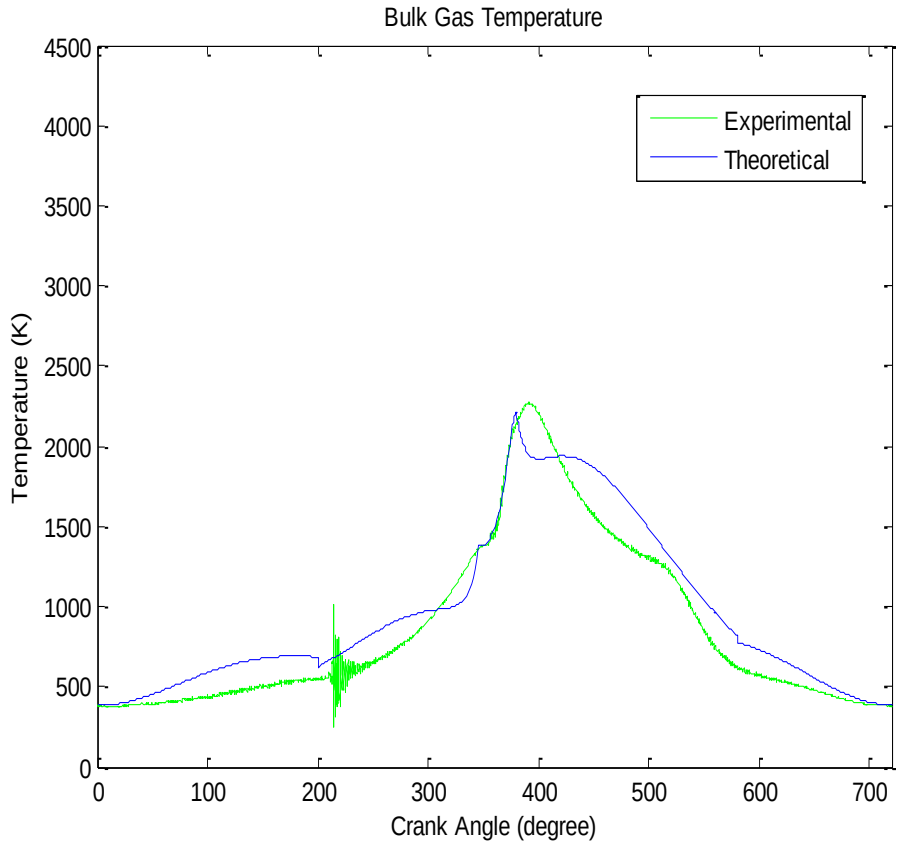

Figure 114 Comparison of experimental and theoretical Bulk gas Temperature

It can be observed from the figure that the bulk gas temperature approximation is less than ideal this is due to the fact of the linear approximations that were made. A comparison between the experimental and simulated results of the pressure and temperature are displayed in the table below.

Table 9 Comparison of Results

Parameter	Petro Diesel Experimental	B-20 Experimental	Theoretical
Max Pressure [MPa]	7.49000	7.3658	7.4904
Max Temperature [K]	2.2735e+003	2.2399e+003	2.2735e+003

These linear approximations created discontinuities in the form of "cusp" or sharp corner. It is known from calculus, that a graph that has a cusp in it is not differentiable at the point where the cusp occurs. Thus a discontinuity results from the formation of the cusp. When the gradients were taken these discontinuities were amplified. The Heat Release approximation is shown below in Figure 115.

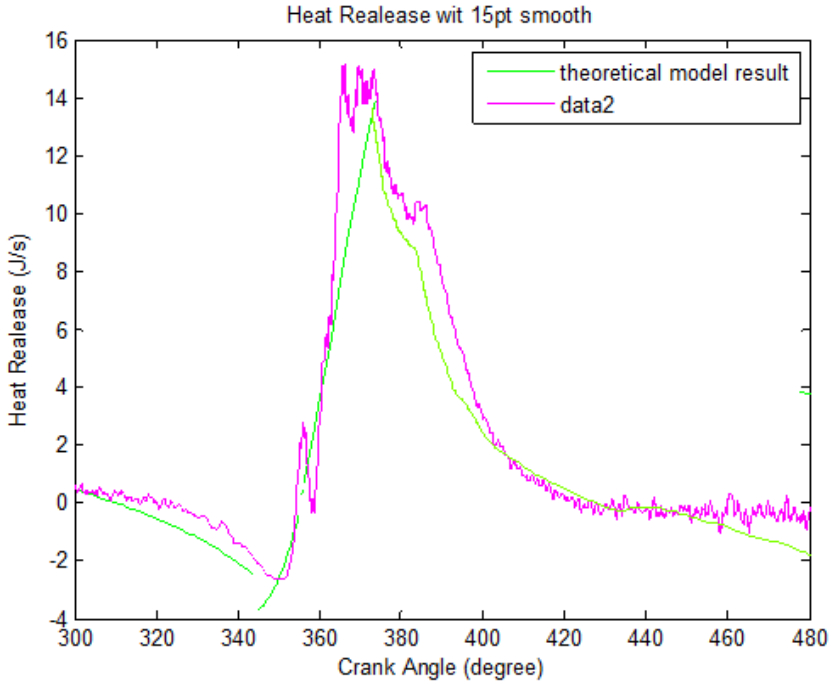

Figure 115 Comparison of experimental and theoretical Heat Release

The approximation of the heat release from the theoretical modeled pressure is a very similar match to the experimentally obtained results. Other theoretical parameters were also calculated for this engine and are presented in the table below.

Table 10 Theoretical Simulation Results

Parameter	Symbol	Unit	Value

Mean Effective Pressure	pe	[MPa]	0.2182
Mean Indicated Pressure	pi	[MPa]	0.2728
Mean Piston Speed	w_{pm}	m/s	5.1333
Pressure at End of Compression	pc	[MPa]	4.4091
Temperate at End of Compression	Te	[K]	936.2220
Mean Indicated Pressure Corrected	pic	[MPa]	0.8069
Ratio of Increase in Pressure during Combustion	λp	N/A	1.6989
Volume of Cylinder at end of Combustion	Vz	[L]	0.0217
Minimum quantity of air necessary for Combustion	Lo	[kmole air/kgfuel]	0.4969
Quantity of Air vs Mass of Fuel before Combustion	N1	[kmole air/kgfuel]	0.6609
Molar Quantity of CO_2	N_{CO2}	[kmole air/kgfuel]	0.0714
Molar Quantity of H_20	N_{H2O}	[kmole air/kgfuel]	0.0665
Molar Quantity of O_2	N_{O2}	[kmole air/kgfuel]	0.0344
Molar Quantity of N_2	N_{N2}	[kmole air/kgfuel]	0.5221
Number of Kmole of Burnt Gas	N2	[kmole bg/kgfuel]	0.6945
Variation of fresh air between start/end Combustion	μ_0	N/A	1.0508
Kmole of Burnt Gas Remaining in Cylinder	Nr	[kmole bg/kgfuel]	2.248e-7
Total Number of kmole at end of Intake at BDC	Na	[kmole / cycle]	8.1809e-6
Kmole of Fresh Air	Npr	[kmole air/ cycle]	7.956e-6
Efficiency of the Exhaust Process	γ_r	[%]	2.8256
Filling Efficiency Coefficient	η_v	[%]	55.05
Burnt Gases at End of Combustion	Nga	[kmole bg/cylce]	8.3601e-6
Whole Mass of Gas into Cylinder in one Cycle	μ	N/A	1.0494
Expansion Pressure	pd	[MPa]	0.2758
Expansion Temperature	Td	[K]	1.3113e3
Mechanical Work during Isobaric Combustion	Wm	[kJ/cycle]	0.0541
Quantity of Fuel that can be completely burnt	Gcycle	[g]	0.012
Heat Quantity that can be obtained	Qtcycle	[kJ]	0.5038
Parameter	**Symbol**	**Unit**	**Value**
Hourly Fuel Consumption	c_{fuel}	[kgfuel/hr]	0.7945
Hourly Air Consumption	c_{air}	[kg air/hr]	0.5251

Break Specific Fuel Consumption	c_e	[g/kWhr]	305.58
Overall Efficiency of Engine	ηe	[%]	28.15
Brake Indicated Fuel Consumption	c_i	[g/kWhr]	244.46
Heat Effectively transformed In Mechanical Work	Qeff	[kJ/kg]	1.1781e6
Heat Consumed to overcome Internal Friction	Qf	[kJ/kg]	1.4608e
Indicated efficiency	ηi	[%]	35.19

Ansys Finite Element Analysis Model

Diesel engines have been used in light and heavy transport for many decades. Due to increasingly stricter requirements for lower fuel consumption and reduced emissions, further investigations into the diesel engine are required in order to help comply with this demand. One possible solution would be the improvement of the combustion process to optimize consumption and reduce emissions. Thus there is a strong demand to explore new combustion concepts capable of meeting stringent emission standards without the destruction of engine components. In the past engine optimization was done by conducting a series of trial and error physical experiments that were both costly and time consuming. By using engine modeling, the amount of testing and cost required is reduced because most of the testing is done virtually through a simulation, thus potential damage to engine components is able to be avoided.

The creation of a new engine model method requires a broad range of experimental data. To make an accurate model, the data must span the entire range of operating conditions. However, only a relatively small amount of data is needed. Therefore, the demand is now able to be satisfied through the development of computer models for engine design, the combination of experimental measurements and validated computer model predictions as to provide an added opportunity for improved understanding of in-cylinder combustion and pollutant-formation

processes. By the creation of an engine model the analysis and comparison of various alternative fuels can easily and efficiency be developed. With this new tool in our arsenal the concept of sustainability is finally visible on the horizon.

With the growing interest in alternative fuels and the need for engine testing, the cost associated with this said testing is steadily rising. In order to combat this increased cost associated with repeated component damage, and help process the interactions between complex geometries, the help of computer aided software will be employed. The software that fits the general purpose of the scope of this paper is ANSYS, which is a finite element modeling package created for numerically solving a wide variety of mechanical, heat, and fluid problems.

Boundary conditions

During engine testing, the main component of importance in terms of potential damage due to fuel properties is that of the piston. When analyzing the piston, it is essential that a pin and connecting rod assembly be incorporated into the study, due to the fact that the dynamic performance of the piston is a function of the contact pressure between the pin and bearing system. In terms of safety it is vital that the forces acting between the piston and pin be analyzed, in particular the forces associated with the pin distortion. The piston using known parameters given by the specifications of the engine was constructed using the Pro-Engineer software. This piston assembly is as shown in the Figure given below.

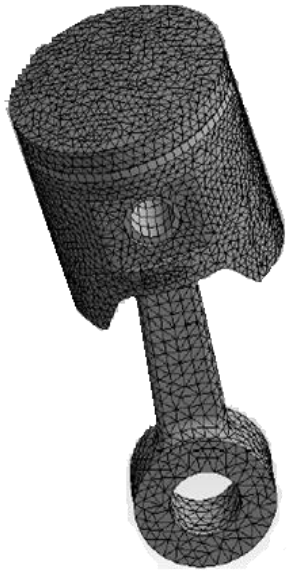

Figure 116 Piston Assembly

This model of the piston was meshed with Solid186 element in the ANSYS workbench. This level of mesh refinement was verified at adequate for continuing with the analysis of the model by the preliminary mesh convergence analysis.

Typically Internal Combustion (IC) engine pistons are comprised of an aluminum alloy versus cast iron from which the cylinder bore is made. Thus the piston has an 80% higher thermal expansion coefficient when compared to the cylinder. The Temperature distribution of the piston is modeled, it is of importance because it leads influence to both thermal deformations and thermal stresses. However, the piston temperature remains constant throughout the working cycle with no influence on the operating state being observed. Assuming a steady state thermal case, and taking into consideration the experimental bulk gas temperature obtain, the figure below shows the boundary conditions applied to the piston at different positions.

Figure 117 Steady State Thermal Boundary Conditions

With A representing the maximum experimental obtained bulk gas temperature, and B,C,D representing heat transfer convection coefficients. The static structural boundary conditions were applied in order to help to simulate the piston behavior accurately and can be seen in the figure below:

Figure 118 Static Structural Boundary Conditions

With C representing an applied load of the maximum experimentally obtained pressure. B represents the area in which a fixed support was applied. A frictionless support was placed the circumference of the piston represented by A in the figure above. This was chosen to simulate the movement of the piston within the cylinder.

In order to fully analyze the component in question the connection between the piston and pin as well as the connection between the pin and connecting rod were changed from the default "bonded" to "no separation" to allow relative translational and rotary motions, which are vital for the evaluation of the influence of a fuel on a piston.

Results

By using the experimental data in correlation with the given engine parameters and applied boundary conditions various models such as the temperature distribution and the von Mises equivalent stress distribution within the piston were able to be derived using the ANSYS software. The temperate distribution within the piston is displayed in the figure given below:

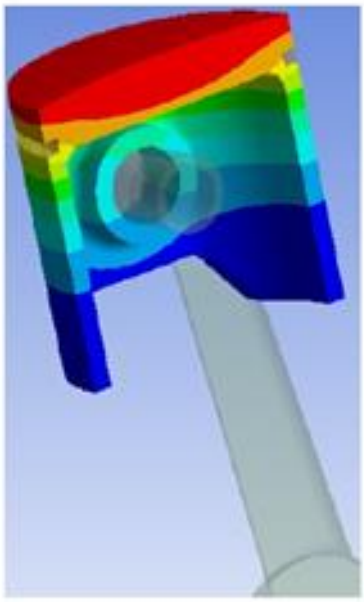

Figure 119 FEA Temperature Distribution

By observing the figure above it becomes evident that for the given operating temperature which in this case is the maximum experimental bulk gas temperature, that this maximum temperature from the combustion of gas in the chamber penetrates the piston crown through nearly 86% of its thickness before the piston ring is able to dissipate any of the heat. However, in the structure following beneath the piston ring the temperature begins to dissipate rapidly. This observation leads to the conclusion in terms of temperature the only area in question is that occurring above the piston ring.

Next the von Mises equivalent stress distribution within the piston is found in order to see what conclusions can be drawn.

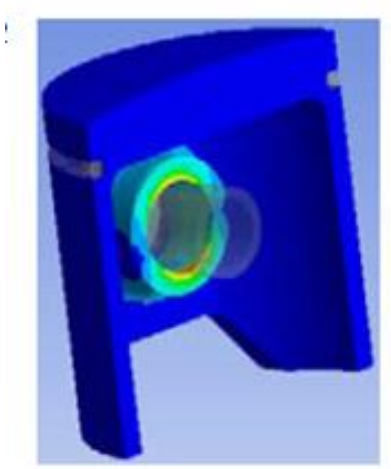

Figure 120 FEA Stress Distribution

From the figure above the following conclusion can be drawn, that being that the compressive stresses on the piston are negligible. However, in order to further verify this analysis the safety factor model associated with the component was also found and is displayed by the figure given below:

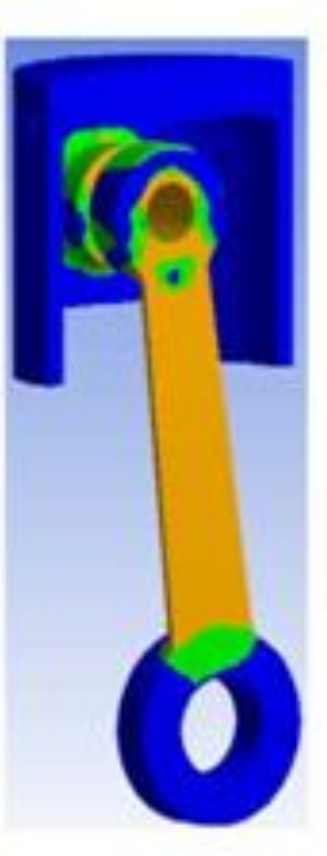

Figure 121 FEA Safety Factor

Based on the figure above, the forces acting on the piston head are transmitted to the pin with a factor of safety of approximately 0.948 for the given operating conditions. Using this process diesel at 2000RPM was investigated under various loads to determine the amount of deformation that would occur and are shown in the table presented below:

Table 11 Maximum Deformation

Engine Loading [%]	**Mean Effective Pressure [**MPa]	**Deformation** [mm]
50%	3.25	0.051

80%	5.15	0.062
100%	5.45	0.079

Based on these results it can be concluded that the material of the piston can withstand the influence of the fuel for the given conditions

Future Research

In order to fully evaluate the effects an alternative fuel has on an engine piston, more detailed analysis should be obtained, in particular the analysis of shear stresses occurring within the cross section of the pin. In time this method of FEA analysis will lead to continued improvement of the combustion process to optimize consumption and reduce emissions. The use of FEA could aid in the selection of new materials for component manufacturing.

CHAPTER 6: CONCLUSION

The authors investigated the injection and combustion of the military aviation fuel, JP-8, a mixture of 20%-50 % by weight in diesel in an indirect injection diesel engine obtained with favorable combustion properties. All of the fuel blends proved to be stable with this composition during the storage for more than 8 months. It was observed that the JP-8 fuel displayed no ignition difficulties in a diesel auxiliary power unit with a high compression ratio. For optimal operation neither intake manifold heating, pilot injection, nor increase in swirl ratio were needed. The ignition delay remained relatively constant at approximately 1.02-1.06 ms for both the diesel and JP-8 blends with the largest value occurring at 2200 rpm for J20. The heat release showed a

favorable development for a diesel engine operation, with both premixed and diffusion combustion phases being compounded into a single event.

The engine investigation proved that 20-50% JP-8 by weight in diesel can be burnt in a diesel engine about 5 ms at 2000rpm resulting in combustion duration of 60-65 CAD, and the engine's continuous power could be reached. The maximum combustion pressure remained relatively constant for all fuel blends, 72.7 bar for diesel and decreased slightly by 0.4 bar for the J50 blend, with the peak pressure position into the cycle being delayed by about 0.5 degrees for the J50 blend for 2000 rpm, with the same trend being able to correlate well with the other speeds. The instantaneous volume averaged gas temperature shifts later in the crank angle as the JP-8 percentage increases, while retaining a higher temperature for a longer, with the position of the occurrence of the maximum temperature of combustion being slightly delayed when compared to diesel. The greatest temperature occurred at the highest speed (2400 rpm) and largest percentage of JP-8 (J50) tested. The exhaust temperatures remained relatively constant for all blends at all test speeds. The heat flux in the engine cylinder showed similar values for all fuels, while the cylinder heat losses were at a minimum during combustion before TDC with increased convection losses at TDC for all fuels and first part of power stroke. The convection flux has a maximum earlier in the cycle compared to the radiation flux and following the zone of maximum turbulence location, while the crank angle to which the maximum radiation flux has been obtained is maximum temperature dependent. The heat losses associated with the system increased slightly with the addition of JP-8 without any phase shifts extending for the duration of cycle. The largest gradient in terms of gross heat release belongs to that of the J50 blend, as it contains both the smallest and largest gross heat release rate value over the tested speeds.

The BSFC increased in relation to speed and decreased in relation to the percentage of JP-8 introduced into the mixture. This correlation became especially strong at higher speeds, where the change could be more dramatically witnessed. However, overall one could conclude that the BSFC remained relatively constant regardless of the amount of JP-8 introduced into the mixture. For example, the BSFC increased by 5% for J20, but returns to just above 1% higher than the initial value of diesel for 2000 rpm. The engine's mechanical efficiency was the lowest for J20 (81.5%) and recovered with the addition of 50 % JP-8 (82.4%) to display similar values with that of diesel (83%) at 2000 rpm. For all blends, it can be seen that the engine's mechanical efficiency was at a maximum when the engine was set at a speed on 2200 rpm. The engine's mechanical efficiency with the JP-8 displayed similar values with that of diesel combustion showing a decrease of less than 1 percent at 2000 rpm, despite the increased lubricity of the JP-8 due to the required Corrosion Inhibitor /Lubricity Improver (MIL-PRF-25017) additive. Taking into account each fuels' corresponding density, the engines' overall efficiency obtained remained relatively constant with the addition of the JP-8.

The highest concentration of NOx occurs for diesel at 2000 rpm. The NOx decreased in relation to speed and percentage of JP-8 introduced into the mixture. Although the smallest concentration of NOx occurred for the J35 blend at 2400 rpm. In terms of emissions based on these findings it can be suggested that simply adding 20% JP-8 by weight into diesel no.2 fuel shall result in a substantial reduction of NOx, especially at higher speeds. The highest concentration of soot occurred for J20 at 2200 rpm. The smoke emissions measured displayed an interesting characteristic of displaying a U-shaped behavior in terms of soot concentration, with the heaviest concentration residing for the J20 blend at 2200 rpm.

The engine ran approximately 50 hours on the JP-8/diesel mixtures. During this time no break-down in the fueling system, piston rings assembly, or crankshaft journals has been recorded. After each investigation, the engine ran for about 30 min with pure diesel fuel to flush the system. The engine was then tested using the reference diesel fuel to ensure the original values obtained could be repeated. This data provides valuable information as it allows researchers to determine which speed and blend will be best for a particular application. The study proved the JP-8 displays combustion characteristics very similar to those of diesel no 2 meaning it is a viable substitution for application in a diesel auxiliary power unit.

REFERENCES

a, E. U., a, K. H., & Yang, S. L. (2005). Numerical Heat Transfer. *An International Journal of Computation and Methodology , 48* (6), 1-23.

Aceves, S. M., Flowers, D. L., Martinez-Frias, J., Smith, J. R., Dibble, R., Au, M., et al. (2001). HCCI Combustion: Analysis and Experiments. *SAE World Congress & Exhibition*, (pp. 1-12). Washing D.C.

Ahmad, T., & Plee, S. L. (1983). Application of Flame Temperature Correlations to Emissions from a Direct-Injection Diesel Engine. *SAE.*

Arcoumenis, C., Cuter, P., & Whitelaw, D. (1998). Heat transfer process in diesel engines. *IChemE 176, Part A.*

Balat, M., & Balat, H. (2008). A critical review of biodiesel as a vehicular fuel. *Energy Conservation Management* , doi:10.1016/j.enconman.2008.03.016.

Blaine, R. G. (1897). *Hydraulic machinery: with an introduction to hydraulics* .

Borman, G., & Nishiwaki, K. (1987). Internal-Combustion Engine Heat Transfer. In *Progress in Energy and Combustion Science* (1 ed., Vol. 13, pp. 1-46).

CHUGHTAI, A., KIM, L., & SMITH, D. (21-43). The Effect of Air/Fuel Ratio on Properties and Reactivity of Combustion Soots. *Journal of Atmospheric Chemistry* , 2002.

Coordinating Research Council, Inc. (1983). *Handbook of aviation fuel properties.* Altanta, Ga: CRC-530.

Cosgrove, J., Church, D., & Pryor, W. (1987). The kinetics of auto-oxidation of poly unsaturated fatty acids. *Lipids , 22*, 299-304.

Culick, F., Heitor, M., & Whitelaw, J. (1996). Unsteady Combustion. *Proceedings of the NATO Advanced Study Institute.* Praia da Granja, Portugal: Springer.

Dibble, R., Au, M., & Girard, J. (2001, May). HCCI Combustion: Analysis and Experiments. *SAE* , 1-12.

Fernandes, G., Fuschetto, J., Filipi, Z., Assanis, D., & McKee, H. (2007). Impact of military JP-8 fuel on heavy-duty diesel engine performance and emissions. *Journal of Automobile Engineering , 221*, 957-971.

Fernandes, G., Fuschetto, J., Filipi, Z., Assanis, D., & McKee, H. (2007). Impact of military JP-8 fuel on heavy-duty diesel engine performance and emissions. *Proceedings of the Institution of Mechanical Engineers: Part D.*

Giannelli, R., Nam, E., Helmer, K., Younglove, T., Scora, G., & Barth, M. (2005). Heavy-Duty Diesel Vehicle Fuel Consumption Modeling Based on Road Load and Power Train Parameters., (pp. 1-13).

Henein, N. (1997). *Autoignition and combustion in diesel engines under cold starting conditions.* Wayne State University, Center for Automotive Research. Detroit: Department of Energy.

Heywood, J. B. (1988). *Internal Combustion Engine Fundamentals.* McGraw-Hill.

Karthikeyan, R., Davis, L., Mankin, K., Erickson, L., & Kulakow, P. (1999). BIODEGRADATION OF JET FUEL (JP-8) IN THE PRESENCE OF VEGETATION. *Conference of Hazardous Waste Research,* (pp. 243-252). Manhattan, KS.

Knothe, G., & Steidley, K. R. (2007). Kinematic Viscosity of Biodiesel Componenets and related compounds at low temperatures fuel. *86 (1)* , 2569-2567.

Kondepud, D. i., & Prigogine, I. (1998). *Modern Thermodynamics: From Heat Engines to Dissipative Structures.* Wiley.

Korres, D. M., Karonis, D., Lois, E., Linck, M. B., & Gupta, A. K. (2008). Aviation fuel JP-5 and biodiesel on a diesel engine. *Fuel , 87* (1), 70-78.

Lakshminarayanan, P. A., & Aghav, Y. V. (2010). *Phenomenology of Diesel Combustion and Modelling.* SpringerLink.

Lesta, S. J., & LePera, M. E. (1992, February). Technology Demonstration of U.S. Army Ground Material Operating on Aviation Kerosene Fuel. *SAE Technical Paper Series: Alternative Fuels for SI and CI Engines* .

Majewski, W. A., & Khair, M. K. (2006). *Diesel Emissions and Their Control* . Society of Automotive Engineers.

Milen, M., & Kiril, B. (2004). INVESTIGATION OF THE EFFECTS OF HYDROGEN ADDITION ON PERFORMANCE AND EXHAUST EMISSIONS OF DIESEL ENGINE. *Fisita World Automotive Congress,* (pp. 23-37). Barcelona.

Nagaraju, V., Henein, N., Quader, A., Wu, M., & Bryzik, W. (2008, April 14-17). Effect of Biodiesel (B-20) on Performance and Emissions in a Single Cylinder HSDI Diesel Engine. *CI Engine Performance for use with Alternative Fuels* , 1-20.

Najt, P. M., & Foster, D. E. (1993). *Compression-Ignited.*

Nelson, D. (2010). *Investigation of Combustion and Emissions (NOx) from Chicken Fat Based Biodiesel in a Diesel Engine with Separate Three Vortex Combustion Chamber.* Georgia Southern University. Statesboro: MSAE Thesis.

Owens, E. C.; LePera, M. E.; Lestz, S. J. (1989). Use of Aviation Turbine Fuel JP-8 as the Single Fuel on the Battlefield. *International Fuels and Lubricants*, (pp. 1-17). Baltimore, Maryland.

Rogers, C. F., Sagabiel, J. C., Zielinska, B., Arnott, W. P., Fujita, E. M., McDonald, J. D., et al. (2003). Characterization of Submicron Exhaust Particles from Engines Operating Without Load on Diesel and JP-8 Fuels. *Aerosol Science & Technology , 37* (4), 355-71.

Said, M. A., Buttsworth, D., & Yusaf, T. (2009). A Review of Radiation Heat Transfer Measurement for Diesel Engines Using the Two-Colour Method. *ICEE 3rd International Conference on Energy and Environment*, (pp. 237-242). Malacca, Malaysia.

Schihl, P., Hoogterp, L., Pangilinan, H., Schwarz, E., & Bryzik, W. (2006). *Modeling JP-8 Fuel Effects on Diesel Combustion Systems.* Report Number: A403654, RDECOM-TARDEC, Warren, MI.

Schihl, P., Hoogterp, L., Pangilinan, H., Schwarz, E., & Bryzik, W. (2006). *MODELING JP-8 FUEL EFFECTS ON DIESEL COMBUSTION SYSTEMS.* RDECOM-TARDEC, Warren, MI.

Shyam, K. A. (2006). *Internal Combustion Engines* . New Age International .

Soloiu, V. (2010, Spring). Design of IC Engines. *Class Notes* . Statesboro, Ga.

Soloiu, V. Y. (2010). Combustion and Emissions Characteristics of a Polypropylene Blended Diesel Fuel in a Direct Injection Compression Engine. *Proceedings of the ASME 2010 Internal Combustion Engine Division Fall Technical Conference ICEF2010.* San Antonio, Texas.

Soloiu, V., Covington, A., & Lewis, J. (2011). Combustion Charateristics in a Small Bore Diesel Auxiliary Power Unit (APU). *ASME ICE.* Morgantown.

Soloiu, V., Covington, A., Nelson, D., & Lewis, J. (2011). Investigations of a Poultry Fat - Fatty Acid Methyl Ester in a Triple Vortex Separate Combustion Chamber Diesel Engine –Stage one: Combustion investigations. *SAE World Congress.* Detroit: SAE 2011-01-1188.

Soloiu, V., Lewis, J., & Covington, A. (2011). Oleic Methyl Ester Investigations in an Indirect Injection Diesel Engine; Stage one: Combustion investigations. *SAE World Congress.* Detroit: SAE 2011-01-0616.

Szybist, J. P., Kirby, S. R., & Boehman, A. L. (2005). NOx Emissions of Alternative Diesel Fuels: A Comparative Analysis of Biodiesel and FT Diesel. *Energy Fuels , 19* (4), 1484-1492.

TARDEC. (2001). JP-8 The Single Fuel Forward: An Information Compendium. *U.S. Army Tank-Automotive and Armaments Command Research, Development, and Engineering Center (TARDEC) Report* .

Tsuji, F., & Neto, L. (2008). *Influence of Vegetable Oil in the Viscosity of Biodiesel.*

Tunestal, P., Wilcutts, M., Lee, A. T., & Hendrick, K. (1999). In-Cylinder Measurement for Engine Cold-Start Control. *International Conference on Control Applications*, (pp. 460-464). Kohala Coast.

U.S. Air Force. (2008). *Jet Fuel Propellant (JP-8) General Facts and Information.* Falls Church, VA: Force Health Protection and Readiness.

US Department of Energy: Energy Efficiency and Renewable Energy. (October 2004). *Biodiesel Handling and Use Guidelines.*

Weston, K. C. (1992). *Energy Conversion.* PWS Pub. Co.

Yu, R., & Shahed, S. (1981). Effects of injection timing and exhaust gas recirculation on emissions from a D. I. diesel engine. *SAE.* (United States.

APPENDIX A

MATLAB COMBUSTION PROGRAM

```
%%%                Enter pressure1=[]; crank2=[];  ps1=[]; (4 DATA SETS 1-4)

%%%%%%%%%%Constants%%%%%%%%%%%%%%%%

%Vs=displacement volume of the piston L

VVs=0.324955479;

Vs=VVs/1000;

%E=compression ratio of engine

E=24.5;

%Vc=Volume of combustion chamber

Vc=Vs/(E-1);

%D=bore (m)

D=77/1000;

%s=stroke (m)

s=70/1000;

%r=radius (m)

r=s/2;

%Ts=Wall temperature of the cylinder (K)

Ts=420;

n=(VVs/22.4);

%connecting rod length is l

l=110/1000;

%R=molar gas constant

R=8.314472;
```

```
%%%%%%%% change units to 10^6 or 10^5 depending on data

u2=10^5

N=2200;

%mean effective pressure (bar)

mep=4.78

%%%%%Piston Movement Analysi%%%%%%%%%%

%Piston move

xm2= ((1-cos((pi/180).*crank2))+((r/l)/4).*(1-cos((pi/180)*2.*crank2)));


xp2=r.*((1-cos((pi/180).*crank2))+((r/l)/4).*(1-cos((pi/180)*2.*crank2)));


%%%%%%%%Temperature Analysi%%%%%%%%%%%%%%%%

%Temperature of the cylinder T

T1=Ts+(((r*pi*(D^2)*(1/4).*xm2)+Vc).*pressure1*u2)*(1/(n*R*0.7));

%dT represents the temperature gradient

dT1=diff(T1)./diff(crank2);

%figure(1),plot(crank2(1:end-1),dT2), xlabel('Crank Angle (degree)'), ylabel('dTemperature/da
(K)'), title('Temperature Gradient'),

%dP is the pressure gradient

dp1=diff(pressure1*u2)./diff(crank2);

%figure(2),plot(crank2(1:end-1),dp1), xlabel('Crank Angle (degree)'), ylabel('dPressure/da'),
title('Pressure Gradient'),

%figure(3),plot(10^-3.*xm2, pressure1), xlabel('Piston Volume (m^3)'), ylabel('Pressure (bar)'),
title('PV Diagram'),

%%%%%%%Work/Energy/POWER Analysi%%%%%%

%Vol2=((r*pi*(D^2))*(1/4).*xm2);
```

```
%volpis2=10^-3.*xm2;

%pw2=u2.*pressure2;

mm=abs(diff(xm2));

imep1=sum(mm.*p1(1:end-1))/2

indicated_work1=trapz(pressure1, xm2)/2

%indicated_work2=trapz(volpis2, pw2)

%N is the rpm

N2=2000;

energy_per_cycle2=(indicated_work1*N2)/(2*60)

%%%%%%%%%%%%Temperature Analysis Dr. Soloiu way%%%%%%%%%%

Vanc2=Vc+xm2.*pi*(D^2)*(1/4)*r;

dVanc2=diff(Vanc2)./diff(crank2);

%dPs5=diff(u2.*ps52)./diff(crank2);

dPs1=diff(u2.*ps1)./diff(crank2);

yy=1.33;

%dQps52=(Vanc2(1:end-1).*dPs52+yy.*ps52(1:end-1).*u2.*dVanc2)./(yy-1);

dQps1=(Vanc2(1:end-1).*dPs1+yy.*ps1(1:end-1).*u2.*dVanc2)./(yy-1);

%dQp1=(Vanc2(1:end-1).*dp2+yy.*pressure2(1:end-1).*u2.*dVanc2)./(yy-1);

%figure(5),plot(crank2(1:end-1),dQps52), xlabel('Crank Angle (degree)'), ylabel('Heat Realease
(J/degree)'), title('Heat Realease wit 5pt smooth'),xlim([300 480])

%figure(7),plot(crank2(1:end-1),dQp2), xlabel('Crank Angle (degree)'), ylabel('Heat Realease
(J/degree)'), title('Heat Realease wit no smooth'), xlim([300 480])

%%% HEAT FLUX AND RADIATION%%%

%Temp of Wall in Kelvin

Tw=500;

%Total area in m^2
```

```
At=2.5*pi*(D^2)*(1/4)+xm2.*pi*2*(D)*(1/2)*r;
%sigma is stepfans boltz constant but Nishiwaki (Soloiu mentor uses 3.3)
sigma=3.3*10^-8;
%epilison is 1 bc its considered to be a back body
ep=1;
dRad1=sigma*ep*((T1.^4-Tw^4))*10^-6;
viscosity1=4.94*(1273.15+110.4)./(T1+110.4).*(T1/1273.15).^(3/2)*10^-5;
ha1=-1.2775*10^(-8).*(T1.^2)+7.6696*10^(-5).*T1+0.00444888;
%density
roe1=pressure1*273*1.3.*(1./T1);
Re1=roe1.*s*N2*(1/30)*D./(viscosity1);
%Ac=constant range (0.3-0.9)
Ac=0.3;
convect1=ha1.*(1/D).*Ac.*((Re1).^0.7).*(T1-Tw)*10^-6;
%Flux1=(convect1(1:end-1)+dRad1(1:end-1));
Flux1=(convect1+dRad1);
dqr1=dRad1.*At.*(0.18/720);
dqc1=convect1.*At.*(0.18/720);
Q111=dqc1(1:end-1)*10^6+dQps1;
Q121=dQps1+dqr1(1:end-1)*10^6+dqc1(1:end-1)*10^6;
%%%%%%%pressure2%%%%%%%
%Temperature of the cylinder T
T2=Ts+(((r*pi*(D^2)*(1/4).*xm2)+Vc).*pressure2*u2)*(1/(n*R*0.7));
%dT represents the temperature gradient
dT2=diff(T2)./diff(crank2);
```

```
%figure(1),plot(crank2(1:end-1),dT2), xlabel('Crank Angle (degree)'), ylabel('dTemperature/da (K)'), title('Temperature Gradient'),

%dP is the pressure gradient

dp2=diff(pressure2*u2)./diff(crank2);

%figure(2),plot(crank2(1:end-1),dp1), xlabel('Crank Angle (degree)'), ylabel('dPressure/da'), title('Pressure Gradient'),

%figure(3),plot(10^-3.*xm2, pressure1), xlabel('Piston Volume (m^3)'), ylabel('Pressure (bar)'), title('PV Diagram'),

%%%%%%%%%Work/Energy/POWER Analysis%%%%%%%%%

%Vol2=((r*pi*(D^2))*(1/4).*xm2);

%volpis2=10^-3.*xm2;

%pw2=u2.*pressure2;

mm=abs(diff(xm2));

imep2=sum(mm.*p2(1:end-1))/2

indicated_work2=trapz(pressure2, xm2)/2

%indicated_work2=trapz(volpis2, pw2)

%N is the rpm

N2=2000;

energy_per_cycle2=(indicated_work2*N2)/(2*60)

%%%%%%%%%Temperature Analysis %%%%%%%%%%%%%%

dPs2=diff(u2.*ps2)./diff(crank2);

dQps2=(Vanc2(1:end-1).*dPs2+yy.*ps2(1:end-1).*u2.*dVanc2)./(yy-1);

%%%%% HEAT FLUX AND RADIATION%%%%%%%

dRad2=sigma*ep*((T2.^4-Tw^4))*10^-6;

viscosity2=4.94*(1273.15+110.4)./(T2+110.4).*(T2/1273.15).^(3/2)*10^-5;

ha2=-1.2775*10^(-8).*(T2.^2)+7.6696*10^(-5).*T2+0.00444888;
```

```
%density
roe2=pressure2*273*1.3.*(1./T2);
Re2=roe2.*s*N2*(1/30)*D./(viscosity2);
convect2=ha2.*(1/D).*Ac.*((Re2).^0.7).*(T2-Tw)*10^-6;
Flux2=(convect2+dRad2);
dqr2=dRad2.*At.*(0.18/720);
dqc2=convect2.*At.*(0.18/720);
Q112=dqc2(1:end-1)*10^6+dQps2;
Q122=dQps2+dqr2(1:end-1)*10^6+dqc2(1:end-1)*10^6;
%%%%%%%%pressure3%%%%%%%%
%Temperature of the cylinder T
T3=Ts+(((r*pi*(D^2)*(1/4).*xm2)+Vc).*pressure3*u2)*(1/(n*R*0.7));
%dT represents the temperature gradient
dT3=diff(T3)./diff(crank2);
dp3=diff(pressure3*u2)./diff(crank2);
%%%%%%%%%%Work/Energy/POWER Analysis%%%%%%%%%%%%
imep3=sum(mm.*p3(1:end-1))/2
indicated_work3=trapz(pressure3, xm2)/2
energy_per_cycle3=(indicated_work3*N2)/(2*60)
%%%%%%%Temperature Analysis %%%%%%%
dPs3=diff(u2.*ps3)./diff(crank2);
dQps3=(Vanc2(1:end-1).*dPs3+yy.*ps3(1:end-1).*u2.*dVanc2)./(yy-
%%%%%%%% HEAT FLUX AND RADIATION%%%%%%%
dRad3=sigma*ep*((T3.^4-Tw^4))*10^-6;
viscosity3=4.94*(1273.15+110.4)./(T3+110.4).*(T3/1273.15).^(3/2)*10^-5;
```

```
ha3=-1.2775*10^(-8).*(T3.^2)+7.6696*10^(-5).*T3+0.00444888;
%density
roe3=pressure3*273*1.3.*(1./T3);
Re3=roe3.*s*N2*(1/30)*D./(viscosity3);
convect3=ha3.*(1/D).*Ac.*((Re3).^0.7).*(T3-Tw)*10^-6;
Flux3=(convect3+dRad3);
dqr3=dRad3.*At.*(0.18/720);
dqc3=convect3.*At.*(0.18/720);
Q113=dqc3(1:end-1)*10^6+dQps3;
Q123=dQps3+dqr3(1:end-1)*10^6+dqc3(1:end-1)*10^6;
%%%%%%%%%%%%%%%%%%%%%%%%%%pressure4!!!!!!!!!!!!!!!!!!!!!!!!!!!!!!!
%Temperature of the cylinder T
T4=Ts+(((r*pi*(D^2)*(1/4).*xm2)+Vc).*pressure4*u2)*(1/(n*R*0.7));
%dT represents the temperature gradient
dT4=diff(T4)./diff(crank2);
dp4=diff(pressure4*u2)./diff(crank2);
%%%%%%Work/Energy/POWER Analysis%%%%%%%%%%%%
imep4=sum(mm.*p4(1:end-1))/2
indicated_work4=trapz(pressure4, xm2)/2
energy_per_cycle4=(indicated_work4*N2)/(2*60)
%%%%%%%%%%Temperature Analysis %%%%%%%%%%%%
dPs4=diff(u2.*ps4)./diff(crank2);
dQps4=(Vanc2(1:end-1).*dPs4+yy.*ps4(1:end-1).*u2.*dVanc2)./(yy-1);
%%%%%%%%%%%%%% HEAT FLUX AND RADIATION %%%%%%%%%%%%
dRad4=sigma*ep*((T4.^4-Tw^4))*10^-6;
```

```
viscosity4=4.94*(1273.15+110.4)./(T4+110.4).*(T4/1273.15).^(3/2)*10^-5;
ha4=-1.2775*10^(-8).*(T4.^2)+7.6696*10^(-5).*T4+0.00444888;
%density
roe4=pressure4*273*1.3.*(1./T4);
Re4=roe4.*s*N2*(1/30)*D./(viscosity4);
convect4=ha4.*(1/D).*Ac.*((Re4).^0.7).*(T4-Tw)*10^-6;
Flux4=(convect4+dRad4);
dqr4=dRad4.*At.*(0.18/720);
dqc4=cnvect4.*At.*(0.18/720);
Q114=dqc4(1:end-1)*10^6+dQps4;
Q124=dQps4+dqr4(1:end-1)*10^6+dqc4(1:end-1)*10^6;
%%%%%IGNITION DELAY%%%%%%%%
yyy=1;
for i=1:length(crank2);
      if fuel1(i)>=146.1;
       fid1(yyy)=[fuel1(i)];
       ids1(yyy)=[crank2(i)];
       tt1(yyy)=[i];
            yyy=yyy+1;

    else
        aaqwdsfv=1;
  end
    i=i+1;
end
```

```
yyy=1;
for a=2050:length(crank2)-1;
      if dQps1(a)<=0;
      dq1(yyy)=[dQps1(a)];
      ide1(yyy)=[crank2(a)];
      ttt1(yyy)=[a];
          yyy=yyy+1;
   else
       aaasdfads=1;
 end
   a=a+1;
end
c1=crank2(tt1(1):ttt1(1));
ahr1=dQps1(tt1(1):ttt1(1));
ahr1=abs(ahr1);
len1=length(c1); %the length of either input could be used, because they are the same
tote1=0; %the total must be initialized
aa=0;
for ii=1:len1-1 %There is one less interval than the number of data points, hence len-1
Wa1=(ahr1(ii+1)+ahr1(ii))/2; %this is the average value of the data
Int1=c1(ii+1)-c1(ii); %this is the time interval
AI1=Wa1*Int1; %this is the total energy for the interval or the area of that interval
tote1=tote1+AI1; %this adds up all of the intervals
aa=aa+1;
TAahr1(aa,:)=tote1;
```

```
end
Look1=tote1*.1;
bb1=linspace(Look1, Look1, length(TAahr1));
c11=c1(1:end-1);
YI1=interp1(TAahr1, c11, Look1);
ID1=(YI1-ids1(1))/(6*N)*10^3
%%%%%%IGNITION DELAY%%%%%%%%%%%
yyy=1;
for i=1:length(crank2);
     if fuel2(i)>=146.1;
      fid2(yyy)=[fuel2(i)];
      ids2(yyy)=[crank2(i)];
      tt2(yyy)=[i];
          yyy=yyy+1;
   else
       aaqwdsfv=1;
  end
   i=i+1;
end
yyy=1;
for a=2050:length(crank2)-1;
      if dQps2(a)<=0;
      dq2(yyy)=[dQps2(a)];
      ide2(yyy)=[crank2(a)];
      ttt2(yyy)=[a];
```

```
        yyy=yyy+1;
    else
        aaasdfads=1;
  end
    a=a+1;
end
c2=crank2(tt2(1):ttt2(1));
ahr2=dQps2(tt2(1):ttt2(1));
ahr2=abs(ahr2);
len2=length(c2); %the length of either input could be used, because they are the same
tote2=0; %the total must be initialized
aa=0;
for ii=1:len2-1 %There is one less interval than the number of data points, hence len-1
Wa2=(ahr2(ii+1)+ahr2(ii))/2; %this is the average value of the data
Int2=c2(ii+1)-c2(ii); %this is the time interval
AI2=Wa2*Int2; %this is the total energy for the interval or the area of that interval
tote2=tote2+AI2; %this adds up all of the intervals
aa=aa+1;
TAahr2(aa,:)=tote2;
end
Look2=tote2*.1;
bb2=linspace(Look2, Look2, length(TAahr2));
c12=c2(1:end-1);
YI2=interp1(TAahr2, c12, Look2);
ID2=(YI2-ids2(1))/(6*N)*10^3
```

```
%%%%%%%%%%IGNITION DELAY%%%%%%%%%%%%
yyy=1;
for i=1:length(crank2);
      if fuel3(i)>=146.1;
       fid3(yyy)=[fuel3(i)];
       ids3(yyy)=[crank2(i)];
       tt3(yyy)=[i];
           yyy=yyy+1;
    else
        aaqwdsfv=1;
  end
    i=i+1;
end
yyy=1;
for a=2050:length(crank2)-1;
       if dQps3(a)<=0;
       dq3(yyy)=[dQps3(a)];
       ide3(yyy)=[crank2(a)];
       ttt3(yyy)=[a];
           yyy=yyy+1;
    else
        aaasdfads=1;
  end
    a=a+1;
end
```

```
c3=crank2(tt3(1):ttt3(1));
ahr3=dQps3(tt3(1):ttt3(1));
ahr3=abs(ahr3);
len3=length(c3); %the length of either input could be used, because they are the same
tote3=0; %the total must be initialized
aa=0;
for ii=1:len3-1 %There is one less interval than the number of data points, hence len-1
Wa3=(ahr3(ii+1)+ahr3(ii))/2; %this is the average value of the data
Int3=c3(ii+1)-c3(ii); %this is the time interval
AI3=Wa3*Int3; %this is the total energy for the interval or the area of that interval
tote3=tote3+AI3; %this adds up all of the intervals
aa=aa+1;
TAahr3(aa,:)=tote3;
end
Look3=tote3*.1;
bb3=linspace(Look3, Look3, length(TAahr3));
c13=c3(1:end-1);
YI3=interp1(TAahr3, c13, Look3);
ID3=(YI3-ids3(1))/(6*N)*10^3
%%%IGNITION DELAY%%%
yyy=1;
for i=1:length(crank2);
    if fuel4(i)>=146.1;
     fid4(yyy)=[fuel4(i)];
     ids4(yyy)=[crank2(i)];
```

```
      tt4(yyy)=[i];
          yyy=yyy+1;
    else
      aaqwdsfv=1;
  end
   i=i+1;
end
yyy=1;
for a=2050:length(crank2)-1;
      if dQps4(a)<=0;
      dq4(yyy)=[dQps4(a)];
      ide4(yyy)=[crank2(a)];
      ttt4(yyy)=[a];
          yyy=yyy+1;
   else
      aaasdfads=1;
  end
   a=a+1;
end
c4=crank2(tt4(1):ttt4(1));
ahr4=dQps4(tt4(1):ttt4(1));
ahr4=abs(ahr4);
len4=length(c4); %the length of either input could be used, because they are the same
tote4=0; %the total must be initialized
aa=0;
```

```
for ii=1:len4-1 %There is one less interval than the number of data points, hence len-1
Wa4=(ahr4(ii+1)+ahr4(ii))/2; %this is the average value of the data
Int4=c4(ii+1)-c4(ii); %this is the time interval
AI4=Wa4*Int4; %this is the total energy for the interval or the area of that interval
tote4=tote4+AI4; %this adds up all of the intervals
aa=aa+1;
TAahr4(aa,:)=tote4;
end
Look4=tote4*.1;
bb4=linspace(Look4, Look4, length(TAahr4));
c14=c4(1:end-1);
YI4=interp1(TAahr4, c14, Look4);
ID4=(YI4-ids4(1))/(6*N)*10^3
imep=[imep1, imep2, imep3,imep4];
ID=[ID1, ID2, ID3,ID4]
mepa=[mep mep mep mep];
mechanical_eff=(mepa./imep).*100
figure(1),plot(crank2,pressure1,'LineWidth',2)
hold on
plot(crank2,pressure2,'r','LineWidth',2)
plot(crank2,pressure3,'g','LineWidth',2)
plot(crank2,pressure4,'c','LineWidth',2)
xlabel('Crank Angle (degree)','FontWeight','Bold')
title('Cylinder Pressure','FontWeight','Bold','FontSize',12)
ylabel('Cylinder Pressure (bar)','FontWeight','Bold')
```

```
legend('Diesel','J20','J35','J50')
xlim([320 400])
ylim([0 80])
set(figure(1),'Units','Inches')
set(figure(1),'Position',[.5,.5,3.5,3.5])
grid on
figure(2),plot(crank2,T1,'LineWidth',2)
hold on
plot(crank2,T2,'r','LineWidth',2)
plot(crank2,T3,'g','LineWidth',2)
plot(crank2,T4,'c','LineWidth',2)
xlabel('Crank Angle (degree)','FontWeight','Bold')
title('Bulk Gas Combustion Temperature (K)','FontWeight','Bold','FontSize',12)
ylabel('Temperature (K)','FontWeight','Bold')
legend('Diesel','J20','J35','J50')
xlim([320 420])
set(figure(2),'Units','Inches')
set(figure(2),'Position',[.5,.5,3.5,3.5])
grid on
figure(3), plot(crank2(1:end-1),dQps1,'LineWidth',2)
hold on
plot(crank2(1:end-1),dQps2,'r','LineWidth',2)
plot(crank2(1:end-1),dQps3,'g','LineWidth',2)
plot(crank2(1:end-1),dQps4,'c','LineWidth',2)
legend('Diesel','J20','J35','J50')
```

```
plot(crank2(1:end-1),Q111,'LineWidth',2)
plot(crank2(1:end-1),Q121,'LineWidth',2)
plot(crank2(1:end-1),Q112,'r','LineWidth',2)
plot(crank2(1:end-1),Q122,'r','LineWidth',2)
plot(crank2(1:end-1),Q113,'g','LineWidth',2)
plot(crank2(1:end-1),Q123,'g','LineWidth',2)
plot(crank2(1:end-1),Q114,'c','LineWidth',2)
plot(crank2(1:end-1),Q124,'c','LineWidth',2)
xlabel('Crank Angle (degree)','FontWeight','Bold')
ylabel('Heat Release (J/degree)','FontWeight','Bold')
title('Gross Heat Release','FontWeight','Bold','FontSize',12)
xlim([300 450])
grid on
set(figure(3),'Units','Inches')
set(figure(3),'Position',[.5,.5,3.5,3.5])
figure(4), plot(crank2,Re1,'LineWidth',2)
xlabel('Crank Angle (degree)','FontWeight','Bold')
ylabel('Reynolds Number','FontWeight','Bold')
title('Reynolds Number','FontWeight','Bold','FontSize',12), xlim([250 450])
hold on
plot(crank2,Re2,'r','LineWidth',2)
plot(crank2,Re3,'g','LineWidth',2)
plot(crank2,Re4,'c','LineWidth',2)
legend('Diesel','J20','J35','J50')
set(figure(4),'Units','Inches')
```

```
set(figure(4),'Position',[.5,.5,3.5,3.5])
grid on
figure(5), plot(crank2,dRad1,'LineWidth',2)
hold on
plot(crank2,dRad2,'r','LineWidth',2)
plot(crank2,dRad3,'g','LineWidth',2)
plot(crank2,dRad4,'c','LineWidth',2)
legend('Diesel','J20','J35','J50')
 plot(crank2,convect1,'LineWidth',2)
hold on
plot(crank2,convect2,'r','LineWidth',2)
plot(crank2,convect3,'g','LineWidth',2)
plot(crank2,convect4,'c','LineWidth',2)
 plot(crank2,Flux1,'LineWidth',2)
hold on
plot(crank2,Flux2,'r','LineWidth',2)
plot(crank2,Flux3,'g','LineWidth',2)
plot(crank2,Flux4,'c','LineWidth',2)
xlabel('Crank Angle (degree)','FontWeight','Bold')
ylabel('Heat Flux (MW/m2)','FontWeight','Bold')
title('Heat Flux W Convection & Radiation ','FontWeight','Bold','FontSize',12)
xlim([300 450])
set(figure(5),'Units','Inches')
set(figure(5),'Position',[.5,.5,3.5,3.5])
grid on
```

```
figure(6), plot(crank2(1:end-1),dQps1,'LineWidth',2)
hold on
plot(crank2(1:end-1),dQps2,'r','LineWidth',2)
plot(crank2(1:end-1),dQps3,'g','LineWidth',2)
plot(crank2(1:end-1),dQps4,'c','LineWidth',2)
legend('Diesel','J20','J35','J50')
xlabel('Crank Angle (degree)','FontWeight','Bold')
ylabel('Heat Release (J/degree)','FontWeight','Bold')
title('Apparent Heat Release','FontWeight','Bold','FontSize',12)
xlim([300 450])
grid on
set(figure(6),'Units','Inches')
set(figure(6),'Position',[.5,.5,3.5,3.5])
figure(7), plot(crank2,dRad1,'LineWidth',3)
hold on
plot(crank2,convect1,'r','LineWidth',3)
plot(crank2,Flux1,'g','LineWidth',3)
plot(crank2,dRad4,'c--','LineWidth',3)
hold on
plot(crank2,convect4,'m--','LineWidth',3)
plot(crank2,Flux4,'y--','LineWidth',3)
legend('Diesel Rad','Convect','Total Flux','B50 Rad','Convect','Total Flux')
xlabel('Crank Angle (degree)','FontWeight','Bold')
ylabel('Heat Flux (MW/m2)','FontWeight','Bold')
title('Heat Flux W Convection & Radiation ','FontWeight','Bold','FontSize',12)
```

```
xlim([300 450])
grid on
set(figure(7),'Units','Inches')
set(figure(7),'Position',[.5,.5,3.5,3.5])
figure(8),plot(crank2,T1,'LineWidth',2)
hold on
plot(crank2,T2,'r','LineWidth',2)
plot(crank2,T3,'g','LineWidth',2)
plot(crank2,T4,'c','LineWidth',2)
xlabel('Crank Angle (degree)','FontWeight','Bold')
title('Bulk Gas Combustion Temperature (K)','FontWeight','Bold','FontSize',12)
ylabel('Temperature (K)','FontWeight','Bold')
legend('Diesel','J20','J35','J50')
xlim([370 400])
set(figure(8),'Units','Inches')
set(figure(8),'Position',[.5,.5,3.5,3.5])
grid on
figure(9), [AX,H1,H2]=plotyy(crank2, fuel1, crank2, pressure1)
set(get(AX(1),'Ylabel'), 'String','Fuel Line Pressure (Bar)','FontWeight','Bold')
set(H1,'Color','b')
set(H2,'Color','b')
set(H1,'LineWidth',2)
set(H2,'LineWidth',2)
set(get(AX(2),'Ylabel'), 'String','Cylinder Pressure (Bar)','FontWeight','Bold')
set(AX(1),'XLim',[320 400],'YLim',[0 600],'YTick',[0:100:600])
```

```
set(AX(2),'XLim',[320 400],'YLim',[0 100],'YTick',[0:20:100])

xlabel('Crank Angle (degree)','FontWeight','Bold'),title('Cylinder and Fuel Line
Pressure','FontWeight','Bold','FontSize',12)

set(figure(9),'Units','Inches')

set(figure(9),'Position',[.5,.5,3.5,3.5])

hold on

[AX,H1,H2]=plotyy(crank2, fuel2, crank2, pressure2)

set(AX(1),'XLim',[320 400],'YLim',[0 600],'YTick',[0:100:600])

set(AX(2),'XLim',[320 400],'YLim',[0 100],'YTick',[0:20:100])

set(H1,'Color','r')

set(H2,'Color','r')

set(H1,'LineWidth',2)

set(H2,'LineWidth',2)

[AX,H1,H2]=plotyy(crank2, fuel3, crank2, pressure3)

set(AX(1),'XLim',[320 400],'YLim',[0 600],'YTick',[0:100:600])

set(AX(2),'XLim',[320 400],'YLim',[0 100],'YTick',[0:20:100])

set(H1,'Color','g')

set(H2,'Color','g')

set(H1,'LineWidth',2)

set(H2,'LineWidth',2)

[AX,H1,H2]=plotyy(crank2, fuel4, crank2, pressure4)

set(AX(1),'XLim',[320 400],'YLim',[0 600],'YTick',[0:100:600])

set(AX(2),'XLim',[320 400],'YLim',[0 100],'YTick',[0:20:100])

set(H1,'Color','c')

set(H2,'Color','c')
```

```
set(H1,'LineWidth',2)
set(H2,'LineWidth',2)
grid on
legend('Diesel','J20','J35','J50')
x=[0 20 35 50];
figure(10),plot(x,[ID1 ID2 ID3 ID4],'LineWidth',2)
xlabel('Percentage of Poultry Fat FAME','FontWeight','Bold')
ylabel('Time (ms)','FontWeight','Bold')
title('Ignition Delay','FontWeight','Bold','FontSize',12)
set(figure(10),'Units','Inches')
set(figure(10),'Position',[.5,.5,3.5,3.5])
grid on
ylim([0 3])
figure(11), [AX,H1,H2]=plotyy(crank2, fuel1, crank2(1:end-1), dQps1)
set(get(AX(1),'Ylabel'), 'String','Fuel Line Pressure (Bar)','FontWeight','Bold')
set(H1,'Color','b')
set(H2,'Color','b')
set(H1,'LineWidth',2)
set(H2,'LineWidth',2)
set(get(AX(2),'Ylabel'), 'String','Apparent Heat Release (J/degree)','FontWeight','Bold')
set(AX(1),'XLim',[320 420],'YLim',[0 600],'YTick',[0:100:600])
set(AX(2),'XLim',[320 420],'YLim',[-5 25],'YTick',[-5:5:25])
xlabel('Crank Angle (degree)','FontWeight','Bold'),title('Ignition
Delay','FontWeight','Bold','FontSize',12)
set(figure(11),'Units','Inches')
```

```
set(figure(11),'Position',[.5,.5,3.5,3.5])
hold on
[AX,H1,H2]=plotyy(crank2, fuel4, crank2(1:end-1), dQps4)
set(AX(1),'XLim',[320 420],'YLim',[0 600],'YTick',[0:100:600])
set(AX(2),'XLim',[320 420],'YLim',[-5 25],'YTick',[-5:5:25])
set(H1,'Color','r')
set(H2,'Color','r')
set(H1,'LineWidth',2)
set(H2,'LineWidth',2)
grid on
legend('Diesel','J50')
[AX,H1,H2]=plotyy(crank2, linspace(147,147,length(crank2)), crank2(1:end-1),
linspace(0,0,length(dQps1)))
set(AX(1),'XLim',[320 420],'YLim',[0 600],'YTick',[0:100:600])
set(AX(2),'XLim',[320 420],'YLim',[-5 25],'YTick',[-5:5:25])
set(H1,'Color','y')
set(H2,'Color','g')
set(H1,'LineWidth',2)
set(H2,'LineWidth',2)

for i=1:length(TAahr1)
   TAa1(i)=TAahr1(i)*100/max(TAahr1);
   i=i+1;
end
for i=1:length(TAahr2)
```

```
    TAa2(i)=TAahr2(i)*100/max(TAahr2);
    i=i+1;
end
for i=1:length(TAahr3)
    TAa3(i)=TAahr3(i)*100/max(TAahr3);
    i=i+1;
end
for i=1:length(TAahr4)
    TAa4(i)=TAahr4(i)*100/max(TAahr4);
    i=i+1;
end
figure(12),plot(c11,TAa1,'LineWidth',2)
hold on
plot(c12,TAa2,'r','LineWidth',2)
plot(c13,TAa3,'g','LineWidth',2)
plot(c14,TAa4,'c','LineWidth',2)
ylabel('Mass Burnt (%)','FontWeight','Bold')
xlabel('Crank Angle (degree)','FontWeight','Bold')
set(figure(12),'Units','Inches')
set(figure(12),'Position',[.5,.5,3.5,3.5])
legend('Diesel','J20','J35','J50')
grid on
figure(13),
plot(crank2(1:end-1),Q121,'g','LineWidth',2)
hold on
```

```
plot(crank2(1:end-1),Q111,'r','LineWidth',2)

plot(crank2(1:end-1),dQps1,'LineWidth',2)

plot(crank2(1:end-1),Q122,'y--','LineWidth',2)

plot(crank2(1:end-1),Q112,'m--','LineWidth',2)

plot(crank2(1:end-1),dQps2,'c--','LineWidth',2)

xlabel('Crank Angle (degree)','FontWeight','Bold')

ylabel('Heat Release (J/degree)','FontWeight','Bold')

title('Gross Heat Release(Convection&Radiation)','FontWeight','Bold','FontSize',12)

xlim([310 450])

legend('Diesel Gross Heat Release','W/ Convection','Net Heat','B50 Gross Heat Release','W/
Convection','Net Heat')

grid on

set(figure(13),'Units','Inches')

set(figure(13),'Position',[.5,.5,3.5,3.5])

Imep=[imep1 imep2 imep3 imep4]

TAa1=TAa1';

TAa2=TAa2';

TAa3=TAa3';

TAa4=TAa4';
```

APPENDIX B

MATLAB THERMODYNAMIC CYCLE SIMULATION PROGRAM

```
%Alternative Combustion
%Vs=displacement volume of the piston L
VVs=0.324955479;
Vs=VVs/1000;
%E=compression ratio of engine
E=23.5;
%Vc=Volume of combustion chamber
VVc=VVs/(E-1);
%D=bore (mm)
D=77;
%s=stroke (mm)
s=70;
%r=radius (mm)
r=s/2;
%Ts=Wall temperature of the cylinder (K)
Ts=370;
 %connecting rod length is l
l=110;
%R=molar gas constant
R=8314;
%Pe is the effective power measured at flywheel [kW]
Pe=2.6;
%i is the number of cylinders
i=1;
%taw = the number of strokes to complete one cycle
taw=4;
%nm is the mechanical efficiency
nm=0.8;
%N is the speed for effective power [rpm]
N=2200;
%Ta is the temperature at the end of intake [K]
Ta=399.2;
%Tr is the average temperature of burnt gas [K] range 600-900K
Tr=850;
%mc= compression polytropic coefficient (1.31-1.37)
mc=1.27;
%md=expansion polytropic coefficient (1.20-1.32)
```

```
md=1.20;
%roe= inital expansion coefficient for CI (1.2-3)
roe=1.5;
%pa=average pressure into the cylinder during intake [MPa];
pa=0.08;
%pev is the pressure into the cylinder during exhaust [MPa]
pev=0.11;
%For diesel fuel
%c = [kgCarbon/kgfuel]
c=0.857;
%h=[kgHydrogren/kgfuel]
h=0.133;
%O=[kgOxygen/kgfuel]
O=0.01;
%For Oleic
Col=(19*12)/296.49;
Hol=36/296.49;
Ool=64/296.49;
%Lambda is the relative air-fuel ratio for CI w seperate combustion chamber
%it needs to be in following range 1.3-1.7
Lambda=1.33;
%p0 [MPa] and T0 [K] are the normal conditions of air
p0=0.101;
T0=273.15;
%Qidiesel is the lower calorific value of diesel fuel [kJ/kg]
Qidiesel=42600;
Qioleic=39930;
nd=0.35665;
np=0.5;
n=180;
ii=n:-1:0;

 %%%%%%%%%%%%%%%%%%START OF CALULATIONS %%%%%%%

%Pl is the effective power per Liter [kW/L]
disp('The effective power per Liter [kW/L] is:')
Pl=Pe/(VVs*i)

%pe=mean effective pressure [MPa]
pe=(30*taw*Pe)/(2*i*VVs*N);
```

```
%p_i = mean indicated pressure for the cycle [MPa]
p_i=pe/nm;

%wpm is the mean piston speed [m/s]
wpm=(s*N)/30*10^-3;

%pce=pressure at end of compression [MPa]
pce=pa*E^mc;

%Tce=temperature at the end of compression [K]
Tce=Ta*E^(mc-1);

%pic= mean indicated pressure corrected
pic=(1/nd)*[p_i+np*(pev-pa)];

%hp is the ratio of increase in pressure during combustion
hp=[((E-1)/(E^mc))*(pic/pa)+((1-(1/(E^(mc-1))))*(1/(mc-1)))]/[roe-1+(roe/(md-1))*(1-
(roe/E)^(md-1))];

%pmax is the maxium pressure during combustion [MPa] should be between 8-15
pmax=hp*pce;

%VVc is the volume of the cylinder at TDC [L]
%VVc=1/((E-1)*VVs);

%Vz is in [L] it is the voulume of the cylinder at the end of combustion
Vz=roe*VVc;

%Lo is the minimum quantity of air necessary for combustion of 1kg fuel
%[kmole air/kgfuel]
Lo=(1/0.21)*(c/12+h/4-O/32);
Lo20=(1/0.21)*(c/12+h/4-O/32)*.8+(1/0.21)*(Col/12+Hol/4-Ool/32)*.2;
Lo35=(1/0.21)*(c/12+h/4-O/32)*.65+(1/0.21)*(Col/12+Hol/4-Ool/32)*.35;
Lo50=(1/0.21)*(c/12+h/4-O/32)*.5+(1/0.21)*(Col/12+Hol/4-Ool/32)*.5;
Lo100=(1/0.21)*(Col/12+Hol/4-Ool/32);

%N1 is the quantity of air vs unity mass of fuel before combustion
%units---> [kmol air/kgfuel]
N1=Lambda*Lo;
```

```
N120=Lambda*Lo20;
N135=Lambda*Lo35;
N150=Lambda*Lo50;

%these are the molar quantities [kmole ../kgfuel]
Nco2=c/12;
Nh20=h/2;
No2=0.21*(Lambda-1)*Lo;
Nn2=0.79*Lambda*Lo;

Nco220=Col/12*.2+c/12*.8;
Nh2020=Hol/2*.2+h/2*.8;
No220=(0.21*(Lambda-1)*Lo20)
Nn220=0.79*Lambda*Lo20;

 %N2 is the number of kmol of burnt gas [kmol bg/kgfuel]
N2=Nco2+Nh20+No2+Nn2;
N220=Nco220+Nh2020+No220+Nn220;

%uo is the variation of the fresh charge between the start of combustion
%and the end during the cycle
uo=N2/N1;
uo20=N220/N120;

%Nr is the kmole of burnt gas that remains in the cylinder [kmol bg/cycle]
Nr=10^3*VVc*pev*(1/(Tr*R));

%Na is the total number of kmole present at the end of intake at BDC
%[kmol/cycle]
Na=10^3*pa*(VVs+VVc)/(R*Ta);

%Npr is the kmol of fresh air [kmol fresh charge/cycle]
Npr=Na-Nr;

%neffex is the efficiency of the exhaust process (amt of residual fuel into the cylinder[%]
neffex=Nr/Npr*100;

%neffv is the filling efficiency coefficient [%]
%this value should be between 80-94% for natually aspirated engines
neffv=R*T0*Npr/(10^3*p0*VVs)*100;
```

```
%Nga is the number of kmol of burnt gases at the end of combustion
%[kmolbg/cycle]
Nga=uo*Npr;
Nga20=uo20*Npr;

%uu is the whole mass of gas that is into the cylinder in one cycle
uu=(Nga+Nr)/(Npr+Nr);
uu20=(Nga20+Nr)/(Npr+Nr);

%Tz is the max temperature during combustion [k]
%It should be in range of 1800-2800K
Tz=hp*roe*Tce/uu;

%pd is the expansion pressure [MPa]
%should be in range of 0.15-0.6 MPa
pd=pmax*(roe/E)^md;

%Td is the expansion temperature [K]
%should be in range of 600-1200 K
Td=Tz*(roe/E)^(md-1);

%Wmech is the mechanical work during the isobaric combustion [kJ/cycle]
Wmech=pmax*VVc*(roe-1);

%Gcycle is the quantity of fuel that can be completely burnt during the
%cycle into the engine cylinder [g]
Gcycle=10^3*Npr/(Lo*Lambda);
Gcycle20=10^3*Npr/(Lo20*Lambda);

Gcycle35=10^3*Npr/(Lo35*Lambda);

Gcycle50=10^3*Npr/(Lo50*Lambda);

Gcycle100=10^3*Npr/(Lo100*Lambda);


%Qtcycle is the heat quantity that can be theoretically obtained by buring
%the amount of Gcycle fuel [kJ]
Qtcycle=10^-3*Qidiesel*Gcycle;
```

```
Qtcycle20=10^-3*Qioleic*Gcycle20;

%chfuel is the hourly fuel consumption [kgfuel/hr]
chfuel=120*10^-3*Gcycle*i*N/taw;
 chfuel20=120*10^-3*Gcycle20*i*N/taw;

 chfuel35=120*10^-3*Gcycle35*i*N/taw;

 chfuel50=120*10^-3*Gcycle50*i*N/taw;

 chfuel100=120*10^-3*Gcycle100*i*N/taw;

%chair is the hourly air consumption [kgair/hr]
chair=chfuel*Lo*Lambda;
 chair20=chfuel20*Lo20*Lambda;

%ce is the brake specific fuel consumption [g/kWhr]
%ce should be in range of 170-270
ce=chfuel/Pe*10^3;
 ce20=chfuel20/Pe*10^3;
 ce35=chfuel35/Pe*10^3;
ce50=chfuel50/Pe*10^3;
 ce100=chfuel100/Pe*10^3;

%ne is the overall efficiency of the engine [%]
%should be in range of 30-45
ne=2.9*10^8/(ce*Qidiesel);
ne20=(2.9*10^8/(ce*Qidiesel))*.8+(2.9*10^8/(ce20*Qioleic))*.2;

%ni is the indicated efficiency [%]
ni=ne/nm*100;
 ni20=ne20/nm*100;

%ci is the brake indicated fuel consumption [g/kWhr]
ci=ce*nm;
 ci20=ce20*nm;

totm=14.23/Lo;
%Qeff is the heat effectively transformed in the mechanical work [kJ/kg]
```

```
Qeff=ne*Qidiesel;

%Qf is the heat consumed to overcome the internal friction [kJ/kg]
Qf=(ni-ne)*Qidiesel;

%Tge is the average exhaust temperature [K]
Tge=0.5*(Td+Tr);

Vo=VVs/n;

pii=pa*[(VVc+n*Vo)./(VVc+ii*Vo)].^mc;

Vy=roe*VVc;

m=360;
 Voo=(VVs-Vy)/m;

jj=0:1:m;

 pj=pmax*[(VVc *roe)./(VVc*roe+jj.*Voo)].^md;

%plot(ii*Vo, pii)
%plot(jj*Voo, pj)

AFR=Lo*totm
AFR20=Lo20*totm
AFR35=Lo35*totm
AFR50=Lo50*totm
AFR100=Lo100*totm
```